Anisotropy and Texture Studies in Magnetic Media

by

Marian Vopsaroiu

A thesis submitted in fulfilment of the requirements of the University of Central Lancashire for the PhD degree

at

Centre for Materials Science
University of Central Lancashire
July 2002

Supervisors:

Prof. Phil R. Bissell

Dr. Jim A. Gotaas

Abstract

The rapid development of magnetic materials for recording media applications increased the demands for new and more precise experimental investigation techniques. In respect with these demands, this project is focused on experimental analyses of advanced particulate media and magnetic thin film samples.

A new extended rotational remanence technique for anisotropy field measurements was developed. The technique is suitable for samples that contain aligned or partially aligned particles and provides both: in-plane anisotropy field distributions and the in-plane anisotropy field. This technique was also extended to out-of-plane anisotropy field measurements.

Rotational hysteresis was introduced as an alternative method for anisotropy field measurements. This applies well in the case of samples without texture or samples having very small magnetic moment (i.e. thin films). The two techniques for anisotropy field measurement compare well and the experimental results were interpreted in terms of inter-particles interactions.

Two measurement methods for determination of the demagnetizing field acting perpendicular to a sample plane were also developed. The first method is based on the in-plane and out-of-plane anisotropy field determination using an extended rotational remanence technique. The second method can provide the demagnetizing field starting from in-plane and out-of-plane transverse hysteresis loops. Comparison between the results from the two methods showed good agreement. Furthermore, the demagnetizing field values were used to calculate the magnetic coating thickness, so the two methods provide a non-destructive method for magnetic thickness measurements in film samples.

The in-plane easy axis distribution (EAD) was experimentally determined using vector VSM techniques. Correlations between in-plane tape texture and magnetic thickness were obtained for a series of advanced MP tapes. A theoretical approach was used in order to relate the orientation ratio to EAD. The out-of-plane EAD was derived from numerical calculations. The out-of-plane distribution also showed a variation with the magnetic thickness. In addition, the microstructure and particle morphology of the advanced MP tapes, as well as the out-of-plane component of magnetization, have been investigated using Mössbauer Spectroscopy. Finally, 3D - EAD maps were produced.

All VSM experiments were fully computer controlled and the routines were designed in the LabView environment as part of this project.

Table of Contents

List of Figures

List of Tables

Acknowledgments

I would like to take this opportunity and thank to my supervisors Prof. Phil R. Bissell and Dr. Jim. A. Gotaas for their help and dedication to this project. Many thanks to Phil who has been a source of inspiration throughout this project and generously has shared with me his rich experience in magnetism.

Special thanks to my collaborator Dr. Victor Kuncser who helped me with the Mössbauer experiments and to Dr. M.F. Thomas from University of Liverpool who did the initial Mössbauer studies.

I would also like to thank my fellows in The Magnetic Materials Research Group and all the people I have met during this project who made my time spent in the basement so enjoyable. Richard Cookson requires a special mention for sharing with me some computing tricks.

Finally, I wish to acknowledge and to express my deep appreciation to University of Central Lancashire, Research Degree Committee and to ORS Committee for their financial support to this PhD project.

Evidences in Chinese documents suggest that magnetism was known as early as around 2000 BC. The ancient Greeks observed magnetic phenomena as early as 700 BC. The existence of magnetic forces is known from observation that pieces of a naturally occurring stone called magnetite (Fe_3O_4) are attracted to iron. The word magnetic comes from the name of Magnesia, on the coast of Turkey, where magnetite was first found. Later in 1600 William Gilbert extended the experiments from magnetite to other materials. Using a compass needle he also suggested that the Earth itself is a large permanent magnet. In 1750, John Michell used a torsion balance to show that magnetic poles exert attractive or repulsive forces on each other and that these forces vary as the inverse square of their separation. Although the force between two magnetic poles is similar to the force between two electric charges, there is an important difference (i.e. electric charges can be isolated whereas magnetic poles cannot be isolated and they are found always in pairs). Only on the early part of the 19^{th} century the scientists established that electricity and magnetism are in fact related phenomena. In 1819, Hans Oersted discovered that a compass needle is deflected when placed near a circuit carrying an electric current. Shortly after Oersted's discover J.B. Biot and F. Savart produced the Bio-Savart law, which gives the magnetic field, produced by a current at some point in space. In 1831, Joseph Henry and almost simultaneously Michael Faraday showed that when a wire is moved near a magnet (or equivalently when a magnet is moved near a wire), an electric current is established in the wire. The microscopic explanation of the magnetic properties starts in 1820 with Ampere's hypothesis of the molecular currents associated with the orbital motion of the electrons and hence generating the orbital magnetic moment. In 1873, James Clerk Maxwell used these observations and other experimental facts as a basis for formulating the laws of electromagnetism. The properties of solids that exhibit magnetic ordering (ferromagnetism) have been explained in 1906 by Pierre Weiss and in 1920s Van Vleck elaborated the quantum theory of dia and para - magnetism. In 1932, L. Neel first predicted the existence of anti-ferromagnetic materials and in 1948 established the theory of ferromagnetic materials.

Honour to those who discovered the magnetic materials and the laws of magnetism

1. Introduction

Magnetic materials represent an important and growing industry. There are numerous applications of magnetic materials [see the reference 1] and they can be separated in two main areas: applications of magnetic materials and properties that provide devices of wide applicability (i.e. permanent magnets, magnetic recording media) and applications of magnetic materials in different magnetic measuring techniques (i.e. nuclear magnetic resonance imaging, magnetic force microscopy, different systems for guiding beams of charged particles, etc).

Permanent magnets are used in different industrial applications but mostly as permanent magnets for electrical motors and generators. Other industrial applications for permanent magnets are in telecommunication, instrumentation and control, acoustic transducers (i.e. loudspeakers, head-phones, microphones, etc) and different mechanical applications. Some of the most important commercial permanent magnets are based on NbFeB, Sm(Fe, Co, Cu, Zr), SmCo or SrFeO.

Magnetic recording media also form part of a major area of magnetic materials applications and have an economic importance, which is comparable to that of semiconductor devices. Especially in the last 50 years, recording media became a multibillion-dollar industry, which in fact is continuously growing. Two most important commercial recording media available are particulate flexible media and thin film disk media.

This rapid development of the magnetic materials and their applications (mainly as permanent magnets and magnetic recording media) has increased the demand for new and more precise magnetic characterisation techniques. One of the goals of this research project is the development of new experimental techniques for recording media / magnetic materials characterisation and also a better implementation of the existing experimental methods. In respect of this, the project is focused on experimental anisotropy and texture studies on advanced particulate recording media and magnetic thin film samples. Magnetic recording materials, both particulate and thin film media are constituted of magnetic fine particles / grains. Single domain magnetic fine particles

can be obtained by reducing the dimensions of a ferromagnetic sample until an equilibrium state is reached, where there are no domain walls and the sample is a single domain with uniform magnetisation. Fine particles present a huge technical interest due to the their high coercivity, and they are used in industry for fabrication of permanent magnets and recording media. A typical example is a bulk sample of MnBi that has a coercivity of 10^2A/m. If the same material is constituted of fine particles, the coercivity increases to 10^6A/m. The dimensions of the fine particles are usually between (100 - 10,000) Å and they can have different shapes. The critical dimension for obtaining a single domain particle can be studied within the classical theory [2,3] and/or micromagnetic theory [4]. However, by reducing further the dimension of the particles, they could reach the critical super-paramagnetic limit where the anisotropy energy of the particles is overcome by the thermal energy and they then behave like super-paramagnets.

Besides these single domain and super-paramagnetic critical dimensions, the anisotropy field of magnetic particles and their orientation distribution are also essential parameters for recording media technology.

Magnetic recording media are often textured by the application of a large magnetic field to the coating before it has dried, which increases the alignment of particle easy axes (see section 1.2.1.1). The degree of texturing can be described by the Easy Axis Distribution (EAD) which can be different in-plane and out-of-plane. The determination of the easy axis distribution is essential to the understanding of bulk magnetic properties and the switching processes in a recording material. The knowledge of these distributions is also very important for the interpretation of other magnetic measurements.

Another important requirement for a magnetic material regarding its applications in recording media is related to the field strength needed to cause magnetic reversal of the moments in the magnetic coating, which is generally characterised by the coercivity. The strength of the magnetic anisotropy or the anisotropy field determines the difficulty of switching and hence the coercivity. The actual coercivity is determined by the anisotropy field of individual particles, by their orientation to the applied field direction and by other factors such as inter-particle interactions. The magnetic anisotropy

distribution is a measure of the potential magnetic properties of the system with perfect particle alignment.

As already mentioned, this project is focused on experimental measurements of the magnetic particles anisotropy field and their texture or easy axis distribution, in metal particle tapes and magnetic thin films. Because the measurements of texture and anisotropy are self-contained, the background and literature review associated with these techniques are presented together with the results obtained in the self-contained chapters 3 and 5.

In the following sections, the concept of magnetic anisotropy and the anisotropy field of a single domain particle in the Stoner – Wohlfarth model is presented, followed by an introduction to magnetic recording materials and an overview of this thesis.

1.1 Magnetic anisotropy

The magnetisation changes can be best understood as involving the switching of the magnetisation direction between preferred directions in single domain magnetic particles. These changes are related to the difficulty of reversing the magnetisation or, in other words the strength of the anisotropy field. Anisotropy is exploited in the design of most magnetic materials of commercial importance and therefore this subject is of extremely practical interest. There are several known types of anisotropy, i.e. magneto-crystalline anisotropy, shape anisotropy, stress anisotropy, exchange anisotropy, induced anisotropy.

However, the *magneto-crystalline anisotropy* and the *shape anisotropy* are of most importance for recording media and they will be discussed in this section, together with the possible responsible physical mechanisms.

1.1.1 Magneto-Crystalline Anisotropy

Magnetic ordered states are a consequence of the exchange interactions between the atomic moments of the constituents atoms / ions. The exchange interactions are considered generally to depend only on the angle between adjacent spins. In reality, the crystals are not isotropic media and they behave differently with respect to the

crystallographic axis directions. An energy component, called magneto-crystalline anisotropy energy, which depends on the direction of the magnetic moments with respect to the crystal lattice, has been considered in order to explain the magnetic anisotropic behaviour of the crystals. The physical origin of the crystal anisotropy is related to the interactions or the coupling of the electron spins or atomic moments. There are four main kinds of interactions taking place in a crystal: spin - spin, spin - orbit, spin - lattice and orbit - lattice. The exchange interactions or the spin – spin coupling is isotropic and does not depend on the direction of the spin axis to the crystal lattice. The spin - spin coupling, therefore, which is a strong interaction (10^8-10^9 A/m), cannot be responsible for the magnetic anisotropy. The orbital – lattice coupling is also very strong because the orientations of the orbitals are fixed to the lattice by the very strong electric crystalline fields. Even large applied magnetic fields cannot change the orbital orientations. Hence the orbital magnetic contribution is negligible and again, not responsible for the magnetic anisotropy. The origins of the magneto-crystalline anisotropy are related to the spin – orbital coupling. If a magnetic field is applied to a crystal, the spins will be free to rotate towards the field direction, while the crystalline field will freeze the magnetic orbital moments. The spin – orbital coupling is a weak interaction (10^5A/m) and the energy required to rotate the spin system of a domain (anisotropy energy) is only the energy required to overcome the spin – orbital coupling.

Analysing the magnetisation curves for a mono-crystal can easily provide evidence for the presence of this magnetic anisotropy in crystals. By applying an external magnetic field H for certain directions, the magnetisation of the crystal reaches saturation faster (at smaller fields) than for other directions of the applied field. The directions for which the crystal is magnetically saturated easier are called "easy axes", while those for which the crystal is saturated at higher fields are called "hard axes".

We are interested in magnetic materials used for recording media (particles/grains for recording media) and the two most common types of magneto-crystalline anisotropy found in these materials are cubic anisotropy and uni-axial anisotropy.

The anisotropy energy of a crystal has been defined using the anisotropy constants, introduced first by Becker and Döring [5]. Akulov showed in 1928 [6] that the anisotropy energy could be expressed in terms of a series expansion of the direction cosines of [1]M_s relative to the crystal axes. An example of a cubic structure, as occurring

[1]) M_s is introduced in the section 2.2.3

in iron crystals, is presented in figure 1.1. For a cubic crystal the anisotropy energy is defined as:

$$W = K_0 + K_1(\alpha_1^2\alpha_2^2 + \alpha_2^2\alpha_3^2 + \alpha_3^2\alpha_1^2) + K_2(\alpha_1^2\alpha_2^2\alpha_3^2) + ... \quad (1.1)$$

where M_s is the saturation magnetisation vector, $\alpha_1,\alpha_2,\alpha_3$ are the cosines of the angles M_s makes with the crystal axes and K_0, K_1, K_2, ...are the anisotropy constants for a particular material. K_0 is independent of angle and can be ignored as well as higher power terms that are too small in comparison with K_1 (including K_2 in some cases).

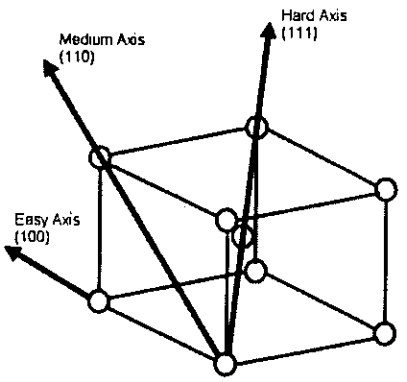

Figure 1.1 The body-centred cubic crystal structure corresponding to Fe. The arrows show the magnetic axes for this cubic crystal.

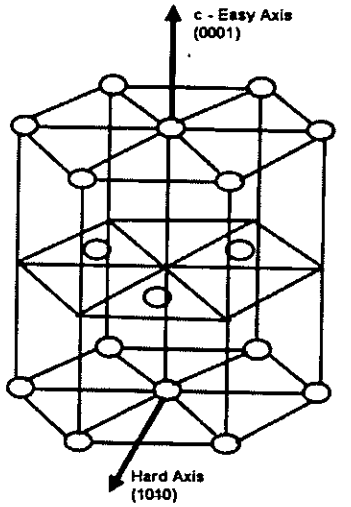

Figure 1.2 The single crystal hexagonal structure corresponding to Co. The c axis is the only easy axis of the crystal and any axis in the basal plane is a hard axis.

The uniaxial anisotropy results from a hexagonal structure as in Co crystals (see figure 1.2) or a tetragonal structure. Usually, there is only one direction of easy magnetisation for a hexagonal structure corresponding to the "c" axis, while any direction in the basal plane is an equally hard axis for positive anisotropy constants. The anisotropy energy for crystals with uniaxial anisotropy depends on only a single angle, namely the angle "θ" between the M_s vector and the easy axis:

$$W = K'_0 + K'_1\cos^2\theta + K'_2\cos^4\theta + ... \quad (1.2)$$

Using the relation: $cos^2\theta = 1 - sin^2\theta$, the anisotropy energy becomes:

$$W = K_0 + K_1 sin^2\theta + K_2 sin^4\theta + \ldots \quad (1.3)$$

1.1.2 Shape Anisotropy

The existence of the shape anisotropy can be shown for a sample with no crystal anisotropy. Practically this could be a polycrystalline sample containing particles / grains with random easy axis orientations. For a spherical shape the specimen will be magnetised in the same way for different directions while for a non-spherical shape it will be more easily magnetised along the long axis than along the short axis. This phenomenon shows that the shape itself can be a source of magnetic anisotropy and this type of anisotropy is called "shape anisotropy". The explanation for the occurrence of the shape anisotropy relies on the existence of the demagnetising fields (H_d). Any physical system always tends to an equilibrium state in which energy is minimised, i.e. it will oppose any action that it is subjected to. In the same way, the demagnetising field is acting in opposite direction to the magnetisation (M) that creates it. Moreover, for uniform magnetisation the demagnetising field is proportional to the magnetisation:

$$\vec{H}_D = -N_D \vec{M} \quad (1.4)$$

The negative sign shows that the demagnetising field is opposed to the magnetisation of a body, and N_d is the demagnetising coefficient. This factor depends on the shape of the magnetised body and can be calculated exactly only for an ellipsoid of revolution. Demagnetising coefficient for other shapes can only be approximately calculated. The maximum value that the demagnetising factor can have is $N_d = 1$, showing that the demagnetising field of a body cannot exceed its magnetisation. The shape anisotropy of a magnetised body can be calculated from the magneto-static energy, which is defined as:

$$W_m = -\int \vec{H} \cdot d\vec{M} \quad (1.5)$$

If there is no applied external field, then the internal field is equal to the demagnetising field defined in the relation (1.5). The magneto-static energy generated by a domain is determined by:

$$W_m = -\int \vec{H} \cdot d\vec{M} = -\int \vec{H}_D \cdot d\vec{M} = \int N_D \vec{M} \cdot d\vec{M} = \frac{1}{2} N_D M^2 \qquad (1.6)$$

In the following, the shape anisotropy for a prolate spheroid (figure 1.3) is derived. A single domain prolate spheroid has a shape anisotropy resulting from the different demagnetising factors acting on the major and minor axes respectively.

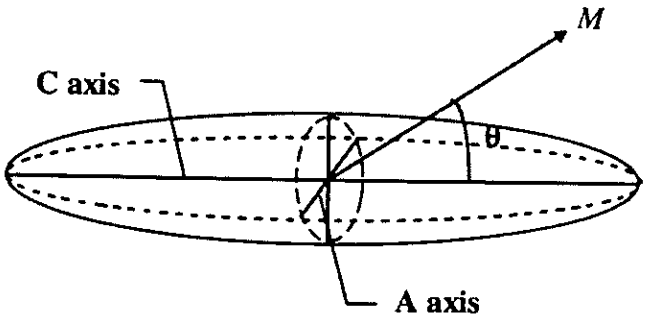

Figure 1.3 An amorphous specimen or a polycrystal in the shape of a prolate spheroid. C is the semi-major axis and A is the semi-minor axis.

Let N_a and N_c be the two demagnetising coefficients corresponding to the two axes. Suppose that the magnetisation M of the prolate domain makes an angle θ with the major axis. The magnetostatic energy for the prolate single domain is calculated for both components of the magnetisation vector, namely the components along the two prolate axes. The relation (1.6) becomes:

$$W_m = \frac{1}{2}\left[(M\cos(\theta))^2 N_c + (M\sin(\theta))^2 N_a\right] = \frac{1}{2} M^2 N_c + \frac{1}{2}(N_a - N_c) M^2 \sin^2(\theta) \qquad (1.7)$$

where the trigonometric relation $cos^2(\theta) = 1 - sin^2(\theta)$ has been used to re-arrange the above expression. It is easy to see that the relation (1.7) has an angle dependent term of the same form as in relation (1.3) for uniaxial crystal anisotropy energy. The shape anisotropy constant K_s can then be defined as:

$$K_s = \frac{1}{2}(N_a - N_c)M^2 \tag{1.8}$$

In the same way that the easy axis of a crystal give rise to the magneto-crystalline anisotropy, the long axis "c" of a prolate spheroid give rise to the shape magnetic anisotropy.

1.1.3 Single domain particle in the Stoner-Wohlfarth model

Stoner and Wohlfarth introduced in 1947 [2] a model which describes the magnetic behaviour of an isolated single domain particle having a uniaxial anisotropy (figure 1.4). The model refers to particles of those magnetisation remains uniform and executes coherent rotations.

The source of the uniaxial anisotropy could be either generated by the shape anisotropy or crystalline anisotropy. In any case the uniaxial anisotropy is defined by:

$$W_a = K_a \cdot \sin^2(\theta) \tag{1.9}$$

where K_a is the uniaxial anisotropy constant and the θ is defined in figure 1.4.

The magnetic properties of the single domain particle are studied in this model through the minimisation of its magnetic energy.

Let the applied field H make an angle ϕ with the easy direction of the particle. The potential energy of the particle in an applied field is:

$$W_p = -\vec{H} \cdot \vec{M}_s = -HM_s \cos(\phi - \theta) \tag{1.10}$$

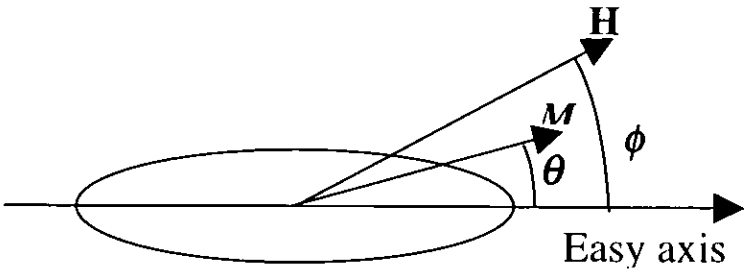

Figure 1.4 A single domain particle having uni-axial anisotropy in the Stoner and Wohlfarth model.

The total energy is:

$$W_t = W_p + W_a = K_a \cdot \sin^2(\theta) - HM_s \cos(\phi - \theta) \tag{1.11}$$

The equilibrium position for the magnetisation vector M_s is given by the condition:

$$\frac{dW_t}{d\theta} = 2K_a \sin(\theta)\cos(\theta) - HM_s \sin(\phi - \theta) = 0 \tag{1.12}$$

$$\Rightarrow \qquad 2K_a \sin(\theta)\cos(\theta) = HM_s \sin(\phi - \theta) \tag{1.13}$$

If the applied field is set normal to the easy axis, then $\phi = 90^0$ and the relation (1.13) becomes:

$$2K_a \sin(\theta)\cos(\theta) = HM_s \cos(\theta) \qquad \Rightarrow \qquad 2K_a \sin(\theta) = HM_s \tag{1.14}$$

The field required to rotate the particle moment 90^0 away from the easy axis ($\theta = 90^0$) is define as the particle anisotropy field, H_a.

$$H_a = \frac{2K_a}{M_s} \tag{1.15}$$

One of the most important limitations of the Stoner – Wohlfarth (S-W) model is related to the assumption that the magnetisation remains uniform in the S-W particle and that the reversal mechanism is coherent. In fact, this means that all the atomic spins of the atoms contained in the single domain particle remain parallel to each other during the reversal process. The reversal mechanism within a single domain particle is very important because it determines magnetic properties such as: remanence, anisotropy field, switching field and the speed of reversal. There are two main forms of reversal mechanism within a single domain particle: coherent reversal (introduced by Stoner – Wohlfarth) and incoherent reversal.

Coherent reversal is an ideal case with limited validity, because it means no contribution to the reversal mode from exchange interactions and it also eliminates the effect of the

demagnetising field during the reversal process. However, it has been found that the field at which the particles reverse in the S-W model is greater than the switching field of real particles [7]. This inaccuracy between the model and the experiment suggested that the assumption of coherent reversal was wrong or incomplete. Other incoherent reversal mechanisms have been suggested [8]: fanning, curling and buckling.

The fanning reversal mode was first introduced by Jacobs and Bean who proposed a model that represented a single domain elongate particle with a chain of spheres [7]. Considering the magnetostatic dipole-dipole interaction energy between the spheres and the applied field energy they found that the coherent rotation increases the magnetostatic energy while the fanning mode reduces it. This effect of increasing the magnetostatic energy in the coherent mode made the fanning reversal a more efficient mechanism.

Buckling is another reversal mechanism that is characterised by moments reversing coherently locally within the particle and could act as nucleation sites for further reversal [9].

Curling is an incoherent reversal mode of rotation that was first investigated by Brown [4] and Frei [9], both in 1957. This mode of rotation is characterised by the existence of no free poles on the particle surface during the reversal process. This is because in this reversal mode the moments rotate so they remain parallel to the surface of the particle and therefore there are no free poles on the surface of the particle resulting in no external magnetostatic fields.

1.2 Magnetic recording media

1.2.1 Particulate recording media

Among all types of recording media, particulate media represent a special class, which has been in continual technological development and growing since its first commercialisation in the mid 40's [10]. The cheap costs of production and the basic principle of recording make particulate media still an attractive alternative for modern recording application, including high-density digital data storage.

A medium consists of a magnetic layer, containing magnetic particles dispersed in an organic binder, supported on a non-magnetic substrate. The medium is configured to form along the track, on the magnetic layer, a pattern of remanent magnetization, so it can store information. The information is written using a recording head, which is an electromagnetic device. The write signal is a time varying current that passes through the coil of the recording head. As the head moves at constant speed along the medium, the spatial variations in remanent magnetization along the length of the medium produce the temporal variations in the head current and represent the recorded signal. The information is read back by passing a read head at the same constant velocity along the medium. The read head detects the out-of-plane magnetic flux emanating from the medium surface and a voltage signal is induced in the coil/head, which is proportional with the rate of change in the remanent magnetization of the medium (i.e. the change in the out-of-plane flux). The "read signal" is not identical with the original "write signal" and represents only an approximate reproduction of it. However, the "read signal" is further electronically processed in order to reproduce the original "write signal" (see also the Appendix 3 for a better description of the magnetic recording process). In most modern systems the original inductive head has been replaced by a magneto-resistive head [11,12], which has much greater sensitivity and allows a reduction in magnetic coating thickness and a much higher data density. The successful recording and reading onto the medium depends on the specific properties of the particulate medium. These properties are especially related to the particles characteristics of the medium, such as: particles size distribution, intrinsic coercivity and switching field distribution. The particles must also be chemically stable and not susceptible to magnetic fluctuations due to thermal energy. One important requirement is that the retained magnetization of a medium must be high enough since it determines the strength of the flux sensed by the read-back head. Another characteristic of a medium is related to the corecivity field (see the chapter 2 for more details) or the mean field strength needed to produce magnetic reversal, which must not be too large because will corrupt the successful writing and also not too small in order to resist signal degradation during the storage time. However, the coercivity of a material does not fully characterize its recording properties and the switching field distribution (explained in chapter 2) should be considered. A broad switching field distribution will have poor recording properties and can have problems

in erasure or overwriting old information. Conversely, a medium with a narrow switching field distribution is more suitable for high-density recording and it allows sharp and well defined magnetic transitions.

The density of a magnetic recording medium is determined by the particle size. There is a constant trend to increase the data densities within particulate media by increasing the particle morphology and reducing the particle size. For a high-density medium with low noise, a recorded bit should contain a large number of particles that should be as small as possible. A large signal to noise ratio is also obtained by minimizing the separation between the medium and the read/write head, which is limited by the roughness of the medium surface. Another limitation is related to the trend of reducing the particle size. Reducing the particle dimensions beyond a certain volume, they are susceptible to magnetic fluctuations due to thermal energy. This limit of magnetic stability occurs when the thermal energy is comparable with the anisotropy energy and is called the super-paramagnetic limit. Considering these requirements for commercial particulate media, over the years, the properties of media have been improved to increase data densities, access speed and archival properties. Subsequent paragraphs list the main types of media in use and their properties.

Gamma oxide

The first commercial magnetic recording tapes were produced in mid 40's using iron oxide particles. The particles used today are acicular in shape with typically length of 0.3-0.4 μm and aspect ratios between 6:1 and 12:1. Current γ-Fe_2O_3 particles have saturation magnetization of about 340 emu/cm^3 and coercivities of 300-400 Oe. The shape anisotropy is the major source of their magnetic anisotropy, together with the magneto-crystalline anisotropy arising from the interaction of the electron spins with the crystal structure of the oxide. Gamma ferric oxide (γ-Fe_2O_3) is useful due to its chemical and physical stability [13,14,15]. Acicular iron oxides are also important in recording technology as precursors for cobalt-modified oxides and metallic particles, which will be discussed in the next paragraphs. These properties combined with low cost and great chemical stabilities suit them very well for some applications.

Chromium dioxide

As the recording densities increased, the relative low coercivity values of the iron oxide particles proved to be a serious limitation. In the mid 60's were first introduced CrO_2 particles as an alternative for higher coercivity particles. These are, like iron oxides, magnetically uni-axial and the anisotropy derives from both their acicular shape and magneto-crystalline anisotropy [16]. Initially, typical length of CrO_2 particles was about 0.5 μm or more but this has been improved and particles as small as 0.1 μm have been reported [17,18] with coercivities of 2800 Oe. Commercially available particles have coercivities around 500-600 Oe and saturation magnetizations of 350-400 emu/cm^3. A limiting factor is that the production process for CrO_2 is very complex requiring high-pressure preparations and material costs. Tapes made with CrO_2 have an unusual low Curie temperature (125^{0}C) and this allow them to be used in thermo-magnetic duplication [19].

Cobalt-modified iron oxides

In mid 70's the most successful magnetic particles were cobalt-modified iron oxides. Most of the practical benefits of the original oxides (low cost, chemical and physical stability, etc) were retained, while the coercivities have been increased well above 1000 Oe, due to Co doping. The particles (Co-Fe_2O_3) can either be cobalt doped into the iron oxide structure [20] or cobalt absorbed onto the oxide surface. The mechanism of coercivity enhancement resulting from Co^{2+} ions in the oxide lattice has been theoretically explained [21,22]. The particles are typically 0.3-0.4 μm length with aspect ratios of 8:1 to 10:1 and saturation magnetization around 350 emu/cm^3. Although practically successful, the cobalt-modified iron oxides are not totally satisfactory for recording applications. They have a strong temperature dependence of the coercivity and can exhibit a progressive loss of short-wavelength signal amplitude with repeated playback as a result of mechanical stress caused by Co doping. More stability with respect to temperature and stress has been obtained by placing the cobalt on or near the surface of the particles.

Metal particles

Metal particles were first introduced in high performance audiocassette tapes and later used in high-density recording media (i.e. digital audio tape) and 8-mm videotapes. Pure metals can have saturation magnetization far in excess of those of oxides. Among them, iron has the highest saturation magnetization of the ferromagnetic elements (1700 emu/cm^3), which is about four times bigger than that of iron oxides and is also very cheap. Therefore, metallic iron particles are very attractive for recording applications. However, the biggest disadvantage is the need for protection against oxidation or other reactions. The iron particles are usually stabilized against corrosion by a controlled oxidation of their surface or by protective action of some organic coating components. The first of these is the most important but has the effect of reducing the average saturation magnetization of particles to almost one-half (800-1000 emu/cm^3) of the value of bulk iron (1700 emu/cm^3). Even in this case, the resulting medium is still superior that of iron oxides [23] or cobalt-modified oxides [24]. The metal particles are acicular in shape with a length of 0.05-0.3 μm, an aspect ratio of 5:1 to 10:1 and coercivities between 700 – 2500 Oe.

Barium Ferrites

Barium ferrites are a special case among recording materials because of their strong uni-axial magneto-crystalline anisotropy. Barium ferrites particles have a hexagonal lattice structure with the easy axis orientated normal to the particle planes and therefore they are interesting for perpendicular recording applications. However, barium ferrite particles exhibit too high coercivities (pure barium ferrite, $BaFe_{12}O_{19}$, has coercivities between 2000-3000 Oe) for recording applications. By substituting Fe with Co and/or Ti ($BaFe_{12-2x}Co_xTi_xO_{19}$) within the barium ferrite structure [25], particles with 0.1 μm diameters and coercivities of around 800 Oe have been obtained. The particles are plate-like structure with thickness around 0.02-0.05 μm, very stable chemically and they exhibit an extremely narrow switching field distribution. In the past years barium ferrite particles have undergone intensive development although they have not yet achieved large-scale commercialisation. The principal deficiency of barium ferrite for advanced recording applications is its relatively low saturation magnetization (about 300

emu/cm^3), although with the development of new GMR heads, this is less limiting and barium ferrite is still seen as a potential competitor for future media applications.

1.2.1.1 Manufacture of particulate media

Different fine magnetic particles are used in particulate media production, depending on the requirements of the finished product. The chemical and technological processes for preparation of various magnetic particles are not discussed here but they are very well described in the reference [26].

Once obtained, fine magnetic particles can be used for particulate recording media production using well-established techniques [27, 28]. The discrete magnetic particles are well dispersed in a polymer binder and different solvents.

The binder has specific properties, which in combination with the particles leads to high volumetric packing fraction, high flexibility, high elasticity, wear resistance and low friction. The binder should also prevent particle sedimentation by reducing further contact between them. There is a large range of different binders but polyurethane has received a great interest. The solvent system should be very cheap and fast drying (i.e. dioxane, toluene, cyclohexanone, etc). However, a too fast evaporation rate can cause problems and usually a combination of solvents with different boiling points is used.

The completed dispersion is then coated onto a substrate through a number of techniques: gravure, knife coating or reverse roll coating [28]. Usually the particles are oriented directly after coating by a strong magnetic field, which is applied while the coating is still wet (except when a magnetically isotropic medium is desired, as for flexible disk medium). The thickness of the created magnetic layer can usually range up to 12 μm (example for audio tapes) but for modern metal particle tapes the magnetic coating may be as thin as 100 nm. A drying process and then a surface finish follows the coating and orienting. The drying of the coating takes place at temperatures of 60 – 100^0 C. The surface finish is to smooth the surface of the magnetic coating. The substrates used in flexible particulate magnetic recording media are almost exclusively films of polyester (PET or PEN) that have very smooth surface and good resistance to wear.

1.2.2 Thin film recording media

The maximum recording density for a longitudinal recording medium is determined by its magnetic thickness [29]. As there is a continuing desire for greater storage capacity, recording on thin films represent a considerable advantage. Magnetic storage is the most economical storage data and hard disk drives provide more than half of all computer storage. IBM developed the first commercial hard disk drive in 1956. It stored approximately 5 Mb of data on 24" at a cost of $100k. The disks in today's computers have typically 3.5" diameter or less and store at least 100 Gb at a cost of about $250. Increases in storage capacity are possible due to new discoveries and developments such as the discovery of giant magneto-resistance (GMR) effect [11,12] and the development of high coercivity media with multi-layer structures.

The key requirements of a magnetic thin film are magnetic and thermal stability of the recorded bit, low noise on replay and high switching speed. These conditions are satisfied for thin films with high coercivity, magnetization saturation and remanence and also large magneto-crystalline anisotropy in the individual grains contained in the magnetic layer. The grain sizes in thin films are in the range of 10 to 50 nm and the size distribution should be as narrow as possible, with the mean size as small as possible, but bigger than the super-paramagnetic limit. The area allocated to one bit is about 0.1 to 1 μm^2, which is much bigger than the size of a grain, so many grains fit into a bit. The materials developments for magnetic thin films have led to a class of Co-Cr based alloy thin films such as Co-Cr-Ta [30] and Co-Cr-Pt [31]. For longitudinal recording thin films the grains should be oriented with their easy axes in the plane of the film and in recording direction that generally coincides with any mechanical texture.

Since it is currently believed that longitudinal magnetic recording will reach its limit, there is an interest in perpendicular recording and perpendicular recording thin films. This is possible because the transition width, δ, (δ can be approximated by $\delta = t \cdot M_r / H_c$, where t is the thickness of the medium [29]) in perpendicular mode is much narrower than that in longitudinal mode and hence higher bit densities are possible. This situation requires a magnetically uni-axial film having a strong perpendicular anisotropy that overcomes the demagnetising energy ($K_1 >> \mu_0 M_s^2 / 2$) and supports magnetization

normal to the film plane. Co-Cr is the main alloy system used for vertically oriented media, in which the level of alloying reduces the M_s and therefore reduces the demagnetising energy. Typical values are saturation magnetization of about 450 emu/cm^3 and coercivities of about 2000 Oe. Iwasaki et al. made in late 1970s the major step in this area by proposing a new recording medium based on Co-Cr alloys and also a novel single pole head which is more efficient in perpendicular recording [32]. A very good review paper on developments of thin film recording media is given in reference [33] and more details about the physics of recording on magnetic thin films can be found in the reference [34].

The next paragraph discusses briefly the most important components of a recording thin film medium and the major preparation techniques used in magnetic thin films technology.

1.2.2.1 Manufacture of thin film media

The preparation of magnetic recording thin films is very similar to technologies used in other films preparation, and the discussion in this paragraph will be focused on features of importance in thin film recording media.

The term of medium refers to the entire recording structure, not only to the magnetic layer. Generally, the structure of a thin film-recording medium consists in a substrate, an undercoat, a magnetic layer and an overcoat. In modern media the magnetic layer may be multi-layered and include Ferromagnetic – Antiferromagnetic components.

Depending on the final application the substrate may be rigid or flexible. Rigid disks are used in rapid access and high density recording media. The most common disk substrates are Al, Al-Mg (4%) alloy or glass. The substrate material must be thermally stable and process compatible since the growth of the several layers on the disk will depend on the substrate material.

The magnetic layer is deposited on a certain underlayer, which has the usual role to promote the growth of a particular crystallographic texture and/or grain size in the magnetic layer. The magnetic layer is without exception a Co-based alloy and Cr is the most common underlayer, because Co-Alloy films grow with a significant degree of heteroepitaxy on Cr. The small head-to-medium spacing is critical for high densities on

rigid thin film disks. However, this generates the risk of mechanical head-disk interactions, which can cause head and disk wear. Wear of the magnetic layer can also occur when the drive starts and stops, because the head contacts the disk at relatively high speeds. The overcoat layer (or the wear resistant overcoat) has the function to preserve the integrity of the thin film disk by minimizing the wear in disk and head. An overcoat should be as thin as possible (usually thickness comparable with the head / disk spacing), and have very good smoothness, wear resistance, protection against corrosion and low static/dynamic friction with the head. The most common overcoat is a thin film of modified carbon or diamond-like carbon film. The overcoat is usually coated with another thin lubricant layer, which is applied by simply dipping the disk into a lubricant solution. There is a strong binding between the overcoat and the lubricant layer, in order to ensure that the lubricant remains between the head slider and the disk when contact occurs and also it is mechanically stable when the disk spins at high speed.

As presented earlier, the magnetic layer is almost exclusively a Co-based alloy deposited on an undercoat, usually Cr. Magnetic thin films can be classified depending on their preparation method: sputtered thin films, metal evaporated thin films and thin films produced by electro-deposition, and they will be briefly presented in the next paragraphs.

Electro-deposition thin films

This was the first developed process for producing commercial magnetic thin film media and even today represents an important approach to rigid disks. The most frequently used plated alloys are Co/Ni/P for longitudinal media, which are electroplated from solution containing Co and Ni salts and hypophosphate (NaH_2PO_2) salts. The phosphor is incorporated in the plating bath, and consequently in the plated alloy, because the phosphorus is a key component in controlling the film coercivity. A similar plating bath is used in auto-catalytic deposition (or electroless deposition) onto surfaces that have been prepared to initiate the reaction [35]. Both electroplating and electroless deposition have an important advantage, namely they are continuous processes and therefore much more convenient than evaporation and sputtering.

Metal evaporated thin films

This technique consists in depositing the evaporated atoms of a ferromagnetic alloy onto a substrate. The process takes place in a vacuum chamber and the production refers mainly to flexible media, such as ME tapes, rather than rigid thin film disks.

Sputtered thin films

The DC/RF sputtering is by far the most convenient production method because of the broad compositional flexibility available through this deposition technique. Co, Co-Cr, Co-Ni-W, Co-Cr-Ta, Co-Re are just a few of the alloys that have been sputtered for thin film media. Sputtering is also the preferred technique for producing non-metallic thin films. For a rapid processing a high-rate sputtered deposition is required. Layers are deposited with little interruptions to avoid contamination and the process of disk production demands a clean-room environment. The sputtering is carried out in a high vacuum system (10^{-6}-10^{-7} Torr) that is then filled with a gas (i.e. argon) up to 10^{-1} – 10^{-3} Torr. A DC (or RF) field will accelerate the ionized gas atoms, which will have enough energy to extract surface atoms from a target material due to mechanical recoil. This forms plasma, from which the deposition onto the substrate occurs. The optimum deposition is achieved by adjusting the sputtering process parameters, which are the DC/RF sputter voltage, the inert gas pressure and the substrate temperature. A DC sputtering system requires conductive target materials, while RF voltage sputtering is used to sputter isolating materials. Commercial deposition systems can produce fully coated disks at rates of more than 600 per hour [33].

1.3 Thesis Overview

The remainder of the thesis is devoted to the experimental measurements undertaken during the PhD project.

Chapter two is related to the instrumentation development, computer interfacing and LabView programming. A short introduction to LabView programming and examples of computer control programs that have been designed in this project are given in this chapter and respectively in the appendix 1.

All the experimental instruments used in this project are also described in detail in chapter two, together with the main magnetic results that could be extracted from each experimental method. The advantages of using a modified vector VSM rather than a standard VSM are well outlined and the main modifications, which need to be applied in order to perform vectorial measurements, are also presented.

An important part of the chapter two is dedicated to the calibration techniques. The calibration corrections are very important and the results are exemplified with experimental graphs showing the effect of base line and calibration on a hysteresis loop measured for a Co-Cr-Ta thin film sample. Vectorial calibration was also described and exemplified with a test graph showing the magnitude compatibility of the signals corresponding to the two normal in-plane directions.

Mössbauer spectroscopy or nuclear gamma resonance has been also used in this project for measuring the mean out-of-plane spin distribution and particle morphology. Therefore, the sections 2.3.1 and 2.3.2 explain the Mössbauer effect and the main hyperfine parameters of a spectrum. A general block diagram of a Mössbauer experiment is also presented in the section 2.3.3.

Mössbauer measurements were carried out in collaboration with Nuclear Research Group at Duisburg University in Germany and in fact, further Mössbauer studies are continuing in collaboration with my colleagues from the Nuclear Gamma Resonance Group in Bucharest, Romania.

Chapter three is focused on magnetic anisotropy field studies and the interactions effects of the anisotropy field. There are many techniques designed for magnetic anisotropy field measurements and a short review of the most popular techniques is given at the beginning of this chapter. The chapter continues with the description of two experimental techniques developed and used in this project for anisotropy field measurements. These are: extrapolated transverse remanent magnetometry and rotational hysteresis. Although both techniques have been previously used, they have novel features that have been introduced in this project. The extrapolated transverse remanent magnetometry method is based on the original transverse remanent magnetometry, which has been extended and improved in this project by introducing the linear extrapolation. The reported results are at least 5 - 10% more precise than those given by the original technique. Rotational hysteresis studies are mostly known as

measured using a torque magnetometer. In this project, however, the technique was successfully implemented on a vector VSM. The two experimental methods have been applied for the two sets of samples and the obtained results are in good agreement.
The two sets of described samples showed a variation of the anisotropy field with the magnetic coating thickness. This result has been related to the inter-particles interactions that are likely to vary as the magnetic thickness changes. It has been shown that exchange interactions have a positive contribution to the anisotropy field (acting towards magnetising the sample), while the magnetostatic interactions have a negative contribution to the anisotropy field (demagnetising the sample). As a consequence, the measured magnetic anisotropy fields are only a kind of effective anisotropy fields because they contain also the interaction effects and there is a clear relationship between magnetic anisotropy and magnetic interaction. The explanations were also supported by the experimental interactions studies (i.e. delta M and Henkel plots) and theoretical studies recently reported in literature. Although both experimental methods are based on switching, they have significant differences and the chapter ends with a very useful review of the advantages and disadvantages of the two techniques.

Chapter four presents the measurement of the demagnetising field acting normal to the sample plane and the applications arising from these measurements (i.e. true magnetisation calibration, demagnetising field corrections and non-destructive magnetic thickness measurements). Related to this topic, two original experimental techniques for demagnetising field measurements have been introduced. These are extrapolated transverse remanent magnetometry and identification of the closure point for hysteresis loops. Although results from the two methods compare well, all the measurement techniques rely on the assumption that the demagnetising factor for the sample is that of an infinite sheet, which it is believed to be not entirely true. A recent modelling study showed that for current media (advanced MP tapes series), the particulate nature does alter the demagnetising factor by about 7%. However, the approximation of an infinite sheet is quite acceptable for particulate recording media where film thickness is small and has good uniformity and this gives a non-destructive measure of the magnetic layer thickness.

Although the determination of the closure point is difficult and susceptible to a certain amount of subjectivity on the part of the investigator, it is available within any laboratory that has standard vibrating sample magnetometer facilities and can provide a useful method for determination of magnetic layer thickness in magnetic tape media.

In chapter five there are presented different texture measurement techniques in magnetic media. Three different experimental equipments have been used for texture investigations. These are standard / vector VSM, Mössbauer spectroscopy and some initial Magnetic Force Microscopy studies. Texture can be represented by the easy axis distribution (EAD) and / or orientation ratio (OR).

In-plane EAD has been directly measured using a vector VSM. Due to the difficulties related to the demagnetising fields, out-of-plane EAD was determined using two indirect measurements, namely the theoretical relationship between the OR and the EAD and theoretical relation between the relative intensities of the 2^{nd} and 5^{th} lines of room temperature Mössbauer spectrum and the angle between the γ - ray and the direction of the magnetic moments. Texture studies were carried out on the series of four MP double-coated tapes. Results showed that both in-plane and out-of-plane texture were strongly related to magnetic coating thickness, probably due to the manufacturing process.

Although not fully understood, an interesting result was obtained from low temperature Mössbauer spectroscopy, which showed that all the spins were perfect aligned in the tape plane. This normally would suggest that there is no real out of-plane orientation of the particles and room temperature results would be only related to thermal effects. This explanation, however, is not consistent with the fabrication parameters as well as the theoretical and experimental evidences related texture in particulate media. Mössbauer spectroscopy was also used to investigate the tape morphology, the results being in good agreement with the magnetic data and fabrication parameters.

Finally, 3D maps of the easy axis distribution have been computed using the experimental in-plane and the derived out-of-plane distribution parameters.

Two appendixes are included and six journal papers that have resulted from the work are also attached, five already published and another one is in press.

2. Experimental instrumentation

There are a large number of experimental methods in magnetism studies [1] and they could be divided in two main groups: bulk techniques and microscopic techniques. This project is mainly experimental and as a bulk technique utilised a standard vibrating sample magnetometer (VSM), which was also designed to work as a vector VSM.

Additional to VSM, two microscopic methods have been used in the experimental investigations: Mössbauer spectroscopy (MS) and some initial studies using a Magnetic Force Microscopy (MFM). Each technique offers different information and depending on the analysed sample and the required information, the most suitable technique can be chosen. However, VSM is by far the most popular experimental tool for magnetic studies and almost exclusively used in any magnetism laboratory.

In the following sections it will be described separately each experimental technique, giving also the details related to the experiments and the main information that can be extracted from each individual technique.

2.1 Foner's VSM

A vibrating sample magnetometer (VSM) is similar in principle to a vibrating coil magnetometer (VCM). Within the VCM a coil vibrates between the sample and a region of free space and thereby acts as a gradiometer by measuring the difference in induction at the two positions [2]. In the case of the VSM, the sample is displaced between the coils, which are kept stationary. The VSM senses the difference in magnetic induction between a region of space with and without the sample present, by vibrating the sample up and down. This gives an output, which is a direct measurement of the magnetisation. *M*. Foner first designed the VSM in 1959 [3].

An electromagnet or a superconductor solenoid is used to produce an external field B, in which the sample is positioned. By vibrating the sample, the flux detected by the coils changes, which in turn changes the magnetic induction. This effect is measured by observing the voltage changes in the pick-up coils. These voltage changes can be calibrated using a reference sample and useful properties can then be extracted by giving the system suitable units.

The instrumentation which makes up the core components of Foner's VSM is shown in figure 2.1. The sample is oscillated perpendicularly to the applied field by the loudspeaker set up. The external magnetic field B is supplied by an electromagnet. The fluctuating magnetic field of the vibrating sample induces a voltage in the stationary detection coils. The magnetic properties of the sample can be deduced from the measurements of this voltage. A second, reference voltage is induced from a sample which maybe a small permanent magnet or an electromagnet. Since the sample and reference are driven synchronously by a common vibrating system, the phase and amplitude of the resulting voltages are directly related. The voltages are proportional to the magnetic moment of the samples. Hence, the magnetic moment of the unknown sample can be found if the two voltages and the magnetic moment of the reference sample are known. This process is called "calibration" and is further described in more detail in the section 2.2.2.

Using this procedure, measurements can be made insensitive to changes of vibration amplitude, vibration frequency, small magnetic field instabilities, magnetic field non-uniformity, and amplifier gain or amplifier linearity.

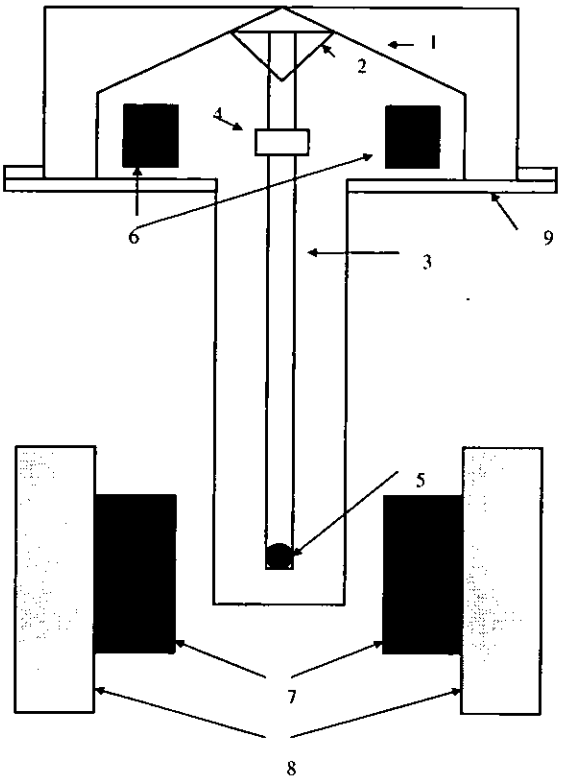

Figure 2.1 A schematic diagram of a Foner vibrating sample magnetometer. (1) loudspeaker vibrating system, (2) Rod support, (3) Metal rod, (4) Reference sample, (5) Sample, (6) Reference coils, (7) Sample coils, (8) Poles of magnet, (9) Metal container

2.2 Vector VSM

The VSM used in this project is rather different from that described by Foner, but the principles remain the same. The system has to be calibrated so that the voltage outputs can be adjusted to more meaningful magnetic units e.g. EMU's. Placing a sample with known magnetic moment in the sample holder and winding the coils up and down to the maximum and minimum saturation points of the sample can achieve the calibration. The reference signal comes straight from the oscillator in the front of the lock-in amplifier and is manipulated together with the signal from the unknown sample in the back of the lock-in amplifier.

In order to perform vectorial measurements, other improvements to the standard VSM instrument have been made by adding to the detection system an extra pair of pick up

coils (namely a double Mallinson arrangement described in section 2.2.1) and a stepper motor which allows the sample to be rotated about a fixed axis perpendicular to the applied field. Therefore, this VSM can be used as a standard VSM as well as a vector VSM (see the diagram 2.2). The double Mallinson coil system and the stepper motor are part of a previous PhD project and have been developed by Franck Schmidlin.

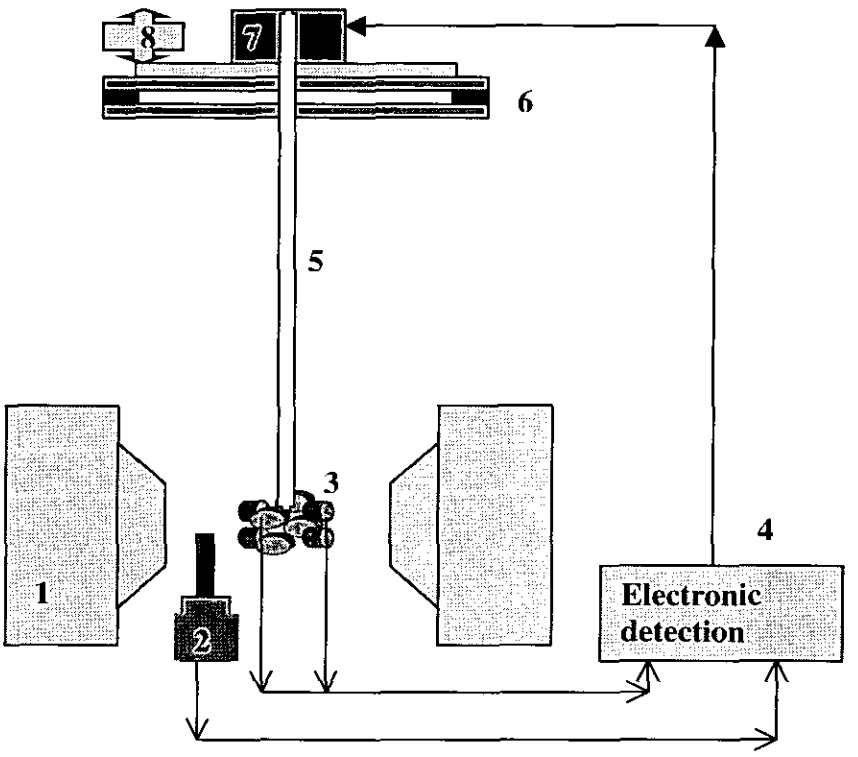

Figure 2.2 A schematic diagram of our vector vibrating sample magnetometer. (1) Poles of the electromagnet, (2) Hall probe, (3) Bi-axial pickup coils arrangement, (4) Electronic detection system, (5) Vibration rod / sample holder, (6) Mechanical bench, (7) Vibration unit, (8) Stepper motor

The vector VSM is built on a water-cooled electromagnet, with 170 mm diameter pole pieces separated by a 45 mm gap. Combined with a 20 A power supply, this magnet can apply a maximum field of 1.2T. The maximum sample size is 10 mm diameter and the coils – sample separation distance is about 10 mm. The stepper motor can operate 100 steps rotation every 180^0, which corresponds to a 1.8^0 for each full step or 200 steps rotation for every 180^0, which corresponds to a 0.9^0 for each half step. The stepper motor is further connected to a gearbox for a better control of the rotation angle. A new GM-05 Hall probe has been installed in this project for direct measurement in T (S.I

units) of the magnetic field. The electronic detection system consists in two lock-in amplifiers that are connected directly to a computer. The system is fully computer controlled using RS232 interfaces and routines in LabView environment that have been also developed as part of this project.

2.2.1 Coils arrangement

On a standard VSM, the sample is placed between two identical pick-up coils connected in series and having the same axis. Spurious vibrations along their common axis will cancel out. However, if two such pairs of coils are connected in opposition and placed parallel one above the other, with the sample vibrating between the two pairs, any background noise will be cancel out, while the signals due to the vibrating moment will add. This is the base for the coil assembly used in most standard VSMs.

Based on the same principle, vector VSMs use a different coil arrangement, which can usually measure two components of the magnetic moment, although the third component could be measured in principle if special coils arrangements are used. The two measurement directions are the case of our instrument and also the reason why we will refer to it as a bi-axial VSM. The applied field direction and the direction perpendicular to it and to the vibration axis represent the two measurement directions. These two also define the plane of rotation. This detection improvement together with the possibility to rotate the sample (or the applied field) considerably extends the range of possible measurements of a vector VSM.

Very important for a vector VSM is the coil configuration. In order to be suitable for measurements of the magnetisation vector, the coil arrangement has to meet the following requirements:

- The coils should be in a bi-axial configuration; in other words, it must be possible to measure the magnetic moment in the applied field direction (Ox) and normal to the applied field direction (Oy) if the sample is assumed to vibrate in Oz direction.
- There must be enough space for the sample between the coils.

- The effect of a magnetic moment normal to the measuring direction on the measured signal (known also as cross talk) must be low.
- The sensitivity for both measuring directions must be sufficient and the dependence of the sensitivity on the position of the sample must be small.

A lot of work has been dedicated to the construction and development of different coil arrangements for vector VSM instruments and techniques. Richter published in 1992 a detailed paper about the construction of a 3D coil detection system for vector VSM measurements [4]. His system was constructed with an eight-coil arrangement designed for high sensitivity measurements on magnetic thin films. Bernards et al. [5] published a technical improvement in the eight-coil detection system for a bi-axial VSM, by using a system consisting of 12 coils. The basis of his system is the same as for the eight-coil arrangement but the noise induced by vibration of the coils in the applied field is low because the coils have their axes parallel to the applied field. In addition to this, the supplementary four coils give an improved sensitivity for the signal in the field direction and minimise the cross-talk effects. His system has an improved dependence of the sensitivity on the sample position not only for the detection of the magnetisation component in the applied field direction but also for the detection on the component perpendicular to it.

Our vector VSM is equipped with an eight-coil detection system composed of two independent sets of four-coils. One set of four-coils is designed for detection in the x direction and the other for the detection in the y direction (see figure 2.3). This coil arrangement had been first proposed and used in 1969 by Gorodetsky et al. [6] and is actually a double Mallinson coil configuration [7]. The advantage of such system is that the two in-plane signals can be directly and simultaneously measured without any need for mechanical or electronic switchers.

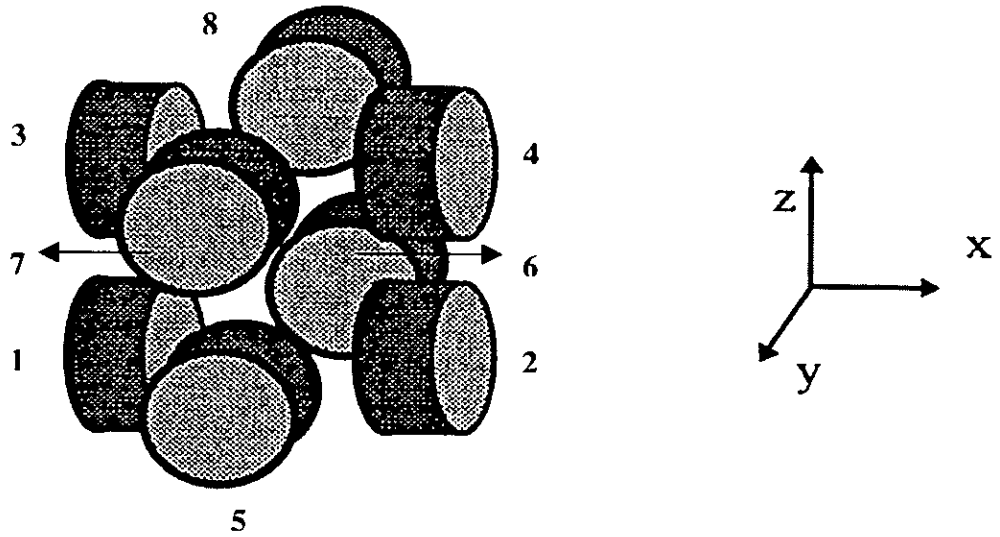

Figure 2.3 The coil configuration used on our VSM for a vectorial determination of the magnetisation.

Table 2.1 shows the way in which the signals from different coils have to be added for the configuration shown in figure 2.3, in order to measure the two-magnetisation components [5].

Table 2.1 The way in which the signals from the coils have to be added to measure the magnetisation components of M_x and M_y for the coils configuration in figure 2.3

Coil number	1	2	3	4	5	6	7	8
M_x	-	-	+	+				
M_y					-	-	+	+

2.2.2 Standard and vectorial calibration

As described earlier, the signal induced in the pick-up coils is being read from the lock-in amplifier as a DC voltage output which is linearly proportional to the moment of the sample. By using a calibration technique, the voltage output should be adjusted to magnetic units. This can be achieved by placing in the sample holder a sample with a

known shape (or mass) and a known magnetic moment. This is usually a $1cm^2$ Ni foil to which corresponds to a saturation magnetisation of M_S^{cal} = 1.2727 emu. The Ni sample is saturated in the plane of the foil and the voltage output signal is recorded from the lock-in amplifier as V^{cal}. The calibration factor, f, is then obtained by formula:

$$f = \frac{M_S^{cal}}{V^{cal}} (emu/volt) \tag{2.1}$$

A magnetisation (M) of an unknown sample, having the same shape as the Ni calibration sample, can be derived then in EMU units by recording the voltage signal (V) from the lock-in amplifier and by using the calibration factor:

$$M = V \cdot \frac{M_S^{cal}}{V^{cal}} (emu) = f \cdot V(emu) \tag{2.2}$$

This calibration factor will not deviate by a significant amount over time, which means that the calibration routine should not need to be repeated, unless major changes occurred to the instrumentation. It is also essential that the shape of the calibration sample should be the same with the shape of the sample to be measured and they should have similar saturation moment.

Besides the calibration factor, there is another correction to the output data that should be considered, especially for the measurements involving magnetisation as a function of the applied field (as in the case of hysteresis loops).

If, for example, the magnetisation voltage data were recorded as a function of the applied field for an empty sample holder, one would be expected to obtain no signal (or a flat line) because no sample is present. However, an approximate straight line with a negative slope is obtained (see figure 2.4). This is called the "base line" and a correction should be always applied by subtracting the base line from the output voltage data. The base line effect is due to the diamagnetic properties of the Perspex sample holder, the double-sided sticky tape used to make the samples and also due to the absence of the air at the interface region of the sample holder with the air, due to the vibration. The

diamagnetic signal is always along the field direction and therefore does not affect the signal along the Y-axis.

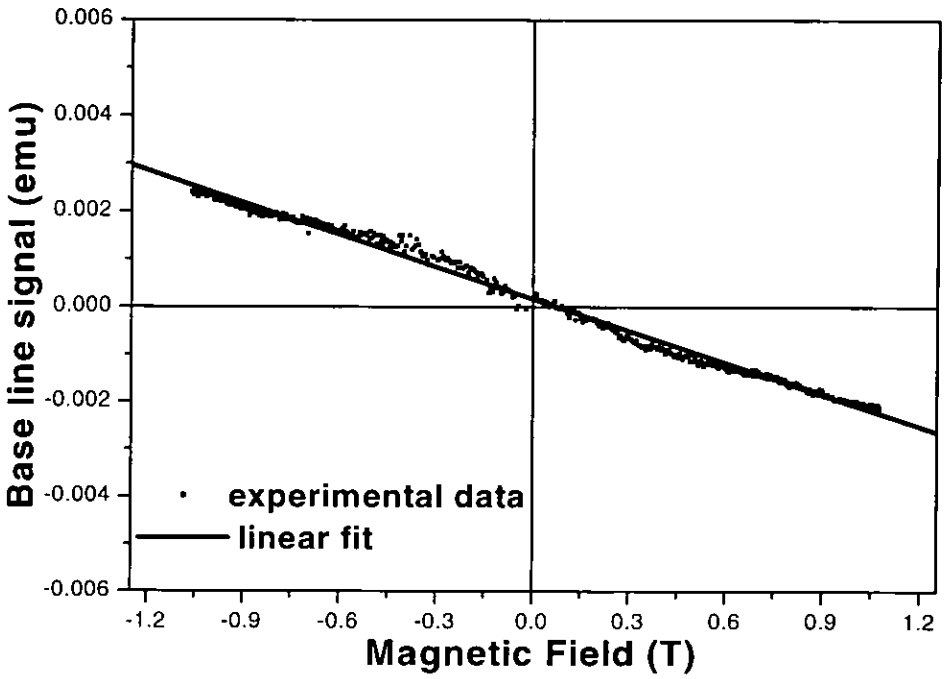

Figure 2.4 Base line signal as a function of the applied field. A straight line could very well approximate the data in order to apply the base line correction.

Finding the slope and the intercept of the base line, and using the equation (2.3) can find the real value of the magnetisation for any value of the voltage output:

$$V_{BL} = S \cdot H + I \tag{2.3}$$

Where S is the slope of the base line, I is the intercept, H is the applied field and V_{BL} is the base line voltage signal;

After a base line correction, the relation (2.2) becomes:

$$M = (V - V_{BL}) \cdot \frac{M_S^{cal}}{V^{cal}}(emu) = f \cdot (V - V_{BL})(emu) \tag{2.4}$$

The base line signal is very small in comparison with the signal from a large magnetic sample. It is usually around $2.5 \cdot 10^{-3}$emu at the maximum applied field of 1.2T. However, the base line signal becomes very important in magnetic thin films investigations, where the diamagnetic signal from the oxygen could be in some cases even bigger than the signal generated by the total moment of a thin film sample. This is very well illustrated in the figure 2.5, where there are represented two hysteresis loops for a thin film sample, with and without base line correction.

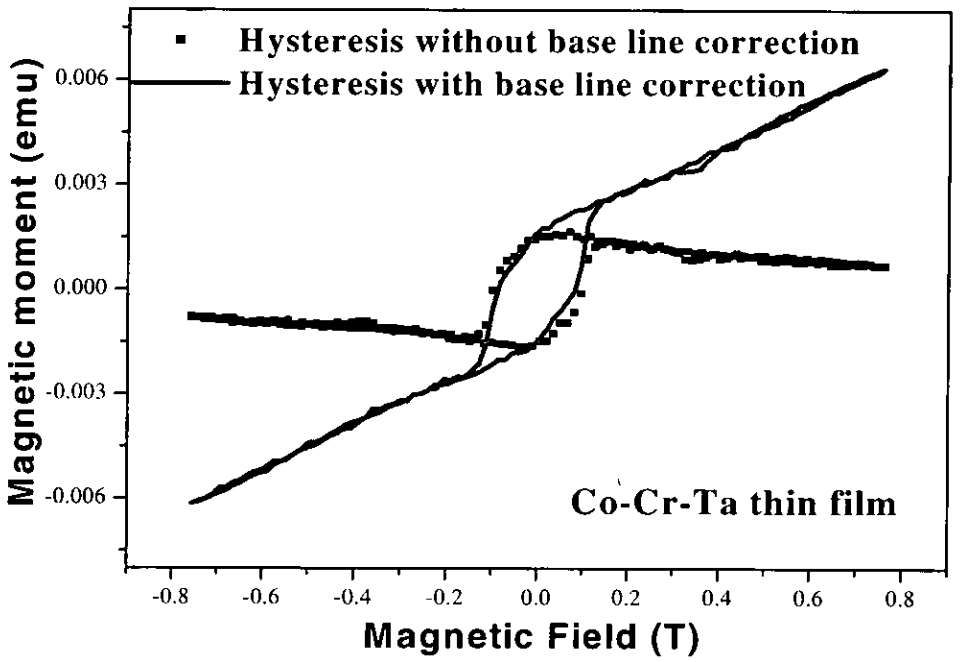

Figure 2.5 Comparison between a thin film hysteresis loop with and without base line correction. The sample is a CoCrTa thin film of 100nm thickness deposited on 50nm Cr underlayer.

Calibration technique, in the case of a bi-axial VSM, is a bit more complicated. The bi-axial calibration method consists of two parts: the calibration of the X coils and the calibration of the Y coils. This vectorial calibration is mainly designed to obtain the two calibration factors corresponding to the coils on each direction. Because most of the bi-axial measurement techniques involve determination of the remanent magnetisation vector as a function of the rotation angle, they do not require any base line correction.

In 1999, Bolhuis et al. proposed an original calibration method for vector VSM measurements [8]. In his technique, the calibration on both directions is made for every angle of interest, in order to minimize the cross talk effect.

Our technique is similar with the one described by Bolhuis, except that only two calibration factors have been obtained, one for each set of coils, rather than one for each rotation angle of interest.

The parallel set of coils was calibrated using a Ni calibration sample with a known moment, as described earlier. For the transverse coils, a hard magnetic sample with longitudinal anisotropy was used for calibration. The sample has been first saturated in its easy axis direction, which was orientated parallel to the field, and the remanent moment has been determinate in that direction. The calibration factor for the parallel coils has been used to calculate the remanent moment in magnetic EMU units. The sample was then rotated 90^0 in remanent state and the calibration factor for the transverse coils has been calculated. As can be seen, it is essential to calibrate first the parallel coils in order to get the calibration factor for the transverse coils.

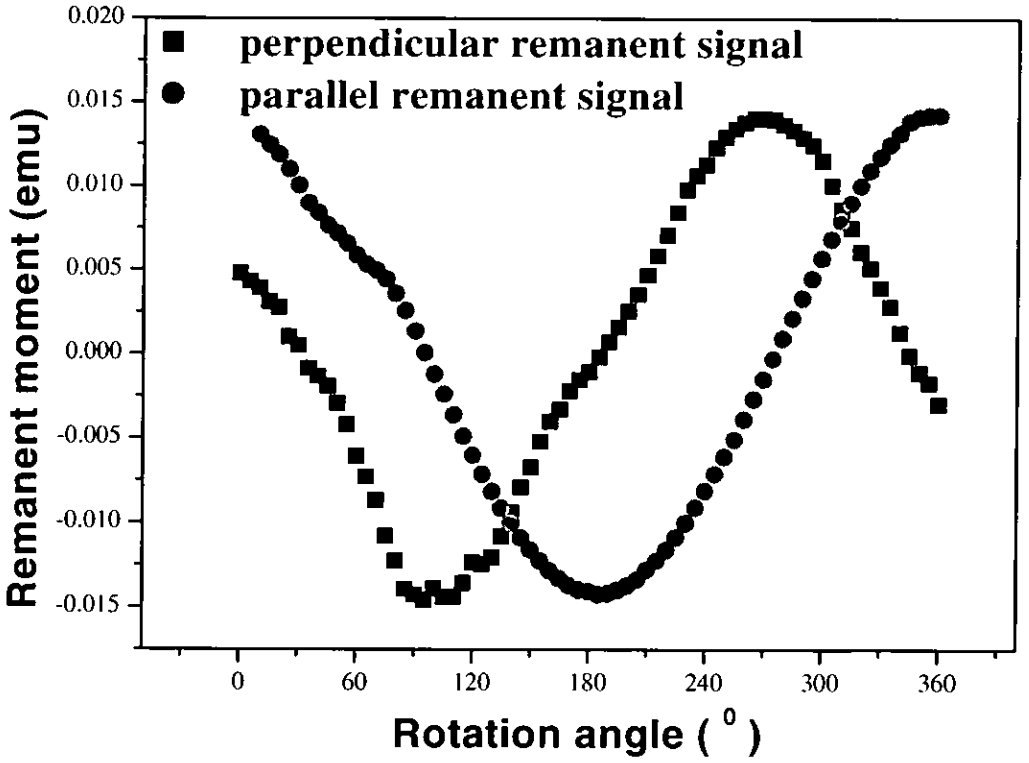

Figure 2.6 The curves indicating the two signals (parallel and transverse) recorded for a sample in saturation remanent state during a full 360^0 rotation

After the calibration, both signals are represented in magnetic EMU units and plotting the saturation remanent signal of a hard magnetic sample as a function of the rotation angle over 180^0, does a direct verification of the accuracy of the calibration (see figure 2.6). The two curves will indicate a correct calibration if they reach maximum at equal values in EMU, which correspond to a 90^0 and 0^0, 180^0 respectively rotation angles.

2.2.3 Magnetic parameters and curves obtained from VSM experiments

The knowledge of magnetic media characteristics is very important for their commercial applications and performances.

The most important magnetic parameters obtained from VSM experiments are: coercivity field (Hc), remanence magnetisation (Mr), saturation magnetisation (Ms), squareness (Sq), switching field distribution (SFD), orientation ratio (OR), anisotropy field distribution, anisotropy field (Ha) and easy axis distribution (EAD). Each of these parameters is obtained by performing certain VSM experiment and they will be discussed briefly in the following part of this section. However, the orientation ratio, anisotropy field and easy axis distribution are the main topic of this thesis and consequently they will be presented in detail in the next chapters.

Hysteresis Loop

The properties of ferromagnetic materials are commonly displayed by curves of magnetisation (M) as a function of the applied field (H), as in figure 2.7. A piece of ferromagnetic material is magnetised to positive saturation field (see point A on figure 2.7)), the field is then reduced in steps to zero value, reversed and increased again until it reaches the negative saturation point (indicated by point B, figure 2.7). If the same process is reversed back to the initial state A, the magnetisation of the sample does not return to zero as in a paramagnetic material, but describes a hysteresis loop.

The following parameters are obtained from a hysteresis loop:

- Remanence magnetisation M_r, is the value of the magnetisation at zero applied field. This is an essential feature of the recording materials, as they are able to retain information magnetically.
- Coercive field H_c, the field value for which the magnetisation becomes zero.

- Saturation magnetisation M_s, the magnetisation corresponding to point A/B in the figure 2.7.

- Squareness Sq, is a derived parameter defined as the remanence magnetisation divided by the saturation magnetisation. For a loop approaching a square shape, Mr/Ms $\rightarrow$ 1 and the response to read/write signals will increase in the recording media. A useful recording medium requires large enough values of Ms, coupled with a value of Sq as close as possible to 1.

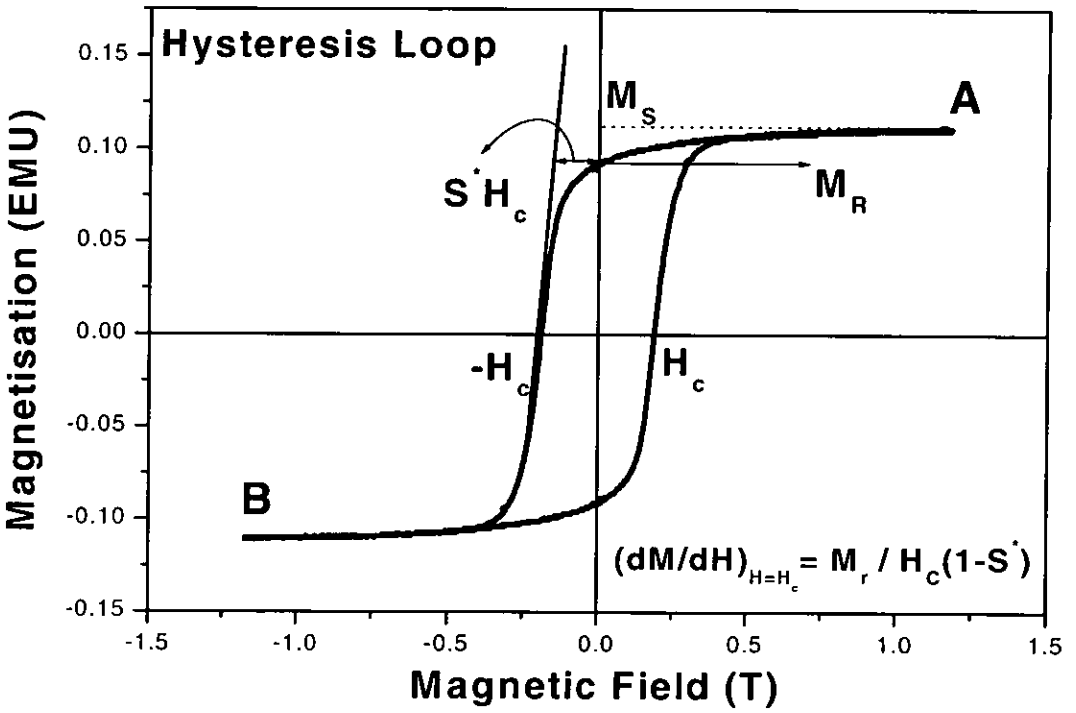

Figure 2.7 Magnetisation as a function of the applied field for a ferromagnetic sample. The curves do not pass through the origin, which means that at zero field the sample retains some magnetisation. This graph is known as a magnetic hysteresis loop.

Isothermal remanence magnetisation (IRM) and DC demagnetisation (DCD)

Although the primary parameters for the characterisation of a recording medium are derived from the hysteresis loops, further useful information can be derived from the remanence curves [9]. The IRM curve is the result of plotting the remanent magnetisation against the applied field (see figure 2.8), when the sample is initially demagnetised and then the remanent magnetisation measured after each application and

removal of the incremental field H, for values between 0 and a maximum saturating field.

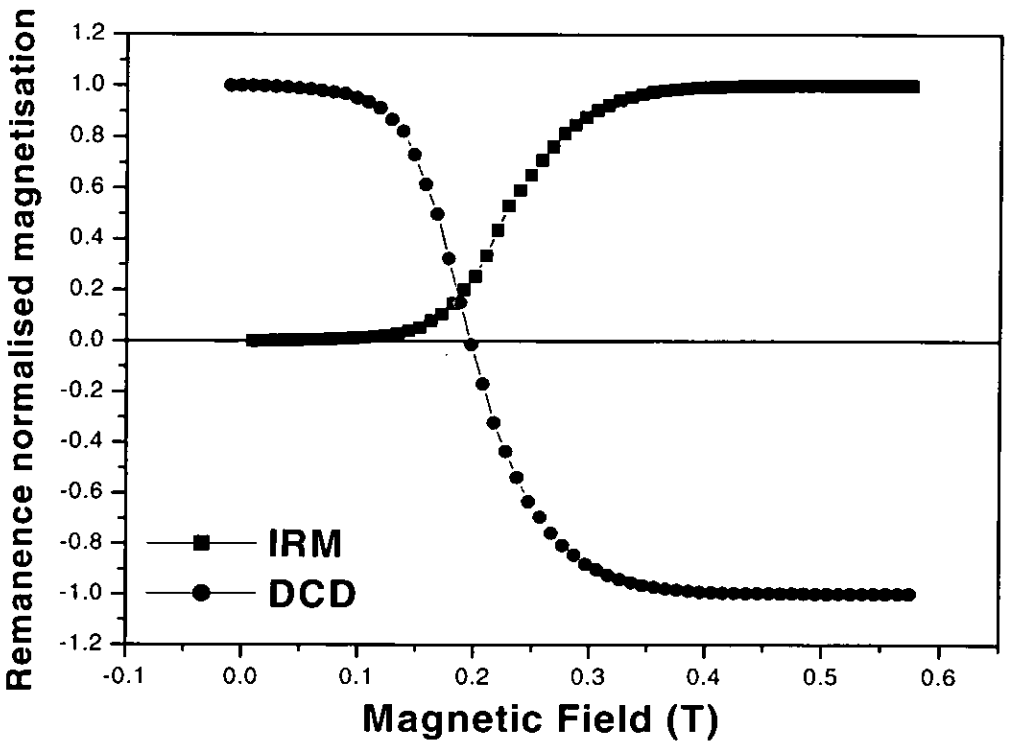

Figure 2.8 Typical IRM and DCD curve for a ferromagnetic material

Using a similar method as the IRM experiment, the DCD curve is produced by measuring the remanent magnetisation as a function of an increasing reverse field applied to a saturated remanent sample, until its net moment is reversed. However, for a better representation of the DCD curve, the DCD data, in figure 2.8, have been plotted against positive fields. Both IRM and DCD are normalised to the saturation remanent magnetisation Mr(∞). Both cases (IRM and DCD) are very useful for providing a measure of particle interactions [10] (known as Henkel plots and Delta M plots) and also the switching field distribution [11,12].

Switching field distribution

The switching field distribution is closely related to parameters such as anisotropy field distribution, particles volume distribution and inter-particle interactions. A recording medium with a broad switching field distribution will have poor recording properties.

Differentiation of the IRM curve provides a detailed measure of the SFD (Chantrell and O'Grady) [13], as shown in figure 2.9. The SFD plot for the DCD curve can be found using the same method as for the IRM curve. The SFD width can be directly measured from this plot (normally done by full width at half maximum or half width at half maximum).

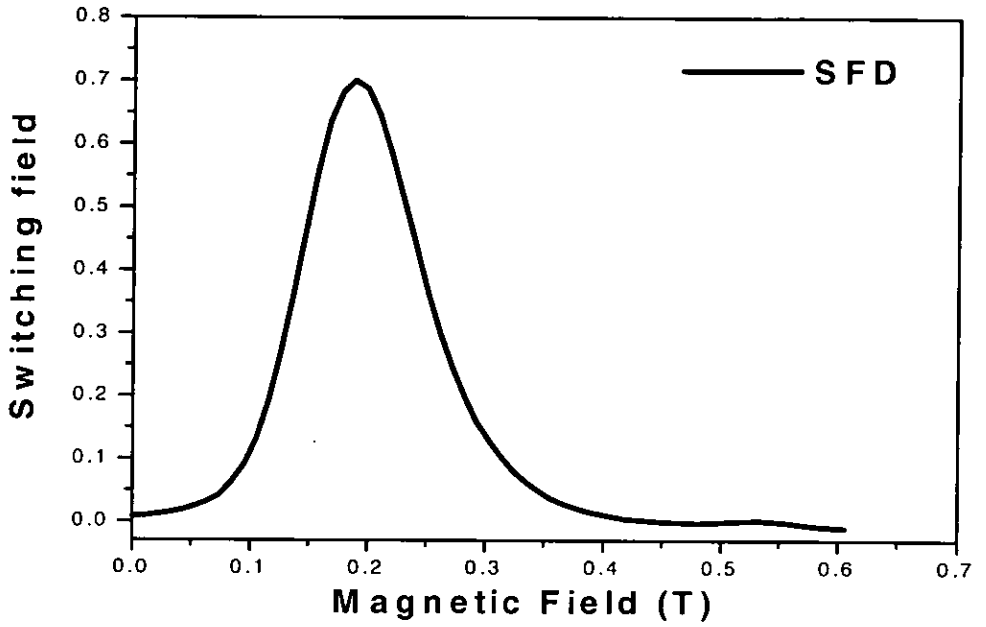

Figure 2.9 Example of a switching field distribution curve

Besides the remanence curves, another direct measure of the width of the SFD is obtained from the Williams-Comstock construction [11] which is shown in figure 2.7. The parameter (1 – S*) characterizes the width of the SFD and is essentially a measure of the slope of the hysteresis loop at H = H_c (see figure 2.7 and equation 2.5).

$$\left(\frac{dM}{dH}\right)_{H=Hc} = \frac{M_r}{H_c(1-S^*)} \tag{2.5}$$

where the quantity S^*H_c represents the length of the line joining the magnetisation axis to a tangent to the curve at H = H_c on the hysteresis loop (see figure 2.7).

2.2.4 Interfacing and software development for VSM measurements

Very complex experimental equipment has been used in this project and consists of a number of devices for experiment controlling and data acquisition. A Stanford SR 810 Lock-in Amplifier has been used for controlling the magnetic field by applying a DC voltage output (0 - 10V) to the power supply and also for acquiring the parallel signal from the pick-up coils. A second EG&G 5205 Lock-in Amplifier has been added to the system, for performing vectorial measurement by reading the transverse signal from the supplementary set of pick-up coils. The magnetic field is measured directly in Tesla (T) - S.I. units using a new GM-05 Hall Probe.

Due to the complexity of the experiments and also the time taken to complete an experiment, the first part of this PhD project was dedicated to complete a full automation of the experiments. The Hall probe and the two lock-in amplifiers were connected to a computer using multiple RS232 interfaces. A high compatibility between the three different serial interfaces and the operating system was achieved by setting the proper values for the Baud Rate, Parity, Data bits, Stop bits and Interrupt request (IRQ), as indicated in the table 2.2:

Table 2.2 Serial SR 232 interfacing parameters

Serial port	Baud Rate	Parity	Data bits	IRQ	Start/Stop bits
COM1	4800	None	8	04	1
COM2	9600	None	8	03	1
COM3	1200	None	8	11	1

where:

- The baud rate is the rate of data transmission in bits per second. The receiver must be compatible with this rate so that no data is lost during transmission.

- Hardware devices use interrupts request (IRQ) channels to signal the motherboard that a request must be fulfilled. Current computers support only 16 IRQs but not all of them available to the user, and therefore they require careful setting in order to avoid any system conflicts.

- Parity is used for checking if data corruption has occurred some time over the transmit/receive cycle. However, this is not normally necessary when data transfer is direct and over small distances.
- "Start bit" signals to the receiver that a data character transmission is about to begin and the "Stop bit" signals the end of a transmission.

The stepper motor was connected to the computer via a digital Input/Output (I/O) card. The I/O card has two ports (A and B) and it was used to send data to the stepper motor driver via port A. Feeding data out (write data) from a user port requires two pieces of information [14]:

- The address of the register required
- The data to be fed out of the register

The data is in the form of an integer lying in the range 0 to 255 and the address in the range 768 to 799. LabView provides VIs for both read/write functions of a user digital port, which must be first initialised in order to function properly. The following settings have been used to operate our digital I/O card (see also Appendix 1):

Table 2.3 Digital I/O user card interfacing parameters

Register	Address	Function	Lines	Control register code
Port A	768	Output data	PA0-PA7	139
Control	771	Control register	-	-

Following the interfacing of the equipment to the computer, a number of complex routines for fully computer-assisted experiments have been developed in LabView environment (see examples in Appendix 1) in the first part of the PhD project. The functions of these routines are:

- Measurement of the magnetisation in the applied field direction
- Measurement of the magnetisation transverse to the applied field direction
- Rotation of the sample
- Controlling the magnetic field
- Measurement of the magnetic field

- Data capture, graphical presentation of the results and calculation of the required parameters

LabView is a programming language, much like various commercial development systems [15]. However, LabView is different from those applications in two points. First of all, other programming systems use text-based languages to create lines of code, while LabView uses a graphical language to create programs in block diagram forms. The other difference is that LabView is very much oriented towards instrumentation interfacing and computer based instrumentation, with a very extended library of pre-written codes capable of controlling specific instruments or to perform very specialised analyses [16,17].

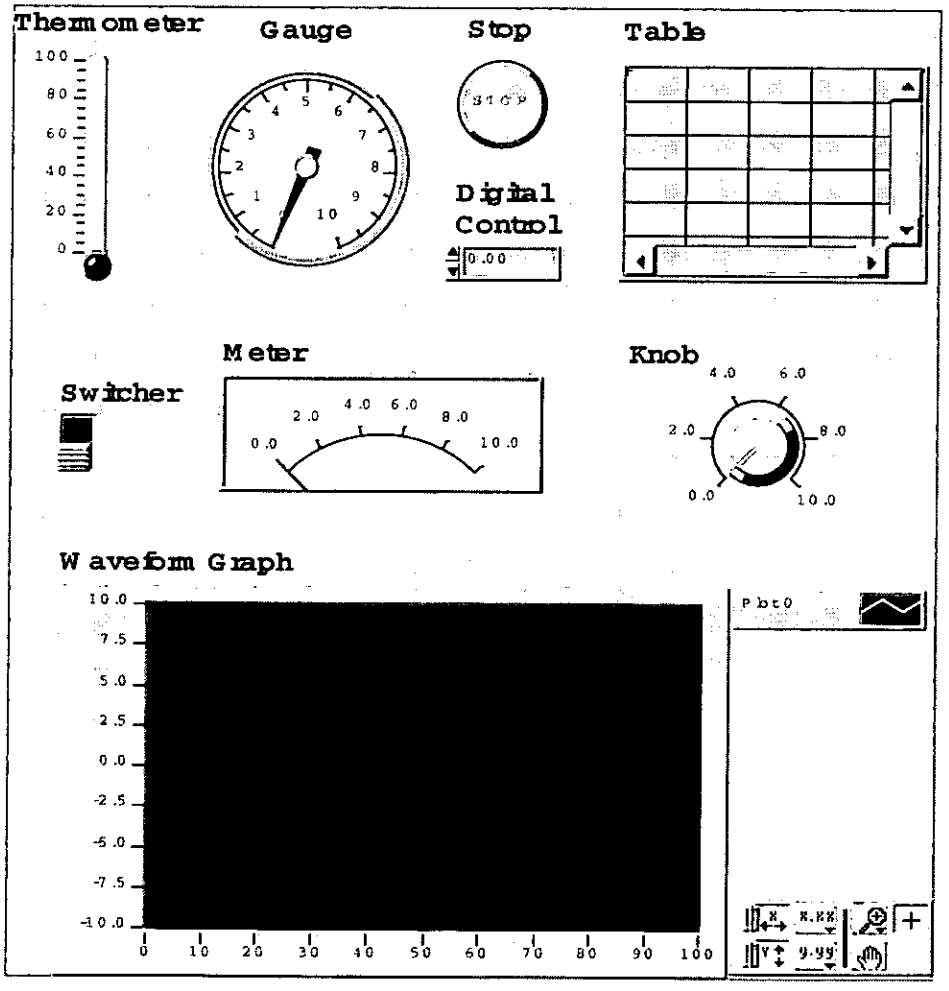

Figure 2.10 Some of the controls and indicators available in LabView

LabView includes libraries for data acquisition, GPIB and SR232 instrument control, data analysis, data presentation and data storage. LabView programs and sub-routines are called virtual instruments (VIs) because their user interfaces imitate the front panel of the real instruments.

Like a real instrument, a virtual instrument is composed of two main parts, front panel and block-diagram. The front panel acts as the interactive user interface and contains either controls / inputs or indicators / outputs. LabView provides the user with a large choice of digital displays, knobs, switches, slides, LEDs and graphs (see figure 2.10).

The block-diagram is equivalent with the electronics of the instrument and actually represents the code of a program or the VI. LabView provides several flow-control structures, like FOR loop, WHILE loop, multiple choices of CASE diagrams, as well as known physical constants (π, c, μ_0,...) and plenty of tools to manipulate and analyse the data. The VIs are hierarchical and modular. They can be used as top-level programs or as subprograms within other programs or subprograms. The icon and connector of a VI work like a parameter so that other VIs can pass data to a subVI. With these features, LabView promotes and adheres to the concept of modular programming. An application is divided into a series of tasks, which can be divided again until a complicated program becomes a series of simple tasks.
For examples of LabView programs developed in this project, please, see the Appendix 1, where both front panel and block-diagram corresponding to some of the main VSM programs are presented.

2.3 Mössbauer Spectroscopy (MS)

2.3.1 Introduction

Since most of the magnetic materials and magnetic recording media are based on Fe compounds, the nuclear gamma ^{57}Fe spectroscopy (or Mössbauer Spectroscopy) is a very attractive method of investigation for the magnetic and microstructure properties of these materials [18].

Mössbauer Spectroscopy is a very sensitive and accurate way of gathering information about the bonding, structural, magnetic, time-dependant and dynamical properties of systems. The Mössbauer effect involves resonant absorption of gamma rays by atoms of the same isotope. The source of the gamma rays is a radioactive isotope of an element which decays into an excited state of the isotope under study, which returns to its ground state by the emission of a gamma ray or electron. For most experiments the main source used is ^{57}Co in Rh matrix, which undergoes a nuclear decay (electron capture) to ^{57}Fe in its (I = 5/2) excited state. This can further decay in two ways as shown by figure 2.11, and the main one gives a 14.4 keV excited state. The decay of this state via gamma rays or conversion electrons is used in Mössbauer spectroscopy of iron systems. Normally, when a gamma ray is absorbed or emitted some of the kinetic energy of the photon is lost as recoil energy. This means that under normal conditions resonant absorption is prevented.

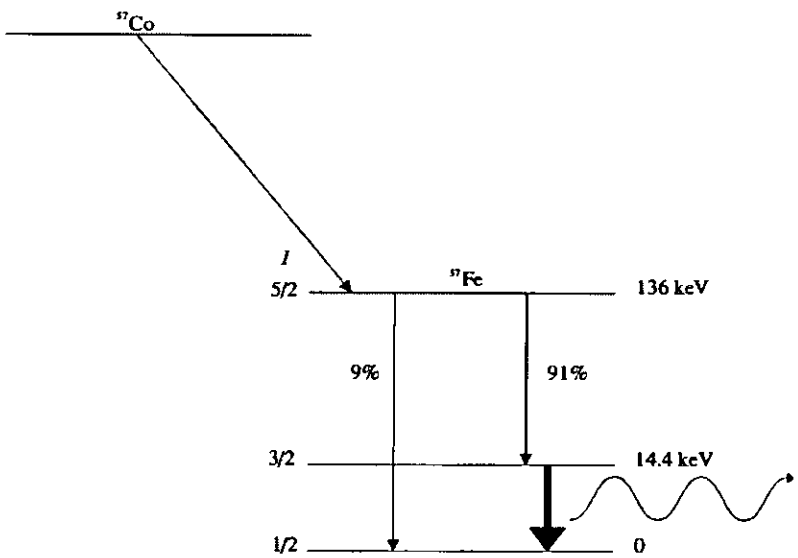

Figure 2.11 Nuclear Decay of ^{57}Co to ^{57}Fe leading to 14.4 keV Mössbauer gamma ray

If, however, the atom is bonded to other atoms in a crystal, then its effective mass is increased by a large factor, reducing the energy it absorbs from the gamma ray, i.e. the "atom" is now so massive it doesn't recoil. In these conditions it is possible to achieve resonant absorption by modulating the energy of the gamma ray beam. By oscillating the gamma ray source, the resulting Doppler shift changes the energy of the photons.

When the modulated beam matches the difference in energy between the ground and first excited state of the absorber (i.e. at resonance), then the gamma rays are resonantly absorbed. This gives a reduction in the number of counts at the detector giving an output like that in figure 2.12, which shows a very simple spectrum for an emitter and absorber in the same surroundings.

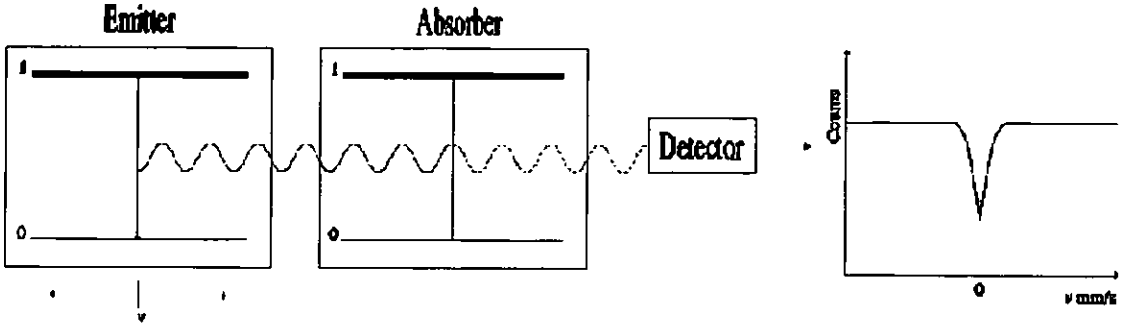

Figure 2.12 Simplest spectrum obtained from emitter and absorber in identical conditions

This output can be affected by temperature and three other factors: isomer shift (IS), quadrupole splitting (QS) and magnetic splitting.

2.3.2 Mössbauer hyperfine parameters

Isomer Shift (IS)

The isomer shift results from the difference in the electron densities at the nuclear sites in the emitting and absorbing atoms. This difference in density changes the Mössbauer transition energy and so the Mössbauer spectrum is shifted (see figure 2.13). In a non-relativistic case the isomer shift is given by the following formula:

$$\delta = \left(\frac{Ze^2R^2c}{5\varepsilon_0 E_\gamma} \right) \cdot [\rho_A(0) - \rho_S(0)] \cdot \left[\frac{\Delta R}{R} \right] mm/s \qquad (2.6)$$

where Z is the atomic number, e is the electronic charge, R is the effective nuclear radius, c is the velocity of light, E_γ is the energy of the Mössbauer gamma ray, the $\rho(0)$

terms are the total electron densities at the nucleus for absorber and source respectively and $\Delta R = R_{excited} - R_{ground}$. This isomer shift gives a way of distinguishing between, for example, different ion charge states as they give different isomer shifts. This is due to the different electronic structures of different types of ion. The s orbitals have the largest density at the nucleus and they cause the isomer shifts. The 3d orbital partially shields the nucleus from the influence of the 3s, and so the ion with the most electrons in the 3d orbital will do the most shielding, i.e. the Fe^{2+}. This smaller density gives a greater magnitude of difference between the emitter and absorber, hence a larger isomer shift.

Quadrupole Splitting (QS)

A quadrupole split spectrum results from a nucleus with an electric quadrupole moment, which experiences an electric field gradient (EFG). In other words, if a nucleus under investigation does not have a spherically symmetric charge distribution, then it will possess an electric nuclear quadrupole moment, Q. This moment interacts with an asymmetric electronic charge distribution to give a splitting, Δ, of nuclear energy levels.

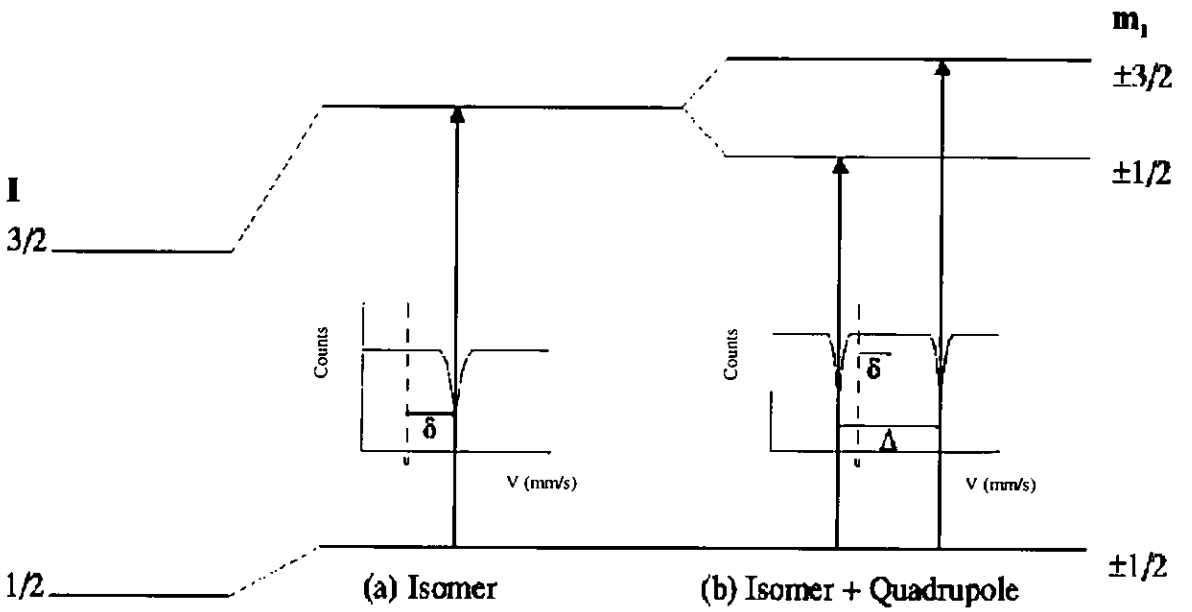

Figure 2.13 Effects of isomer shift and quadrupole splitting on Mössbauer

For example ^{57}Fe has no quadrupole moment on the ground state but the excited I = 3/2 state has a quadrupole moment, Q. The interaction of this with the EFG leads to two states $m_1 = \pm 1/2$ and $m_2 = \pm 3/2$ (see figure 2.13).

As the quadrupole moment is fixed for each state/isotope, this can be used to probe the electronic configuration. The largest component of the electric field gradient, V_{zz}, is given by the formula:

$$V_{zz} = \frac{\partial^2 V}{\partial z^2} = \frac{1}{4\pi\varepsilon_0} \sum_i q_i r_i^{-3} (3\cos^2 \theta_i - 1) \qquad (2.7)$$

The spectra are characterised by the quadrupole splitting constant (QSC), which is the product of V_{zz} (the principal component of EFG) and eQ (the electric quadrupole moment of the nucleus, where e is the charge on the proton).

For Mössbauer transitions between nuclear states with spin 1/2 and 3/2, the spectra are simple doubles, which are split by an amount Δ known as quadrupole splitting (QS) and is one half of the QSC of the 3/2 state:

$$\Delta = \frac{eQV_{zz}}{2} \qquad (2.8)$$

Magnetic Splitting

A nucleus with a magnetic moment placed in a magnetic field has a dipole interaction with the field. The interaction raises the degeneracy of nuclear states with angular momentum quantum number I > 0 to 2I+1. For example the ^{57}Fe ground state I = 1/2 splits into two, and excited state I = 3/2 splits into four. The selection rule of $\Delta m_I = 0, \pm 1$ gives six possible transitions (see figure 2.14).

The splitting is directly proportional to the magnetic field applied and so Mössbauer provides a way of measuring it. The field experienced by the system is a combination of the applied and hyperfine field. The effective hyperfine field (Be) can be calculated from the different contributions to it. They are related by the formula (2.9).

$$B_e = B_{hf} \pm B_{app} \pm B_d = B_c - \left(\frac{3\cos^2 \theta - 1}{2} \right) B_{dip} \pm B_{orb} \pm B_{app} \pm B_d \qquad (2.9)$$

where: B_{hf} is the hyperfine field, B_{app} is the applied external field, B_d is the demagnetising field, B_c is the contact field due to the unpaired electrons (3d for

transitional metals or 4f for rare earth) which polarised the s electrons that have a finite density at the nucleus, B_{dip} is the magnetic hyperfine field produced by the dipolar field of the spins of the 3d or 4f electrons, B_{orb} is the magnetic hyperfine field produced at the nucleus by the orbital motion of the electrons.

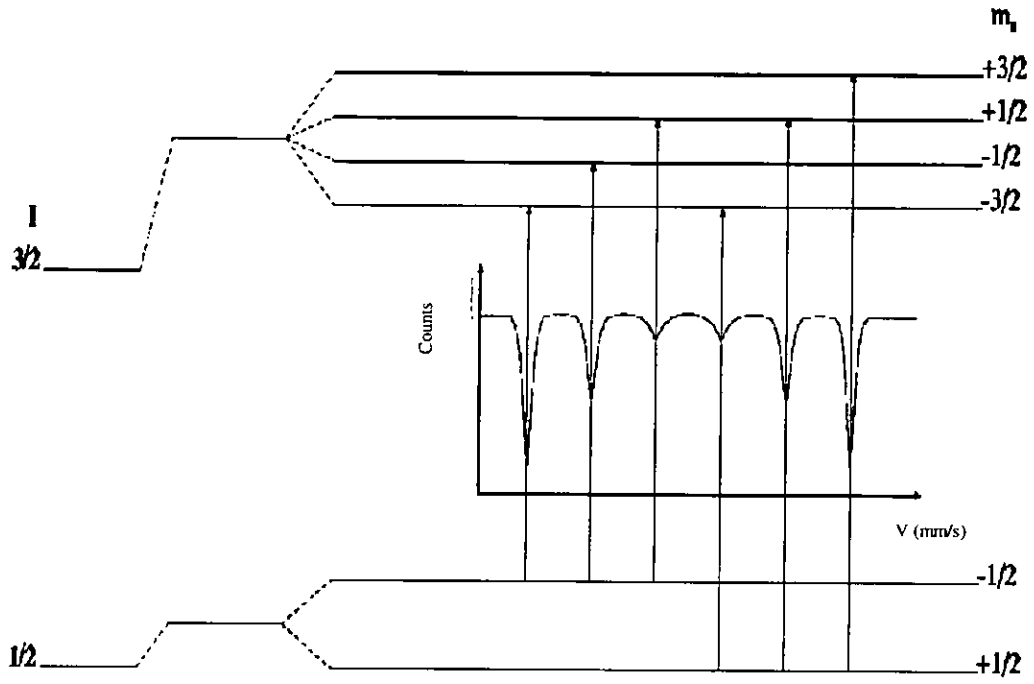

Figure 2.14 Effect on Mössbauer spectra produced by magnetic splitting

2.3.3 Experimental Set-up

Although there are some differences in apparatus used for room temperature and cryostat experiments, the method of data acquisition is basically the same and it can be summarised by the block diagram in figure 2.15.

The most usual experimental arrangement for Mössbauer spectroscopy involves a radioactive source containing the Mössbauer isotope in an excited state and an absorber consisting of a material to be investigated which contains the same isotope in its ground state. In a normal transmission experiment, the gamma rays emitted by the source pass through the absorber, where they may be partially absorbed, and then pass to a suitable detector.

In order to investigate the nuclear energy levels in the absorber it is necessary to modify the energy of the gamma rays emitted by the source so that they can have the correct energy for a resonant absorption.

The modification of the emitted gamma rays energy is usually accomplished by moving the source relative to a stationary absorber. This will give the gamma rays an energy shift as a result of the first-order relativistic Doppler effect. The motion of the source is oscillatory and is produced by an electromechanical transducer.

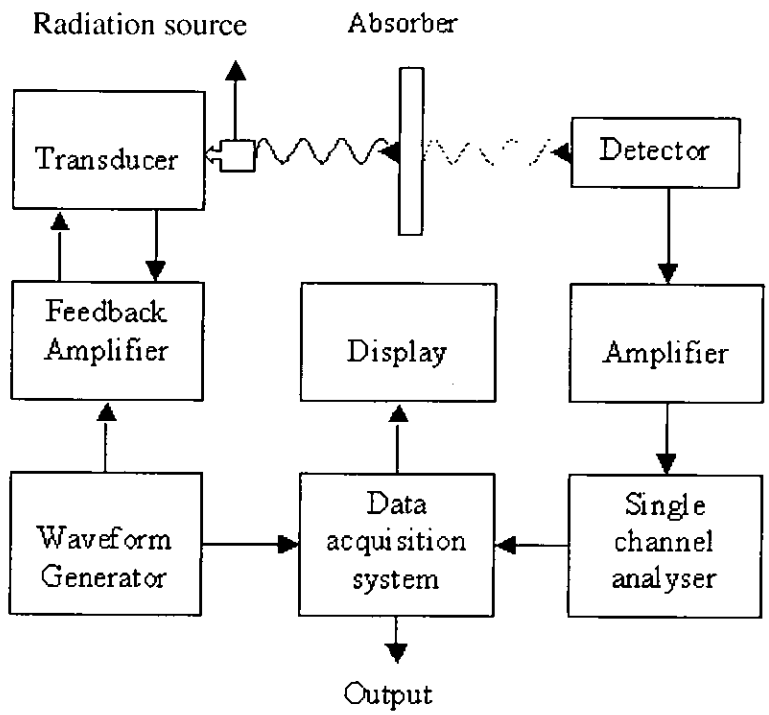

Figure 2.15 The block diagram of a typical Mössbauer spectrometer [17]

The detection system is dependent on the energy of the particular gamma ray and is essentially a single channel analyser selecting the counts corresponding to the Mössbauer gamma ray. The gamma ray counting and the source motion are synchronised by a microprocessor system in which the counts are accumulated in channels corresponding to the velocity of the source relative to the absorber. A spectrum is accumulated for a period of hours or days during which it may be monitored on a display screen. When a spectrum with a satisfactory signal-to-noise ratio has been obtained, it is normally stored on magnetic disk for subsequent computer analyses.

All spectrometers need to be calibrated, usually by using a film of metal containing the Mössbauer isotope (i.e. a foil of metallic ^{57}Fe at room temperature), in order to determine things like non-linearity in the oscillators. All further spectra and isomer shifts are quoted relative to the calibration spectrum.

The experimental aspects of Mössbauer spectroscopy are well developed and documented in the references [19,20]. The implementation of a Mössbauer spectroscopy experiment discussed in this section refers only to transmission geometry. However, there are also other types of Mössbauer spectroscopy that involves a scattering experiment rather than a transmission one. These are applicable for very thick samples where a transmission experiment is not possible, or even thin samples but when a surface analysis is required. A scattered Mössbauer experiment measures the conversion electrons, which are associated with the absorption process. These are more exotic experiments and they are considered in detail in the reference [21,22].

2.4 Summary

There are a large variety of experimental methods for magnetic materials analysis. Standard vibrating sample magnetometer, nuclear depolarisation, nuclear gamma resonance, nuclear magnetic resonance, magnetic force microscopy, neutron diffraction, torque magnetometer or magneto-optic effect are just some of the most important techniques used in magnetic materials characterisation.

The equipments used for experimental investigations in this project are a vibrating sample magnetometer, a nuclear gamma spectrometer and a magnetic force microscope. This chapter represents a glimpse over the first two experimental instruments and offers to the reader a good introduction to the techniques and to the main magnetic results that could be extracted from each one. For a better understanding, the graphic representations and schematic diagrams accompany the description throughout this chapter.

Firstly, the functionality principle of a standard VSM was presented and then the modifications needed to be applied to it in order to perform vectorial measurements. The eight coil detection system, which equips our vector VSM, is presented together with the way that signals from each coil should be add in order to measure the two components of the magnetisation.

The accuracy of the measurements depends very much on the calibration method and on different signal corrections, i.e. base line. The base line correction and the calibration of a VSM are treated in the section 2.2.2. The results are exemplified with experimental graphs showing the effect of base line and calibration.

Mössbauer spectroscopy or nuclear gamma resonance has been also used in this project. The Mössbauer experiments were carried out in collaboration with the Nuclear Gamma Resonance group at the University of Duisburg, Germany. The Mössbauer effect and the main hyperfine parameters of a spectrum are explained in the sections 2.3.1 and 2.3.2. A general block diagram of a Mössbauer experiment is also presented in the section 2.3.3.

An important part of the project was also dedicated to interfacing and development of the computer programs for full automation experiments. The computer routines were designed in LabView environment and a short introduction to LabView programming language is given in the section 2.2.4. In the appendix 1, I also give examples of some of the main LabView routines for VSM experiments, which were developed during this PhD project.

The following chapters contain the main results achieved in this project, followed by the conclusions and appendixes.

3. Experimental magnetic anisotropy studies in magnetic recording media

3.1 Introduction and review of the experimental techniques

As introduced in the section 1.1.3, the anisotropy field is defined as the field required to be applied at 90^0 from a particle easy magnetization direction in order to reverse the magnetisation of this particle. This definition is valid for an isolated particle or grain, but in reality there are no isolated particles within a recording medium. The field strength required to produce switching is influenced by inter-particle interactions such as exchange and magneto-static interactions. Other important factors that affect the anisotropy field are the nature of the material and its crystallographic structure and the particle volumes. A real material will contain particles having a distribution of the volumes (usually log-normal distribution) rather than perfect identical particles. Therefore, it is impossible to measure directly the anisotropy field and all the existing techniques measure the average effect of the distribution of the anisotropy fields within a medium. The average anisotropy field is then usually chosen as the most probable value of the distribution, i.e. the position of the maximum. Measuring anisotropy field distribution, other properties of the sample are excluded so that results relate more to the potential of a "particle type" rather than to the specific coating under investigation. This is because a single domain particle makes a contribution to the anisotropy field related to its switching field when its easy axis is aligned with the applied field but it is still under the influence of interactions with other constituent components of its magnetic environment. On the other hand, a particle contribution to coercivity is related to its switching field with the particle easy axis in its present orientation to the applied field.
This chapter discusses experimental techniques for anisotropy field and anisotropy field distribution measurements in modern recording media. Many techniques in literature describe the measurement of the anisotropy field and anisotropy field distribution and they could be separated in two different classes. The first class is represented by techniques involving switching processes and the second class is related to non-

switching techniques. The switching techniques depend upon the non-reversible switching of magnetic moments in the analysed material while the non-switching techniques (or "stiff techniques") measure the reversible rotation of the moments under an applied field without actually switching them.

3.1.1 Switching techniques

3.1.1.1 Rotational transverse remanent magnetometry

Rotational transverse remanent magnetometry is very similar to remanent torque magnetometry, except that direct measurement of the magnetization is used rather than torque measurement. This method is more suitable for automating computer-assisted experiments carried out on a modified vector VSM. Sharrock [1] and Speliotis [2] have used this technique to measure the anisotropy field of acicular and metal particles in magnetic recording media. The method determines the minimum field necessary to rotate the magnetisation into the field direction when it is applied at 90^0 to the mean of the EAD. This technique has been extended and improved in the present work and will be described in more detail in the section 3.2.1.

3.1.1.2 Rotational hysteresis (RH)

Despite this very time consuming technique, RH remains one of the most popular methods for anisotropy field measurements. Unlike other techniques, RH is applicable to any kind of magnetic material and does not depend on the orientation of the particles within the sample or the crystallographic structure of the sample. The anisotropy field value is identified as the field value where the rotational hysteresis loss (W_{RH}) curve reaches zero value. This technique was experimentally and theoretically introduced by Jacobs [3] and Luborsky et al. [4]. Since then, it has been intensively used. Bottoni [5] and Templeton et al. [6] have used this method to measure the magnetic anisotropy of metal particles for magnetic recording and M. Igaki et al. [7] has also studied acicular particles for recording media using RH. Anisotropy fields of Fe doped CrO_2 – particles have been analysed by Keller and Schmidbauer [8] using RH and the magneto-

crystalline anisotropy constants of inter-metallic compounds were determined by Wyslocki et al. [9] via rotational hysteresis energy studies. Besides the information related to the anisotropy field, which is obtained from rotational hysteresis loss curves, another important parameter might be derived from RH, namely the rotational hysteresis integral (J_{RH}):

$$J_{RH} = \int \frac{W_{RH}}{M_S} d\left(\frac{1}{H}\right) \tag{3.1}$$

J_{RH} is a parameter that is weakly dependent on particle interactions and gives only information about the reversal mechanism [10].

Since Rotational Hysteresis is also one of the main experimental tools used in this thesis, the description of the experiment, results and further details are given later in section 3.2.2.

3.1.2 Non-switching techniques

3.1.2.1 Torque magnetometry

This technique has long been recognized as one of the most direct methods for the measurement of the anisotropy. The sample is usually disk shape with the easy axis contained in the disk plane and suspended on a torsion wire. First the sample (considered as uniaxial crystal) is saturated in a large magnetic field. In an applied field, by rotating the sample easy direction away from the equilibrium position (parallel to the field direction), then the torque generated on the sample can be recorded as a function of rotation angle. The instrumentation is usually home made and various methods are used for torque experiments, which are all based on the same principle. The anisotropy energy W_a, for a sample having uniaxial anisotropy is given by:

$$Wa = K_0 + K_1 \sin^2(\theta) + K_2 \sin^4(\theta) + \ldots \tag{3.2}$$

When the energy of a system depends on an angle, the derivative of the energy with respect to the angle is the torque, τ. If we neglect K_2, then the torque exerted by M_s on the crystal is:

$$\tau(\theta) = -\frac{dW_a}{d\theta} = -2K_1 \sin(\theta)\cos(\theta) = -K_1 \sin(2\theta) \tag{3.3}$$

where K_1 and K_2 are the anisotropy constants and θ is the angle between saturation magnetisation of the crystal (M_s) and easy axis direction of the crystal. In figure 3.1 is plotted a torque curve as a function of angle. For $\tau = 0$, the slope of the torque curve is negative for the equilibrium positions ($\theta = 0$ and $\theta = 180^0$) and positive for the unstable position ($\theta = 90^0$).

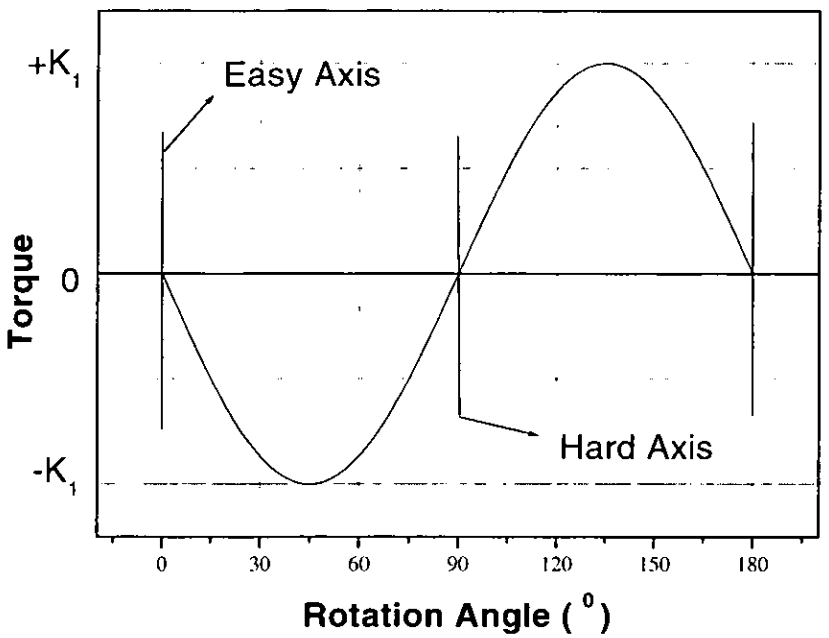

Figure 3.1 Variation of the torque with the rotation angle for a uni-axial crystal, obtained from the equation 3.3.

Experimentally, the value of K_1 is found simply from the maximum amplitude of the torque curve. An alternative method of extracting the value for K_1 and also the value for K_2 is by fitting the torque curve to a Fourier series. Keeping higher order terms in the energy expression (3.2), the torque becomes:

$$\tau(\theta) = -\frac{dW_a}{d\theta} = (K_1 + K_2)\sin(2\theta) - \frac{1}{2}K_2 \sin(4\theta) \tag{3.4}$$

and the anisotropy constants can both be extracted by least-squares fitting the torque curve. In this case all the experimental data in the torque curve is used to determine the anisotropy parameters, unlike the first technique where the peak value is enough to extract K_1. From the original torque magnetometry technique, many techniques have been developed.

Flanders and Shtrikman have successfully applied this method in 1962 [11]. They reported an experimental technique for determination of the anisotropy field distribution in ferromagnetic powders using remanent torque measurements. Uesaka et al. [12] have introduced a derived method called "45^0 out-of-plane torque method" in which they measured the anisotropy constant in Co-Cr-Ta thin film media for both randomly and oriented disks. Bertram also showed that micromagnetic simulations of the "45^0 out-of-plane torque method" give very accurate H_a values [13]. Pearson has given a very useful review of torque instruments and experimental techniques in the ref. [14] and Penoyer in [15].

3.1.2.2 Torsion pendulum

This method of measuring the anisotropy is very similar to torque magnetometry. The specimen is again a disk, suspended by a torsion wire in the air gap of an electromagnet. The sample is assumed to be a crystal with uniaxial anisotropy contained in the plane of the disk. Initially, the disk has the easy axis direction aligned to the applied field, this corresponding to the minimum energy position. The disk is rotated through a small angle away from the equilibrium position, released and allowed to oscillate with respect to the field direction. When the disk is displaced from the equilibrium position, two different torques act on the disk: the torque in the wire and the torque due to the crystal anisotropy that tries to rotate the disk back to its minimum energy position. The disk will oscillate with the frequency f that has to be experimentally measured and is given by the relation:

$$\frac{1}{f} = 2\pi\sqrt{\frac{I}{C_1 + C_2}} \tag{3.5}$$

$$C_2 = \frac{dT}{d\theta} = \frac{d^2W}{d\theta^2} \tag{3.6}$$

where C_1 is the torsion constant of the wire, C_2 is the rate of change of torque with the angle, I is the moment of inertia of the suspended disk and W is the magnetic anisotropy energy. Since C_1 and I can be determined experimentally from oscillations in zero field, by measuring the frequency f, C_2 may be calculated and hence the anisotropy constant. The torsion pendulum has been described and used by Rathenau and Snoek [16], and a more detailed reference is Zijlstra's paper [17].

3.1.2.3 Transverse susceptibility

This method consists of the application of a small perturbing AC field at right angle to a DC field that can be varied. The AC transverse susceptibility (χ_T) for the sample is then measured in the AC field direction. The AC field causes the particle dipole moments to oscillate around their local orientations. At the anisotropy field, large oscillations occur for those particles having their easy axis directions in the AC field direction. The peak position in the χ_T curve for both the positive and negative field directions gives the anisotropy field value (see figure 3.2).

The use of the transverse susceptibility as a characterisation method for magnetic materials was first theoretically introduced in 1957 by Aharoni et al. [18] and later experimentally demonstrated by Pareli and Turilli [19]. Despite this complicated technique of measurement, different authors have used transverse susceptibility successfully. Bissell and Sollis [20] have used the transverse susceptibility technique for anisotropy field measurements and magnetic thickness calculation on CrO_2 systems. Also, Chantrell et al. [21] and Jones [22] developed techniques for de-convoluting the anisotropy field distribution starting from χ_T experiments and using maximum entropy and neural networks.

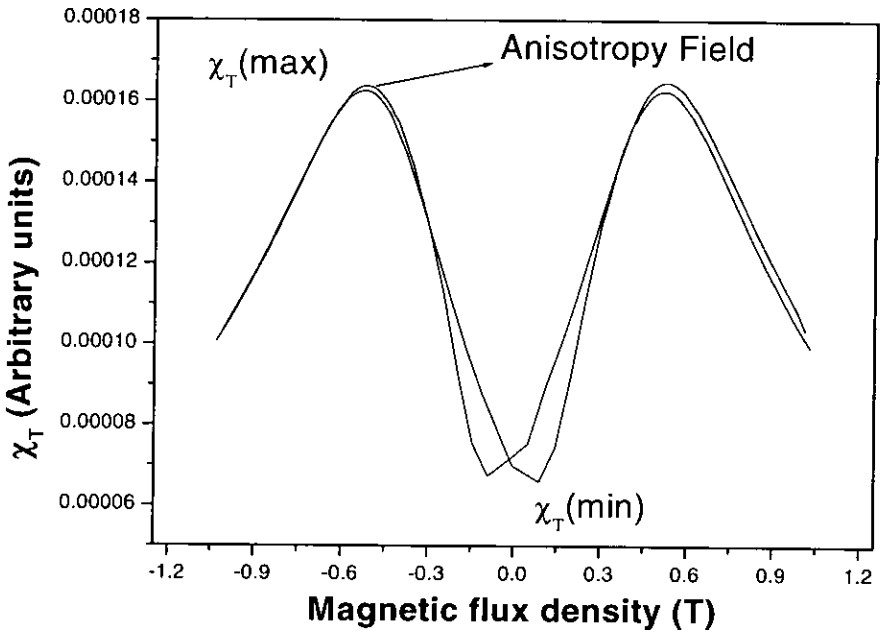

Figure 3.2 Example of Transverse Susceptibility plot showing the two anisotropy field peaks. (This plot is generated by Richard Cookson, another member of our research group)

3.1.2.4 Ferromagnetic resonance

Ferromagnetic resonance measurements represent a way of sampling the internal fields of a sample. Ferromagnetism is a cooperative phenomenon in which the individual atomic moments are aligned parallel due to exchange coupling. In a single domain particle all the atomic moments remain parallel generating a net moment for the particle. Each moment experience an effective field inside the sample, which is the sample's internal field plus the external magnetic applied field. A magnetic moment will orient itself along the direction of the effective field acting in the sample and executes a precession around the effective field. A small alternating field is applied perpendicular to the DC field. In a strong enough DC field, the AC field will be applied almost perpendicular to the effective field and therefore to the moment. If the damping effect is small, when the frequency of the AC field matches the natural precession frequency of the system, will resonate.

Two basic techniques are known to produce a ferromagnetic resonance curve, either by varying the frequency of the AC field in order to find the resonance position while DC field is kept constant [23], or by varying the DC field while the AC field frequency is kept constant [24].
Ferromagnetic resonance (FRM) is a well-established technique [25] and measurements have been carried out on magnetic recording media [26].

3.1.2.5 Singular point detection

According to the singular point detection theory (Asti and Rinaldi [27]) the magnetisation curve of a magnetic polycrystalline material plotted as a function of the magnetic field includes singularities located at values of H equal to the anisotropy fields for the individual components. These singular points become visible in the successive derivatives of the magnetisation with respect to the field. Only a small fraction of the crystallites in the sample are involved in the process, namely those having their hard axis parallel or near parallel to the field direction.

Bottoni et al. [28] applied this technique to different types of recording media. They proposed a method for determination of the anisotropy field distribution starting from "in plane" hysteresis loops measured with the field applied transverse to the mean easy axis direction. The demagnetising branch of the hysteresis loop, included between saturation and remanence, is fitted by a suitable function (after the remanence is subtracted). The relation (3.7) gives anisotropy field distribution and the second derivative is performed on the fitting function:

$$P(H_a) = -H\frac{d^2M}{dH^2} \tag{3.7}$$

3.2 Vector VSM techniques for anisotropy field measurements

3.2.1 Extrapolated transverse remanent magnetometry

As it has been discussed in section 3.1.1.1, transverse remanent magnetometry is a technique based on vectorial VSM measurements and has been developed mainly for anisotropy studies. The technique can be applied successfully to recording media that contain orientated particles / grains. With some limitations it could be also used for randomly oriented systems. However, the method is not very precise because changes in magnetisation are measured perpendicular to the applied field direction and consequently are very small. Therefore, the technique has been improved in this project by the introduction of extrapolation.

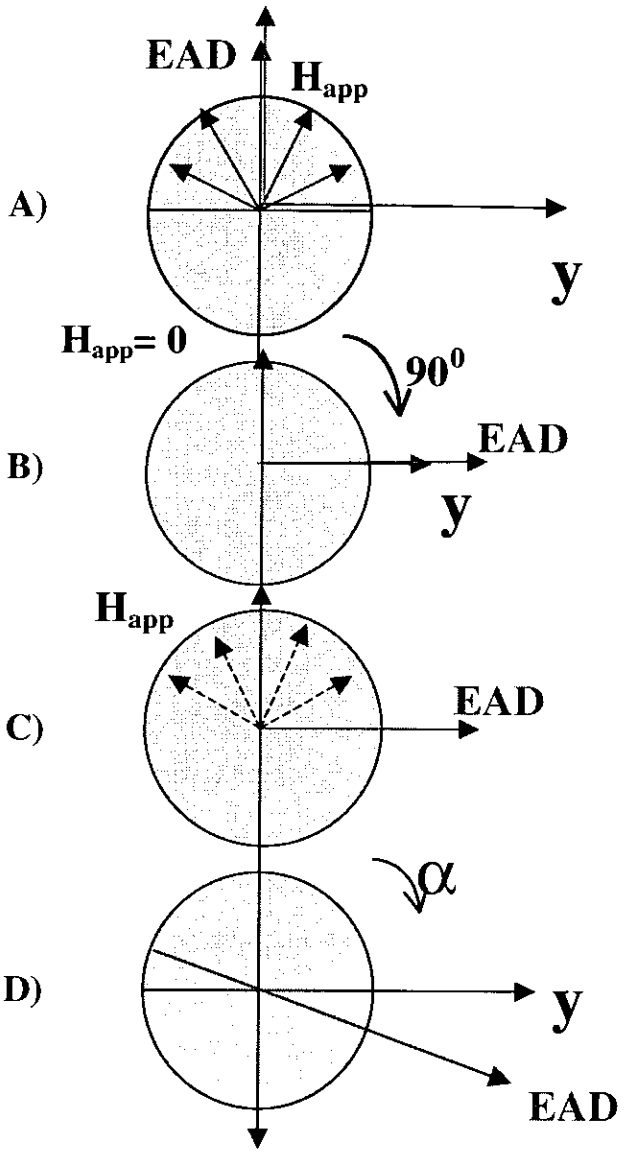

Figure 3.3 The representation of the experimental steps during a "transverse remanent magnetometry" experiment.

The technique is similar to remanent torque magnetometry, except that direct measurement of the magnetization change is used rather than torque measurement. The effective anisotropy field is measured by identifying the field value required to produce switching if applied at an angle close to 90^0 to the *in plane* symmetry direction of the sample easy axis distribution (EAD). This mean direction was determined by measuring saturation remanence as a function of angle. The direction

corresponding to maximum value was taken as the centre of the EAD on the assumption that the distribution was symmetric about this direction.

Figure (3.3 A) shows the initial state generated by the application and removal of a saturating field in the direction of the mean EAD, when all the moments are switched into directions making an acute angle with the applied field.

Starting from this point, the sample was rotated through 90° as indicated in (figure 3.3 B) and a saturating field was applied and removed again (see figure 3.3 C). This operation ensured that all the particles having their easy axis transverse or almost transverse to the mean EAD are switched back to their easy direction and only those particles having the axis transverse or almost transverse to the field direction were left in the remanent state. In this remanent state, the sample was rotated through a small angle, α (figure 3.3 D). A small field was applied and removed and the change in the remanence signal perpendicular to the applied field direction was recorded. Using gradually increasing fields, the change in remanence was due to the reversal of particle moments lying between 90° and $(90 + \alpha)^{\circ}$ to the centre of the EAD.

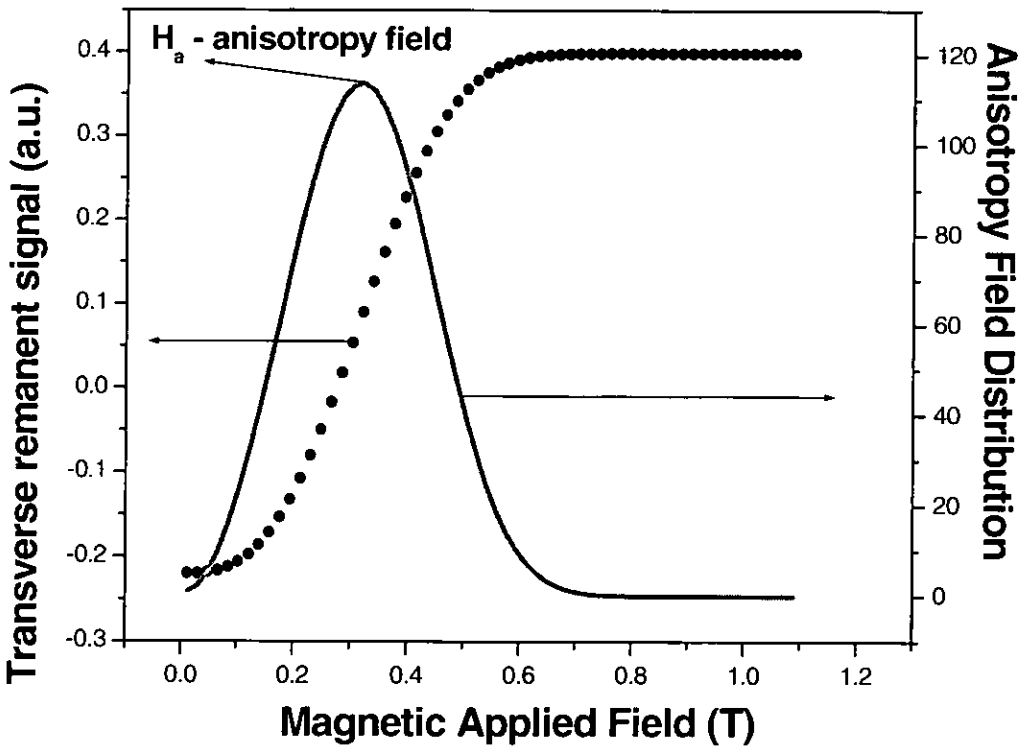

Figure 3.4 The dotted curve shows the transverse signal recorded during a TRM experiment. The continuous curve is the anisotropy field distribution obtained by differentiating the transverse signal.

For small α, this corresponds to particle moments reversing at their anisotropy field. The differential of the remanence curve (figure 3.4), or approximately the variation in the transverse remanent moment between two successive field applications and removals H_i and H_{i+1}, is the anisotropy field distribution of the particles. This indicates how many particles with their easy axes between 90^0 and $(90 + \alpha)^0$, have an anisotropy field value between H_i and H_{i+1}. In figure 3.4 is presented the in-plane anisotropy field distribution measured for a 5^0 rotation angle and the mean anisotropy field is taken as the field value corresponding to the curve peak (figure 3.4).

Strictly speaking, this is only an approximate measure and it will only be a true measure of anisotropy field as $\alpha \rightarrow 0$. Measurements at $\alpha = 0$ are impossible since the OY axis becomes a symmetry axis and the transverse signal is zero. Moreover, measurements for smaller angles are difficult as the signal also becomes too small to measure and the error increases. Therefore, most reported measurements using this technique work with an angle of at least 5^o. In this project, the technique has been extended in order to derive the true anisotropy field corresponding to the $\alpha = 0$ direction of measurement.

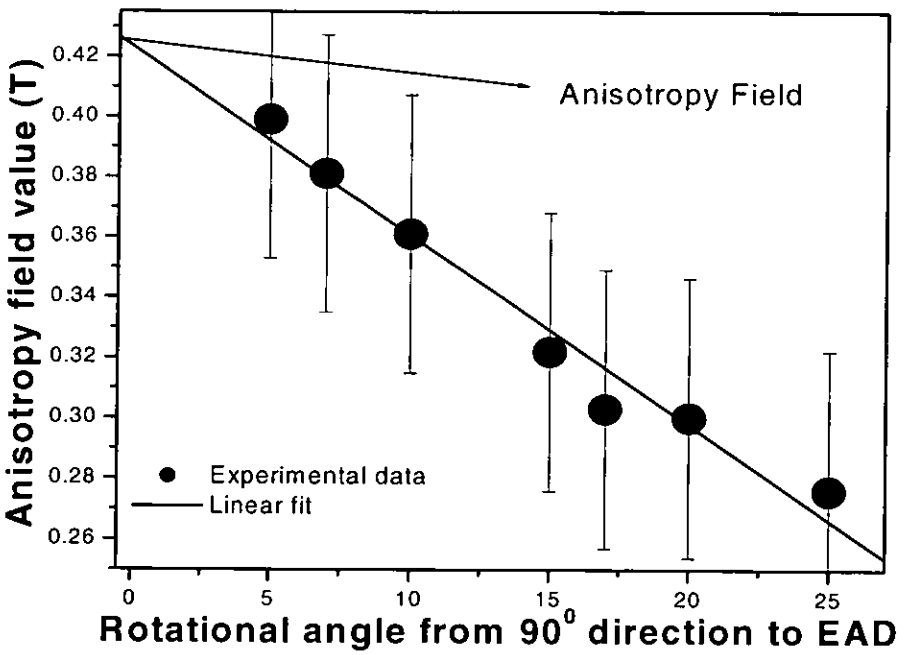

Figure 3.5 Experimental anisotropy fields as a function of the angle. The figure shows the linear extrapolation for determining the real anisotropy field. The error bars are evaluated from the standard deviation of the data giving a precision of ± 50 mT.

The same technique has been used but the experiment was repeated for up to 7 different rotational angles from 5^0 to 25^0. By plotting the peak field value against the rotational angle, it was found that these values lie approximately on a straight line which can be extrapolated back to $\alpha = 0$ (see figure 3.5).

The intersection point of the extrapolated line with the field axis gives a more accurate value of the anisotropy field. This technique is first introduced in the ref. [29]. It is worth mentioning that usually, the raw experimental data should be processed before extracting the anisotropy field distribution and the anisotropy field. The transverse remanence curve is first smoothed and interpolated and then fitted by an appropriate function. Only after these steps, the curve is ready for differentiation. A series of samples has been investigated using this extended method and the results are presented in the next section.

3.2.1.1 Results and discussions

This new technique has been used for the investigation of a set of four samples. These are a new generation of experimental double-coated advanced metal particle (MP) tapes. A complete description of the samples analysed in this thesis is given in the Appendix 2 together with the code names and other properties of the samples. For simplicity, the sample codes defined in the Appendix 2 will be used throughout the thesis.

In order to achieve accurate results, a very careful preparation of the samples is required before running any kind of vector VSM experiment in general, or a transverse remanent experiment in particular. Bi-axial experiments were carried out at room temperature on 1 cm diameter disk samples made of stacks of 16 single layers glued together to maintain their tape orientation. This produced a sample corresponding to 12.5 cm^2 and increased the signal to noise ratio to satisfactory levels without compromising the sheet demagnetisation factor of the sample. The disk samples were mounted in the VSM with the sample plane and the rotational axis coincident. Transverse remanent magnetometry has been performed as described in section 3.2.1. Figure 3.6 shows the anisotropy field distribution for the four analysed samples corresponding to a measurement at 5° rotation angle. Although the anisotropy field is determined by extrapolation to 0^0, it is believed

that the shape of the distribution measured at 5^0 is the same or at least very close to the one at 0^0, except the central position, which is shifted towards smaller fields.

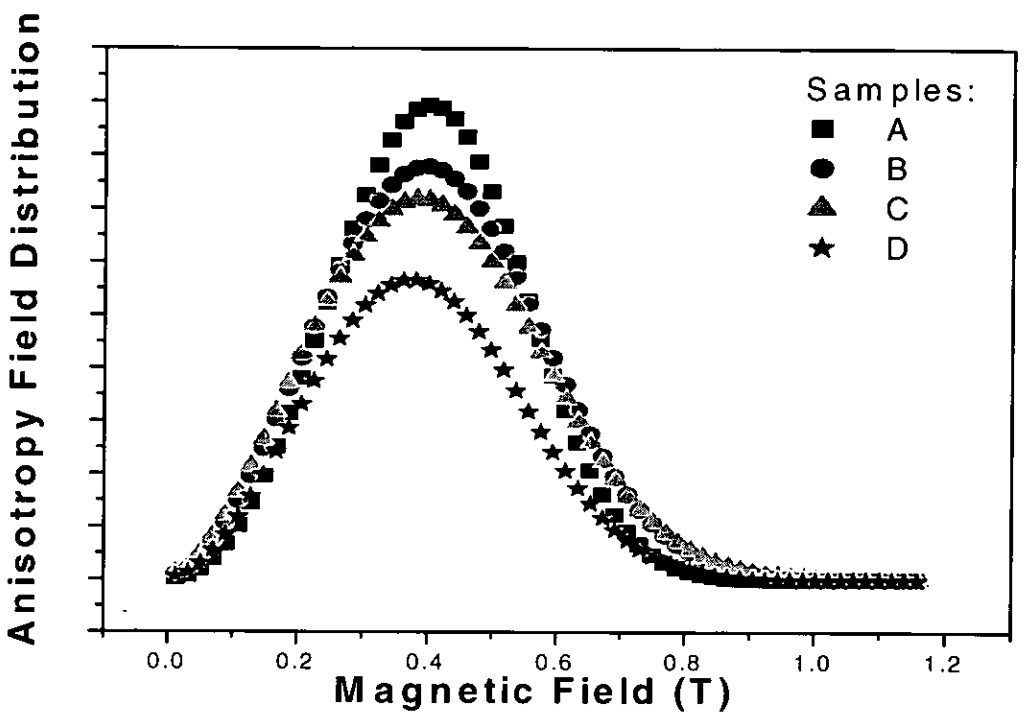

Figure 3.6 Anisotropy field distribution for the four MP tape samples, measured for a 5^0 rotation angle.

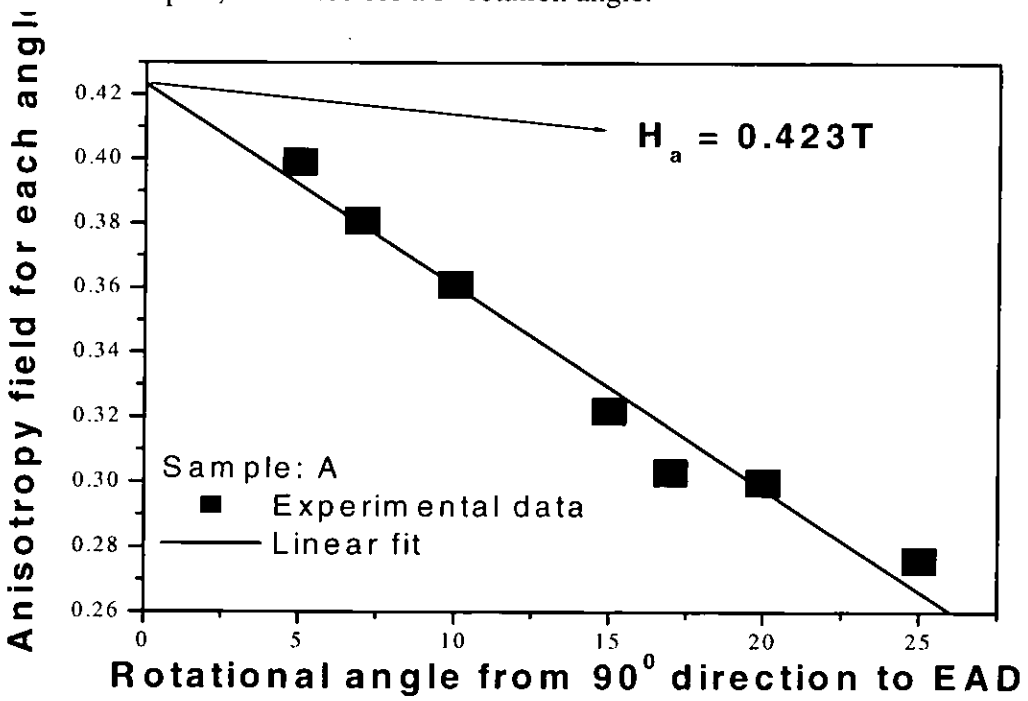

Figure 3.7 Transverse remanent magnetometry experimental data and the linear extrapolation showing the anisotropy field value for sample A.

Figures 3.11 to 3.14 show the linear extrapolations and the appropriate anisotropy fields for the four samples.

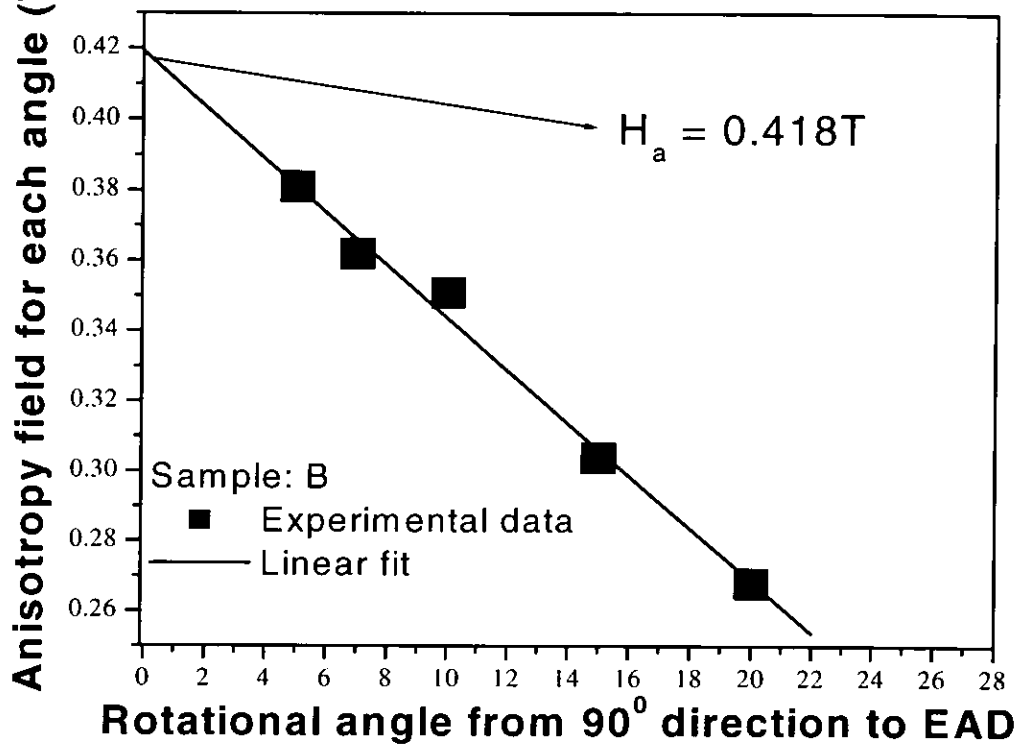

Figure 3.8 Experimental data from transverse remanent magnetometry and the linear extrapolation showing the anisotropy field value for sample B.

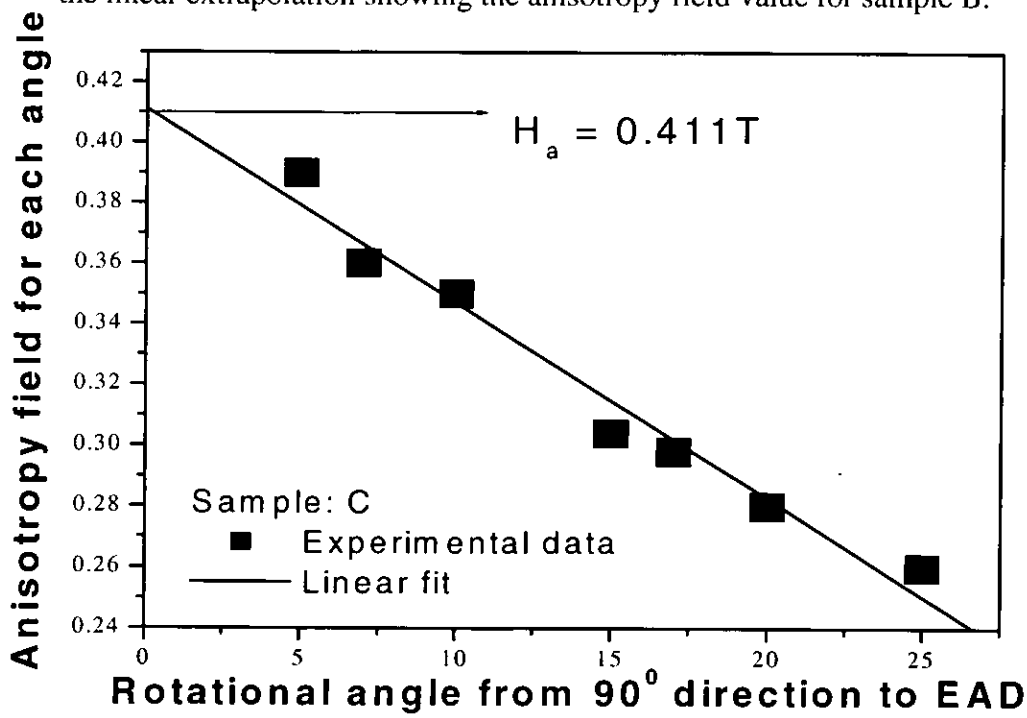

Figure 3.9 Experimental data from transverse remanent magnetometry and the linear extrapolation showing the anisotropy field value for sample C.

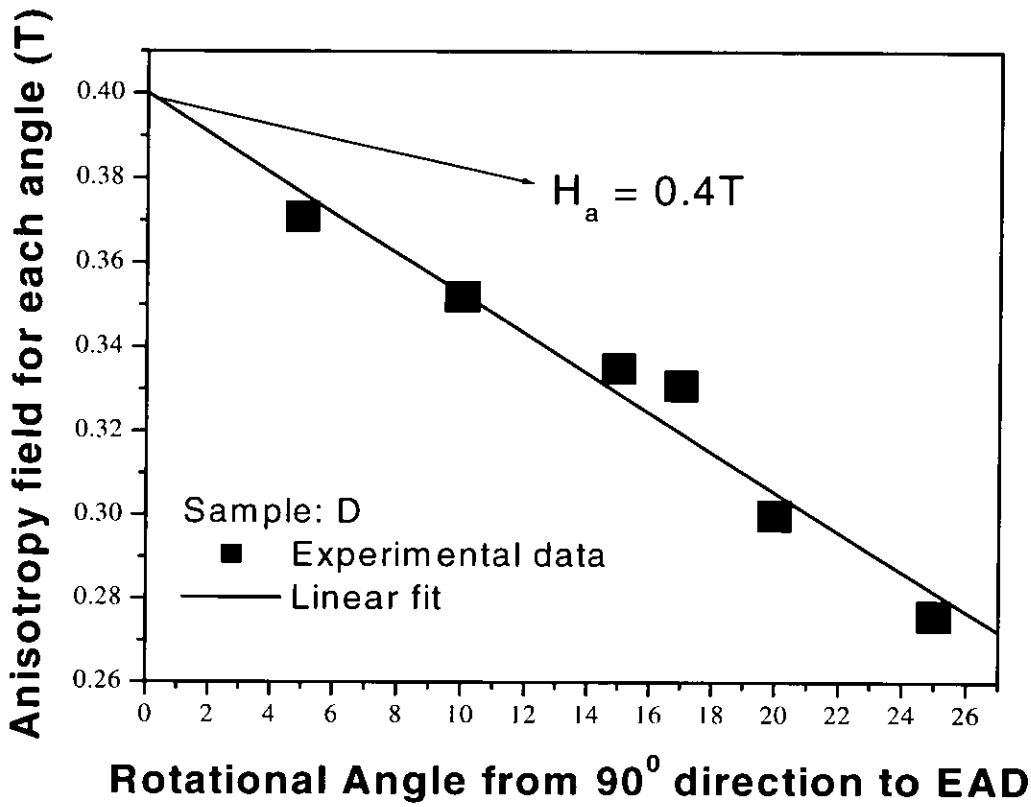

Figure 3.10 Experimental data from transverse remanent magnetometry and the linear extrapolation showing the anisotropy field value for sample D.

Table 3.1 gives the anisotropy results for this set of samples.

Table 3.1 Anisotropy fields, obtained using the extrapolated transverse remanent magnetometry technique, for the series of MP tape samples

Samples	Fe-Co metal-particle tapes			
	A	B	C	D
Anisotropy field H_a (mT)	423	418	410	400

Normally, one would expect the measured anisotropy field for samples belonging to the same set to be the same, since they were prepared in the same conditions and also contain identically components. However, it can be seen that the H_a values are not the same and a variation of the anisotropy field with respect to the magnetic thickness was found, as shown in figure 3.11.

For the MP tapes it has been shown that a thinner magnetic layer is associated with a smaller anisotropy field. This result is explained in terms of interactions between particles. In a system of magnetically isolated particles, the measured anisotropy field would be the distribution of fields of the individual particles. However, in a real system,

the magnetic anisotropy field is reduced by inter-particle magnetostatic interactions [30].

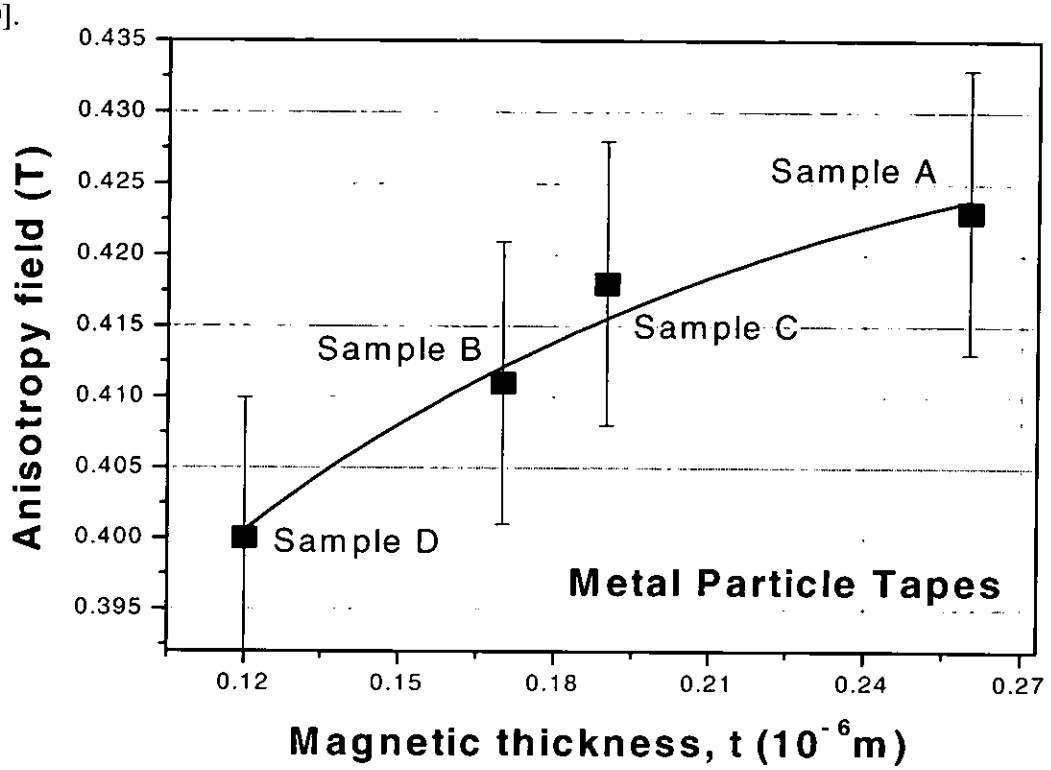

Figure 3.11 Anisotropy field variation with respect to the magnetic coating thickness. The thinner the sample, the smaller the anisotropy field. The error bars are evaluated from the standard deviation of the data giving a precision of ± 50mT.

Therefore, the measured anisotropy field values represent a mean effective anisotropy field, which includes also the interaction effects. Recently, theoretical investigations on the magnetostatic interactions in particulate media have revealed a clear dependence of the magnetostatic interactions with the magnetic coating thickness [31]. It has been shown that a network of 2D particles has an enhanced magnetostatic interaction distribution over that of a 3D system of particles. As a consequence, the interaction effects are more pronounced for a thinner medium. Since the anisotropy field of metal particles is reduced by the inter-particular magnetostatic interactions, as explained earlier, for a thinner medium, the anisotropy field is smaller. This theoretical result [31] is in agreement with our experimental data (see figure 3.11), where the anisotropy field increased as the magnetic thickness increased. Furthermore, the change of the interactions with thickness has been also experimentally confirmed by experimental remanence curves [32], which have been determined for all samples in order to generate

the well-known Henkel [33] and ΔM plots [34]. These are accepted as a useful indication of the sign of the interactions in a magnetic material and of their variation with sample properties.

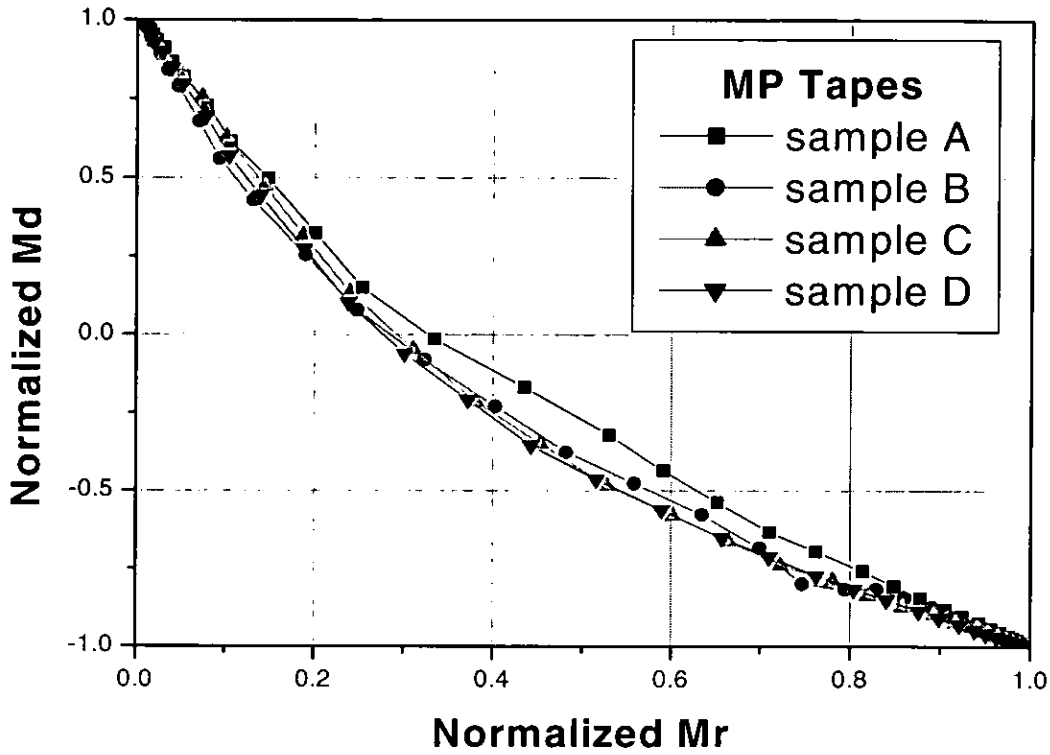

Figure 3.12 Henkel plots for the remanence measurements in the direction parallel to the applied field (longitudinal remanence measurements). The negative deviations indicate the presence of demagnetising (negative) magneto-static interactions within the analysed media.

The isothermal remanence magnetisation (IRM) and the DC - demagnetisation (DCD) curves [32] were measured using the techniques described in the section 2.2.3. Henkel plots (see figure 3.12) have been produced by representing Md as function of Mr, where Md and Mr are IRM and DCD values normalised to the saturation remanence magnetisation. Henkel plots and ΔM plots are both useful as they show different things. Henkel plots contain no displayed field information and so can be used to compare materials with different coercivity, whereas ΔM plots display interactions as a function of field (see figure 3.13), which is in fact the deviation from the Wohlfarth relation [35], as a function of the applied field: $\Delta M = Md - (1 - 2Mr) = \Delta M(H)$.

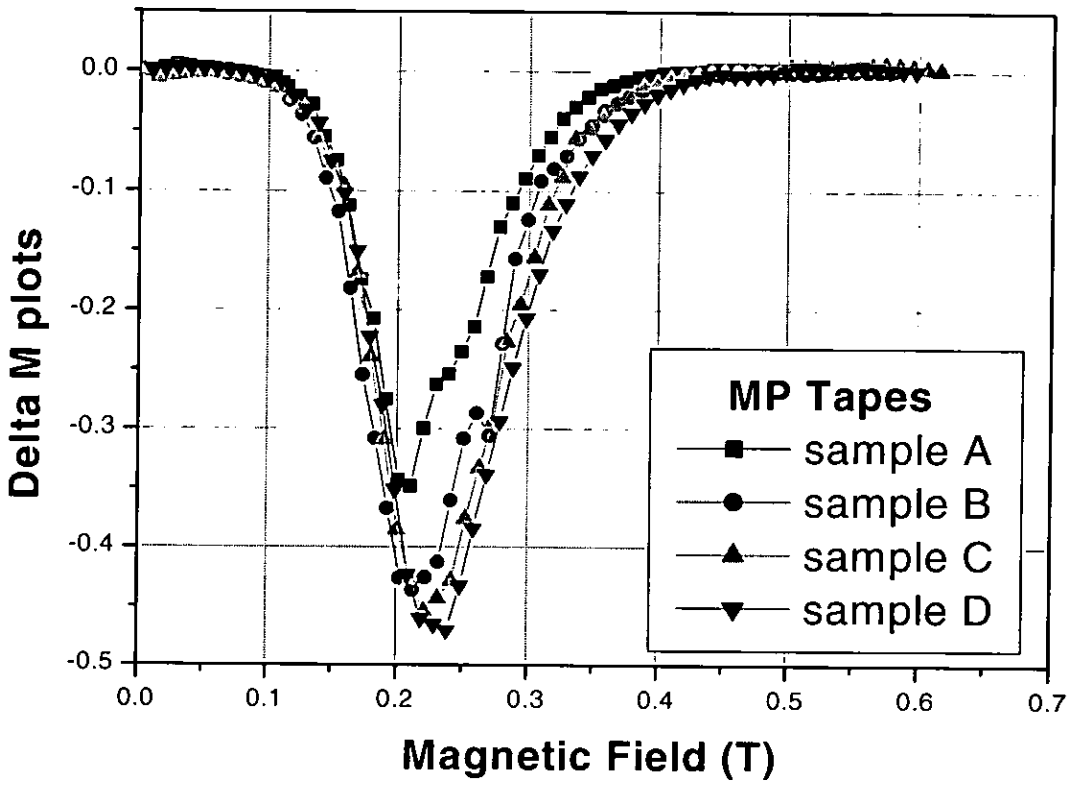

Figure 3.13 Delta M plots. The negative peaks indicate the presence of demagnetising (negative) magneto-static interactions within the analysed media.

A Henkel plot for an ideal medium with no interactions will present a straight diagonal line and a ΔM plot value will be zero for all fields. In the case where there are interactions within the medium demagnetising (negative), the curve is below the line and above the line for interactions, which oppose demagnetisation (positive). As can be seen from figures 3.12 and 3.13, the experimental remanence studies indicate negative interactions throughout the entire field range, as expected for acicular particle systems, but they become stronger as the magnetic coating is reduced in thickness.

3.2.2 Rotational hysteresis (RH)

Rotational hysteresis energy (W_R) is defined as the work necessary to rotate the moment of a sample through 360^0 in the presence of a magnetic field. This is determined by measuring the torque T exerted on a sample by a rotating magnetic field H. Mathematically it can be expressed as:

$$T(\theta) = \vec{M} \times \vec{H} = MH \sin\theta = M_{\perp} H \tag{3.8}$$

$$W_R = \int_0^{2\pi} T(\theta) d\theta = \int_0^{2\pi} MH \sin(\theta) d\theta \tag{3.9}$$

Since the torque is proportional with the perpendicular magnetisation of the sample, again, instead of measuring the torque, the rotational hysteresis energy was determined by using a vector VS-M. During the experiment, a disk sample is rotated through 360^0 about its axis with the field direction always in-plane and the signal transverse to the magnetic field ($M_\perp$) is recorded as a function of the rotation angle. A numerical value of the rotational hysteresis energy is obtained by integrating the "torque" curve, which in this case is the curve $M_\perp = M_\perp(\theta)$. The integral value is the area under the experimental curve and represents the rotational hysteresis energy. However, valuable information can only be obtained from the rotational hysteresis loss (W_{RH}) rather than rotational hysteresis energy (W_R). The rotational hysteresis loss is determined by the algebraic sum of the rotational hysteresis energies measured for a full 360^0 clockwise rotation followed by a full anticlockwise rotation.

$$W_{RH} = W^{cbw}{}_R + W^{acbw}{}_R = \int_0^{2\pi} T(\theta) d\theta + \int_{2\pi}^{0} T(\theta) d\theta = \oint T(\theta) d\theta \tag{3.10}$$

Qualitatively speaking, the loss arises from the delay that the magnetisation M suffers with respect to the rotating applied field. If the applied field is small, H cannot induce any irreversible variation of the magnetisation and no rotational hysteresis loss occurs. When the applied field is very large (bigger than the anisotropy field, H_a) the magnetisation follows the field and is almost always parallel to it. This time there is no difference in the irreversible changes during the two rotations and so there is no rotational hysteresis loss. At intermediate fields, unlike the two previous cases, the magnetisation tries to follow the rotation of H and suffers irreversible variations. The rotational hysteresis loss is no longer zero and in this range W_{RH} initially increases with the field. These transitional phases can be visualised in the figure 3.16, section 3.2.2.1, where the transverse signal was recorded for a full 360^0 rotation in clockwise and anticlockwise directions for a range of different applied fields values. After a distinct

maximum, the rotational hysteresis loss decreases back to zero at $H = H_a$ (figure 3.14) and this gives a direct measurement of the anisotropy field. Experimentally, a disk sample is rotated through 360^0 clockwise and anticlockwise in an applied field using steps of 10^0 rotation angle. The transverse signal is recorded after each 10^0 rotation throughout the experiment. The rotational hysteresis loss is determined by calculating the integral values (as defined earlier) and the difference between the two obtained areas represents the W_{RH}. This is repeated for different applied field values, starting at H = 0T and up to high fields that exceed the anisotropy field. The W_{RH} values are calculated for each experiment. By plotting the calculated W_{RH} versus applied field values, the anisotropy field can be identified for that sample as the field where W_{RH} become zero (figure 3.14).

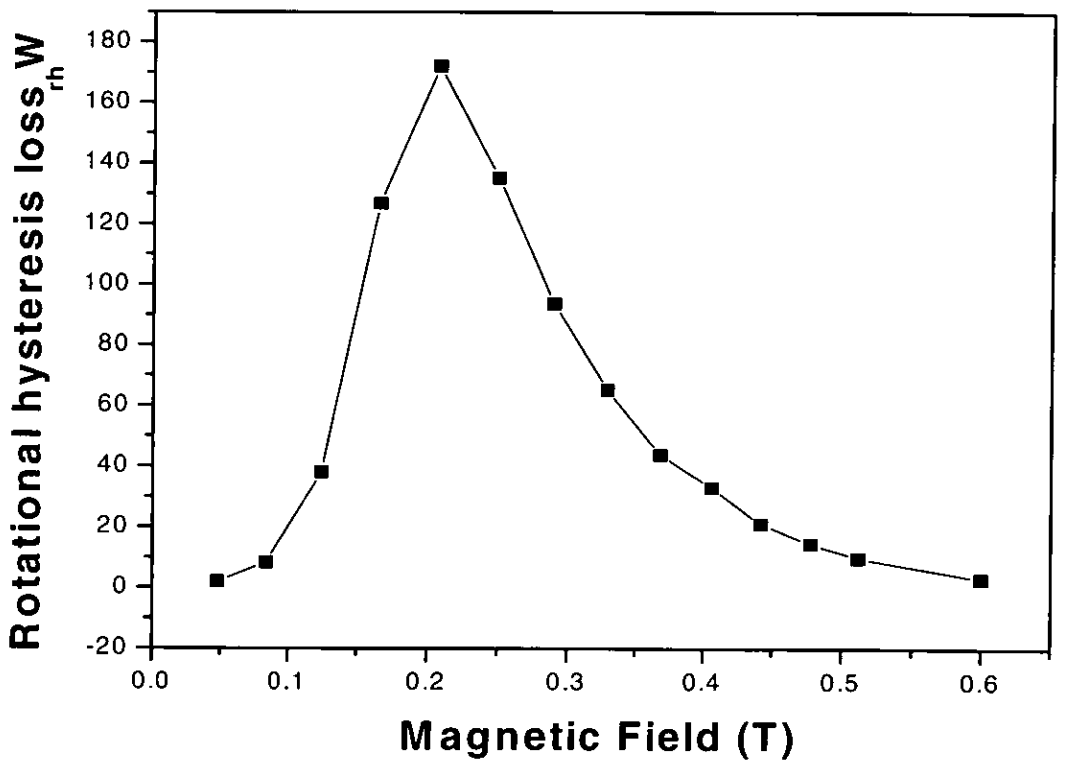

Figure 3.14 Rotational hysteresis loss as a function of applied field.

A better representation is given by plotting W_{RH} as a function of the inverse applied magnetic field 1/H (figure 3.15). From this graph, the anisotropy field is easily obtained by extrapolating the initial linear slope to $W_{RH} = 0$, where the intercept gives the values $1/H_a$. A rotational hysteresis experiment is quite time consuming and before starting

one, a few details must be carefully analysed in order to avoid any possible faults. The full clockwise and anticlockwise rotations are performed in applied field at different values. If the step field and the maximum field are not chosen properly, is very likely to miss the anisotropy field by rotating the sample up to maximum fields that are either lower or much higher than H_a.

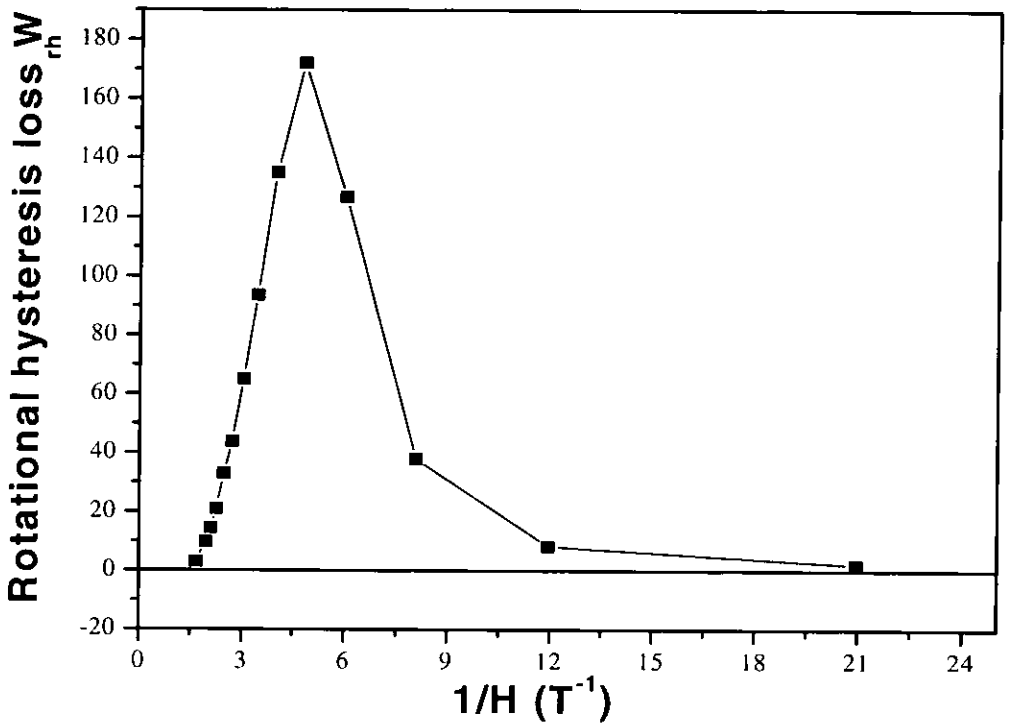

Figure 3.15 Rotational hysteresis loss as a function of the inverse applied field. This plot shows clear the linear part of the graph that can be extrapolated back to zero for H_a determination.

Therefore, the rotational hysteresis experiment requires some initial study to determine the range of fields of interest. For a very large step field, it could happen that the anisotropy field to be contained within the first two/three step fields and that will lead to an inaccurate determination of the H_a.

Contrary, if the step field is too small, it could generate a very long experiment that might be stopped even before reaching the anisotropy field.

The solution for this technical problem comes from an empirical observation. The graph of rotational hysteresis loss (W_{RH}) as function of the applied field (figure 3.14) will always have a peak at an approximate value equal to the coercivity field (H_c) of the sample. On the other hand, the anisotropy field is always bigger than the coercivity: H_c

$< H_a$. Therefore, in order to choose the best step field and the best maximum field for a rotational hysteresis experiment the coercivity field of the sample must be known first.

3.2.2.1 Results and discussions

The same set of MP tapes has been used for rotational hysteresis studies. The experimental procedure has been fully explained in section 3.2.2. In figure 3.16 there are represented the variation of the transverse signal with respect to the rotation angle for a full 360^0 clock-wise and anti-clockwise rotation. The graph shows only a few representative data that correspond to different step fields during a rotational hysteresis experiment performed on the vector VSM.

As can be seen from figure 3.16 A, a full rotation in a very small magnetic field (50 mT), will induce very small irreversible changes of the magnetisation and almost no rotational hysteresis loss occurs.

As the field increases (140 mT – 300mT), the magnetisation tries to follow the rotation of the applied H and suffers irreversible variations (figures 3.16 B, C and D). For rotations taking place in large applied magnetic fields ($H \geq 478$ mT), which are even bigger than the anisotropy field, the magnetisation follows the field direction almost parallel to it and almost no irreversible variations occur (see figure 3.16 E). These experimental curves are then processed in order to obtain a numerical value of the rotational hysteresis loss.

All four MP samples have been measured using rotational hysteresis. Figure 3.17 shows rotational hysteresis loss data plotted against the reverse field for the set of MP tape samples.

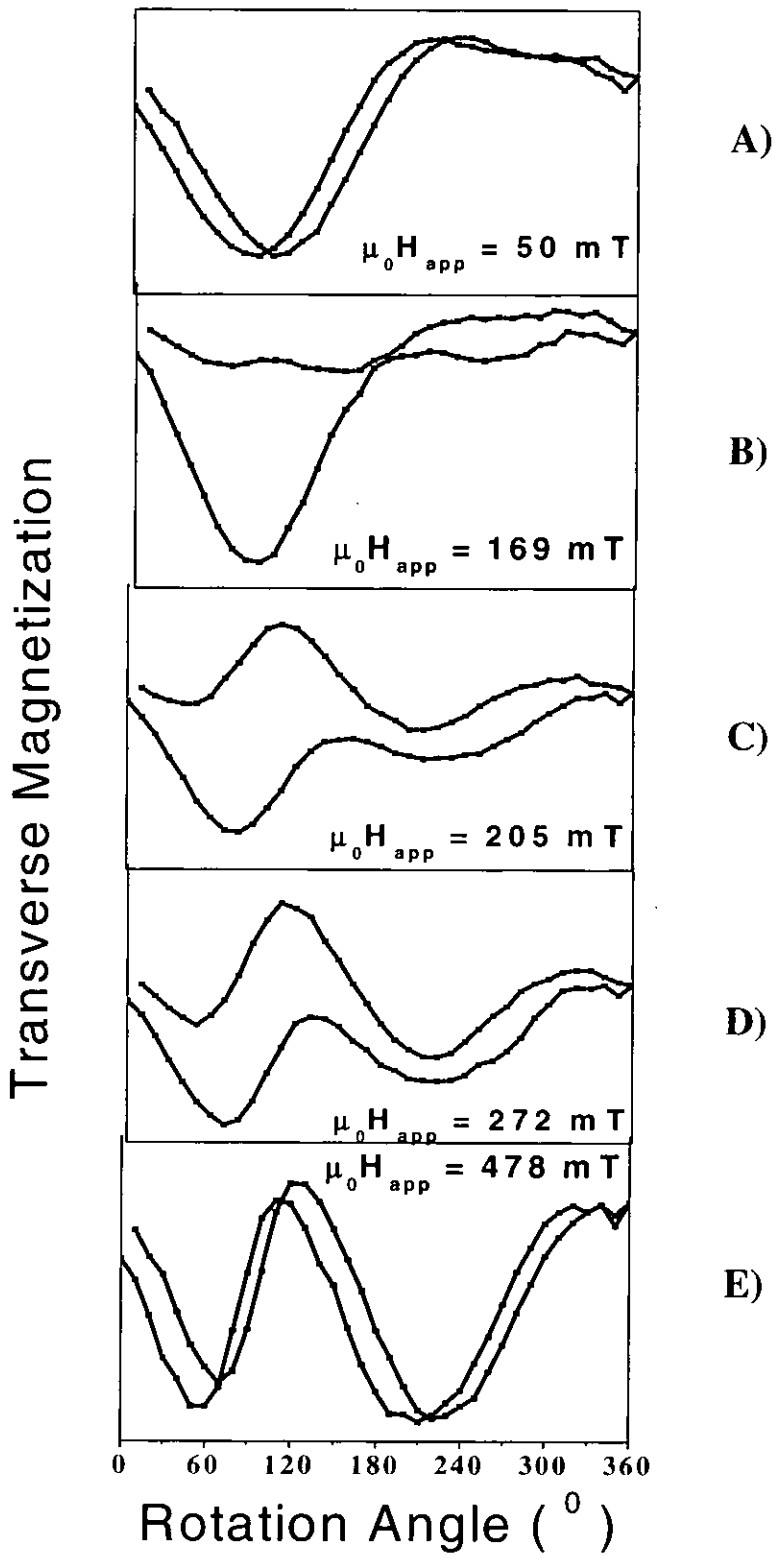

Figure 3.16 Experimental data recorded during a RH experiment on a vector VSM. The diagrams show the transverse signal recorded, for sample A, as a function of angle for incremental applied fields.

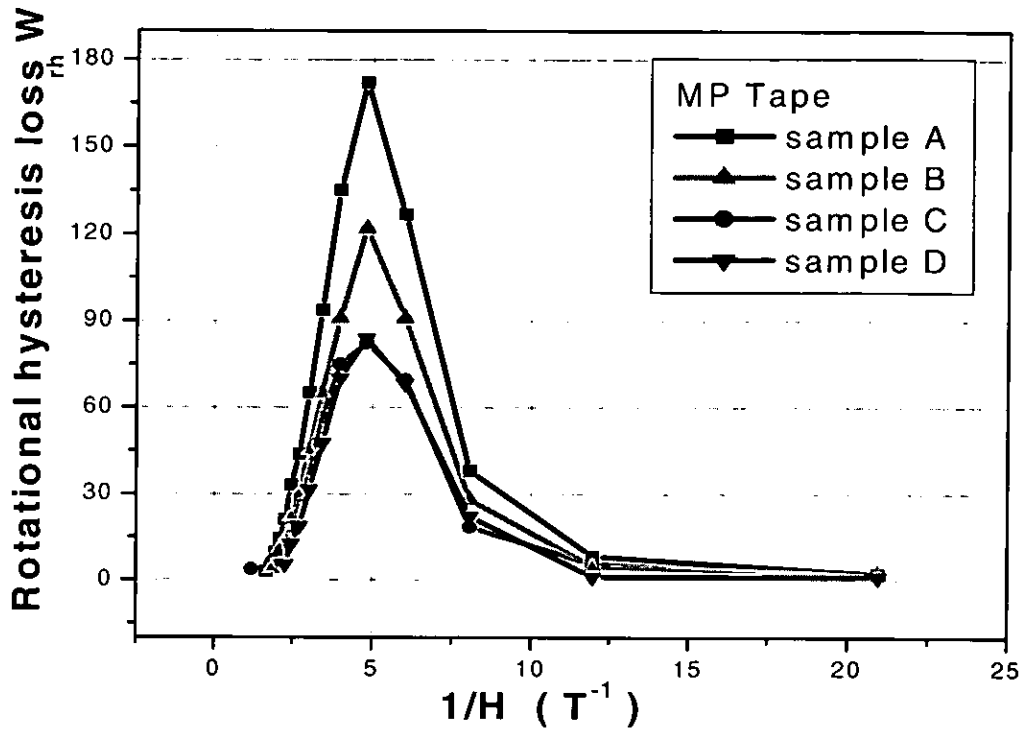

Figure 3.17 Rotational hysteresis loss as a function of the reverse field.

The rotational hysteresis anisotropy data are in good agreement with those obtained from the transverse remanent magnetometry (see for a direct comparison table 3.2 and figure 3.18).

Table 3.2 Comparison between anisotropy fields experimentally obtained from the two techniques

Samples	A	B	C	D
H_a - Rotational Hysteresis (mT)	420	413	409	395
H_a – Transverse Remanent Magnetometry (mT)	423	418	411	400

Supplementary, RH has been used for analysing the set of Co-Cr-Ta thin films samples, as well. As explained earlier, the transverse remanent magnetometry is applicable only within certain limitations.

Although other thin film samples were successfully measured using transverse remanent magnetometry, the experiments for Co-Cr-Ta failed in producing reliable results because the samples had moments which were too small to produce measurable

changes. Thus rotational hysteresis was the only accessible way to measure the magnetic anisotropy for these thin film samples.

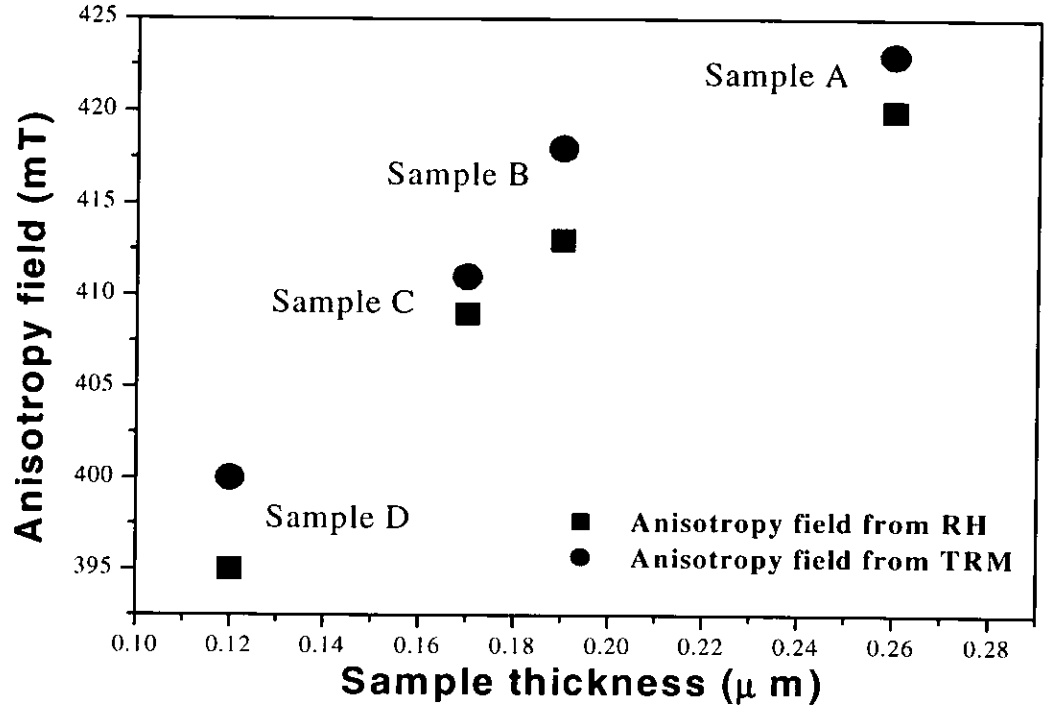

Figure 3.18 Comparison between anisotropy experimental data obtained from extrapolated transverse remanent magnetometry and rotational hysteresis. The presented results are for the series of MP tape samples and the H_a are plotted as a function of magnetic thickness

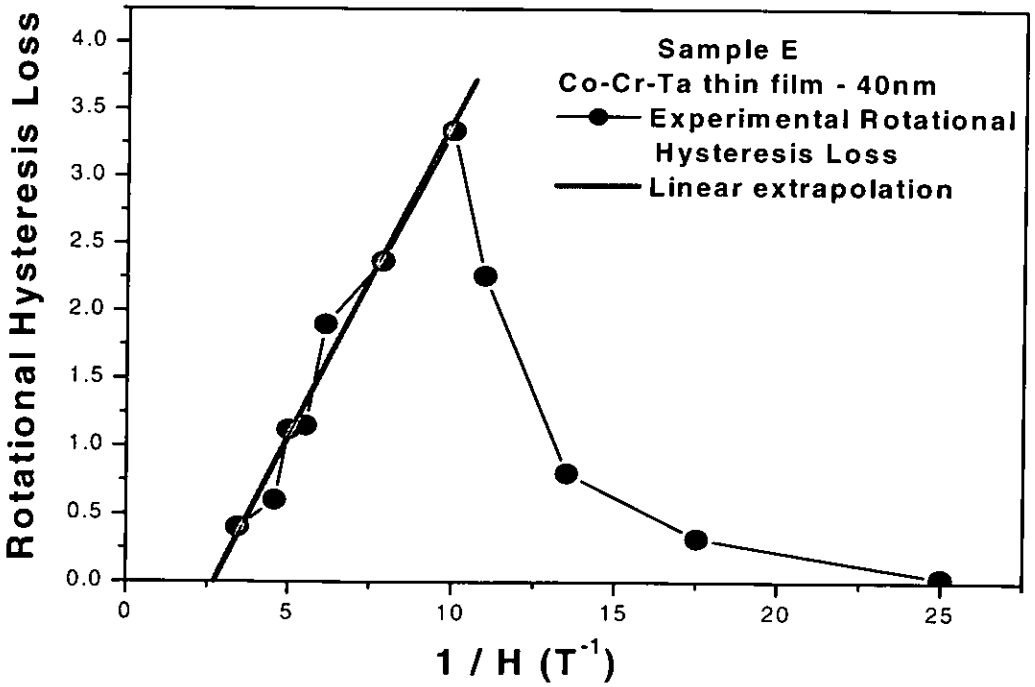

Figure 3.19 Rotational hysteresis loss as a function of the reverse field for the thin film sample E and the linear extrapolation for H_a determination.

The magnetic properties of Co-Cr-Ta thin films are very interesting due to their particular preparation method by transfer deposition (see Appendix 2). In figures 3.19 to 3.22 there are represented the rotational hysteresis loss for the four Co-Cr-Ta thin films.

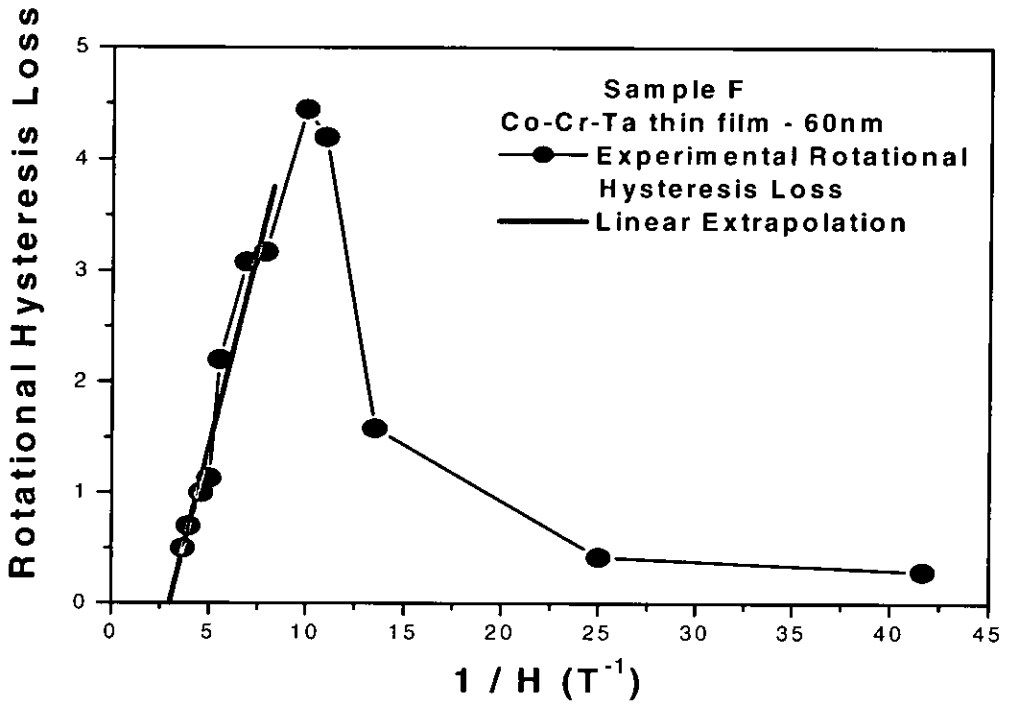

Figure 3.20 Rotational hysteresis loss as a function of the reverse field for the thin film sample F and the linear extrapolation for H_a determination.

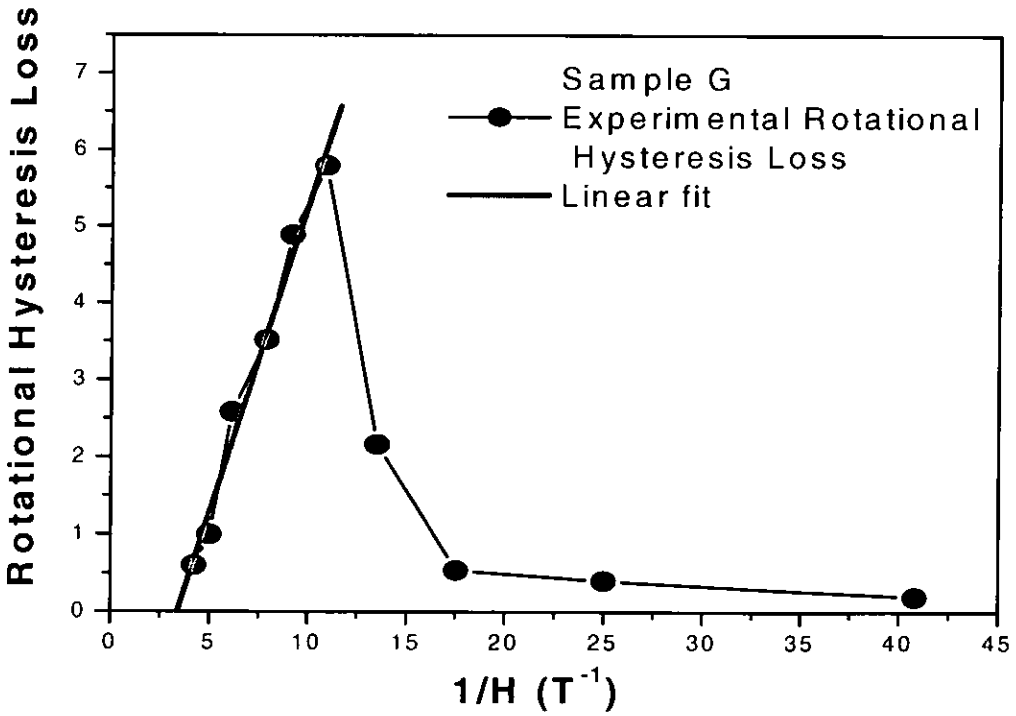

Figure 3.21 Rotational hysteresis loss as a function of the reverse field for the thin film sample G and the linear extrapolation for H_a determination.

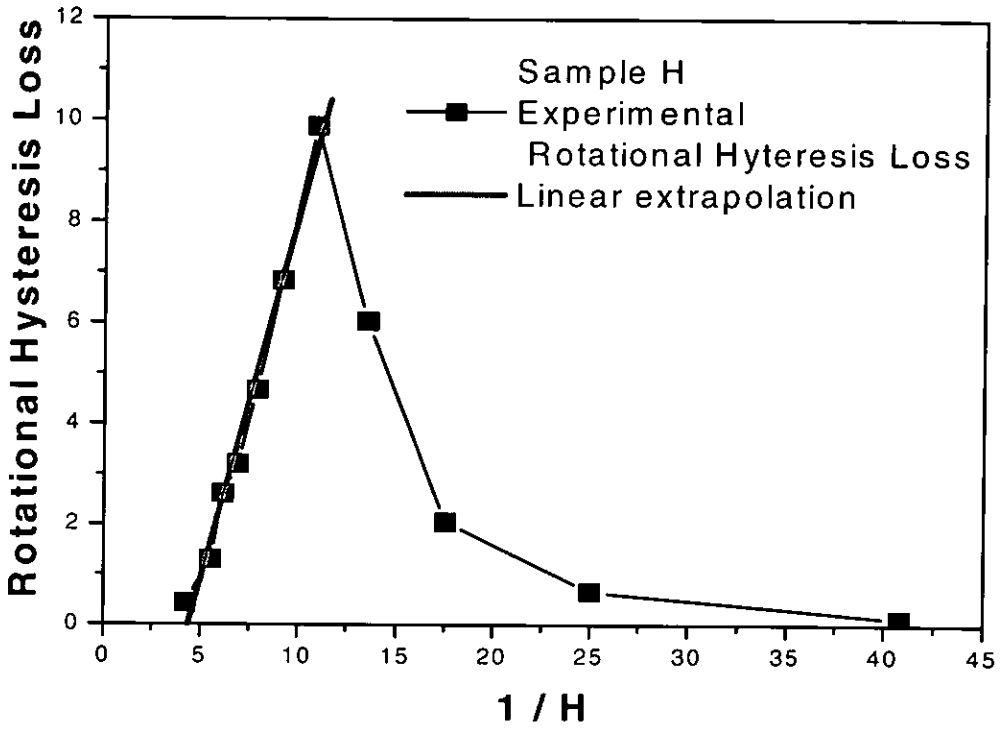

Figure 3.22 Rotational hysteresis loss as a function of the reverse field for the thin film sample H and the linear extrapolation for H_a determination.

The anisotropy fields derived from the linear extrapolation in the RH loss curves are summarised in the table 3.3.

Table 3.3 Anisotropy fields, obtained using rotational hysteresis technique, for the series of Co-Cr-Ta thin film samples

Samples	Co-Cr-Ta thin films			
	E	F	G	H
Anisotropy field H_a (mT)	360	330	290	220

The measured anisotropy fields corresponding to the thin film samples also have a variation with the magnetic thickness but, unlike the particulate tapes, they show the opposite behaviour i.e. the thinner the magnetic layer, the higher the anisotropy field (see figure 3.23).

This is a direct effect of the positive exchange interactions that are dominant in these thin film media. Although the exchange coupling between neighbouring grains is a positive short-range interaction, it is not obvious why the strength of the exchange coupling should be thickness dependent.

The explanation for that comes from the preparation procedure (see also Appendix 2). These thin films are prepared using transfer deposition and this will facilitate the formation of a bowed columnar structure that would generate strong exchange anisotropy effects. Since the preparation time and the transit of the substrate in front of the target is fixed, as the magnetic layer gets thicker, the columnar structure becomes less bowed and reduces the in-plane anisotropy. This also reduces the strength of the positive exchange coupling.

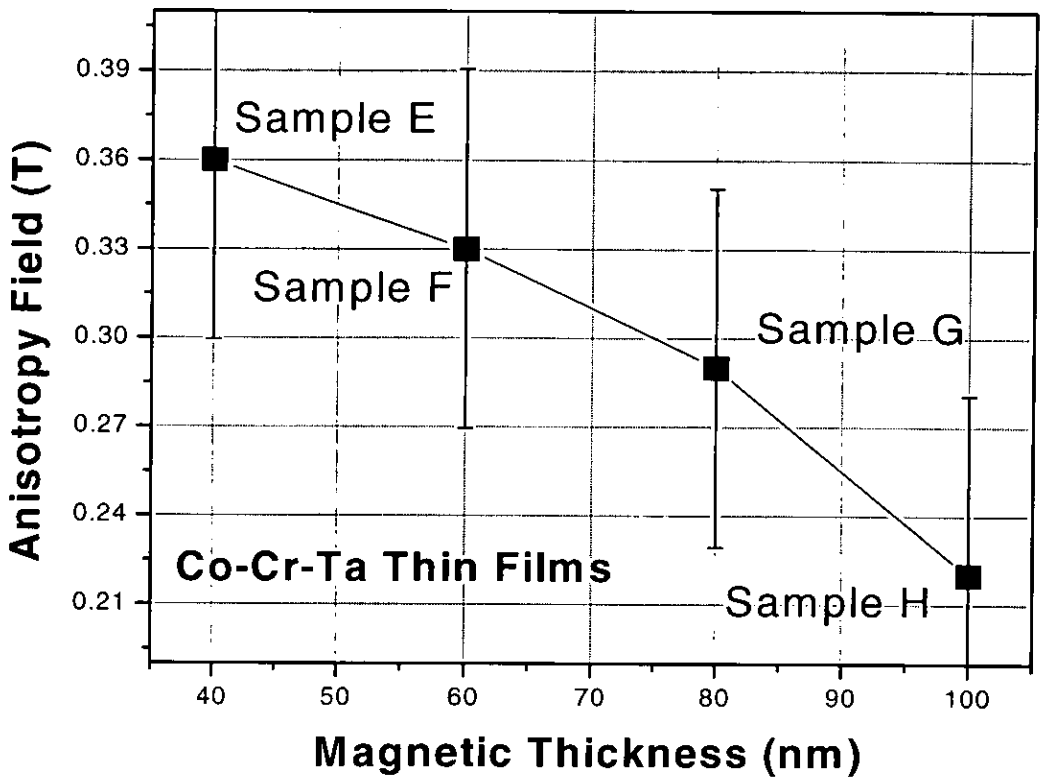

Figure 3.23 Anisotropy field variation with respect to the magnetic thin film thickness. The thinner sample, the higher the anisotropy field. The error bars are evaluated from the standard deviation of the data giving a precision of ± 60 mT.

The change in the strength of the coupling is also confirmed by the remanence curves shown in figures 3.24 and 3.25, where the strongest positive interactions are for the thinnest Co-Cr-Ta thin film.

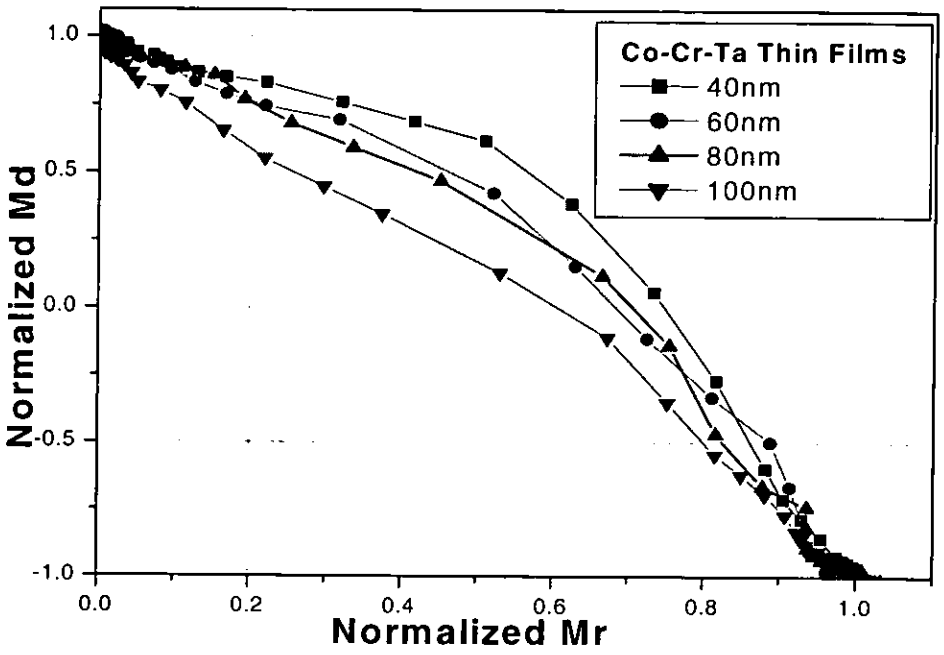

Figure 3.24 Henkel plots for the remanence measurements in the direction parallel to the applied field (longitudinal remanence measurements). The positive deviations indicate the presence of positive local exchange interactions within the analysed media.

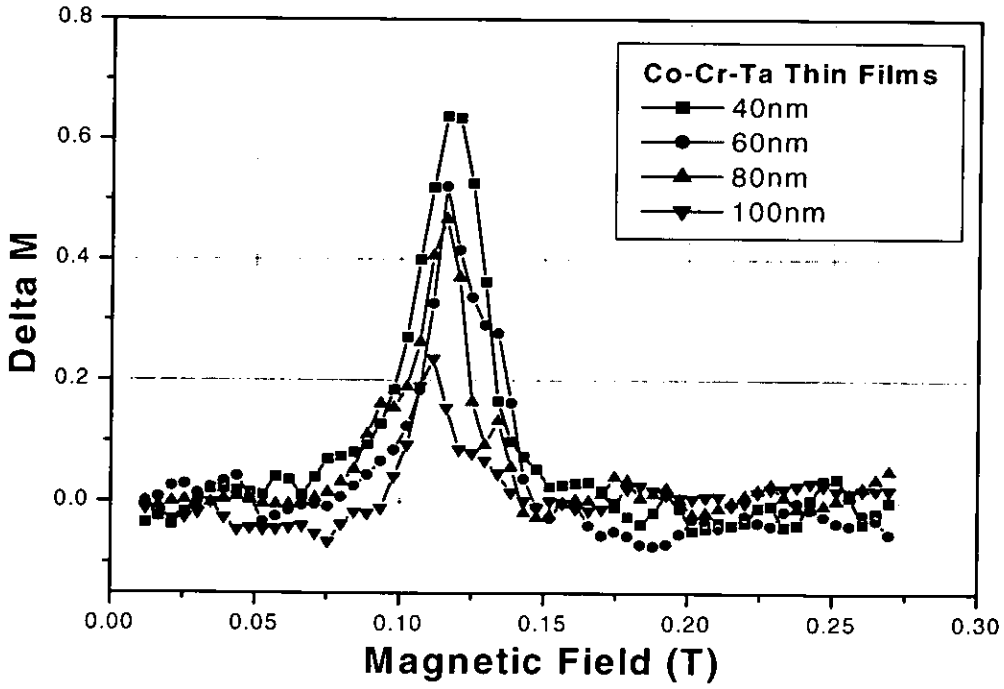

Figure 3.25 Delta M plots. The positive peaks indicate the presence of positive local exchange interactions within the analysed media.

Another reason for the enhanced exchange anisotropy in thinner films could be the effect of the Cr underlayer on the crystallographic properties of the Co-Cr-Ta thin film [36]. It's been proved that Cr microstructure influences the grain morphology and the crystallographic texture of the sputtered magnetic film [37]. Consequently a thicker magnetic layer will suppress the effect of Cr underlayer on the in-plane anisotropy properties of the sputtered film.

3.4 Summary

The topic of this chapter is the anisotropy field. A review of the most popular techniques for magnetic anisotropy measurements has been presented within this chapter together with some theoretical aspects of this topic.

Two experimental techniques have been introduced and described in detail: Transverse remanent magnetometry and rotational hysteresis. Transverse remanent magnetometry is an original extended technique that has been developed and improved first time as part of this project [see also ref. 29]. The two experimental methods have been successfully applied for two sets of different samples. Results obtained from the two techniques corresponding to the tape samples are in good agreement. Experimental data have been discussed and reliable explanations were produced. The remanence experimental curves and theoretical studies [31] support the achieved results.

The two techniques described are related to each other since both are experimental methods based on switching of the particle moments. The measured magnetic anisotropy fields are only a kind of effective anisotropy field because they contain also the interaction effects. It has been proved that there is a clear relationship between magnetic anisotropy and magnetic interaction and that should be carefully considered in any magnetic recording studies.

The presented techniques will produce anisotropy fields either higher or underestimated, depending on the dominant interactions within the analysed medium. The overestimation of the H_a determined from rotational hysteresis method has been also experimentally observed and reported by Inaba et al. [38]. However, the information

obtained is still valuable since it represents magnetic anisotropy properties of a real medium.

Although both experimental methods are based on switching, they have significant differences, advantages and disadvantages from each other. It is very important to know exactly what technique is suitable for use, depending on the sample and also what are the limitations of one particular experiment. In the following, a summary of the main advantages and disadvantages of the two techniques is described in order to offer a fuller picture of these two experimental tools.

Extrapolated transverse remanent magnetometry

Advantages

- Easy to apply on a vector VSM or even a conventional VSM if either the sample or the field can be rotated through controlled angles
- Gives a more accurate value for the anisotropy field
- Gives also the anisotropy field distribution
- It is suitable for extensions that allow demagnetising field measurements and non-destructive magnetic thickness calculations (see chapter 4, section 4.2.1)

Disadvantages

- Applicable only to samples that contain orientated particles or grains and non-applicable on randomly oriented media
- It requires some data processing after the experiment
- Very difficult to apply on extremely thin samples (less than 30nm thickness) with very small magnetic moment
- As a switching technique will incorporate in the anisotropy fields the interaction effects

Rotational Hysteresis

Advantages

- A very simple technique and easy to implement on any VSM or torque magnetometer

- Applicable to any kind of magnetic samples: poly-crystals, single-crystals, amorphous materials and magnetic recording media
- Applicable to recording media containing both orientated and non-orientated particles/grains
- When applied on a torque magnetometer, for recording media studies, it provides information not only about the anisotropy field but also about the reversal mechanism taking place in the single domain particles (via a parameter called: rotational hysteresis integral). In principle this information is available from vector VSM measurements but requires additional data manipulation steps, which increases errors.

Disadvantages

- It requires initial study of the samples (i.e. a prior knowledge of some magnetic properties such as coercivity field or saturation magnetisation)
- It's a very time consuming experiment
- Very difficult to apply on extremely thin samples (less than 30nm thickness) with very small magnetic moment
- As a switching technique will incorporate in the anisotropy fields the interaction effects

4. Measurement of the demagnetising field in recording media and its applications

4.1 Introduction

With the development of new generations of magnetic recording media, measurement of magnetic coating thickness using mechanical techniques has become almost impossible. Other techniques such as electron microscopy require specially prepared samples and introduce uncertainty through mechanical damage during preparation. These difficulties are related to the extremely thin magnetic coatings and also to the presence of multiple layers and coatings in recording media, as those in double-coated MP tapes where only the top layer is magnetic or Co-Cr-Ta thin films deposited on Cr substrates and silicon wafers (see Appendix 2).

In this chapter an alternative non-destructive magnetic technique for thickness measurements and true magnetisation calibration is presented. The method is based on the measurement of the demagnetising field acting normal to the sample plane and has been previously described [1] for transverse AC susceptibility measurements. This involved measurement of the sheet-demagnetising field of a tape sample by observing the transverse AC susceptibility anisotropy peak with an applied DC field in-plane and out-of-plane. The position of the peak is very closely associated with particles with an orientation in the AC field direction so that the shift of the peak between the two measurements can be taken to be the difference in the demagnetising fields experienced by these particles for the two DC field applications. This allows corresponding VSM hysteresis loop measurements to be calibrated in terms of magnetization. When combined with the usual calibration for total moment against a reference sample and the known area of sample, then the thickness can be determined as well as magnetisation rather than the total moment.

Here the principle of this technique is extended to other magnetic properties of recording media samples that have features specifically related to the applied magnetic

field, which can be applied parallel and perpendicular to the plane of the tape. Based on this, two further methods have been added to the transverse susceptibility measurement. They have been first introduced in this PhD thesis and these are:

1) Extended remanent rotational magnetometry, which involved the switching of particles perpendicular to an applied field direction

2) Comparison of the closure point of the transverse and perpendicular hysteresis loops

Results from these two additional methods are described in reference [2] where they are also compared with transverse susceptibility measurements. All three methods gave comparable values for magnetic layer thickness. In the next sections the two methods for demagnetising field measurement are introduced followed by the section that describes their applications.

4.2 Demagnetising field measurements

4.2.1 Demagnetising field derived from the transverse remanent magnetometry

A method for demagnetising field measurements has been developed from the transverse remanent magnetometry technique, which has been introduced in the section 3.2.1. The method for the in-plane anisotropy field measurements [3] has been conveniently extended to alternative out-of-plane anisotropy field determination. The out-of-plane experiments were carried out following the same remanent magnetometry technique except that the method was repeated with the applied field pointing out of the sample plane. The difference between the two in-plane and out-of-plane anisotropy field values gives the demagnetising field acting perpendicular to the sample plane, as will be discussed in this section.

Figure 4.1 shows the anisotropy peak values for both in-plane and out-of-plane components, corresponding to one thin film test sample using the extrapolated transverse remanent magnetometry technique. The intersection points of the two linear fitting lines with the field axis give the most accurate value for the anisotropy field. It can be seen that the line corresponding to the out-of-plane component has a bigger

slope. The anisotropy peak value for the out-of-plane component is shifted to a higher value, H_{a2}, by the rotation of the DC field, which is applied perpendicular to the sample plane. The anisotropy shift is mainly associated with the demagnetising field, $H_D = H_{D2}$, acting perpendicular to the sample plane.

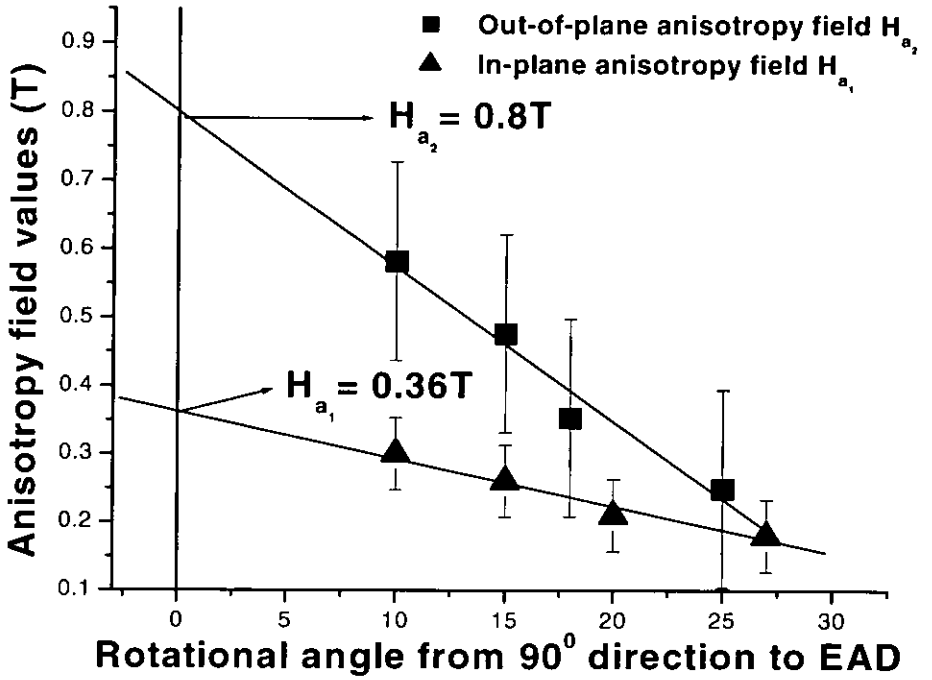

Figure 4.1 In-plane and out-of-plane anisotropy fields plotted as a function of the rotation angle, using the extrapolated transverse magnetometry. The linear extrapolations show the real anisotropy field at the intercept with the field axis. This example is for a Co sputtered thin film disk. The error bars are evaluated from the standard deviation of the data.

This is based on the fact that the anisotropy field of the particles is the same for both orientations (i.e. the in-plane components are rotated through 90^0 for the out-of-plane measurements) and the in-plane demagnetisation factor is 0 for an infinite sheet. In fact, the intersection points of the two linear fits with the field axis give the values of the anisotropy field plus the demagnetising field, for both in-plane and out-of-plane orientations. Mathematically, it can be written as:

$$H_{a1} = H_{k1} + H_{D1} \quad \text{and} \quad H_{a2} = H_{k2} + H_{D2} \tag{4.1}$$

where:

- H_{a1} and H_{a2} are the in-plane and out-of-plane anisotropy peaks;
- H_{k1} and H_{k2} are the in-plane and out-of-plane anisotropy fields;
- H_{D1}, H_{D2} are the demagnetizing fields acting on both directions;

Assuming that all the particles are identical, the anisotropy fields for the two orientations should be the same:

$$H_{k1} = H_{k2} = H_k \tag{4.2}$$

Therefore, according with relations (4.1) and (4.2), the difference between the two-anisotropy peak values becomes:

$$H_{a2} - H_{a1} = H_{D2} - H_{D1} \tag{4.3}$$

But, the demagnetizing field is defined as: $H_D = N_D M$. Hence, we can write:

$$H_{a2} - H_{a1} = N_{D2}M_2 - N_{D1}M_1 \tag{4.4}$$

where: $N_{D1,2}$ are the demagnetizing factors for the two orientations and they are functions of the shape and the orientation of the sample.

The analysed samples are either squares or disks with the dimension about L = 1cm. The magnetic thickness of the samples is of h ~10^2nm order (see figure 4.2).

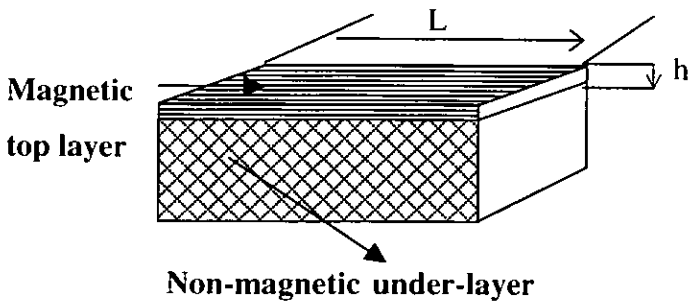

Figure 4.2 A section through a double-coated MP tape showing the magnetic coating and the non-magnetic under-layer.

It is obvious that L >> h and our samples can be approximated, and, in particular, magnetic recording media, with an infinite plane. For an infinite sheet uniformly

magnetized, the demagnetization factor for in-plane direction is 0 ($N_{D1} = 0$) and for out-of-plane is 1 ($N_{D2} = 1$). Hence the relation (4.4) becomes:

$$H_{a2} - H_{a1} = H_{D2} = N_{D2}M_2 = H_D \qquad (4.5)$$

The relation (4.5) reveals that by measuring the in-plane and out-of-plane anisotropy fields, it is possible to derive the demagnetizing field.

Although the out-of-plane demagnetising factor is generally accepted as 1 for an infinite sheet, is has been theoretically shown [4] to be different than 1 for current media and generally the particulate nature does alter the demagnetising factor by about 7%.

4.2.1.1 Experimental results

This extended technique has been applied for the series of four MP tape samples. Figures 4.3 to 4.6 show the experimental results for the four analyzed samples.

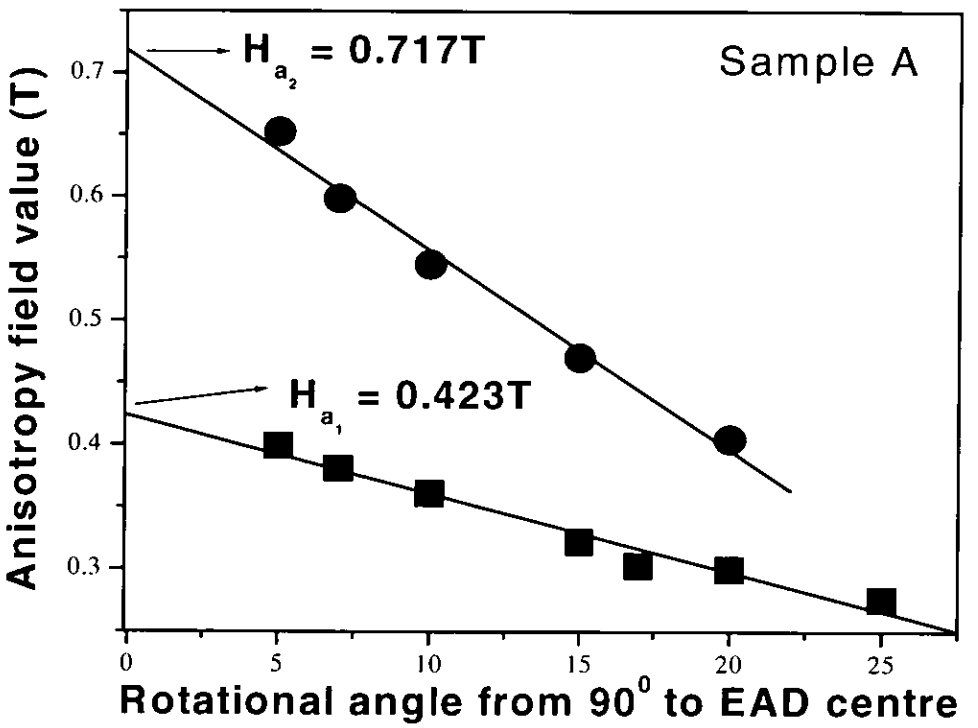

Figure 4.3 Linear extrapolations of the experimental data, showing the two in-plane and out-of-plane anisotropy fields corresponding to sample A.

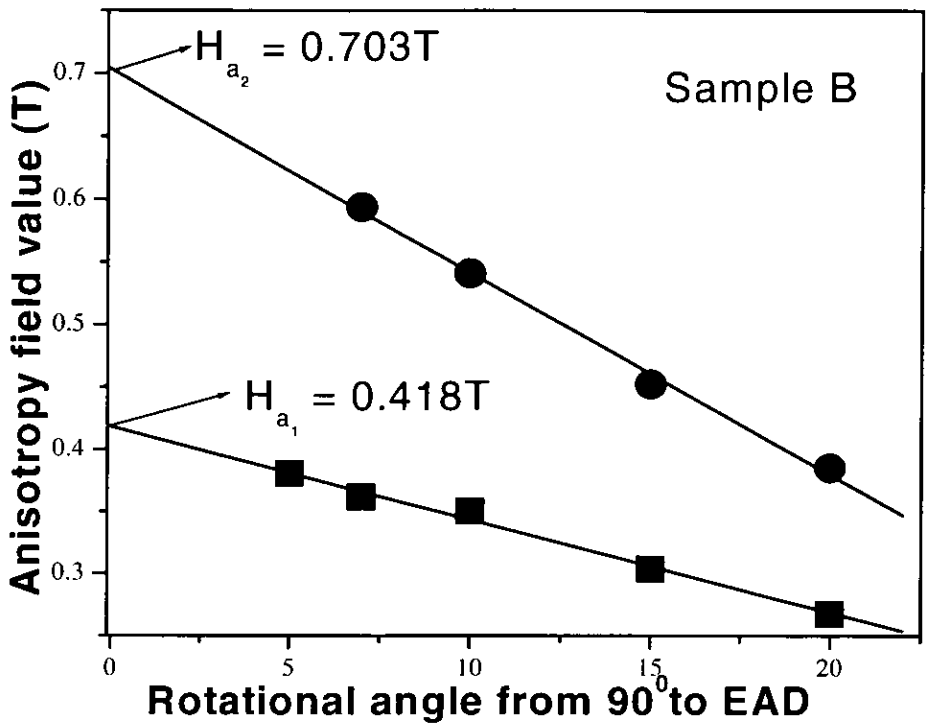

Figure 4.4 Linear extrapolations of the experimental data, showing the two in-plane and out-of-plane anisotropy fields corresponding to sample B.

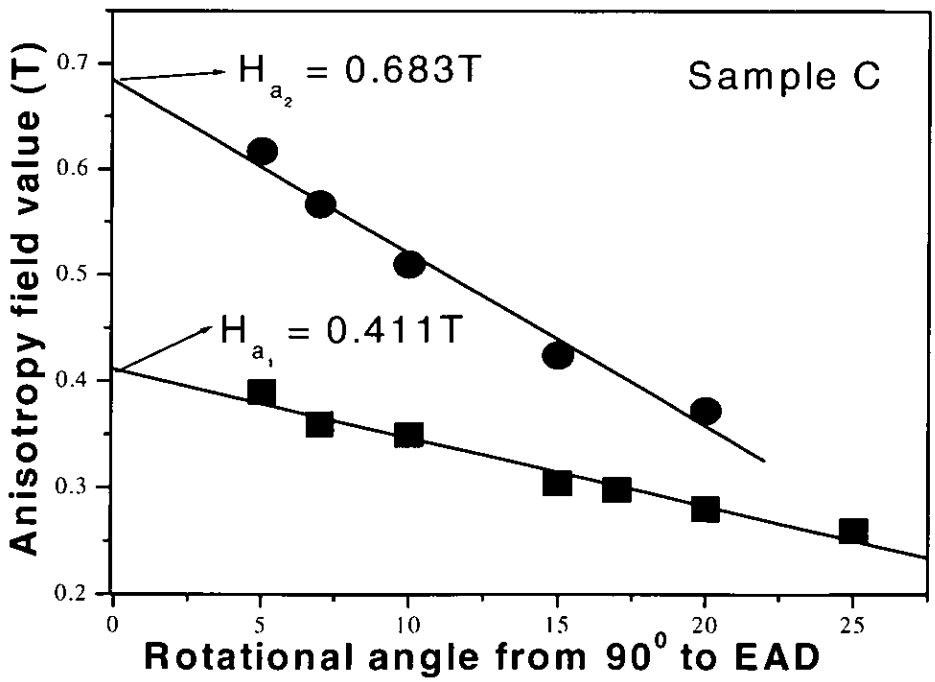

Figure 4.5 Linear extrapolations of the experimental data, showing the two in-plane and out-of-plane anisotropy fields corresponding to sample C.

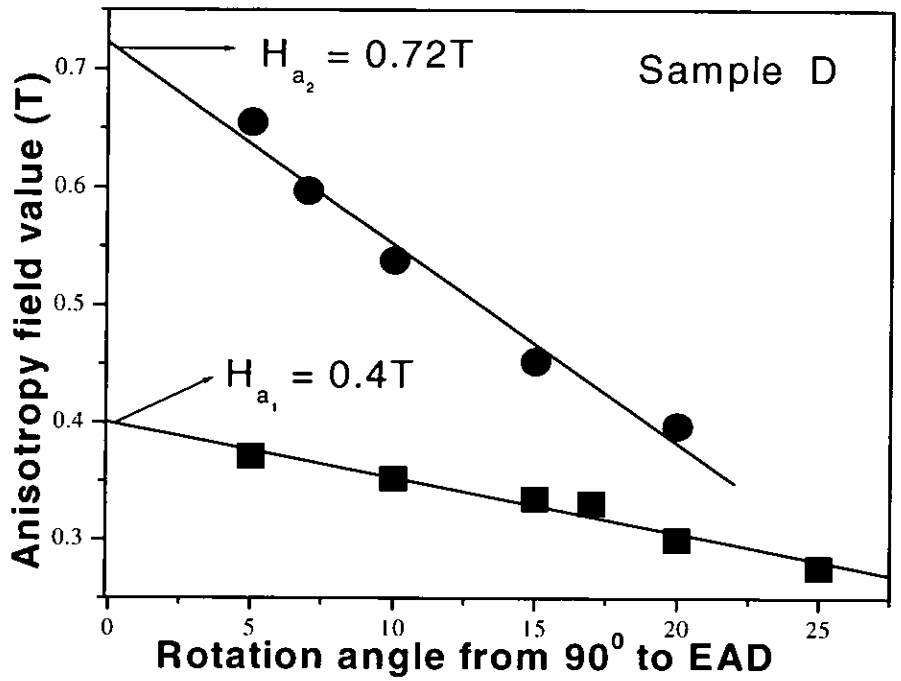

Figure 4.6 Linear extrapolations of the experimental data, showing the two in-plane and out-of-plane anisotropy fields corresponding to sample D.

The demagnetizing fields have been derived using equation (4.5) and are presented in table 4.1. It is shown in the next section that these are consistent with the results obtained from the second experimental method.

Table 4.1 The experimental in-plane / out-of-plane anisotropy fields and the corresponding demagnetising fields for the MP tapes series.

Sample codes	In-plane anisotropy H_{a1} (mT)	Out-of-plane anisotropy H_{a2} (mT)	Demagnetizing field H_D (mT)
A	423	717	294
B	418	703	285
C	411	683	272
D	400	720	320

4.2.2 Demagnetizing field calculation from hysteresis loop measurements

The second method was performed on a standard VSM and involved measurement of the in-plane and out-of-plane hysteresis loops of a sample. The closure points of the loops were determined and compared for in-plane and out-of-plane loops. The difference was again related to the demagnetizing field. A hysteresis loop will close at a field when all the particles have switched. For Stoner Wohlfarth particles, this will correspond to the reversal of the particles with the largest anisotropy field and with their easy axes aligned with the applied field direction. In this case, unlike the anisotropy field determination techniques, the closure points measured in-plane and out-of-plane will be determined by different particles. However, the particles that reverse incoherently, which is likely to be the case for current recording particles, those with the highest coercivity are likely to be at 90^0 to the field direction [5,6]. This would mean that the closure point of the two loops again corresponds to the same particles and makes the techniques consistent with transverse susceptibility and the extrapolated transverse remanent magnetometry. This is also confirmed by checks on the closure points of in-plane aligned and transverse loops, which indicate that results are consistent with the other technique within experimental error.

Figures 4.7 to 4.10 show an in-plane transverse and out-of-plane hysteresis loops. The difference in the field values for the closure points is taken as the difference in the demagnetizing fields of the sample. If the H_1 is the closure point for the in-plane hysteresis loop and H_2 is the closure point for the out-of-plane hysteresis loop, then the demagnetizing field is given by:

$$H_D = H_2 - H_1 \qquad (4.6)$$

The method is also original and has the advantage that it can predict with reasonable accuracy the value of the demagnetising field starting from the in-plane and out-of-plane hysteresis loops. Because it is accessible and easy to experiment in any magnetism laboratory, this technique has practical application. Unlike the previous method, or the transverse susceptibility technique, where the demagnetising field is

measured as the difference between the effective in-plane and out-of-plane anisotropy fields, in this case the demagnetising field is determined by measuring and comparing the closure points of the in-plane transverse loop and out-of-plane hysteresis loop (figures 4.7 to 4.10), on the basis that these represent the upper end of the switching-field distribution for the particles that lie nearly perpendicular to the field direction.

4.2.2.1 Experimental results

The transverse in-plane and out-of-plane loops for the MP tape series have been measured and the closure points have been identified (see figures 4.7 to 4.10). Although this process seems very straightforward, in fact is more complicated and requires a lot of preparation prior to finding the closure points.

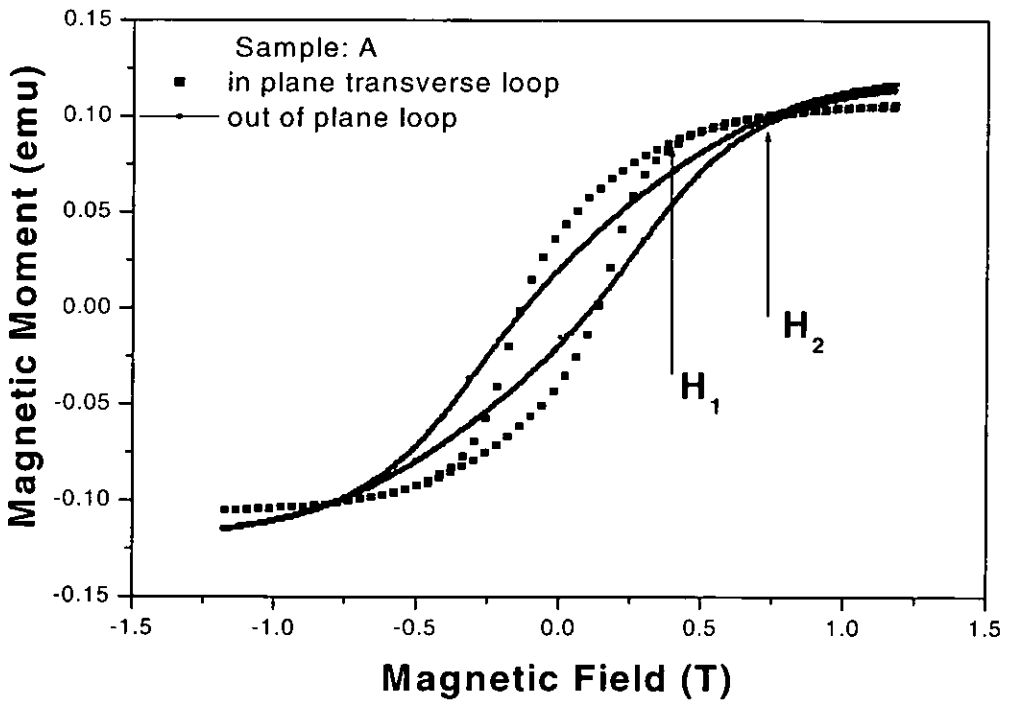

Figure 4.7 In-plane and out-of-plane loops for sample A, showing the corresponding closure points.

The raw data corresponding to the part of the loop between remanence and saturation is separated from the main loop and then interpolated / fitted by an appropriate function, in order to increase the accuracy of the method.

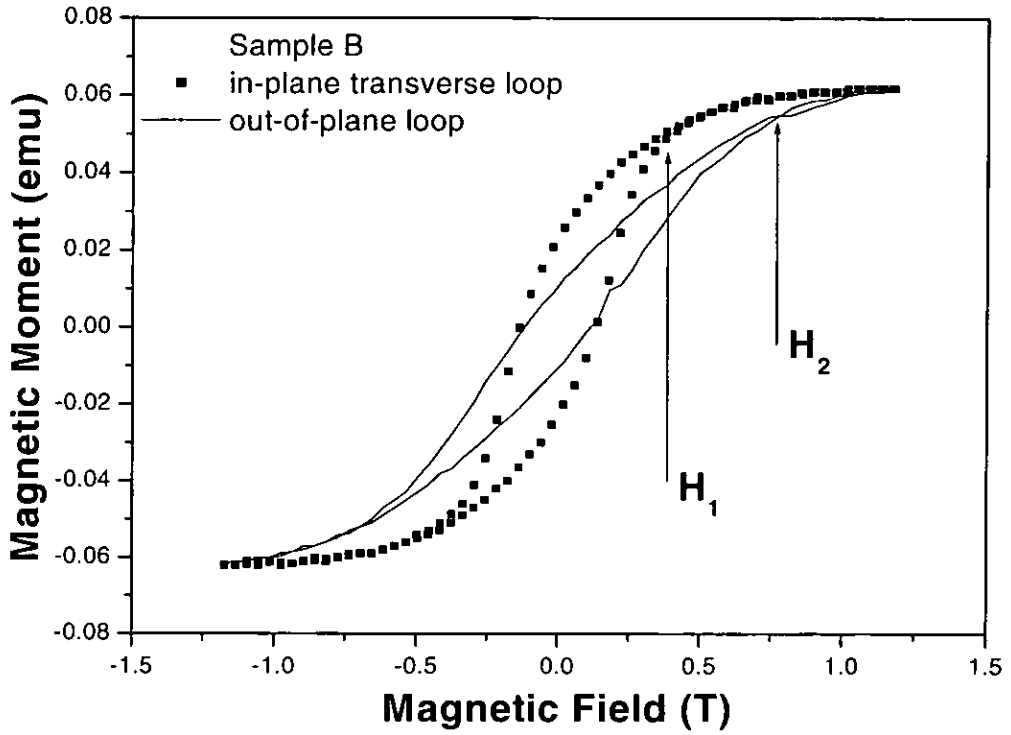

Figure 4.8 In-plane and out-of-plane loops for sample B, showing the corresponding closure points

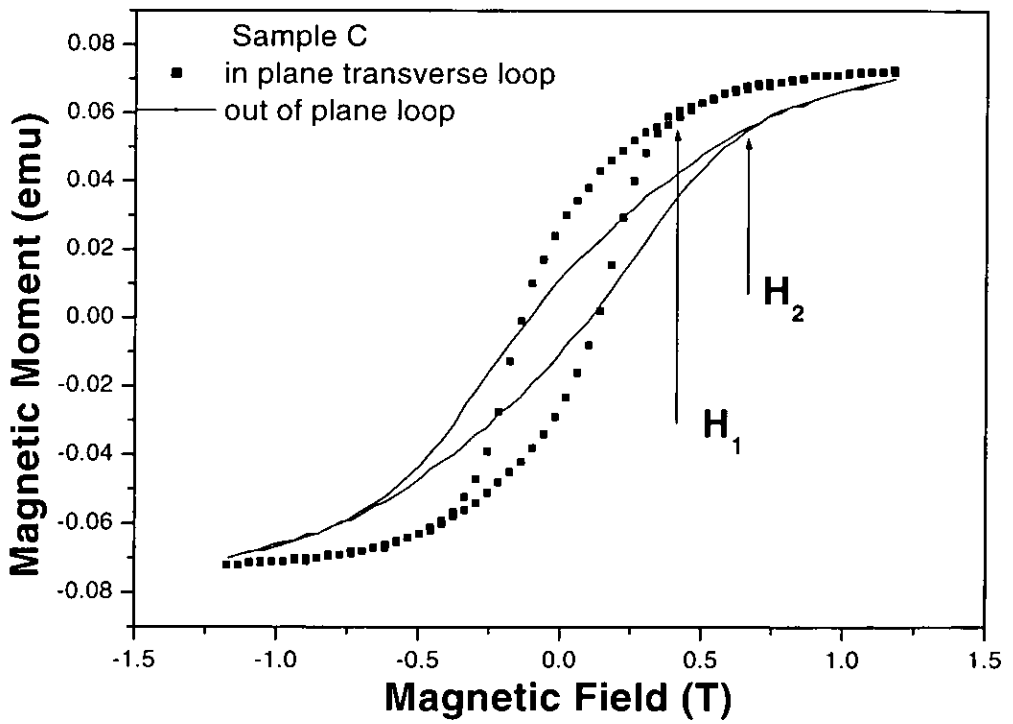

Figure 4.9 In-plane and out-of-plane loops for sample C, showing the corresponding closure points

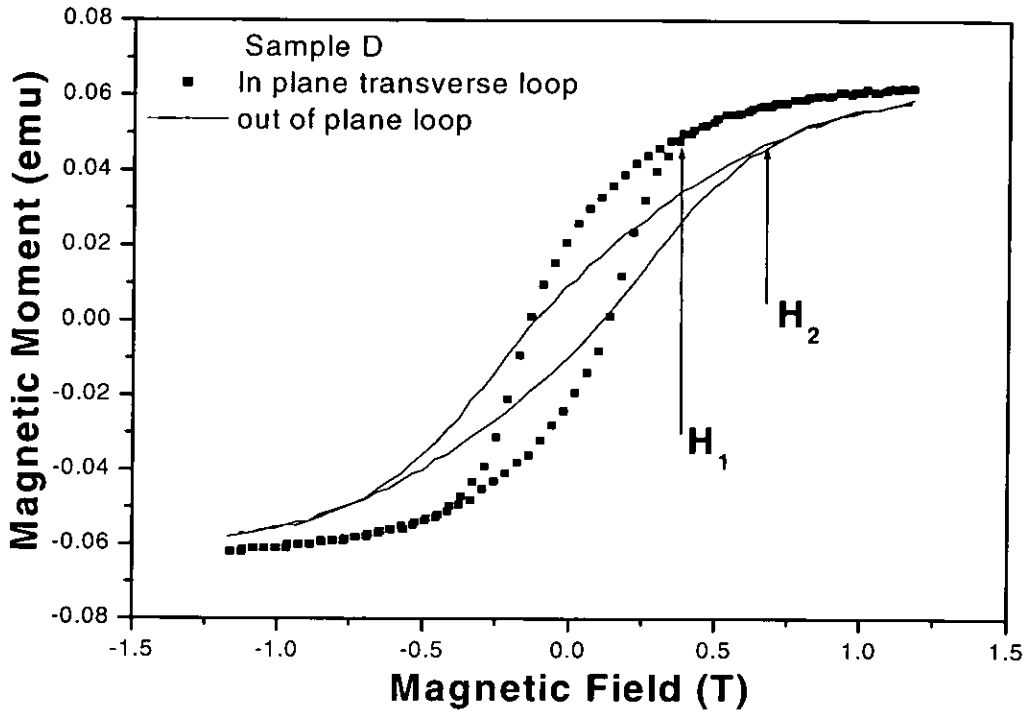

Figure 4.10 In-plane and out-of-plane loops for sample D, showing the corresponding closure points

Table 4.2 gives the results for all four MP tape samples analysed for demagnetising field using the two methods. Supplementary, the data is compared with those obtained from transverse susceptibility measurements [2]. The results from the three different techniques are in good agreement.

Table 4.2. Comparison between the demagnetizing fields calculated from the two methods described in this chapter and from transverse susceptibility*.

Sample codes	In-plane closure H_1 (mT)	Out-of-plane closure H_2 (mT)	Demagnetizing field (closure point) H_D (mT)	Demag. field (trans.magnetom) H_D(mT)	Demag. field (trans.suscept.) H_D(mT)
A	426	723	297	294	284
B	459	726	267	285	267
C	421	710	289	272	261
D	463	750	292	320	301

*Measured by R.D. Cookson

4.3 Applications of the demagnetizing field measurements

4.3.1 True magnetisation calibration and demagnetising field correction

Knowing the demagnetising field offers the possibility to calculate and calibrate a hysteresis loop in terms of true magnetisation (kA/m) rather than (emu/cm^2). Very often it is also required to calculate certain magnetic parameters for the out-of-plane orientation (i.e orientation ratio – OR) and that demands, for higher accuracy, the demagnetising field correction. Another important application of the demagnetising field measurements is the magnetic thickness calculation, which will be discussed in section 4.3.2.

By applying one of the two described techniques for demagnetising field measurements and using again the relation 4.5 ($H_{a2} - H_{a1} = H_D = N_D M_2$), the transformation relation for the true magnetisation and the effective field can be derived. On the out-of-plane loop the magnetic moment corresponding to the field H_{a2} is identified as μ_2 (emu). The magnetisation of the sample at the field H_{a2} is also $M_2 = H_D/N_D$ (kA/m). A calibration factor "f" can now be defined in order to transform the magnetisation data of the hysteresis loop from (emu) units to (kA/m): $f = M_2/\mu_2$ and the transformation relation is:

$$M = \mu \cdot f = \mu \frac{M2}{\mu_2} = \mu \frac{H_D}{N_D \mu_2} \tag{4.7}$$

where: M is the wanted magnetisation data in kA/m and μ is the measured magnetisation data in emu. For the infinite sheet approximation $N_D=1$ and the relation (4.7) becomes:

$$M = \mu \cdot f = \mu \frac{M2}{\mu_2} = \mu \frac{H_D}{\mu_2} \tag{4.8}$$

As mentioned before, the out-of-plane loop is affected by the demagnetising field and very often it is important to apply the appropriate demagnetising corrections. If the H_{app} is the external field exerted by the VSM and H_{eff} is the field, in which the sample is subjected after demagnetisation correction, then the transformation relation is:

$$H_{eff} = H_{app} - M \tag{4.9}$$

where M is the internal polarisation of the sample due to the demagnetising field corresponding to a certain value of the applied field. By combining the relations 4.8 and 4.9, the effective field is derived:

$$H_{eff} = H_{app} - \frac{\mu}{\mu_2} H_D \tag{4.10}$$

Figure 4.11 gives an example of a corrected hysteresis loop for the demagnetisation field using the transformation 4.10.

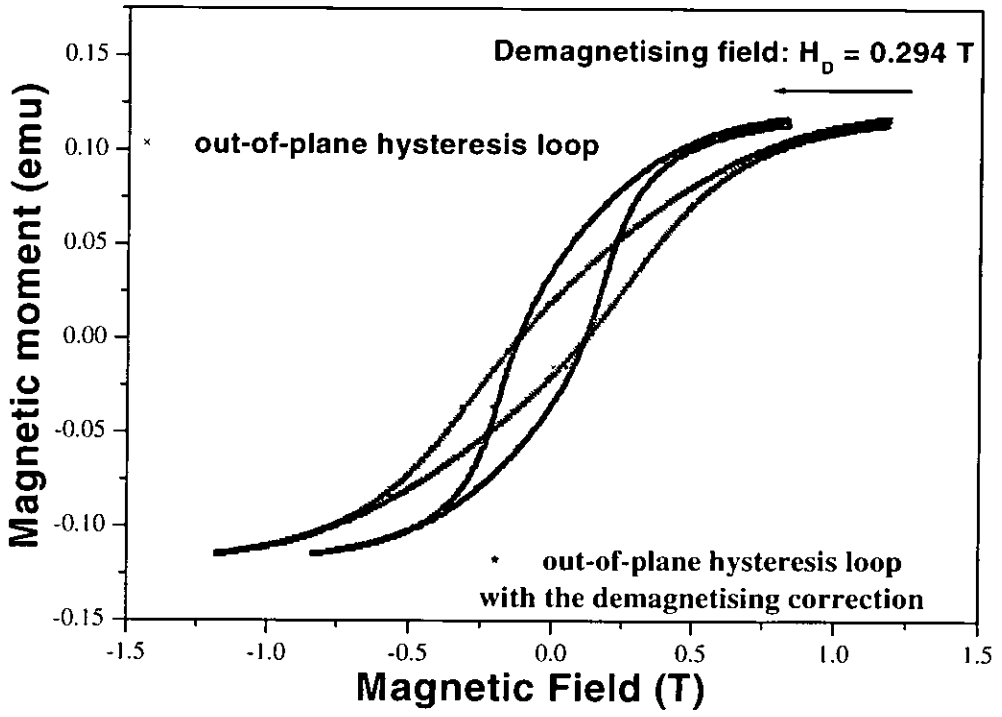

Figure 4.11 Example of corrected and un-corrected out-of-plane hysteresis loops corresponding to sample A.

4.3.2 Magnetic thickness calculation

The ability to measure the magnetic coating thickness in magnetic recording media is very important, especially with the development of the high-density media where the particles are smaller and the magnetic coatings are thinner. Based on the new described techniques for demagnetizing field measurements, which have been introduced in the

previous sections, an alternative non-destructive magnetic technique for measuring the magnetic coating thickness has been developed. The idea has been described previously [Bissell, 1991], where transverse susceptibility measurements were used for demagnetizing field and magnetic thickness determination on CrO_2 systems.

By using the extrapolated transverse remanent magnetometry technique, as described in the section 4.2.1, the demagnetizing field can be measured according to the relation (4.5). Therefore, by placing a sample in a VSM so that the applied field is perpendicular to the sample plane and equal to H_{a2}, the sample magnetic moment, μ_2, can be measured (see figure 4.11). If V is the sample volume, A is the sample area and t is the thickness then:

$$\mu_2 = V \cdot M_2 = t \cdot A \cdot M_2 \qquad (4.7)$$

and the magnetic thickness is:

$$t = \mu_2 / A \cdot M_2 \qquad (4.8)$$

16 layers of $1cm^2$ samples with a total area of $16cm^2$ were used for experiments. A calculation example is given for sample A for which the demagnetizing field measurement is shown in figure 4.3 and the out-of-plane hysteresis loop is shown in figure 4.12.

The following experimental data have been extracted:

$H_{a1} = 423$ mT, $H_{a2} = 717$ mT and $H_D = H_{a2} - H_{a1} = 294$ mT

which according to relation (4.5) gives a corresponding value for magnetization: M_2 = 234 kA/m (234 emu/cm^3).

Comparison with the magnetic moment, $\mu_2 = 0.098$ emu, measured at the field H_{a2} = 717 mT gave a calculated tape magnetic thickness of t = 0.26 μm corresponding to sample A.

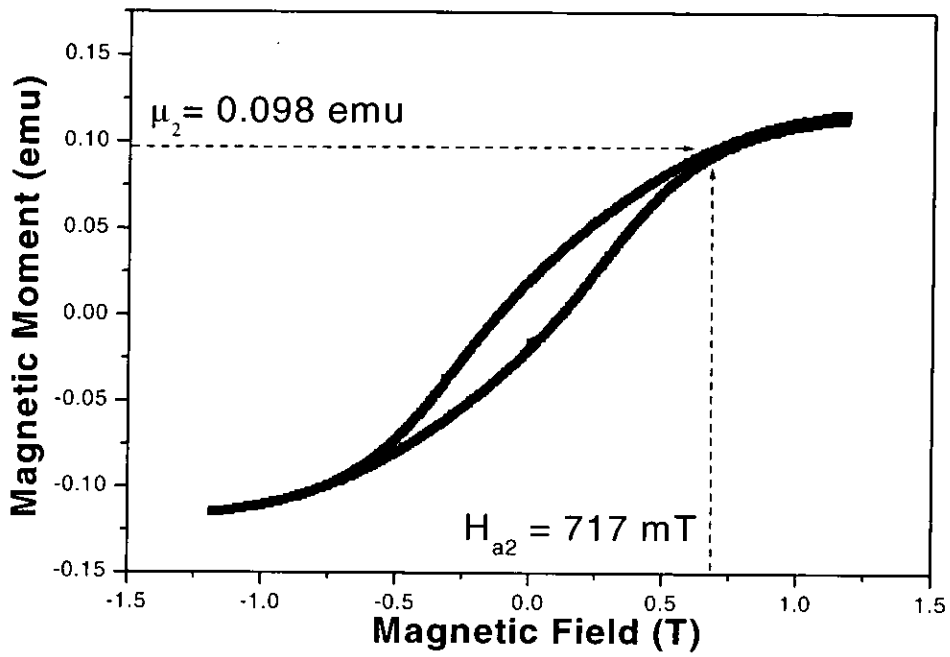

Figure 4.12 Example of identification of the magnetic moment corresponding to an applied field equal to the out-of-plane anisotropy field, on the out-of-plane hysteresis loop.

Table 4.3 shows the results for magnetic thickness calculation and the Mrt* values corresponding to the four MP tapes. The results were obtained using the transverse remanent data and they are in good agreement with the sample characteristics.

Table 4.3 Magnetic thickness and Mrt* values calculated from transverse remanent magnetometry and closure point method data.

Samples Code	Mrt (memu/cm^2)	Calculated Mrt (memu/cm^2)	Magnetic thickness (trans. magnetometry) (μm)	Magnetic thickness (closure point) (μm)
A	6	5.73	0.261	0.250
B	4.5	4.47	0.190	0.155
C	4	3.92	0.171	0.152
D	3	3.12	0.120	0.131

* Mrt parameter represents the saturation remanent magnetization multiplied by magnetic thickness (Mrt = $M_r \times t$). The Mrt values in the second column are the values

provided by the manufacturer and the Mrt values in the third column are those calculated after the magnetic thickness had been determined.

The closure point technique is also applicable to magnetic thickness calculation. In this case however, the magnetic thickness is derived by identifying the magnetic moment μ_2 corresponding to the closure field H_2 on the out-of-plane hysteresis loop.

Figure 4.13 shows the magnetic thickness calculated from the two techniques as function of Mrt values. The results are in good agreement and the magnetic thickness also is directly proportional to the Mrt values. Hence, it is a valid approximation to refer to the Mrt values as a substitute or as a measure of the magnetic thickness (see figure 4.13).

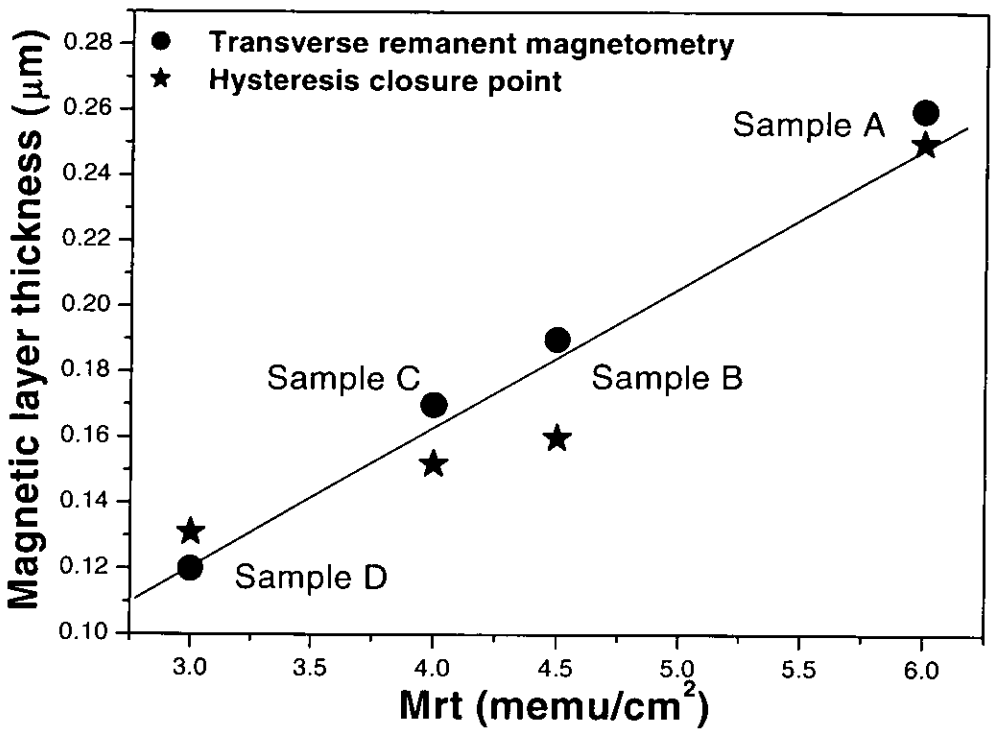

Figure 4.13 Magnetic thickness variation with the Mrt values.

4.4 Summary and discussions

The measurements of the demagnetizing field and magnetic thickness have been discussed in this chapter. Related to this topic, two original experimental techniques for demagnetizing field measurements have been introduced. They can be further used for applications as: magnetic coating thickness calculation, true magnetization calibration and demagnetization corrections. Although results from the two methods compare well, it should be noted that determination of the closure point for hysteresis loops is difficult and is susceptible to a certain amount of subjectivity on the part of the investigator. In addition, all the measurement techniques rely on the assumption that the demagnetizing factor for the sample is that of an infinite sheet. Two aspects of this assumption require some comments:

- First is related to the effect of stacking layers in order to increase the signal to noise ratio. Because the magnetic layer thickness is much less than the spacing between layers (magnetic layer to substrate thickness < 0.03), a simple application of Gauss' Law indicates that the demagnetising field within a magnetic layer is unaffected by magnetic layers other than itself. Thus, stacking of infinite layers has no effect on the sheet demagnetising factor, but for finite sheets, there is an effect resulting from the free edges of the sample. This is small because of the dilution effect of the wide spacing of individual magnetic layers.

- The second aspect refers to the effect of the particulate nature of the magnetic layers where thickness has been reduced to the order of a particle length. This has been the subject of a modelling study [4], which shows that for current media, the particulate nature does alter the demagnetising factor by about 7%. However, this will increase as the magnetic layer thickness is decreased unless there is an equivalent reduction in particle dimensions.

From this comparative study, it can be concluded that the two methods to determine the demagnetising field of the sample give satisfactory results. On the assumption that the demagnetising factor is that of an infinite sheet, which is a good approximation for a

particulate recording media where film thickness is small and has good uniformity, this gives a non-destructive measure of the magnetic layer thickness. Although the measure of the closure points on the hysteresis loops has added experimental errors associated with determination of the closure points and the added assumption about the particle distribution, it is available within any laboratory that has standard vibrating sample magnetometer facilities. This technique therefore provides a useful method for determination of magnetic layer thickness in magnetic tape media.

5. Texture measurements in particulate media

5.1 Introduction and review of the experimental techniques

The degree of particle alignment, or the texture, can be described by the easy axis distribution. The knowledge of the easy axis distribution is beneficial for the recording performances of a medium and is also very important for the interpretation of other magnetic measurements.

For instance, the effect of texturing increases the squareness of the hysteresis loop in the texture axis direction and reduces the switching field distribution (SFD), which is beneficial to recording performance. A magnetic recording medium with randomly orientated particles will have Sq = 0.5 and a very broad SFD. Such a magnetic medium will have poor recording properties characterised by a wide transition width, which will reduce the data densities that can be achieved, will have a small replay signal and a poor signal to noise ratio.

Another example that shows the importance of the EAD, is the calculation of the damping constant of a magnetic tape from ferromagnetic resonance spectra (FRM) measurements. Particle orientation can strongly affect the FRM spectrum and the accurate knowledge of the distribution function can be used to deconvolute the spectrum in order to obtain the damping constant [1].

The easy axis distribution is also extremely important in theoretical micro-magnetic studies, as input data in different simulation programs.

Given the importance of the easy axis distribution in recording media studies, it is clear that a full accurate experimental evaluation of the EAD is required. The experimental determination of the easy axis distribution is the topic of this chapter and has been also widely investigated as subject of many studies and published papers.

5.1.1 VSM based experiments for EAD measurements

In 1960, Shtrickman and Treves first introduced a model for extracting the easy axis distribution from experimental measurements of the angular dependence of remanence [2]. In their technique, the remanence is measured as a function of the angle between the applied field and the easy axis direction, in the plane defined by the easy axis and the applied field. Under the assumption that the orientation distribution is axially symmetric and that the particles are non-interacting, Shtrikman and Treves derived a rather complex solution for the EA distribution as a function of the transverse or parallel remanence signals, involving also a series expansion of Legendre polynomials. A limitation of their technique, as they pointed out, is related to highly orientated samples for which the solution yields inaccurate results.

Following the original Shtrikman and Treves method, el-Hilo et al. [3] have looked at the special case of a two-dimensional distribution. They showed that the distribution function could be written in a harmonic series with coefficients involving integral expansions of the parallel remanent signal, Ip. Although el-Hilo technique is a simplification of the Shtrikman and Treves method, it is still quite complex and an accurate and more straightforward technique for determining the distribution function is desirable. This is also a major part of this chapter and will be discussed in detail in the section 5.2.1.

5.1.2 Torque magnetometry experiments for EAD measurements

Although torque magnetometry is best known as a technique for experimental anisotropy studies, it has been also successfully used for texture measurements. Hoon and Paige [4] have introduced an interesting method for both anisotropy field and orientation distribution measurements. They have used a torque magnetometer to measure the hysteretic loss during forward-reverse cycles of the field orientation. The novelty of the technique lies in measuring the loss over small angular cycles ~ 10^0. The loss, dependent on both the magnitude and the orientation of the field relative to the

particle axis, yields a map of the orientation distribution of the particles and anisotropy fields. They applied the method to random and aligned samples of CrO_2 and Co doped γ-Fe_2O_3.

However, the easy axis distribution can be also derived from torque measurements using Shtrickman and Treves treatment, after suitable processing of the torque data in order to extract only the perpendicular remanent signal, It.

5.1.3 Maximum entropy method for EAD determination

Maximum entropy is a numerical method, which permits solution to positive, linear superposition problems without requiring an initial form of the functional or an absolute value of the solution [5]. Skilling has developed the theoretical algorithm in the reference [6]. The maximum entropy has been used for solving various physical problems involving the determination of a distribution function, starting from a set of experimental data corresponding to a variable that is related to the distribution function. Zolla et al. [6] determined the size distribution of Ni precipitates in Ag-Ni from high field magnetisation curves and using maximum entropy method. J.A. Potton et al. [7] determined the particles volume distribution from super-paramagnetic measurements and using also the maximum entropy algorithm.

Easy axis distribution has been also determined using this technique. J.W. Harrell et al. [8] reported in 1997 comparative results between Shtrickman and Treves based method and maximum entropy algorithm. In their work they carried out experiments on commercial Co-γ-Fe_2O_3 recording tapes and showed that there is a good agreement between the two methods for EAD measurement.

5.1.4 Mössbauer Spectroscopy as a technique for EAD measurements

Over the past years Mössbauer Spectroscopy has become a useful tool for studying the chemical and magnetic properties of magnetic storage media [9,10,11]. Among different types of Mössbauer Spectroscopy, the ^{57}Fe Mössbauer Spectroscopy is by far the most

important and exclusively used for studies in recording media materials. A ^{57}Fe Mössbauer spectrum consists of a number of components, which could be singlets, doublets or sextets, depending on the analysed material or/and the different magnetic components within a sample. A magnetically ordered material will present a sextet spectrum or a superposition of sextets. The orientation distribution function of the moments in a magnetic material can be obtained from the relative intensities ratio of the lines in a sextet spectrum. The 14.4 keV nuclear transition in ^{57}Fe spectroscopy has a magnetic dipole nature, which leads to angle dependent expressions for the relative intensities of the lines. The relative intensities are expressed as function of the angle between the gamma ray beam and the magnetisation direction and have been summarised by Greenwood and Gibb in 1971 [12]. ^{57}Fe Mössbauer Spectroscopy has been also used as an experimental tool in this project in order to analyse the particles morphology and the out-of-plane orientation distribution in advanced double-coated metal particle tapes. The experimental technique has been introduced in the section 2.3 and the experimental results in the section 5.3.2.

5.2 In-plane texture measurement

5.2.1 Orientation Ratio (OR) measurements

For simplicity of characterization, the texture is often represented by the orientation ratio (OR). This is defined as the ratio of the remanent magnetization along the recording direction to that transverse to it. For a sample with randomly orientated particles OR = 1, while an OR > 1 indicates a partial alignment of the particles [13]. As will be seen later in this chapter, OR is a crude measure of the texture, which is insensitive to the distribution width corresponding to OR in the range 1 to $\approx$ 2. Therefore, a full measurement of the easy axes distribution gives more detail [14,15] and is more accurate. However, for certain studies only the knowledge of the OR is enough. Measurement techniques of the OR are given in the next two sections.

5.2.1.1 Orientation Ratio measurements from hysteresis loop

As has been defined earlier, the OR represents the ratio of the longitudinal remanent magnetisation along the mean easy axis direction to that transverse to it:

$$OR = \frac{M_r^{along}}{M_r^{transvesre}} \tag{5.1}$$

Another hysteresis loop parameter, the squareness *(Sq)*, is defined as the ratio of the remanent magnetisation to the saturation. The squareness has a maximum value, $Sq^{max} = 1$.

$$Sq = \frac{M_r}{M_s} \tag{5.2}$$

Since the saturation magnetisation is the same for different orientations ($M_s^{along} = M_s^{transverse} = M_s$), then the OR can be also defined using the squareness parameters:

$$OR = \frac{M_r^{along}}{M_r^{transvesre}} = \frac{Sq^{along}}{Sq^{trnsverse}} \tag{5.3}$$

where: Sq^{along}, $Sq^{transverse}$ are the squareness parameters corresponding to the in-plane parallel loop and transverse loop, respectively. The measurement of the OR parameter from a hysteresis loop is very simple and only requires obtaining two in-plane hysteresis loops. The first hysteresis loop is measured for the sample placed with the track direction along the magnetic field and the second loop is determined with the sample mean EAD direction positioned normal to the applied field direction (see figure 5.1).

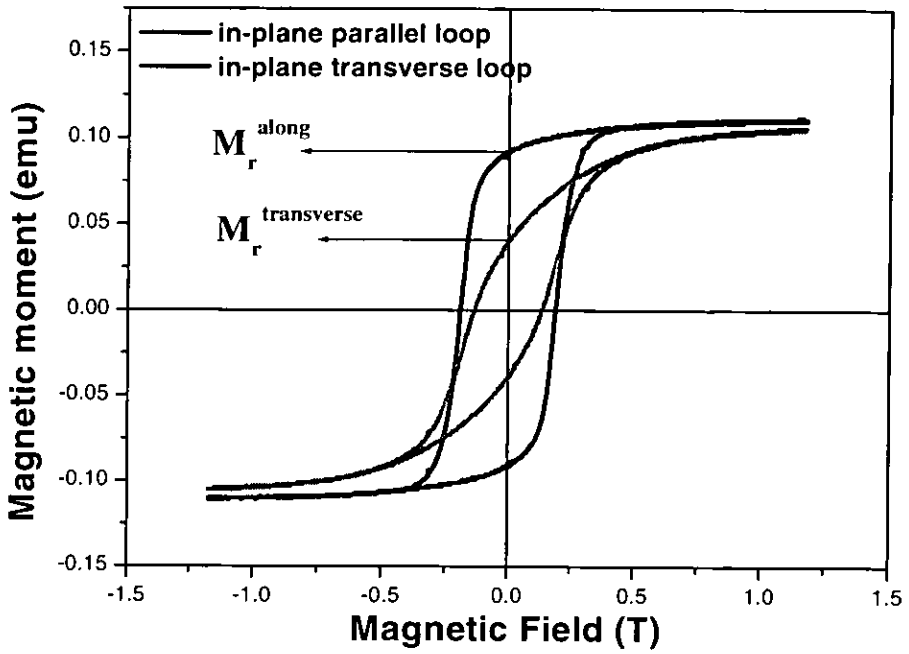

Figure 5.1 Example of the in-plane parallel and transverse loops corresponding to sample A.

For both series of samples the OR has been determined from hysteresis loop measurements. In table 5.1 the experimental results are summarised.

Table 5.1 In-plane OR parameters obtained from hysteresis loops.

Samples	Sq^{along}	$Sq^{transverse}$	OR
A	0.82	0.37	2.21
B	0.83	0.36	2.30
C	0.81	0.36	2.25
D	0.82	0.35	2.34
E	0.84	0.80	1.05
F	0.78	0.73	1.06
G	0.78	0.70	1.11
H	0.71	0.64	1.10

5.2.1.2 OR measurements using MFM

While VSM is a bulk technique, Magnetic Force Microscopy (MFM) can provide a microscopic technique for the measurement of the OR. There are several publications [16-18] where quantitative information has been obtained from longitudinal media using MFM, but they are not related to the orientation properties of the media. However, Yen et al. [19] published a paper in which they reported measurements of the OR in CoCrPtTa longitudinal thin films using MFM techniques. Following their technique, in order to test the technique and to compare the results with those obtained from VSM, an initial investigation was made using the MFM facilities in the Centre for Materials Science, University of Central Lancashire.

The analysis used by Yen et al. to determine orientation ratio from MFM images is based on the disorder noise model. It is well known that the noise due to the disorder (σ), in recording media with uniaxial anisotropy, it can be represented by the relation [20,21]:

$$(\frac{\sigma}{M_s})^2 = 1-(\frac{M}{M_s})^2 = 1-m^2 \qquad (5.4)$$

where: M and Ms represent the magnetisation and respective saturation magnetisation; m is the magnetisation normalised to the saturation. For a sample in the remanent state ($\sigma = \sigma_r$) the relation (5.4) becomes:

$$(\frac{\sigma_r}{M_s})^2 = \overline{\sigma}_r^{\,2} = 1-(\frac{M_r}{M_s})^2 = 1-m_r^{\,2} \qquad (5.5)$$

Yen et al. proposed that the standard deviation of the magnetic roughness, which can be derived from pixel intensity mapping of an MFM image (δ), should be equal with the disorder noise (σ) multiplied by a transfer function. The transfer function is difficult to measure directly but instead it is possible to normalize the MFM images in a way that eliminates the transfer function. All the MFM images in this technique were collected

from samples in the remanent state. The samples have been previously exposed to a saturating DC field along to a specified direction. In order to normalize the MFM data, firstly two MFM images have been acquired in the same conditions from the same sample, but the previous saturating field was applied in two orthogonal directions: in-plane (along track) and out-of-plane. Calculating the ratio (5.6) can eliminate the transfer function:

$$\frac{\delta^{in-plane}}{\delta^{out-plane}} = \frac{\overline{\sigma}^{in-plane}}{\overline{\sigma}^{out-plane}} \tag{5.6}$$

Hence, from relations (5.5) and (5.6):

$$(\frac{\delta^{in-plane}}{\delta^{out-plane}})^2 = \frac{(1-m^2{}_{r(in-plane)})}{(1-m^2{}_{r(out-plane)})} \tag{5.7}$$

$m_{r\ (out\text{-}plane)}$ is very small in longitudinal recording media and it can be neglected in the first order. The relation (5.7) becomes:

$$m^2{}_{r(in-plane)} = 1-(\frac{\delta^{in-plane}}{\delta^{out-plane}})^2 \tag{5.8}$$

By combining the definition of the orientation ratio (5.1) with the relation (5.8), I obtain:

$$OR = \frac{\left[1-\left(\frac{\delta^{along}}{\delta^{out-plane}}\right)^2\right]^{\frac{1}{2}}}{\left[1-\left(\frac{\delta^{transverse}}{\delta^{out-plane}}\right)^2\right]^{\frac{1}{2}}} = \sqrt{\frac{(\delta^{out-plane})^2-(\delta^{along})^2}{(\delta^{out-plane})^2-(\delta^{transverse})^2}} \tag{5.9}$$

The δ values in the relation (5.9) can be easily derived from analysing three remanent MFM images corresponding to the same sample, but previously exposed to saturation fields in three orthogonal directions.

The MFM images have been acquired using a phase contrast detection mode. They represent a map of the out-of-plane stray field from the media and the variation in the stray field is considered to be media noise for longitudinal media [17]. The MFM data requires further processing using the appropriate software in order to obtain the magnetic average roughness and hence δ values.

Two samples, each corresponding to a different series, have been analysed using this technique. Figures 5.2 and 5.3 show the MFM pictures for a MP tape sample and for a CoCrTa thin film sample, respectively.

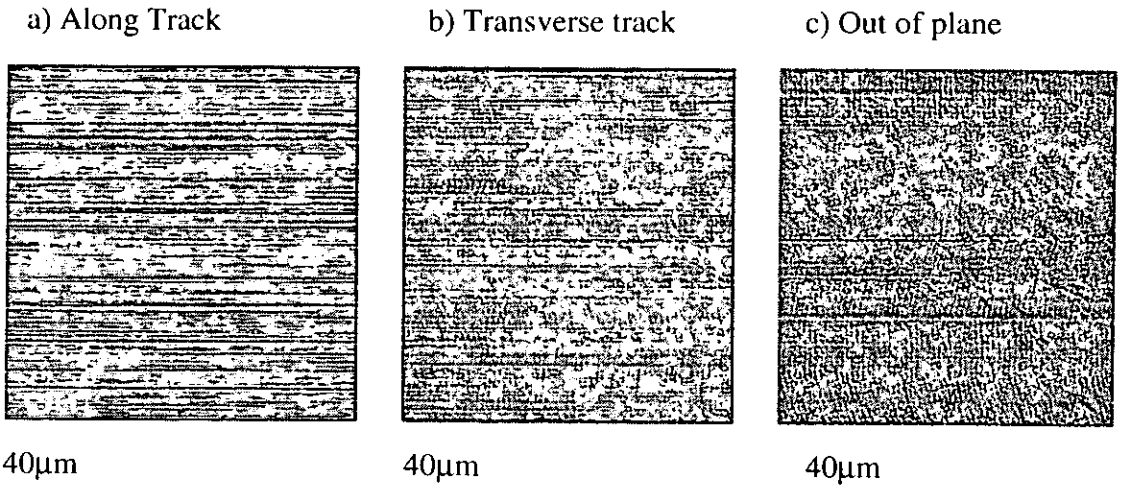

Figure 5.2 A set of representative MFM pictures of the same sample (MP tape sample A) pre-treated with saturation field applied: a) Along track direction, b) Transverse track direction, c) out-of-plane direction

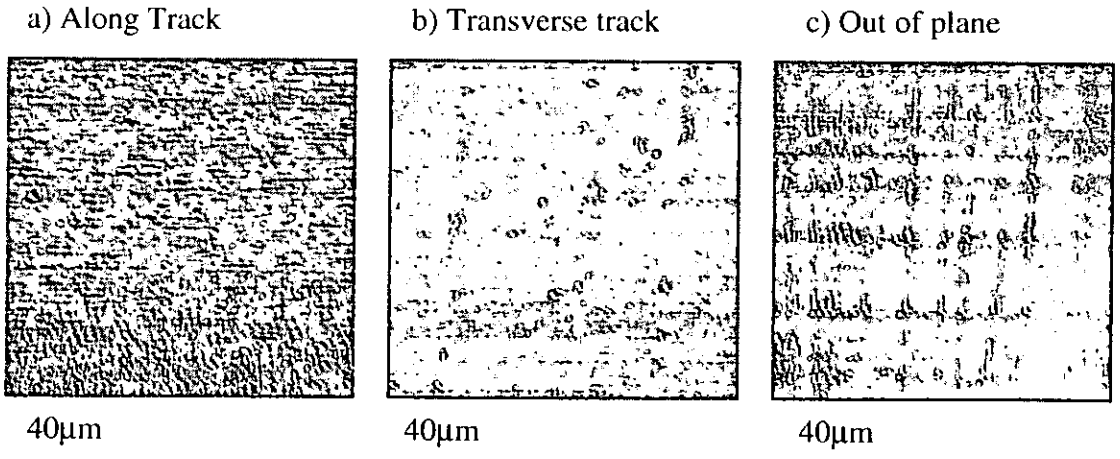

Figure 5.3 A set of representative MFM pictures of the same sample (Co-Cr-Ta thin film sample H) pre-treated with saturation field applied: a) Along track direction, b) Transverse track direction, c) out-of-plane direction

In table 5.2 there are summarised the results from MFM experiments.

Table 5.2 The average magnetic roughness corresponding to the three images and the OR values obtained from MFM images in comparison with the OR from VSM.

Samples	$\delta^{\text{out-plane}}$	δ^{along}	$\delta^{\text{transvesre}}$	OR from MFM	OR from VSM
A	30.9	14.1	29.7	**3.35**	**2.21**
H	28.2	16.8	26.2	**2.16**	**1.10**

As can be seen from the table 5.2, the OR data from the two techniques give a poor match. In both cases, the OR values obtained from the MFM technique are overestimated.

Since the VSM method is well established and also known as very accurate, it is concluded that the MFM technique is quite inaccurate. This is due to the systematic errors that are accumulated during the process of analysing the MFM images. Theses errors are also enhanced by the strong approximation, in which the out-of-plane remanent magnetisation ($m_{r\ (out\text{-}plane)}$) for longitudinal media was considered very low and accordingly neglected (see the relations (5.7) and (5.8)). However, this is not entirely true. For example, the sputtered Co-Cr-Ta thin films were produced by transfer deposition. Because of this dynamic fabrication method, the deposition angle changes throughout the film thickness and this process leads to a bowed columnar structure in the transfer direction. Therefore, the Co-Cr-Ta thin films will have an important out-of-plane component and the mentioned approximation does not work.

This explanation is also supported by the experimental data, which show that the OR values obtained from MFM are overestimated. For the MP tape sample has been obtained an overestimated value by 52 %, while for the Co-Cr-Ta thin film sample the OR is overestimated by 97 %. This big difference in the case of the thin films could be directly related to the bowed internal structure of the samples, and therefore to the wrong approximation in relation (5.8).

Because of the poor match, the MFM technique was not pursued beyond the initial investigations.

5.2.2 In-plane EAD measurements using vector VSM techniques

The present experiment is based on a bi-axial VSM technique and is similar to the one implemented by Schmidlin et al. [14]. The bi-axial VSM assembly, as has been introduced in the section 2.2, allows the measurement of a sample moment to be made both in the field direction and orthogonal to it.

The samples used for experiments were circular disks mounted in the VSM with the sample plane and the rotational axis coincident. The mean easy axis direction of the sample was first determined by measuring saturation remanence as a function of angle, as follows: the sample was saturated in a large magnetic field, the field was removed and the remanent magnetisation in the field direction was measured. The mean EAD of the sample was detected by repeating this step at different orientations until a maximum remanent magnetisation in the applied field direction was achieved. The direction corresponding to maximum value was taken as the centre of the EAD on the assumption that the distribution was symmetric about this direction $\alpha = 0$ (see figure 5.4,a). All further measurements were made relative to this direction.

Once the EAD centre has been identified, the experimental procedure to determine the EAD of the sample is the following: the sample was saturated in a large magnetic field in its EAD axis direction, so that all the particle or grain moments are switched into the field direction (see figure 5.4, a).

When the field is removed, they return to a remanent state occupying their easy axis directions closest to the field direction (figure 5.5,a).

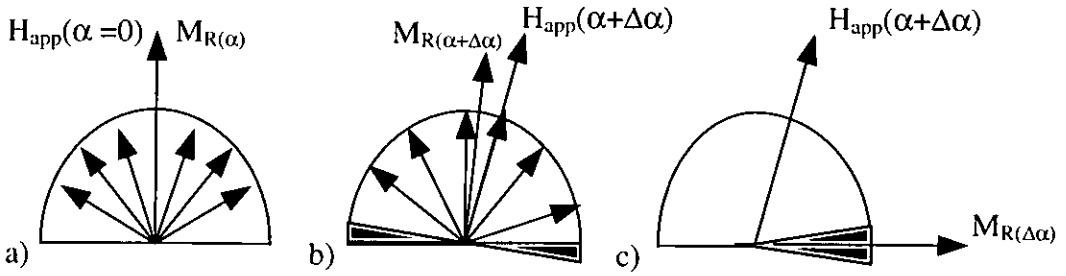

Figure 5.4 Schematic representation of the particles orientated within a medium:
(a) after the application of a saturating field in the easy axis centre ($\alpha = 0$)
(b) after the application of a saturating field at an angle ($\alpha+\Delta\alpha$)
(c) the switched remanent magnetisation of the moment between applied field directions of α and $\alpha+\Delta\alpha$.

If the sample is now rotated through an angle $\Delta\alpha$ (see figure 5.4,b), saturated in the applied field direction and the field removed again, the change in the remanence vector will be the result of the moment switching for grains with easy axes direction between 90^0 and $90^0 + \Delta\alpha$ to $\alpha = 0$. By repeating the measurement process for an incremental increase in α from 0^0 to 180^0, the easy axis distribution can be obtained in that plane of measurement. The remanent signal measured transverse to the applied field direction is proportional to the number of moments that have their easy axes lying within the angle $2\Delta\alpha$ (see figure 5.5,c). The difference between the remanent transverse signals corresponding to α and $\alpha+\Delta\alpha$ directions for consecutive saturation and removals represent the number of particles where easy axis lie between α and $\alpha+\Delta\alpha$.

Let us suppose a rotation of the sample from θ to $\theta + \Delta\theta$ (see figure 5.5). The magnitude of the transverse signal is a measure of the particles that lay with their easy axes within $90^0 + \theta$ and $90^0 + \theta + \Delta\theta$, represented in the figure 5.5 by the shaded area. Assuming that there is a distribution of the easy axes within the sample, $f(\theta)$, then the amount of magnetic moment between $90^0 + \theta$ and $90^0 + \theta + \Delta\theta$ is Δm, where:

$\Delta m \sim f(\theta + 90^0)\cdot\Delta\theta$. As we can see in the diagram, the left side of the disk is "loosing" an equivalent amount Δm after rotation, while the right side "gains" the same amount. If the $M_\perp$ is the transverse signal, then:

$$M_\perp(\theta + \Delta\theta) = M_\perp(\theta) - \Delta m\cdot\sin(\Delta\theta - \pi/2) + \Delta m\cdot\sin(\Delta\theta + \pi/2) \quad (5.10)$$

But

$$\Delta m \sim f(\theta + 90^0)\cdot\Delta\theta \quad (5.11)$$

$$M_\perp(\theta + \Delta\theta) \approx M_\perp(\theta) - f(\theta + 90^0)\cdot\Delta\theta\cdot\sin(\Delta\theta - \pi/2) + f(\theta + 90^0)\cdot\Delta\theta\cdot\sin(\Delta\theta + \pi/2) \quad (5.12)$$

$$\sin(\Delta\theta - \pi/2) = -\cos(\Delta\theta) \text{ and } \sin(\Delta\theta + \pi/2) = \cos(\Delta\theta) \quad (5.13)$$

The equation can now be written as:

$$M_\perp(\theta + \Delta\theta) \approx M_\perp(\theta) - f(\theta + 90^0)\cdot\Delta\theta\cdot(-\cos(\Delta\theta)) + f(\theta + 90^0)\cdot\Delta\theta\cdot\cos(\Delta\theta) \quad (5.14)$$

$$M_\perp(\theta + \Delta\theta) \approx M_\perp(\theta) + 2\cdot f(\theta + 90^0)\cdot\Delta\theta\cdot\cos(\Delta\theta) \quad (5.15)$$

$$M_\perp(\theta + \Delta\theta) - M_\perp(\theta) \approx 2\cdot f(\theta + 90^0)\cdot\Delta\theta\cdot\cos(\Delta\theta) \quad (5.16)$$

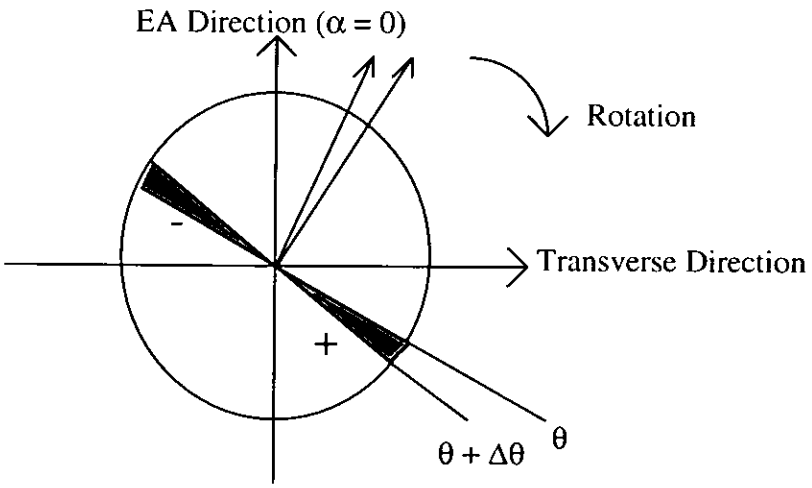

Figure 5.5 The shaded area represents the amount of particles, which are switched after applying the saturating field between the two directions θ and θ + Δθ

For very small rotational angles, $\Delta\theta \rightarrow 0$ and in this case $\cos(\Delta\theta) \cong 1$

$$\Rightarrow M_{\perp}(\theta + \Delta\theta) - M_{\perp}(\theta) \approx 2 \cdot f(\theta + 90^0) \cdot \Delta\theta$$

$$\Rightarrow f(\theta + 90^0) \approx (M_{\perp}(\theta + \Delta\theta) - M_{\perp}(\theta)) \cdot \frac{1}{2 \cdot \Delta\theta} \qquad (5.17)$$

But
$$\lim_{\Delta\theta \rightarrow 0} \left(\frac{(M_{\perp}(\theta + \Delta\theta) - M_{\perp}(\theta)}{\Delta\theta}\right) = \frac{dM_{\perp}}{d\theta} \qquad (5.18)$$

From relations (5.17) and (5.18) it can now be written the distribution function of the easy axes as:

$$\text{a) } f(\theta + 90^0) \approx \frac{dM_{\perp}(\theta)}{d\theta} \quad \text{or} \quad \text{b) } f(\theta) \approx \frac{dM_{\perp}(\theta - 90^0)}{d\theta} \qquad (5.19)$$

According to the equations (5.19), the easy axis distribution is represented by the variation in the normal component of magnetisation with respect to the rotation angle and therefore, easy axis distribution is proportional with the derivate of the transverse signal. Since the scanning of the sample was between 0 – 180^0, then the centre of the distribution would normally be at $\alpha = 90^0$, as can be seen from relation 5.19, a. By

subtracting 90^0 from the experimental data, the obtained distribution will be between -90^0 to 90^0, centred on $\alpha = 0$ (see relation 5.19, b and figures 5.6, 5.7). This result will be used in the procedure for EAD determination.

5.2.1.1 Results and discussions

The series of four MP tape samples (A - D) were experimentally analysed in order to determine the in-plane EAD. Although the parameters from hysteresis loops show no major differences between the samples (see the appendix 2), the experimental data from vectorial measurements proved that the samples have different magnetic texture varying with the magnetic coating thickness.

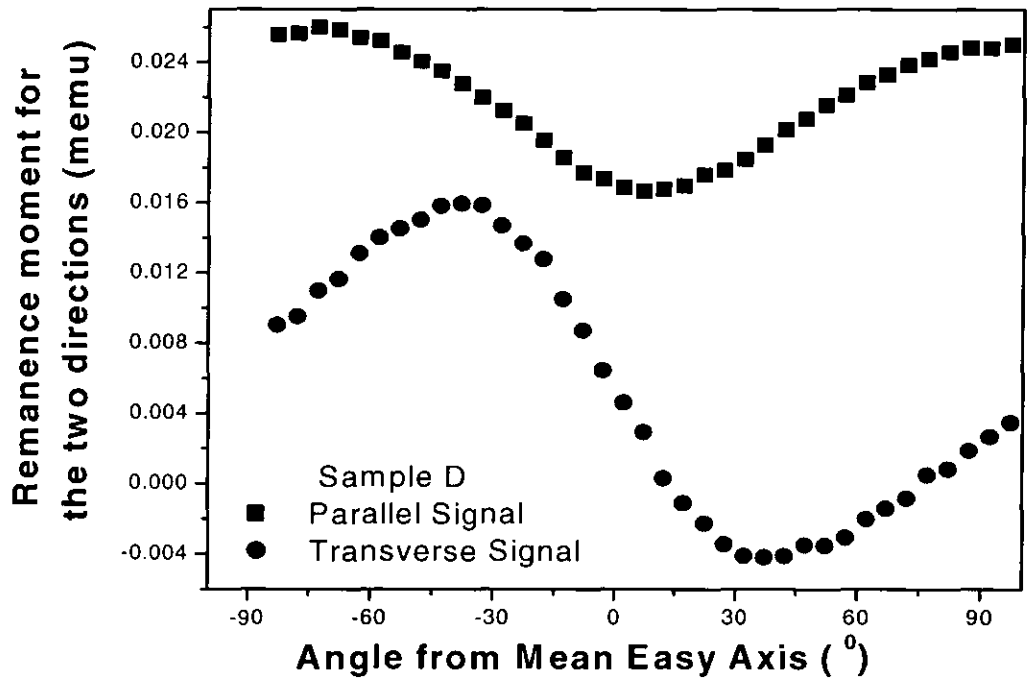

Figure 5.6 The remanent parallel and transverse signals as a function of the rotation angle.

Figure 5.6 shows an example for the experimental measurement of both in-plane magnetisation components using the vector VSM assembly. Both signals are plotted in magnetic (memu) units and the experimental signals were calibrated following the technique described in the section 2.2.2, which is also similar to the one described by Bolhuis et al.[22].

The parallel coils were calibrated using the standard technique with a Ni calibration sample having a known magnetic moment. For the transverse coils, a hard magnetic sample in remanent state was used for calibration. The sample has been first saturated in its EAD, which was orientated parallel to the field, and the remanent moment was determined in that direction. The calibration factor for the parallel coils has been used to calculate the remanent moment in magnetic EMU units. The sample was rotated 90^0 in remanent state and then the calibration factor for transverse coils was calculated.

Once the transverse signal was measured, the in-plane EAD can be derived according to the relation 5.19. The experimental data have been fitted by a Lorentzian distribution function, in order to obtain a numerical measure of the distribution width. A Lorentzian distribution function $f(\alpha)$ is defined as:

$$f(\alpha) = f_0(\alpha) + \frac{A}{4\pi} \cdot \frac{w}{4(\alpha - \alpha_c)^2 + w^2} \tag{5.20}$$

where: A is a normalisation parameter representing the area of the distribution

w is the distribution width

α_c is the centre of the distribution

$f_0(\alpha)$ is the minimum value of the distribution

The experimental data have been acquired for $f_0(\alpha) = 0$, $\alpha_c = 0$, and after the normalisation to the area of the distribution, A = 1.

The new distribution function is:

$$f(\alpha) = \frac{a'w}{4\alpha^2 + w^2} \tag{5.21}$$

where: a' = $1/4\pi$

Re-arranging the terms it is obtained:

$$f(\alpha) = \frac{a'w}{4\alpha^2 + w^2} = \frac{a'w}{4(\alpha^2 + (\frac{w}{2})^2)} = \frac{a'}{2} \cdot \frac{\frac{w}{2}}{\alpha^2 + (\frac{w}{2})^2} = \frac{ab}{\alpha^2 + b^2} \tag{5.22}$$

where: b = w/2 is the distribution parameter and a = a'/2 is the new normalisation parameter;

$$f(\alpha) = \frac{a \cdot b}{\alpha^2 + b^2} \tag{5.23}$$

Here $f(\alpha)$ represents the magnitude of the EAD, α represents the in-plane angle with respect to the sample easy axis direction and a is a normalisation parameter obtained according with the condition:

$$\int_{-90}^{90} f(\alpha) d\alpha = 1 \tag{5.24}$$

In figure 5.7 the experimental EAD are plotted for all four samples. Because the signal for a single layer disk sample is very small, in order to increase the signals level, a stack of 16 disks glued together to maintain their magnetic orientation was used. This produced a sample corresponding to 12.5 cm^2 which increased the signal to noise ratio to satisfactory levels without compromising the sheet demagnetisation factor of the sample. It is estimated that the easy axis distribution width is determined with a precision of $\pm 2.5^0$, which is half of the rotational step angle.

At the extremes of the EADs, the measured signal became increasingly noisy. This was a consequence of the measurement technique, which involves measuring changes in magnetization at right angles to the applied field direction. At angles further away from the EAD direction, the amount of particles switched from consecutive saturating field directions became increasingly small and the background noise within the system started to dominate.

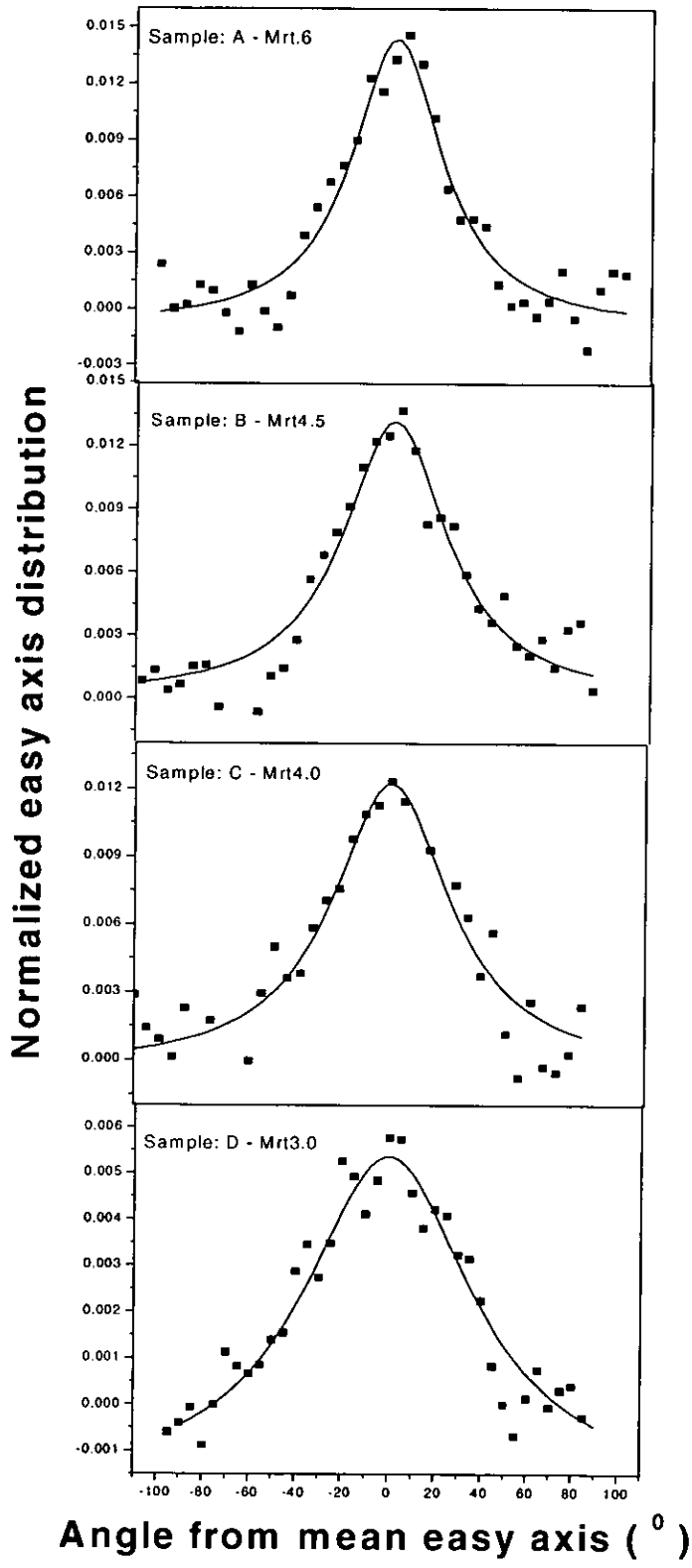

Figure 5.7 In-plane experimental easy axis distributions measured for all four MP tape samples. The continuous lines represent the Lorentzian fitting functions and the data points are the experimental data.

The experimental results in figure 5.7 have been fitted using a Lorentzian distribution function and the fitting results are summarised in table 5.3.

Table 5.3 The in-plane EA distribution parameters

Sample	Mrt (memu/cm^2)	Distribution width (w^0)	Distribution parameter (b =w/2)
A	6.0	42.19	21.09
B	4.5	48.5	24.25
C	4.0	55.3	27.65
D	3.0	65.33	32.66

In-plane easy axis distribution measurements show that width of the distribution increases as the magnetic coating thickness (represented here by the Mrt values) is decreased. There is a clear trend, which can be related to the Mrt value (see figure 5.8). This indicates that, as the magnetic layer becomes thinner, the *in-plane* particle orientation is reduced resulting in a broader distribution. It is believed that this result is a direct consequence of the manufacturing process when a thinner coating will dry more rapidly and so reduce the effectiveness of the orienting magnets or be associated with changed rheology of the wet coat. The diffusion of the particles from the magnetic layer into the non-magnetic sub-layers has also a contribution to the texture degree and that is again related to the thickness.

The experimental variation of the distribution parameter with the magnetic coating thickness (figure 5.8) was fitted using an exponential function:

$$b = b_0 + A \cdot e^{-\frac{Mrt}{B}} \qquad (5.25)$$

where: b = distribution width

b_0 = minimum distribution width

Mrt = remanence×thickness

A = 19.8 (constant) and B = 1.5 (constant)

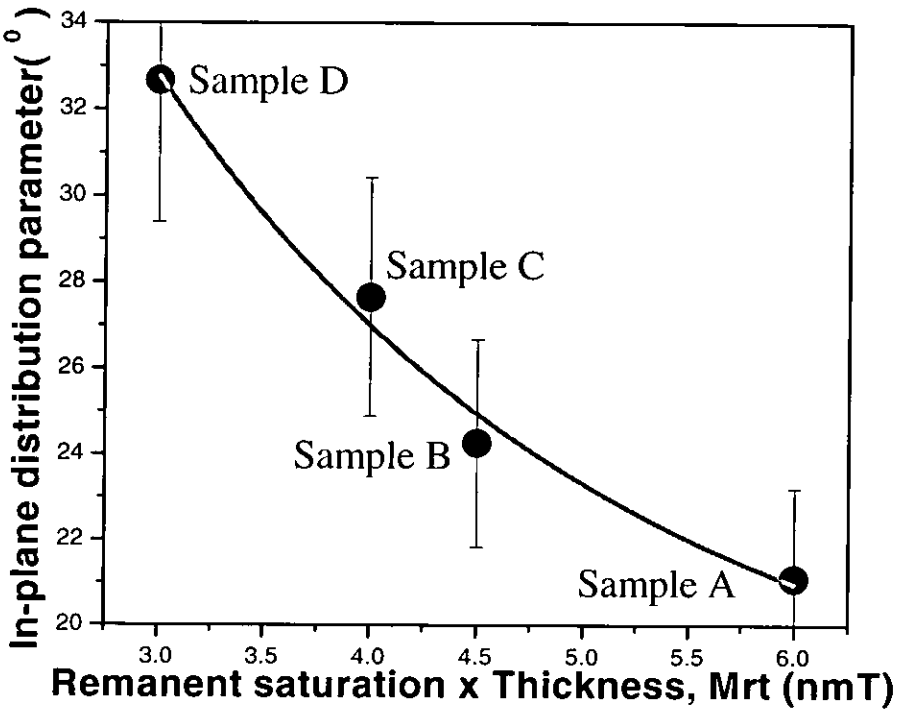

Figure 5.8 Easy axis distribution parameter variations as a function of the sample thickness. The thinner the sample, the bigger distribution parameter. The error bars are evaluated as 10% of the data. This gives a precision of $\pm 2.5^0$ that is comparable with half of the rotation step angle.

The fitting function (5.25) can be used to predict, for this class of metal particle tape samples, the distribution parameter values for different magnetic thickness that can be controlled during the fabrication process.

5.3 Out-of-plane texture measurements

The degree of alignment, or texturing, is very process dependent and will be related to wet coating properties such as viscosity, the rate of drying and the shear applied to the particles by mechanical means and the aligning magnetic field. In double coated systems these effects are likely to be exaggerated by the thinness of the top coat, as indicated by the variations observed and reported in this chapter. The Easy Axis Distribution (EAD) is 3 dimensional (3D) and can be different in-plane and out-of-plane. The in-plane EAD measurement has been already described in the section 5.2. This section describes two techniques for out-of-plane EAD measurements, which are based on VSM magnetometry and Mössbauer spectroscopy. The two methods have been successfully applied to the series of four metal particle (MP) tapes.

5.3.1 Out-of-plane EAD derived from OR measurements

Out-of-plane measurements of the EAD are very difficult, if not almost impossible to measure with any reasonable accuracy. This is because of demanding demagnetising field corrections after each rotation of the sample, in order to keep the internal field constant in a fixed direction. In order to avoid these complications, a theoretical relation between OR and distribution parameter has been used to determine the out-of-plane EAD.

5.3.1.1 The relation between OR and EAD

The OR measurements can be used as an alternative tool for determining the EAD. Let us consider a disk sample or diameter 2R with the magnetic moments lying in the disk plane. Let us suppose that the sample is first saturated in its mean easy direction (Ox), which is also the applied field direction. After removing the saturating field, the magnetic moments can be considered distributed in the remanent state only in a half disk, as indicated in the figure (5.4,a). If the easy axis distribution of the particle easy directions is a function $f(\alpha)$ and if I_s is the saturation remanent magnetisation, then it is

proposed to calculate the mean remanent magnetisation M_r of the sample in the Ox direction. In other words, what is the mean value of the M_r when I_s can have any possible orientation in the half disk?

Let us consider the angle α between I_s and the Ox direction. Then the corresponding M_r will be: $M_r = I_s \cdot cos(\alpha)$. The mean $<M_r>$ of the sample, when all the particles are distributed according with the distribution function $f(\alpha)$ will be:

$$< M_r >= \frac{\int M_r \cdot f(\alpha) dA}{\int f(\alpha) dA} = \frac{\int I_s \cdot \cos(\alpha) f(\alpha) dA}{\int f(\alpha) dA} = I_s \frac{\int \cos(\alpha) f(\alpha) dA}{\int f(\alpha) dA} \qquad (5.26)$$

$$dA = r \cdot dr \cdot d\alpha \qquad (5.27) \qquad <M_r> = M_x \qquad (5.28)$$

From (5.26), (5.27), (5.28) and also considering the integrating limits: $0 < r < R$, and $-\pi/2 < \alpha < \pi/2$, the relation (5.26) becomes:

$$M_x = Is \frac{\int_0^R r dr \int_{-\pi/2}^{\pi/2} \cos(\alpha) f(\alpha) d\alpha}{\int_0^R r dr \int_{-\pi/2}^{\pi/2} f(\alpha) d\alpha} = I_s \int_{-\pi/2}^{\pi/2} f(\alpha) \cos(\alpha) d\alpha \qquad (5.29)$$

where: $\int_{-\pi/2}^{\pi/2} f(\alpha) d\alpha = 1$

If the disk sample is subjected to an applied saturating field H_{app}, after it has been rotated through an angle β from the mean easy axis direction, and then the field is removed, the magnetic moments of each particle will relax along the easy axis direction closest to β. The remanent magnetisation in the Ox direction will be:

$$M_x(\beta) = I_s \int_{\beta - \frac{\pi}{2}}^{0} f(\alpha) \cos(\alpha - \beta) d\alpha + I_s \int_{0}^{\beta + \frac{\pi}{2}} f(\alpha - \pi) \cos(\alpha - \beta) d\alpha \qquad (5.30)$$

Equation (5.31) gives the resulting normalised remanent magnetisation along the field direction ($\overline{M_x}(\beta) = \frac{M_x(\beta)}{I_s}$) after the rotation through an angle β and after applying and removing a saturating field in the Ox direction:

$$\overline{M}_x(\beta) = \frac{M_x(\beta)}{I_s} = \int_{\beta-\frac{\pi}{2}}^{0} f(\alpha)\cos(\alpha-\beta)d\alpha + \int_{0}^{\beta+\frac{\pi}{2}} f(\alpha-\pi)\cos(\alpha-\beta)d\alpha \tag{5.31}$$

Having the expression (5.31), the Orientation Ratio of the sample can be calculated using its definition: OR is the ratio of the remanent magnetisation along the recording direction (M_x) to the remanent magnetisation along the transverse direction (M_y):

$$OR = \frac{M_x(0)}{M_x(\frac{\pi}{2})} = \frac{\overline{M_x}(0)}{\overline{M_x}(\frac{\pi}{2})} = \frac{\int_{-\frac{\pi}{2}}^{0} f(\alpha)\cos(\alpha)d\alpha + \int_{0}^{\frac{\pi}{2}} f(\alpha-\pi)\cos(\alpha)d\alpha}{\int_{0}^{0} f(\alpha)\cos(\alpha-\frac{\pi}{2})d\alpha + \int_{0}^{\pi} f(\alpha-\pi)\cos(\alpha-\frac{\pi}{2})d\alpha} \tag{5.32}$$

It is assumed that the distribution $f(\alpha)$ indicates the probability of having a particle with easy direction at an angle α from the mean easy direction. The fact that a magnetic moment can point towards either of two directions along the easy axis, is represented mathematically by:

$f(\alpha) = f(\alpha - \pi)$ (5.33)

Considering also that: $\cos(\alpha - \pi/2) = \sin(\alpha)$ (5.34)

and the integral: $\int_{0}^{0} f(\alpha)\cos(\alpha-\frac{\pi}{2})d\alpha = 0$ (5.35)

After a few simplifications, the relation (5.32) becomes:

$$OR = \frac{\int_{-\frac{\pi}{2}}^{\frac{\pi}{2}} f(\alpha)\cos(\alpha)d\alpha}{\int_{0}^{\pi} f(\alpha)\sin(\alpha)d\alpha} \tag{5.36}$$

For an easy axis distribution described by a Lorentzian function: $f(\alpha) = \frac{a \cdot b}{\alpha^2 + b^2}$ and starting from the theoretical equation (5.36), the variation of the orientation ratio as a function of the distribution width can be calculated using the relation (5.37):

$$OR = \frac{\int_{-\pi/2}^{\pi/2} \frac{\cos(\alpha)}{\alpha^2 + b^2} d\alpha}{\int_{0}^{\pi} \frac{\sin(\alpha)}{\alpha^2 + b^2} d\alpha} \tag{5.37}$$

Giving different values for the distribution parameter (b), the OR can be calculated by performing numerical integration in the expression (5.37). Table 5.4 shows the results for the numerical integrations, whish were performed using Easy Plot software.

Table 5.4 Orientation Ratio calculated for different given values of the distribution parameter, b.

b	b^2	$\int_{-\pi/2}^{\pi/2} \frac{\cos(\alpha)}{\alpha^2 + b^2} d\alpha$	$\int_{0}^{\pi} \frac{\sin(\alpha)}{\alpha^2 + b^2} d\alpha$	Orientation Ratio OR
1	1	3.05978	0.14689	20.83
2	4	1.52379	0.12516	12.17
3	9	1.00075	0.11158	8.96
5	25	0.58278	0.09415	6.18
7	49	0.40414	0.08263	4.89
10	100	0.27079	0.07049	3.84
15	225	0.16809	0.05695	2.95
20	400	0.11763	0.04762	2.46
25	625	0.08799	0.04065	2.16
30	900	0.06870	0.03519	1.95
35	1225	0.05529	0.03078	1.79
40	1600	0.04552	0.02714	1.67
45	2025	0.03815	0.02409	1.58
50	2500	0.03243	0.02151	1.50

In order to obtain the OR variation as a function of the distribution parameter, the values calculated in the table 5.4 have been plotted (see figure 5.9). This is a very important result because it allows the distribution width to be calculated for a sample if

the OR is known and under the assumption that there is a Lorentzian distribution for the particle easy axes within that sample.

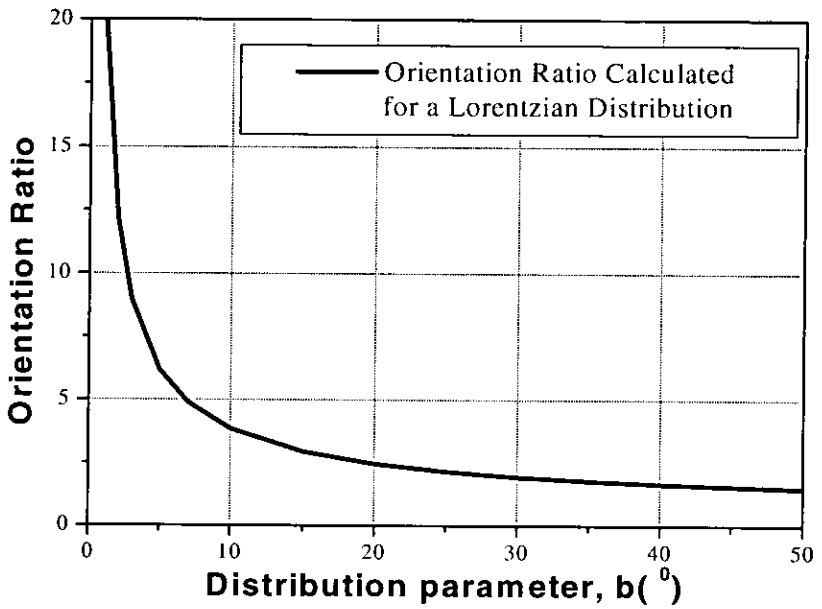

Figure 5.9 Numerical calculation of the Orientation Ratio for a Lorentzian distribution with different distribution parameters

The orientation ratio is a magnetic parameter that is easy to determine from hysteresis loops. By fitting the numerical curve with an appropriate function it is possible to derive any *b* distribution parameter for any OR value using the equation (5.38):

$$OR = 1.5 + 7.16 \cdot e^{-\frac{b}{9.61}} + 32.6 \cdot e^{-\frac{b}{1.072}} \qquad (5.38)$$

It can be seen in figure (5.9) that for distribution widths greater that $b \cong 20^0$, OR is insensitive to increasing *b*, i.e. for wide distributions, as in the case of the in-plane measurements, OR is not an effective measure of the EAD. However, as OR increases it can be used to estimate the distribution width more precisely and is more effective for out-of-plane distribution measurements because they are usually narrower than the in-plane ones (i.e. $b < 20^0$). Although minimum OR is 1, which corresponds to a randomly system of particles, from the equation (5.38) it appears that the minimum OR is 1.5. This is due to calculation method in which are considered only samples with distribution widths up to 100^0 (or $b = 50^0$ distribution parameter). This is a good

approximation for our studies, since most of the recording media are textured for increasing the alignment of the particles. If required, however, the theoretical variation can be easily extended to higher values of the distribution width.

5.3.1.2 Results and discussions

The theoretical relation between OR and the distribution parameter has been used in order to calculate the out-of-plane EAD. Out-of-plane OR was experimentally determined using the in-plane transverse loop and the out-of-plane hysteresis loop, the latter being prior corrected for demagnetising effects (see the section 4.3.2).
Figure 5.10 shows a comparison of the experimental results with the theoretical calculation.

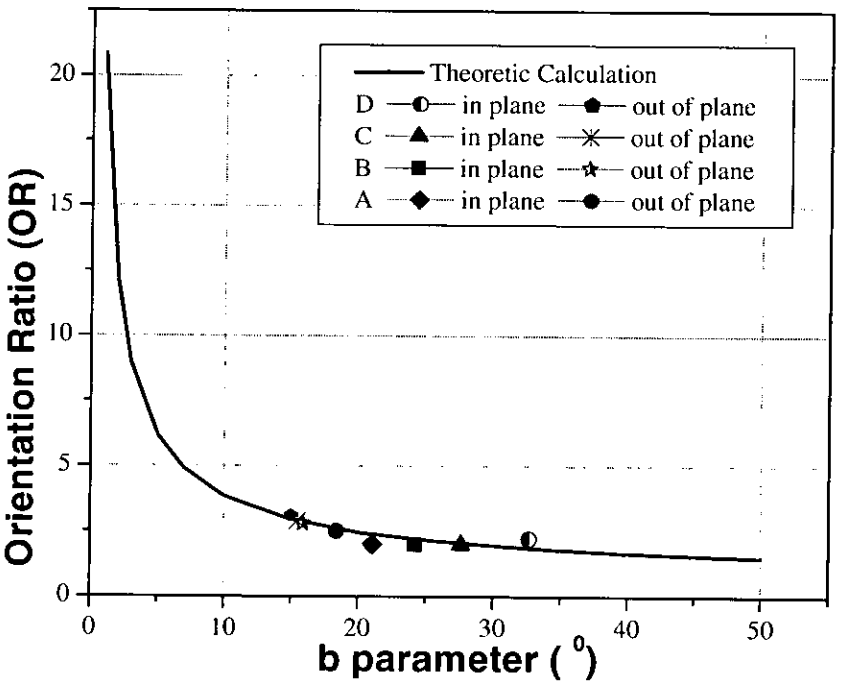

Figure 5.10 Measured in-plane distribution parameter (*b*) and OR for all four samples, shown on the theoretically derived relation. Out-of-plane measured OR values are also plotted on the theoretical curve to show the derived values of b.

Out-of-plane OR can be used to predict the out-of-plane distribution widths with more accuracy. This is a very useful method since out-of-plane EAD is almost impossible to

measure and the experiments are very time-consuming, having also a high percentage of errors. Using the experimentally determined out-of-plane OR values and the equation (5.38), the out-of-plane distribution parameters corresponding to the series of MP tape samples have been estimated. The results are summarised in the table 5.5.

Table 5.5 Out-of-plane OR and out-of-plane distribution parameters for MP tapes

Sample	Mrt (memu/cm^2)	Distribution width (w^0)	Distribution parameter (b = w/2)	Orientation ratio OR
A	6.0	36.9	18.4	2.5
B	4.5	31.14	15.7	2.8
C	4.0	31.10	15.5	2.9
D	3.0	30	15	3.1

As expected, the out-of-plane distribution parameters show a variation with the magnetic thickness (represented here by the Mrt values). However, unlike the in-plane distribution parameter (see figure 5.8), the out-of-plane trend is in the opposite sense (see the figure 5.11).

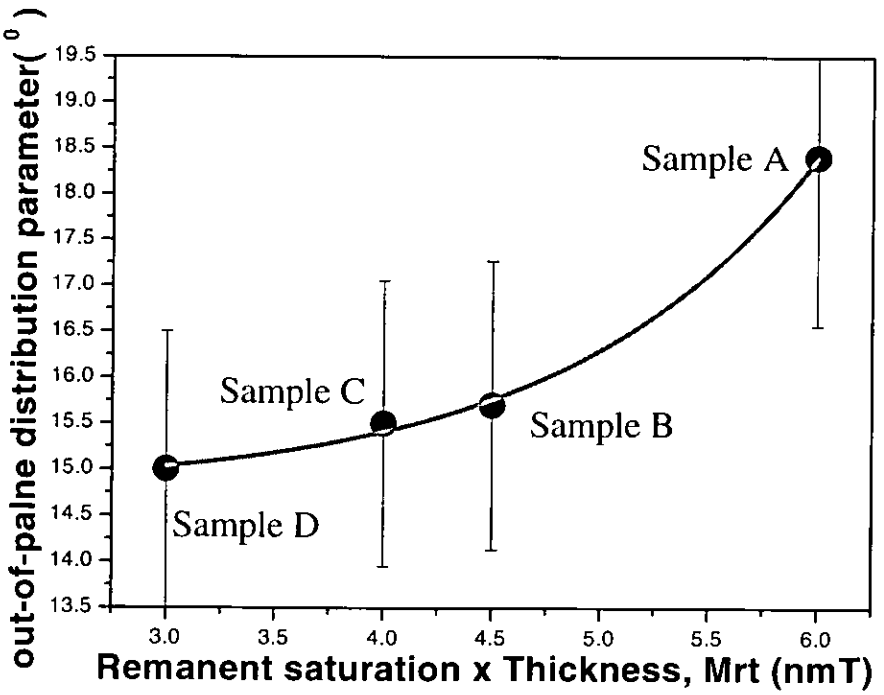

Figure 5.11 Out-of-plane distribution parameter variation as a function of the magnetic thickness. The thinner the sample, the smaller distribution parameter. The error bars are evaluated as 10% of the data giving a precision of ± 1.5^0.

The thinnest sample has the smallest out-of-plane distribution parameter, contrary to the in-plane EAD where the thinnest sample had the biggest distribution parameter. This may be due to the geometrical influence of the magnetic thickness to the tape texture, where the finished magnetic coat thickness is approximately equal to the particle length, as well as to the mechanical shearing effects of the knife coater or doctor blade. The observed trend out-of-plane is much smaller than in-plane. In addition, all the out-of-plane distribution widths are much smaller than those measured in plane. Again this is probably related to the mechanical properties of the coating process.

5.3.2 Out-of-plane EAD derived from Mössbauer spectroscopy

Since most of the magnetic materials contain iron-based compounds, ^{57}Fe Mössbauer spectroscopy represents a powerful tool for providing both particles morphology and spin orientation [9,10,11]. In this study, Mössbauer spectroscopy has been used to analyse double-coated MP tapes. Valuable information regarding the out-of-plane distribution and the internal structure, have been obtained. A full description of a Mössbauer experiment is given in the section 2.3.

The Mössbauer spectra were obtained in collaboration with the Nuclear Gamma Resonance group at the University of Duisburg, Germany. The spectra have been acquired in transmission geometry using a spectrometer with symmetrical waveform and a ^{57}Co source in an Rh matrix. Spectra were obtained at both room temperature (RT) and liquid helium temperature. Inserting the sample in a variable temperature cryostat performed the measurements down to 4.2 K. The γ-ray direction was in both cases perpendicular to the sample plane (see figure 5.14).

5.3.2.1 Internal structure and particle morphology

The Mössbauer spectra of the four analysed samples taken at room temperature (RT) are presented in figure 5.12. They consist of a broad and large sextet with a hyperfine field around 49 T, a less split sextet with a hyperfine magnetic field of around 35 T and a central paramagnetic component. Excepting the less-split sextet, which can be unambiguously assigned to the α-Fe(Co) metallic phase, some doubts persists to the

assignment of the central pattern and the broad external sextet which may be due to either a mixture of different oxides (distributed Fe sites) or dynamical effects related to only one oxide phase.

In order to solve this problem, Mössbauer spectra have been taken at 4.2 K (see figure 5.13). The low temperature spectra show clearly only two magnetic phases. The much narrower line for the external sextet stands therefore for dynamical aspects related both to the external sextet and the central pattern in the RT spectra. This is the reason that finally the dominant outer sextet in the RT spectra has been fitted by a distribution of hyperfine fields related to relaxation aspects. The main hyperfine parameters, isomer shift (IS), quadrupole splitting (QS), hyperfine magnetic field (B_{hf}), relative intensity ratios ($R_{23}=I_2/I_3$) and relative areas (RA) of the two magnetic sextets are presented in table 5.6.

Table 5.6 Mössbauer hyperfine parameters, relative intensity ratio and relative areas for the two magnetic sextets in the Mössbauer spectra measured at RT and 4.2K

Phase	T	Oxide					α-Fe(Co)				
Sample	(K)	IS (mm/s)	QS (mm/s)	B_{hf} (T)	R_{23}	R.A (%)	IS (mm/s)	QS (mm/s)	B_{hf} (T)	R_{23}	R.A (%)
A	4.2	0.38	-0.19	53.0	2.1	86.2	0.06	0.00	36.9	4.1	13.8
	295	0.26	-0.21	49.5	2.0	64.4	-0.06	0.00	35.9	3.6	23.7
B	4.2	0.38	-0.18	53.0	2.1	88.8	0.05	0.00	36.8	4.1	11.2
	295	0.26	-0.21	49.5	2.0	70.1	-0.07	0.00	35.8	3.5	20.0
C	4.2	0.38	-0.18	53.0	2.1	91.0	0.06	0.00	36.8	4.0	9.0
	295	0.26	-0.21	49.4	2.0	72.1	-0.07	0.00	35.8	3.7	18.1
D	4.2	0.38	-0.19	53.0	2.1	93.0	0.05	0.00	36.8	4.0	7.0
	295	0.26	-0.21	49.4	2.0	74.6	-0.07	0.00	36.0	3.6	18.8

It may be observed that for all the analysed samples the relative area of the external sextet decreases from 4.2 K to 295 K with around 20% whereas the relative area of the inner sextet increases with around 10%. Therefore, the RT super-paramagnetic central pattern could be developed only from the external sextet and consequently it has to be assigned to the oxide phase. Hence, the only trace of the metallic phase in the Mössbauer spectra belongs to the inner sextet.

The increase of their relative area versus temperature should be explained by the different temperature dependence of the Debye-Waller factor (f_{DW}) in the two implied phases, because usually f_{DW} decreases faster for an oxide than for a metallic phase.

The oxide could be most probably assigned from the values of hyperfine fields and isomer shifts to a α-Fe_2O_3 or γ-Fe_2O_3 phase [12,23].

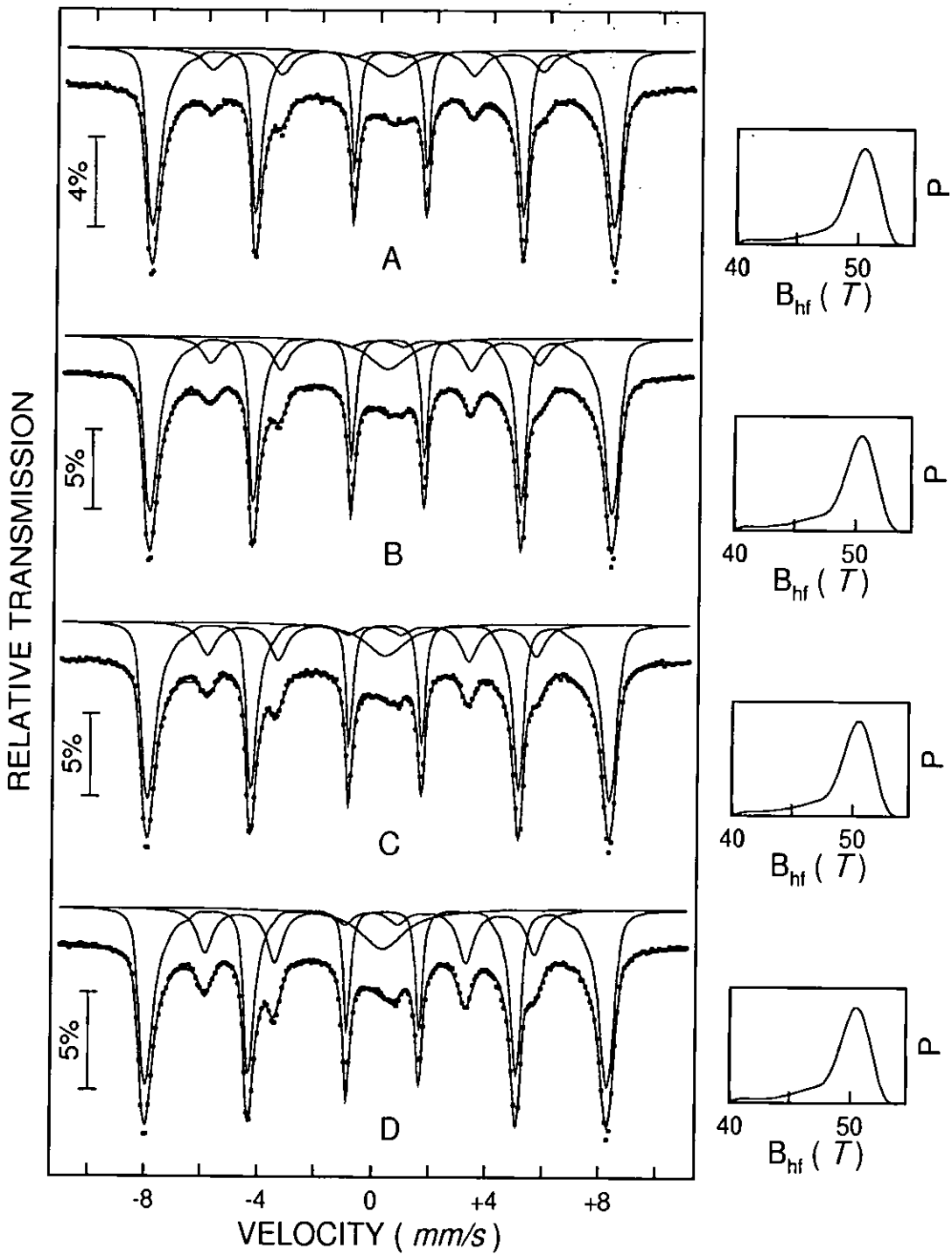

Figure 5.12 Room temperature Mössbauer spectra of the analysed samples

The negative quadrupole splitting evidenced at room temperature as well as the absence of the Morin transition over the analysed temperature range (see the quadrupole split behaviour in table 5.6) should rather infer the presence of a γ-Fe_2O_3 phase. However, magnetic measurements suggest that the Mrt value is related primarily to the top magnetic coating and that the underlayer is essentially non-magnetic. The γ-Fe_2O_3 phase is ferrimagnetic whereas α-Fe_2O_3 is weak ferromagnetic above the Morin transition and antiferromagnetic below it. Because there is no Morin transition, the negative value of the quadrupole split over the whole temperature range correlated with the above magnetic result points strongly to a defected anti-ferromagnetic α-Fe_2O_3 phase in the underlayer.

The higher hyperfine field in the metallic α-Fe(Co) phase is due to both the presence of the Co ions and interfacial interaction with the oxide layer. Taking into account the above Mössbauer parameters as well as the preparing procedure we may assume the particle morphology as consisting of a metallic α-Fe(Co) core surrounded by an oxide layer.

It is worth noticing that only the low temperature spectra, where the two f_{DW} factors are comparable, give valuable information about the relative amount of the two iron phases. The results indicate (see table 5.6), as we mentioned above, only two iron phases. These are distributed in around 10% for the metallic α-Fe(Co) core and the rest of approximately 90% for the oxide which is present in both passivation layer and non-magnetic underlayer. There is magnetic evidence that the passivation layer on the α-Fe(Co) particles, expected to be around 2nm thick, does not contribute to the particle moment and is also non-magnetic. The volume fraction corresponding to such a thin passivation layer represents much below 10% from the metallic phase, that means below 1% from the total Mössbauer absorption area. Therefore, the Mössbauer data, which show only two distinct iron phases, give reliable information only about the metallic phase and the iron oxide in the non-magnetic underlayer.

The line-width behaviour of the outer sextet stands for a distribution of oxide nano-particles that behave in the regime of collective excitation. The small fraction of

superparamagnetic phase identified by the central doublets in the RT spectra corresponds to the smallest particles from this distribution.

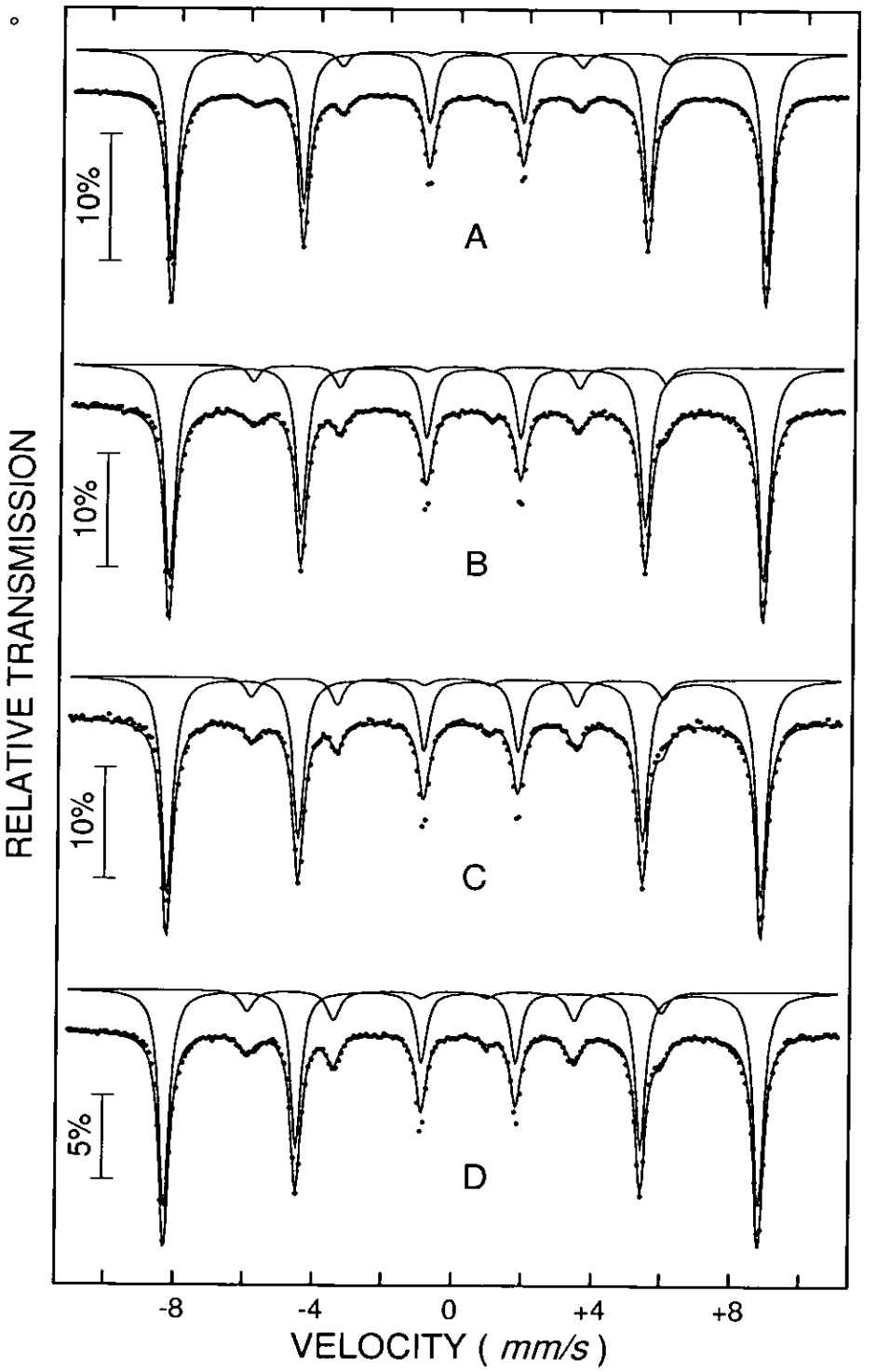

Figure 5.13 Mössbauer spectra of the analysed samples, taken at 4.2 K

5.3.2.2 Out-of-plane distribution, results and discussions

Besides the information about the internal structure, room temperature Mössbauer spectroscopy has been also used as a complementary technique to derive the mean out-of-plane distribution angle. If the six lines in a magnetically split Mössbauer spectrum are numbered from left to right as 1 to 6, valuable information can be obtained, about the out-of-plane distribution of the particle magnetic moments, from the intensity ratios R_{23}, defined as the ratio of the intensity of the line 2 or 5 to the line 3 or 4. Greenwood and Gibb have theoretically calculated the intensities of the transitions for general cases [12]. For our particular case, where Ψ is the angle between the γ - ray beam and the direction of the effective hyperfine field at nucleus B_{eff} (see the figure 5.14), the probabilities of transition or the intensities of the six lines in a magnetically split spectrum, for an axial symmetry of the electric field gradient (quadrupole interaction is zero), are [12]:

$$I_1 = I_6 = 3(1+\cos^2(\Psi)) \tag{5.39}$$

$$I_2 = I_5 = 4\sin^2(\Psi) \tag{5.40}$$

$$I_3 = I_4 = \cos^2(\Psi) + 1 \tag{5.41}$$

The relative intensities of the six lines in the magnetically split spectrum are:

$$R_{13} : R_{23} : R_{33} : R_{44} : R_{54} : R_{64} \quad \text{or} \quad 3 : \frac{4\sin^2(\psi)}{1+\cos^2(\psi)} : 1 : 1 : \frac{4\sin^2(\psi)}{1+\cos^2(\psi)} : 3 \tag{5.42}$$

As can be seen from the relation (5.42), only the relative intensities of the 2nd and 5th lines depends on the angle Ψ between the magnetisation direction and the γ - ray beam which is perpendicular to the plane of the sample (see figure 5.14). Therefore, in the following treatment the results will be discussed using the relative intensity ratio, R_{23} defined as:

$$R_{23} = \frac{4\sin^2(\psi)}{1+\cos^2(\psi)} = \frac{I_2}{I_3} \qquad (5.43)$$

i) For $\Psi = 0$, which means that the magnetisation is perpendicular to the plane of the sample, $R_{23} = 0$. This is, for example, useful in studying perpendicular recording media where all the moments point normal to the sample plane. Hence, the Mössbauer spectrum will present a sextet in which the 2nd and the 5th lines are completely absent. The relative intensities of the six lines will be: 3 : 0 : 1 : 1 : 0 : 3.

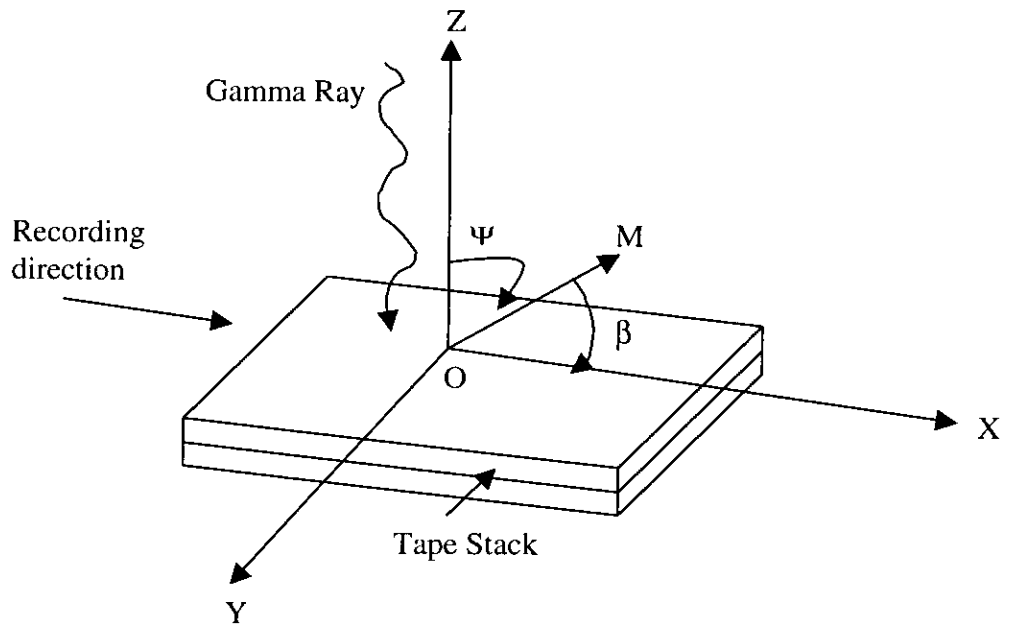

Figure 5.14 Geometrical arrangement used for obtaining the Mössbauer spectra.

ii) For $\Psi = 90^0$, which means that the magnetisation is in the plane of the sample, $R_{23} = 4$. This is, for instance, the case of the longitudinal recording media in which all the particle moments are oriented in the sample plane. A Mössbauer spectrum for such a sample will be a sextet with the intensities of the six lines in the ratio: 3 : 4 : 1 : 1 : 4 : 3.

iii) An intermediate value of R_{23} between 0 and 4, corresponds to either a particular value of Ψ between 0 and 90^0, or to a distribution of values of Ψ. A value $R_{23} = 2$, will indicate a particular value of $\Psi = 54.7^0$, a completely random distribution of

magnetisation directions, or a whole family of possible distributions leading to $R_{23} = 2$. The spectrum will have the relative intensities: 3 : 2 : 1 : 1 : 2 : 3.

The mean angle, β, between the "dispersed" spins and the sample plane is simply deduced by the relation $\beta = 90° - \Psi$, where Ψ is the angle between the Fe spin and the direction of the γ ray, and is obtained from the measured R_{23} ratio. The solution of the equation (5.43) is:

$$\psi = ar\cos\left(\sqrt{\frac{4-R_{23}}{4+R_{23}}}\right) \qquad \text{and} \qquad \beta = 90^0 - \psi = 90^0 - ar\cos\left(\sqrt{\frac{4-R_{23}}{4+R_{23}}}\right) \qquad (5.44)$$

From the experimental R_{23} values obtained at RT, the angles β have been deduced for sample A, B, C and D respectively (see table 5.7). Although the results from Mössbauer data do not show the trend obtained from OR measurements, they are still comparable within the error limits.

Table 5.7 Comparison between the out-of-plane distribution angles obtained from Mössbauer spectroscopy and OR measurements.

	A	B	C	D
Out-of-plane distribution parameter b (^{0}) from OR measurements	18.4	15.7	15.5	15.0
Out-of-plane β (^{0}) angle derived from Mössbauer spectroscopy	13.2	14.9	11.5	13.3

Considering that the OR and gamma ray spectroscopy are two techniques very different from each other, the fact that the results are comparable but they do not perfectly match is understandable. The OR and VSM techniques are bulk experimental methods, which measure the statistical properties of the magnetic moments as a whole, while Mössbauer spectroscopy is a nuclear technique from which the information is extracted as an average of the individual behaviour of each iron nucleus in each magnetic particle or grain.

Another important observation is related to the R_{23} values of the spectra taken at 4.2 K (see figure 5.13 and table 5.6). The obtained values ($R_{23} \approx 4$) at low temperatures

indicate for all samples that the iron spins in the metallic core are all in the tape plane. In other words, the room temperature out-of-plane distribution measured using both orientation ratio and Mössbauer spectroscopy would be only related to dynamical aspects when the spins starting to oscillate along the longitudinal direction due to the thermal excitation. This means that, in fact, the particles are all perfectly aligned in the tape plane. Although not shown here, this result is also supported by the spectra taken for sample D at five different temperatures (between 295 K and 4.2 K). They were fitted in similar conditions and the results indicate clear a continuously increasing trend of the intensity ratio (R_{23}) vs. temperature. In this case, however, the out-of-plane angles derived from room temperature OR technique and from room temperature Mössbauer spectroscopy are still real and they represent the out-of-plane distribution of the particle magnetic moments rather than physical out-of-plane distribution of the particles. Since most of recording media applications are used at room temperature, the out-of-plane measurements are valid and practically important.

However, this is a rather controversial explanation. There are numerous experimental evidences (i.e. electron microscopy, magnetic measurements, etc.) showing that particulate media contain particles that are 3D oriented. Although longitudinal media is seen as having 2D particles dispersed in the magnetic film, this is only the ideal case of a medium, since it is impossible to manufacture perfect 2D media, in which the particles have no out-of-plane orientation at all. Therefore, another more acceptable explanation is yet under investigation and further experimental and theoretical work is required.

5.4 3D easy axis distribution

Using the experimental in-plane and out-of-plane distributions, an overall 3D representation of the particle easy axis within a medium was obtained and is given by the function $\gamma(\alpha,\beta)$. The 3D distribution function, $\gamma(\alpha,\beta)$, was computed using the relation:

$$\gamma(\alpha,\beta) = f(\alpha)\cdot g(\beta) = \frac{a_\alpha \cdot b_\alpha}{\alpha^2 + b_\alpha{}^2} \cdot \frac{a_\beta \cdot b_\beta}{\beta^2 + b_\beta{}^2} \tag{5.45}$$

Where:

$f(\alpha) = \frac{a_\alpha \cdot b_\alpha}{\alpha^2 + b_\alpha{}^2}$ is the in-plane normalised Lorentzian distribution function;

$g(\beta) = \frac{a_\beta \cdot b_\beta}{\beta^2 + b_\beta{}^2}$ is the out-of-plane normalised Lorentzian distribution function;

- $a_{\alpha,\beta}$ are the normalization factors and $b_{\alpha,\beta}$ the distribution parameters (i.e. widths) of the two Lorentzian distributions; For generating the 3D functions, the out-of-plane distribution parameters were those experimentally obtained from OR measurements.
- α and β are the in-plane and the out-of-plane angles, measured with respect to the centre of the EAD. The normalization condition for the 3D EAD function, $\gamma(\alpha,\beta)$, became:

$$\iint f(\alpha) \cdot g(\beta) d\alpha d\beta = \iint \gamma(\alpha,\beta) d\alpha d\beta = 1. \qquad (5.46)$$

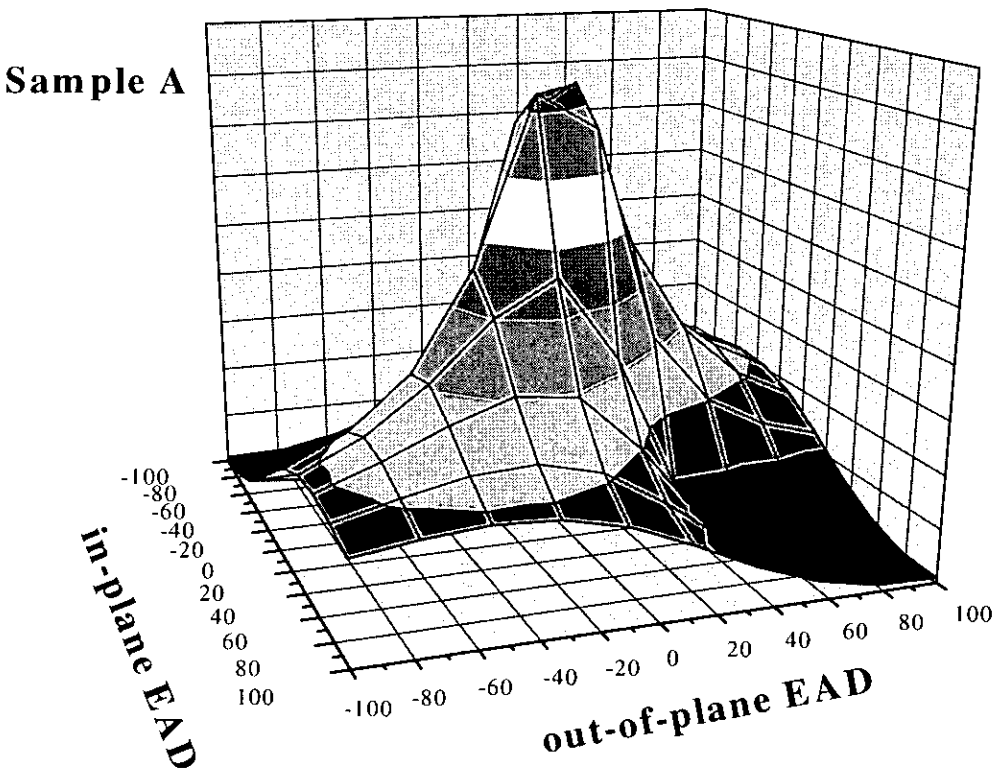

Figure 5.15 3D Easy axis distribution represented sample A

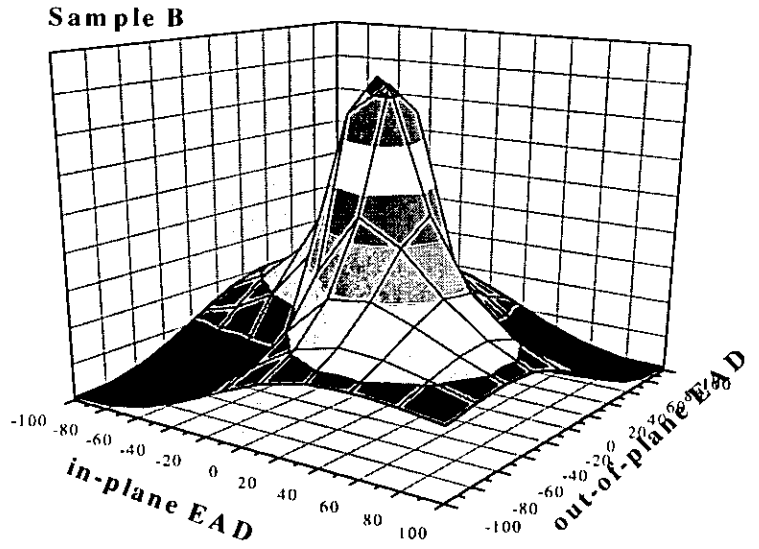

Figure 5.16

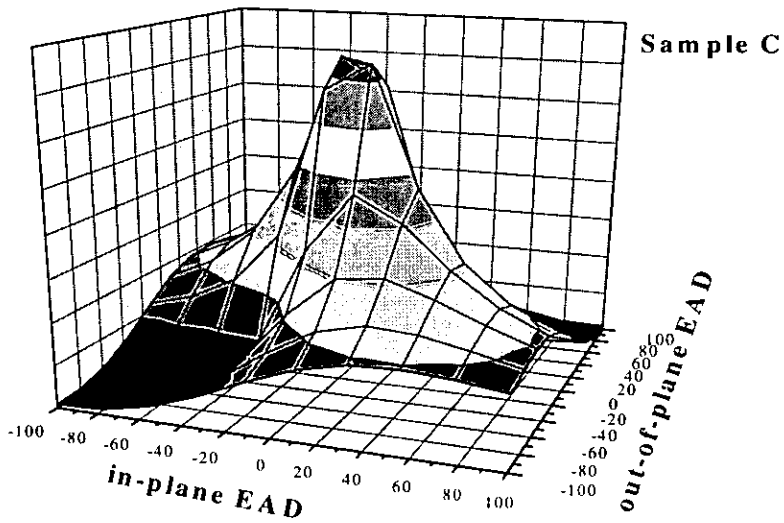

Figure 5.17

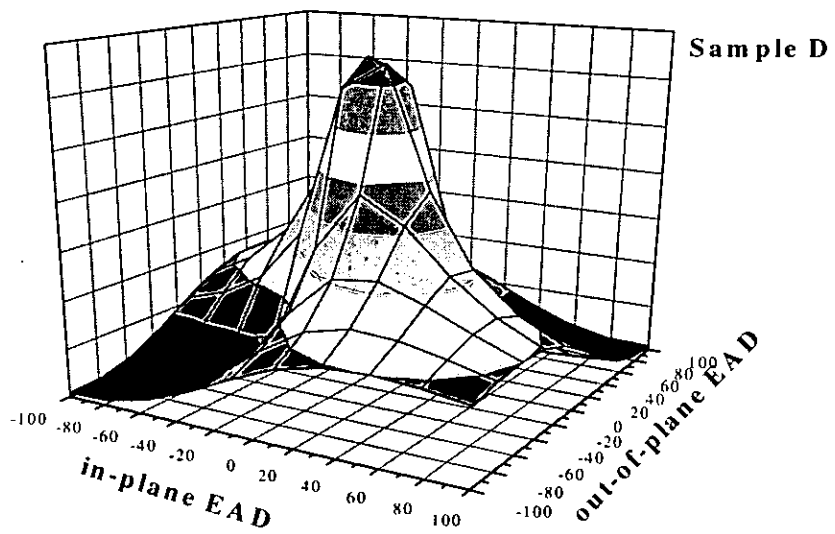

Figure 5.18

Figures 5.16 to 5.18: 3D maps of the easy axis distribution, represented for MP tape samples B, C and D

The 3D function was computed assuming that the two functions $f(\alpha)$ and $g(\beta)$ are not correlated. This assumption is quite inaccurate considering the source of the two distributions. A system of 3D particles will have an out-of-plane component and an in-plane component, both given by the projections of moments on the two directions. Therefore, the two distributions are related to each other as they refer to the distribution of particles moments projections. Although not entirely accurate, this is an acceptable approximation considering that is impossible to measure the two components separately. 3D maps of the easy axis distribution have been produced for all samples (see figures 5.15 to 5.18).

5.5 Summary and discussions

Different texture measurement techniques in magnetic recording media have been presented in this chapter. It has been demonstrated that bulk techniques like standard and vector VSM, as well as microscopic methods like Mössbauer spectroscopy, can be very powerful tools for texture investigation in information storage media. The easy axis distribution (EAD) fully describes the degree of texturing and this is 3 dimensional (3D). The in-plane and out-of-plane are the two different directions that compose the 3D distribution and they can have different distribution widths. Knowledge of the EAD is very important and is the subject of many publications [3,14,15]. Alternatively, the texture can be also represented by the orientation ratio (OR). This is only a rough estimation of the texture but is very useful for certain studies [13]. VSM and magnetic force microscopy (MFM) techniques have been used for in-plane OR measurements. However, ORs determined from initial MFM investigations proved to be inaccurate and the technique was not further pursued.

A number of experiments, leading to the direct determination of the in-plane and out-of-plane EAD, were developed in this PhD project and described in this chapter. The in-plane EAD has been measured using a vector VSM technique. Out-of-plane EAD is

more complicated to measure using conventional or vector VSM and I used instead, two indirect methods:

i) The theoretical relationship between the OR and the EAD

ii) The theoretical relation between the relative intensities of the 2^{nd} and 5^{th} lines of a Mössbauer spectrum and the angle between the γ - ray and the direction of the magnetic moments

The developed techniques have been used to analyse the series of four MP double-coated tapes (A - D). Results showed that the in-plane / out-of-plane texture was strongly related to magnetic coating thickness, probably due to the manufacturing process.

Tape morphology and out-of-plane distributions have been investigated using Mössbauer spectroscopy, the results being in good agreement with the magnetic data and fabrication parameters. 3D EAD functions have been computed using the experimental in-plane and the derived out-of-plane distribution parameters.

Finally, low temperature Mössbauer spectroscopy revealed that an out-of-plane component at low temperatures is too small to measure, suggesting that the out-of-plane EAD at room temperature is only related to thermal effects. This explanation, however, is not consistent with the manufactured parameters and experimental evidence in literature. Therefore, further investigations are required in order to clarify the low temperature behavior.

6. Conclusions and further work

In parallel with the rapid developments in recording media technology there is a considerable increase in academic research concentrated on the fundamental understanding of the physical processes and magnetic behaviour of these magnetic materials, and also the understanding of the relationship between these processes and media performances in their commercial application. In order to examine these physical processes, several new measurement techniques have been developed as part of this project. Experimental investigations have been carried out using a vibrating sample magnetometer, a nuclear gamma spectrometer and some initial texture studies using a magnetic force microscope. Two sets of samples have been used in the experimental investigations: a set of four advanced metal particles tapes (A - D) as LTO and DLT formats for high density digital storage and four sputtered Co-Cr-Ta thin films (E - H) specially prepared in order to enhanced their exchange coupling. Both sets of samples are fully described in appendix 2.

Technically, the main topics reported in this project are outlined below:

1) Anisotropy field distribution measurements and the relationship between the anisotropy field and the rotational angle with respect to the mean easy axis direction;

2) In-plane and out-of-plane anisotropy field measurements using the extrapolated rotational remanence technique;

3) Experimental evaluation of the inter-particle interactions effects on the anisotropy field;

4) Evaluation of the demagnetising field acting perpendicular to the sample plane in the approximation of an infinite magnetic sheet;

5) Non-destructive magnetic technique for magnetic coating thickness calculation;

6) In-plane texture studies using orientation ratio and easy axis distribution measurements;

7) Out-of-plane easy axis distribution measurements using the theoretical relationship between orientation ratio and easy axis distribution;

8) Out-of-plane spin distribution angles and particle morphology studies using room temperature and low temperature Mössbauer spectroscopy;

9) Additional to these, the research work was supported by a systematic development of computer interfacing and LabView computer programs for VSM instrumentation control;

Regarding the magnetic anisotropy field studies undertaken in chapter 3, it has been demonstrated that a vector VSM is a powerful tool for anisotropy field measurements. The two experimental techniques developed on a vector VSM and introduced in this project (extrapolated transverse remanent magnetometry and rotational hysteresis) involve new developments to improve the original techniques. For instance, the extrapolated transverse remanent magnetometry method has been extended and improved in this project by introducing the linear extrapolation. Rotational hysteresis has also novel characteristics, which unlike the previous techniques that were applied on a torque magnetometer, was successfully implemented using a vector VSM. Results obtained from the two methods showed good agreement and their applicability limits are presented at the end of the chapter 3.

Anisotropy fields were experimentally determined for the two series of samples. Both sets of samples showed a variation of the anisotropy field with the magnetic coating thickness, but the trends were in opposite sense. The anisotropy fields for metal particle tapes varied with magnetic thickness so a thinner magnetic coating will have a smaller anisotropy field, while the anisotropy fields for the Co-Cr-Ta thin films vary with the magnetic thickness in a way that a thinner magnetic film will generate a bigger anisotropy field.

This result has been related to the inter-particle interactions that are likely to vary as the magnetic thickness changes. It has been experimentally shown that the effect of the interactions on the anisotropy field has a positive contribution to the anisotropy field, i.e. tending to magnetise the sample, in the case of exchange interactions and a negative interactions contribution to the anisotropy field, i.e. tending to demagnetise the sample, in the case of magnetostatic interactions. There is a clear relationship between magnetic anisotropy and magnetic interaction, which should be carefully considered in any magnetic anisotropy studies.

Besides the in-plane anisotropy field measurements, the extrapolated transverse remanent magnetometry method has been also extended to out-of-plane anisotropy studies. The knowledge of the in-plane and out-of-plane anisotropy fields allows deriving the demagnetizing field acting normal to the sample plane. This is a very important parameter, especially for the applications arising from its measurements (i.e. true magnetisation calibration, demagnetising field corrections and non-destructive magnetic thickness measurements).

The measurement technique relies on the assumption that the demagnetising factor for the sample is that of an infinite sheet, which in some cases could be an approximation. Recent modelling studies showed that for current advanced MP tapes series, the demagnetising factor is altered by about 7%. However, the approximation of an infinite sheet is quite acceptable for particulate recording media where film thickness is small and has good uniformity and this gives a non-destructive measure of the magnetic layer thickness, as described in chapter 4.

Related to this topic, another original experimental technique for demagnetising field measurements has been introduced, i.e. identification of the closure point for hysteresis loops. This is very useful since it is available within any laboratory that has standard vibrating sample magnetometer facilities. Results from the two methods compare well and both provide a useful non-destructive magnetic technique for determination of magnetic layer thickness in particulate media.

Texture measurement in magnetic media represents another research direction of this project. Recording media is textured during the manufacturing process in order to increase the degree of particles alignment. Texture can be described by the easy axis distribution (EAD) or a more general parameter, i.e. orientation ratio (OR) and is an essential characteristic for the recording performances of a medium. The magnetic particles can have a 3D orientation so the texture or easy axis distribution can be different in-plane and out-of-plane. Texture investigations have been undertaken in this project, on the series of four MP double-coated tapes, using both bulk technique (standard / vector VSM) and a microscopic technique (Mössbauer spectroscopy measurements that were carried out in collaboration with another research group in Germany). In-plane easy axis distribution measurements have been directly measured

using the vector VSM, while the out-of-plane EAD was determined using two indirect measurements, i.e. theoretical relationship between the OR and the EAD and theoretical relation between the relative intensities of the 2^{nd} and 5^{th} lines of room temperature Mössbauer spectrum. A direct measurement of the out-of-plane EAD is almost impossible due to the difficulties related to the demagnetising field corrections after each rotation.

Experimental studies indicate a relationship between both in-plane and out-of-plane texture and magnetic coating thickness.

The EAD for in-plane particles is reduced as the magnetic layer becomes thinner, so the thinner sample, the broader easy axis distribution. The out-of-plane distribution showed an opposite variation with respect to the magnetic thickness, i.e. thinner magnetic layer generates a narrower out-of-plane distribution. These results were linked to the manufacturing process. It has been concluded that during manufacturing a thinner coating will dry faster and hence the effectiveness of the orienting magnets will be reduced, this generating a broader in-plane distributions in thinner magnetic coatings. In the case of out-of-plane distribution the explanation may be the geometrical influence of the magnetic thickness, where magnetic coat thickness is in the range of a particle length, as well as the mechanical effects of the "doctor blade" or finishing knife. All these aspects should be considered during manufacturing in order to achieve a desired texture for a particular magnetic coating thickness.

Additional to the out-of-plane texture measurements using room temperature Mössbauer spectroscopy, low temperature Mössbauer spectroscopy showed a perfect in-plane alignment of the particles. This would normally suggest that the particles have no real out-of-plane orientation and room temperature results would be only related to thermal effects. However, the result is not fully understood and is not consistent with the fabrication parameters and other experimental evidences.

The investigations in this project are far from being completed or fully understood. Therefore, further theoretical and experimental work is required. First of all, it would be very interesting to study more deeply the inter-particle interactions and their effects on the anisotropy field. This is related to the variation of the interactions with the magnetic thickness and theoretical simulations could provide valuable information about the

geometrical influence on the anisotropy field and about the intimate relationship between the interactions and magnetic coating thickness.

Another research direction is related to the magnetic non-destructive thickness measurements. The techniques presented in chapter four have been successfully applied only to advanced MP tapes. In order to have full advantage of these techniques, thickness measurements on thin film media is desirable. So far, the experiments have failed in producing reliable results on thin film media and some efforts should be put into improvement of the experimental techniques by increasing the sensitivity and by improving for example the software averaging routines.

Further work will be also dedicated to investigate not only the out-of-plane texture using Mössbauer Spectroscopy, but also the in-plane texture. In fact, experimental in-plane spin distribution studies are being carried out at the moment in collaboration with the members of the Nuclear Gamma Resonance Group from National Institute for Materials Science, Bucharest, Romania.
The out-of-plane component of the EAD may be obtained from Mössbauer experiments in perpendicular geometry whereas the in-plane spin component could be obtained from experiments in non-perpendicular geometry, at different azimuth angles between the anisotropy main axis and the incident γ-ray direction. This offers the possibility to deconvolute the Mössbauer spectra in order to obtain the in-plane spin distribution. The results could then be compared with the easy axis distributions obtained from vector VSM measurements. Finally, the low temperature Mössbauer spectra that indicate a total in-plane alignment should be further investigated in order to produce a more consistent explanation of the results.

APPENDIX 1

Examples of LabView programs for VSM experiments

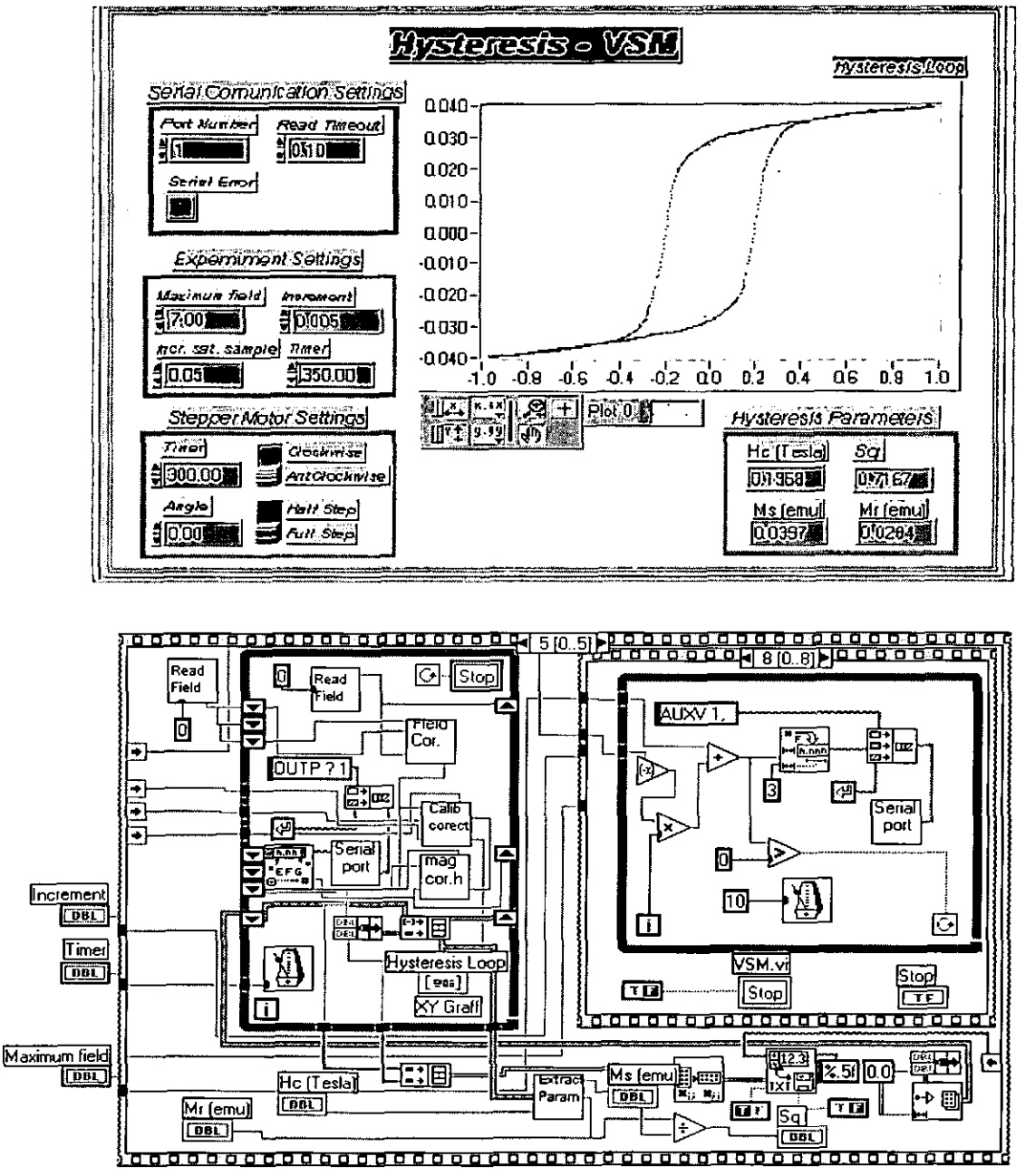

Figure A1.1 LabView routine for hysteresis loop measurements. The front panel and the main back diagram are shown.

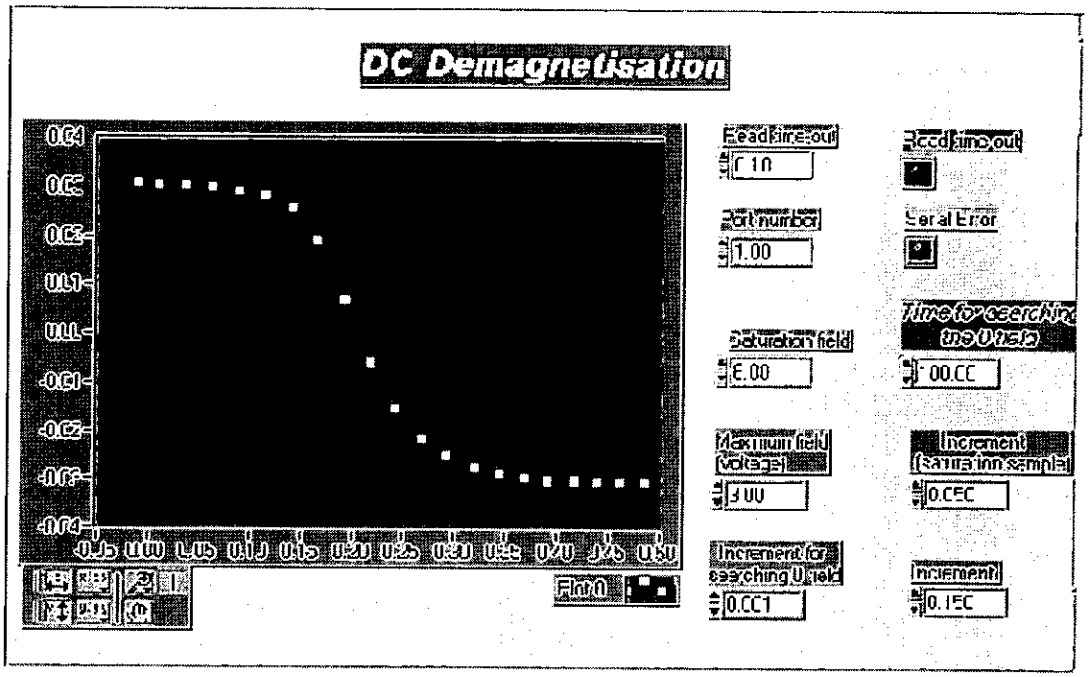

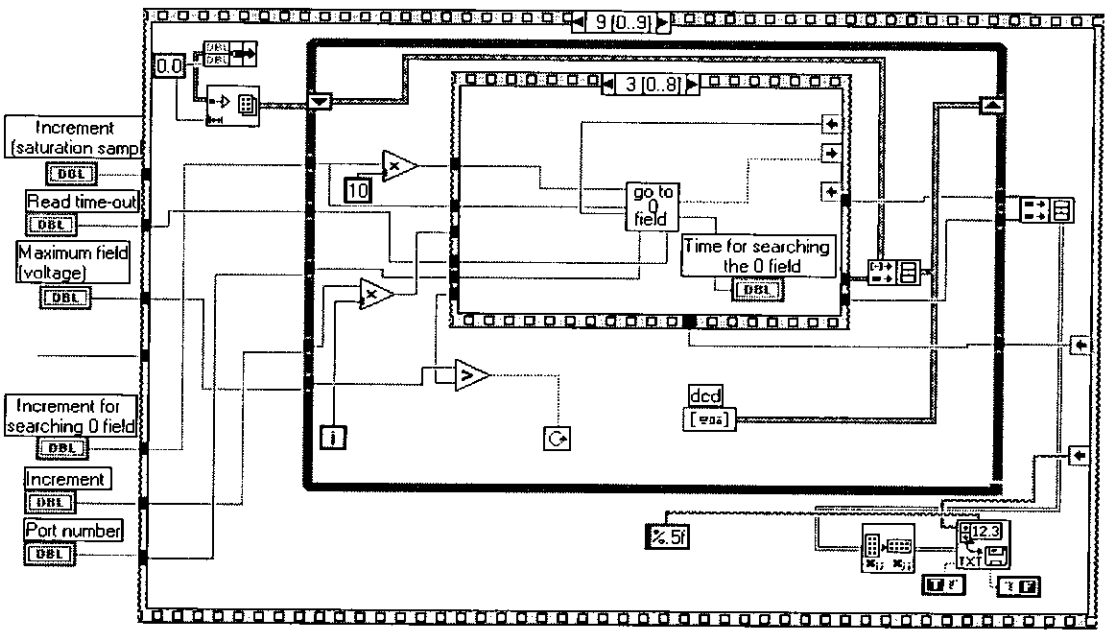

Figure A1.2 LabView routine for DCD measurements. The front panel and the main back diagram are shown in this figure.

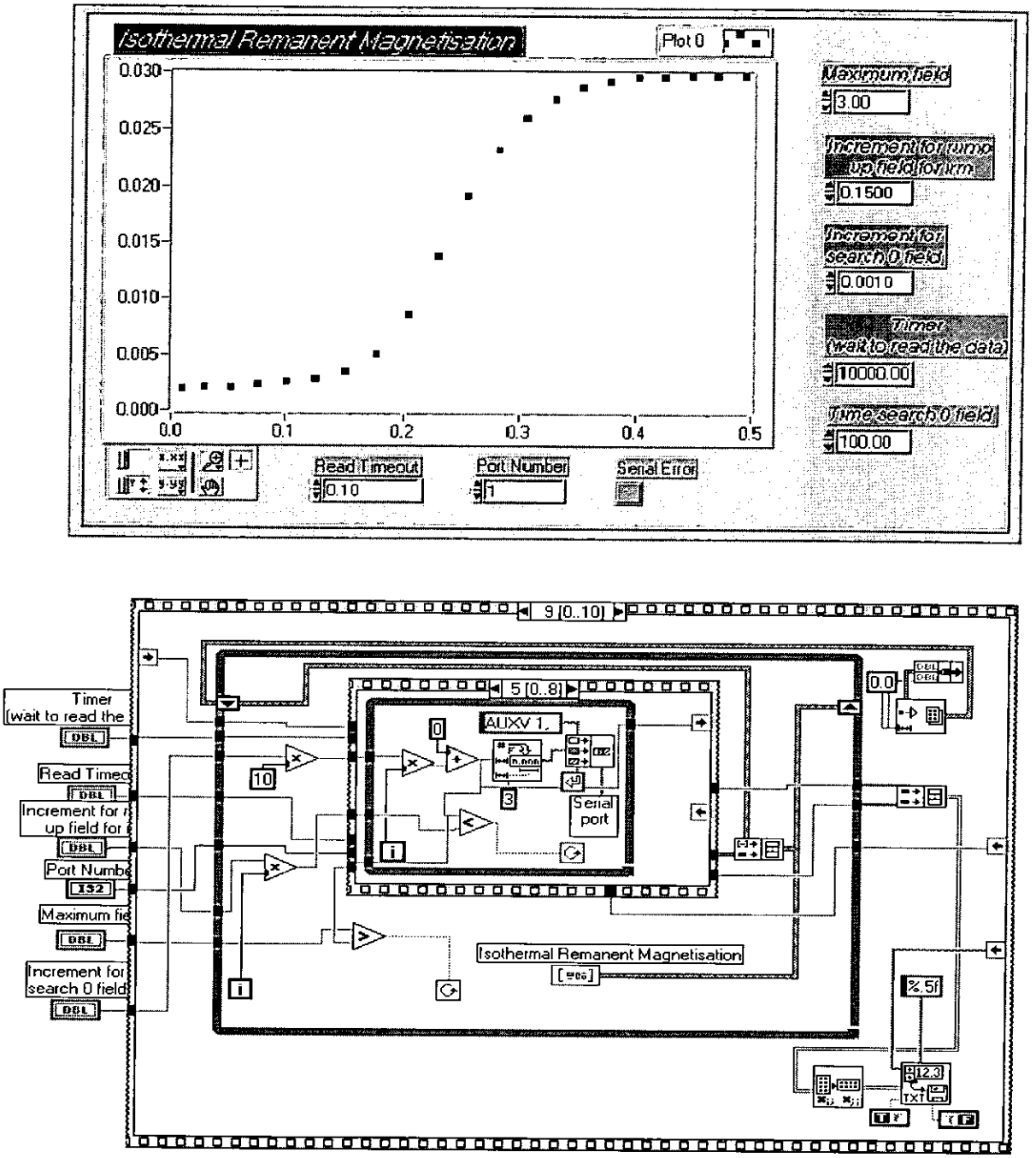

Figure A1.3 LabView routine for IRM measurements. The front panel and the main back diagram are shown in this figure.

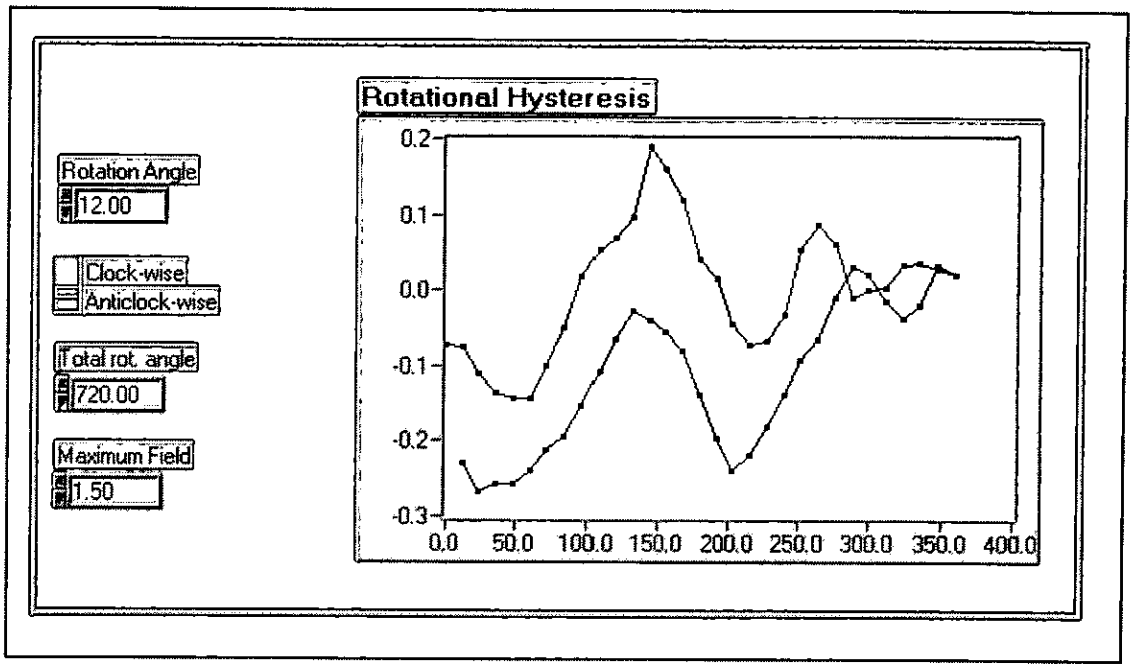

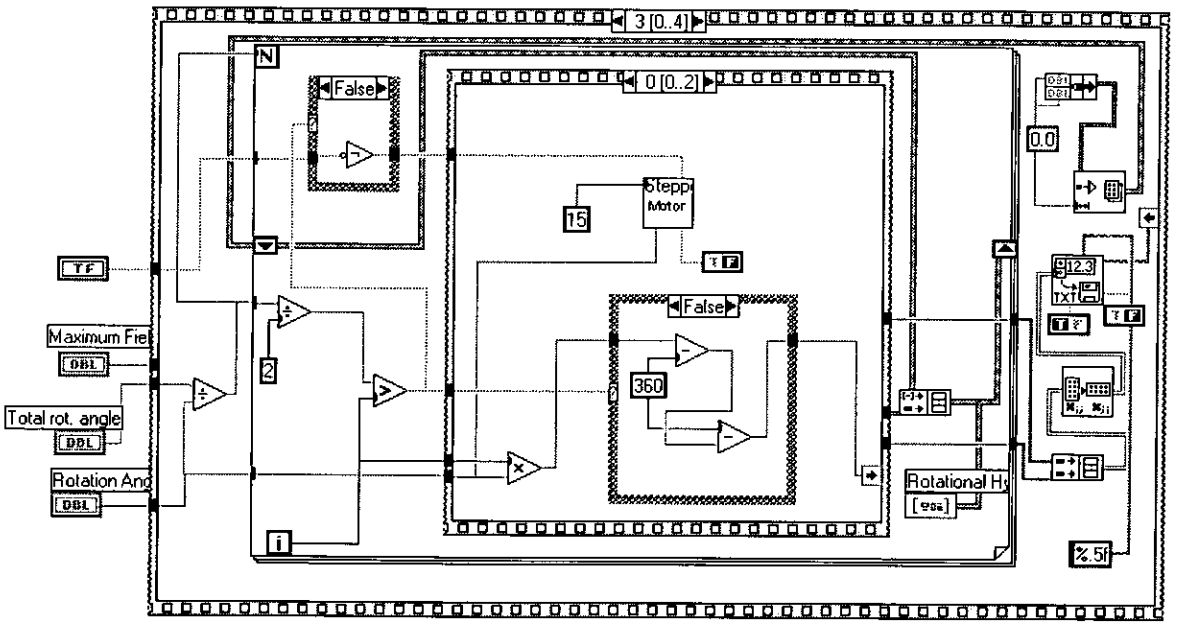

Figure A1.4 LabView routine for rotational hysteresis measurements. The front panel and the main back diagram are shown in this figure.

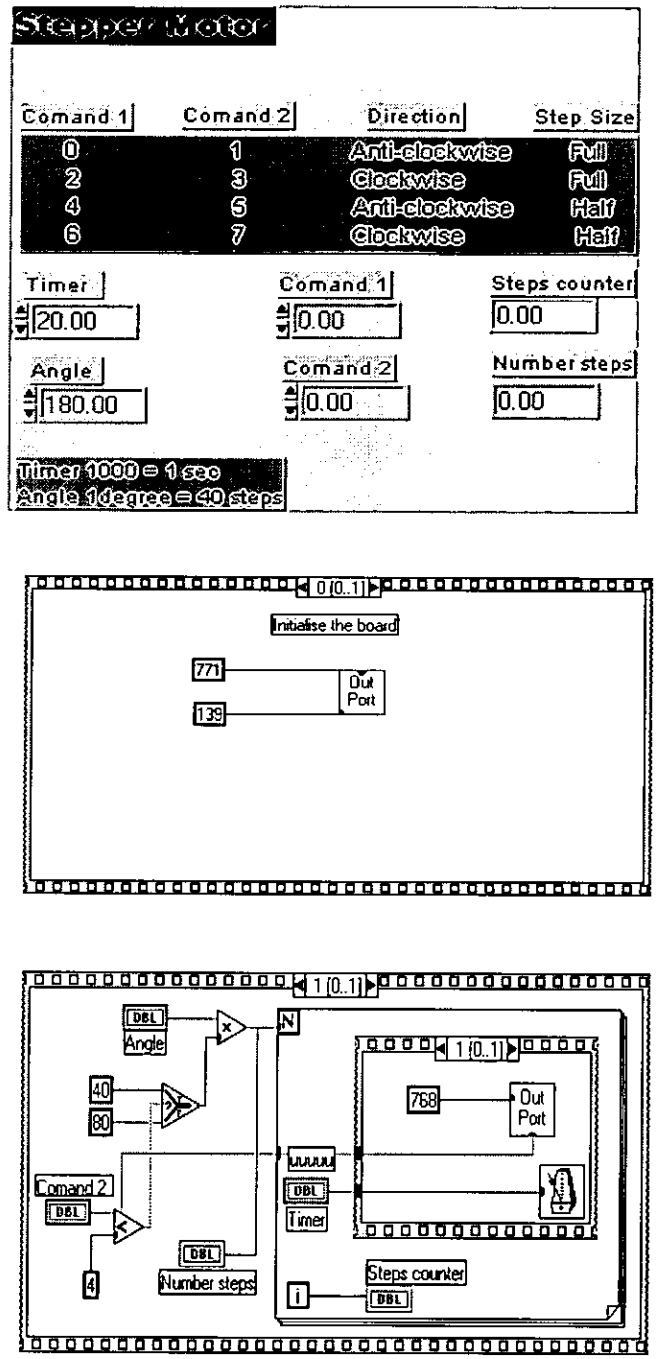

Figure A1.5 LabView routine for stepper motor control. The front panel and the two main sequence back diagrams are shown in this figure.

APPENDIX 2

Experimental samples and their properties

Series 1: Double coated (Fe-Co) metal particle tapes

Recently developed particulate tapes have been analyzed in this paper. These were industrially produced experimental samples of double-coated advanced metal particle (MP) tapes as those used for linear archival data storage such as the LTO and DLT formats. They were chosen because of their similar magnetic properties but different thickness and orientation distribution [1]. The tapes consisted of a thin magnetic coating on top of a non-magnetic underlayer. The magnetic layer varied across the set of four samples from t = 0.12 μm to 0.26 μm. The non-magnetic underlayer is most probable a α-Fe_2O_3 iron oxide [2] while the magnetic top layer contains Co-Fe metallic particles approximately 100nm in length and with an aspect ratio ~ 5:1. It is expected that shape anisotropy will be significant in these particles, although doping with a small amount of Co will also increase their intrinsic coercivity. They have been also passivated (for protection against corrosion) by an induced oxidation of the surface and subsequently uniformly distributed in a non-magnetic polymer matrix using normal manufacturing techniques and alignment in a magnetic field prior to drying. It is assumed that the same process has been use to produce all four samples and that the only significant difference is the thickness of the magnetic coating. Standard in-plane/out-of-plane VSM experiments were made on single layer square samples with a total area of 1 cm^2 and the data are given in table A2.1.

However, the vectorial measurements require a more careful sample preparation. Due to symmetry and demagnetizing field considerations, the experiments involving magnetic measurements as a function of the rotation angle should be performed on circular disk samples rather than square shape samples. Moreover, the signal generated by a single layer disk sample is very small. Hence, in order to increase the signal level a stack of 16 layers was used. The stack was obtained by folding the tape along the recoding direction and then gluing it carefully in order to maintain the magnetic orientation.

Table A2.1. In-plane magnetic parameters for MP tapes obtained from VSM measurements.

MP tapes Samples	Magnetic Thickness (μm)	Coercivity Hc (mT)	Orientation Ratio (OR)	Squareness Sq (Mr/Ms)
A	0.26	191	2.1	0.82
B	0.19	194	2.2	0.83
C	0.17	192	2.1	0.81
D	0.12	194	2.2	0.82

Finally, the stack was punched with a special disk shape puncher. This produced a sample that has a total area of 12.5 cm^2 and increased the signal to noise ratio to satisfactory levels without compromising the sheet demagnetization factor of the sample.

Series 2: Sputtered Co-Cr-Ta thin films

Uniaxial crystal anisotropy of the films is the major source of the magnetic anisotropy in cobalt based alloy thin films and strongly influences their magnetic properties. It has been reported [3-6] that the crystallographic orientation of cobalt based alloy thin films such as Co-Cr-Ta, depends strongly on the orientation of the underlayer as this affects the orientation of the thin film during growth. In addition, other factors such as inter-grain interactions influence the magnetic properties of the films. Co based alloy films produced by magnetron sputtering are very convenient for generating high-density recording media. Usually, thin film media are sputtered on a rigid disk substrate during a static process. An alternative producing method is transfer deposition, where the substrate is slowly moved passing the sputtering target on a continuous production line. In the case of sputtering perpendicular to the film plane on a static substrate, it would be expected that the magnetic properties would be isotropic in the film plane. Contrary, in the case of transfer deposition, the incidence angle will vary throughout the film thickness and this may generate an anisotropy in the film. Because the deposition angle changes throughout the film thickness, this process leads to a bowed columnar structure in the transfer direction [7]. Due to the induced anisotropy, the samples were selected as a series of four Co-Cr-Ta thin films on a Cr underlayer and produced by this technique. They have been extensively analysed and reported previously [8,9] and their main properties and the codification are given in table A2.2.

Table A2.2 Magnetic parameters for Co-Cr-Ta thin film samples obtained from VSM measurements

Co-Cr-Ta Samples	Co-Cr-Ta Thickness (nm)	Coercivity Hc (mT)	Orientation Ratio (OR)	Squareness Sq (Mr/Ms)
E	40	117	1.05	0.84
F	60	106	1.06	0.78
G	80	98	1.11	0.78
H	100	96	1.10	0.71

The magnetic thickness has been varied from 40 nm to 100 nm in steps of 20 nm, while the Cr underlayer thickness was kept constant at 50 nm. The films were deposited on silicon wafers using a circuit processing apparatus in-line DC magnetron transfer sputtering system [10,11]. In order to reduce texture effects of the substrate, naturally oxidised wafers were used and coated with 50 nm Cr underlayer before depositing the magnetic layer in the same system. The Co-Cr-Ta deposition rates varied from 1 nm/s to 2.5 nm/s for film thickness of 40 nm and 100 nm, respectively. During deposition, each disk has been subjected to the same range of deposition angles and this produced a different depth profile for films of different thickness. The substrate temperature was fixed at 250^0 C.

1 cm square samples were cut from the wafers and used for standard VSM experiments. Rotational hysteresis measurements were carried out using 1 cm diameter disk samples. Both, the square and circular disk samples were cut using a diamond knife. The circular disk films were initially obtained by cutting a square film in a hexagon-like shape and then further processed / polished (using an extremely fine grinder) until a circular disk shape was formed.

APPENDIX 3

Introduction to the principles of magnetic recording

This appendix gives a brief tutorial introduction to basic concepts of the magnetic recording technology. However, a more detailed mathematical presentation of the physics of magnetic recording can be found in the references [12,13].

The recording process is defined as the mechanism of imprinting magnetic information on a recording medium and then reading back the information in its original form, which can be analogue or digital data. Therefore, for magnetic recording a recording head and a magnetic medium are needed. Different types of recording media have been already described in the section 1.2.

The recording head is an electromagnet with a gap that has to be located near the medium. The information to be recorded is contained in the current that passes through the head coil (see figure A3.1, a).

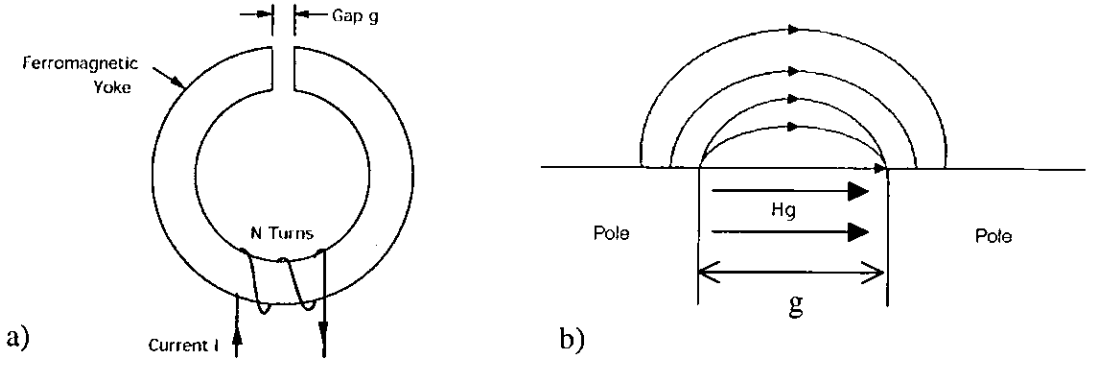

Figure A3.1 a) An ideal write-head showing the core (yoke), the coil and the gap.
b) The fringing field around the top of the gap of a write head.

By moving the head at constant speed relative to the medium, the fringing fields from the head gap (see figure A3.1,b) permanently magnetize the medium and the information is stored. Modern recording media require that the gap field (H_g) to be around three times bigger than the coercive field of the medium ($H_g = 3 \cdot H_c$) and smaller than 60% of the saturation flux density of the pole ($H_g \leq 0.6 \cdot Bs$). The gap field H_g is given by the relation [14]:

$$H_g = \frac{N\eta I}{g} \tag{A3.1}$$

where: N is the number of turns, I the current carrying the signal to be recorded and η is the writing head efficiency (usually $\eta = 0.8$). Assuming the above introduced conditions fulfilled, the longitudinal component (H_x) of the fringing field above the gap, at a point P, is given by the Karlqvist approximation [15]:

$$H_x = \frac{H_g}{2\pi}\left[\arctan\left(\frac{g/2+x}{z}\right)+\arctan\left(\frac{g/2-x}{z}\right)\right] \tag{A3.2}$$

where: g is the gap distance (see figure A3.1,b), x and z are the P coordinates in respect with the geometry described in figure A3.2.

Figure A3.2 shows the geometry of the magnetic recording process, where the head moves relatively to the medium in the longitudinal (x) direction with a constant velocity v. The figure also indicates that the medium is magnetised in the (x) longitudinal direction, which is true for all longitudinal recording media.

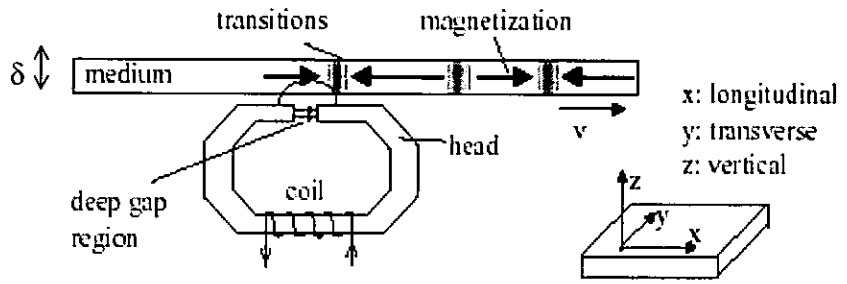

Figure A3.2 Geometry of the longitudinal recording process and the coordinate system associated with it.

Considering only the longitudinal magnetisation and field component and supposing the written magnetisation is sinusoidal: $M_x(x) = M_r \cdot \sin(kx)$, where M_r is the maximum amplitude of the written magnetization and k is the wavenumber ($k = 2\pi/\lambda$), then the two components of the fringing field of the magnetized medium at a point (x, z) below/above the medium are:

$$H_x = -2\pi M_r\left(1-e^{-k\delta}\right)e^{-kz}\sin(kx) \tag{A3.3}$$

$$H_z = 2\pi M_r\left(1-e^{-k\delta}\right)e^{-kz}\cos(kx) \tag{A3.4}$$

where δ is the thickness of the medium;

When reading back the information, the medium is moved past the read head and the flux emanating from the medium and entering the head give rise to a read-back signal. If the track width is "w", the distance head-to-medium is "d" and "g" is the gap length, then for the sinusoidal recording the flux Φ to a coil of a reading head is given by:

$$\Phi(x) = -4\pi M_r w \frac{\left(1 - e^{-k\delta}\right)e^{-kd}}{k} \frac{\sin(kg/2)}{kg/2} \sin(kx) \tag{A3.5}$$

For a read-head coil with N turns the read-out voltage is proportional to the rate of change in time of the flux:

$$V = -\frac{d(N\Phi)}{dt} = -N\frac{d\Phi}{dt} = -N\frac{d\Phi}{dx}\frac{dx}{dt} = -Nv\frac{d\Phi}{dx} \tag{A3.6}$$

where v is the speed of the medium;

Introducing relation A3.5 into A3.6, the read-out voltage is obtained as:

$$V = 4\pi N v M_r w\left(1 - e^{-k\delta}\right)e^{-kd} \frac{\sin(kg/2)}{kg/2} \cos(kx) \tag{A3.7}$$

which is proportional to the number of coil turns, the head-to-medium velocity and written magnetisation. The factor between the brackets is called thickness loss and it shows that the head is not able to read magnetisation patterns written too deep into the medium, the exponential e^{-kd} represents the spacing loss and the factor $\frac{\sin(kg/2)}{kg/2}$ is called the gap loss.

The read-head can be either the same as the write-head or a different one. The information in most common read-heads is retrieved inductively, as described above. However, for high recording densities, inductive read-back heads no longer provide sufficiently sensitivity and modern magneto-resistive (MR) read-heads are used [16,17]. This is because a MR head senses the flux rather than the flux change, which makes the read-out voltage independent on the relative velocity between the head and the medium.

References

Chapter 1

[1]. C. Heck, Magnetic materials and their applications, 1974

[2]. E.C. Stoner, E.P.Wohlfarth, Royal Soc. Phil. Trans., 1947

[3]. L. Neel, C.R. Acad. Sci. Paris, 224, 1947

[4]. W.C. Brown, Phys. Rev., 105, pp. 1479, 1957

[5]. R. Beker, W. Doring, Ferromagnetismus, Sringer-Verlag, Berlin, 1939

[6]. N.S. Akulov, Zeit. Physik, 52, 389, 1928

[7]. I.S. Jacobs, C.P. Bean, Phys. Rev., vol 100 (4), pp. 1060-1067, 1955

[8]. C.D. Mee, E.D. Daniel, Magnetic recording, McGraw-Hill book company, 1987

[9]. E.H. Frei, S. Shtrikman, D. Treves, Phys. Rev., vol. 106, pp. 446-45, 1957

[10]. M.P.Sharrock, Particulate Magnetic Recoring Media, IEEE Trans. on Magn, vol. 25, (6) 1989

[11]. M.N. Baibich, J.M. Broto, A. Fert, F. van dau Nguyen, F. Petroff, ..., Phys. Rev. Lett. 61, pp. 2472, 1989

[12]. J. Brug, L. Tran, M. Bhattacharyya, A. Jander, T.H. Nickel, T.C. Anthony, J.Appl. Phys., 79, pp.4491, 1996

[13]. A.E.Berkowitz, R.P. Goehner, E.L. Hall, J.Appl. Phys., vol 57, pp.3928-3930, 1985

[14]. S.J. Andress, A. Benedetti, A.R. Corradi, G. Fagherazzi, IEEE Trans. on Magn, vol. 22, pp. 1341-1348, 1986

[15]. A.E.Berkowitz, E.L. Hall, P.J.Flanders, IEEE Trans. on Magn, vol. 35, pp. 3816-3819, 1987

[16]. E. Koster, I.E.R.E Conf. Proc., No.26, pp. 213-222, 1973

[17]. U. Kullman, E. Koster, B. Meyer, IEEE Trans. on Magn., MAG-20, pp. 742-744, 1984

[18]. P. Maestro, D. Andriamandroso, G. Demazeau, M. Pouchard, P. Hagenmuller, IEEE Trans. on Magn., MAG. 18, pp. 1000-1003, 1982

[19]. G.R. Cole, L.C. Bancroft, M.P. Chouinard, J.C. McCloud, IEEE Trans. on Magn., MAG-20, pp. 19-23, 1984

[20]. A.E. Berkowitz, R.P. Goehner, E.L. Hall, P.J. Flanders, J.Appl. Phys., vol. 57, pp. 3928-3930, 1985

[21]. J.C. Slonczewski, Phys. Rev., vol. 110, pp. 1341-1348, 1958

[22]. M. Tachiki, Prog. Theoret. Phys., vol.23, pp. 1055-1072, 1960

[23]. G. Akashi, Proc. of the ICF 3, Centre for Academic Publication, Japan, 1981, pp. 548-552

[24]. R. Chubachi, N. Tamagawa, IEEE Trans. on Magn, vol. 20, pp. 45-47, 1984

[25]. O. Kubo, T. Ido, H. Yokoyama, IEEE Trans. on Magn., 18, pp. 1122-1124, 1982

[26]. G. Bate, ed. E.P. Wohlfarth, N. Holland Publ., pp. 381-507, 1980

[27]. K. O'Grady, R.G. Gilson, P.C. Hobby, JMMM, 95, pp. 341-355, 1991

[28]. C. Denis Mee, Eric D. Daniel, Magnetic recording technology, vol.1, 1987

[29]. G. Bate, J.Appl. Phys., 37, pp.1164, 1966

[30]. R.D. Fisher, J.C. Allan, J.L. Pressesky, IEEE Trans. on Magn., 22, 352, 1986

[31]. T. Shimatsu, S. Yokota, D.D. Djayaprawira, M. Takahashi, T. Wakiyama, IEEE Trans. on Magn., 9, 34, 1994

[32]. S. Iwasaki, Y. Nokamura, IEEE Trans. on Magn., 13, pp. 1272, 1977

[33]. P.J. Grundy, J. Phys. D: Appl. Phys, 31, pp. 2975-2990, 1998

[34]. H.J. Richter, J. Phys. D: Appl. Phys., 32, pp. 147-168, 1999

[35]. A. Brenner, G.E. Riddell, J. Res. Natl. Bur. Stand., 37, 31, 1946

Chapter 2

[1]. H. Zijlstra, Exp. Methods in Magnetism, North-Holl. Pub. Com., Amsterdam, 1967

[2]. D.O. Smith, Rev. Sci. Instruments, Vol. 27, No.5, pp. 261-268, 1956

[3]. S. Foner, vol 30, 1959

[4]. H.J. Richter, JMMM 111, pp. 201-213, 1992

[5]. J.P.C. Bernards, G.J.P. van Engelen, H.A.J. Cramer, JMMM 123, pp. 141-146, 1993

[6]. G. Gorodetsky, L.M. Levinston, Solid State Comun., 7 (1969) 67

[7]. J. Mallinson, J. Appl. Phys., 37, pp. 2514, 1966

[8]. T. Bolhuis, L. Abelmann, J.C.Lodder, E.O. Samwel, JMMM, 193, pp. 332-336, 1999

[9]. G.W.D. Spratt, P.R. Bissell, R.W. Chantrell, E.P. Wohlfarth, JMMM, 75, pp. 309-318, 1988

[10]. P.E. Kelly, K.O'Grady, P.I. Mayo, R.W. Chantrell, IEEE Trans. Magn., 25, pp.3880, 1989

[11]. M.L. Williams, R.L. Comstock, AIP Conf, 5 (1971), 738

[12]. O. Henkell, Phys. Status Solidi, 7, 919, 1964

[13]. R.W. Chantrell, K. O'Grady, J.Phys. D: Appl. Phys. 25 (1992), pp. 1-23

[14]. P.A. Bates, PC Interfacing using LabView, Univ. of Central Lancashire, 1998

[15]. LabView User Manual, National Instruments, 1998

[16]. B.E. Paton, Sensor, Transducers & LabView, Prentice Hall, 1998

[17]. J. Essick, Adanced LabView Labs, Prentice Hall, 1999

[18]. C.E. Johnson, J. Phys. D: Appl. Phys. 29 (1996), pp. 2266-2273

[19]. D.P.E. Dickson, F.J. Berry, Mossbauer Spectroscopy, Cambridge Univ. Press, 1986

[20]. K. Wertheim, Academic Press, New York, 1964

[21]. U. Gonser, Springer – Verlag, Berlin, 1975

[22]. I.J. Guverman, 1965-74, Vols. I-IX, Plenum Press, New York

Chapter 3

[1]. M.P. Sharrock, IEEE Trans. on Magn., vol. 26 (1), 1990

[2]. [4]. Dennis E. Speliotis, IEEE Trans. on Magn., vol. 26 (5), 1990

[3]. I.S. Jacobs, F.E. Luborsky, J. Appl. Phys., 28, No. 4, 467, 1957

[4]. G. Bottoni, JMMM 155 (1996), pp. 16-18

[5]. G. Bottoni, JMMM 140-144 (1995), pp. 2207-2208

[6]. T.L. Templeton, A.S. Arrot, J. Appl. Phys., 81 (8), 1997, pp. 3797-3799

[7]. M. Igaki, H. Nagamori, T. Shimatsu, M. Takahashi, JMMM 183, pp. 209-219, 1998

[8]. R. Keller, E. Schmidbauer, JMMM, 187, No.2, pp.160-168, 1998

[9]. J.J. Wyslocki, W. Suski, P. Pawlik, K. Wochowski, B. Kotur, O.I. Bodak, JMMM, 162, pp. 239-246, 1996

[10]. S. Shtrikman, D. Treves, Journ. De Phys. Et le Radium, 20, pp.286-289, 1959

[11]. P.J. Flanders and S. Shtrikman, J. Appl. Phys. vol.33 (1), pp. 216-219, 1962

[12]. Y. Uesaka, K. Yoshida, Y. Nakatani, N. Hayashi, J. Appl. Phys., 77 (10), 1995, pp. 5303-5309

[13]. Y. Uesaka, Y. Nakatani, N. Hayashi, H. Fukushima, N. Inaba, IEEE Trans. on Magn., vol. 35 (5), 1999

[14]. R.F. Penoyer, Conf. MMM, Boston, 1956

[15]. R.F. Pearson, J. de Phys. Et. Radium, 20, 409-413, 1959

[16]. G.W. Rathenau, J.L. Snoek, Physica, 8, 555-575, 1941

[17]. H. Zijlstra, Rev. Sci. Instr., 32, 634-638, 1961

[18]. A. Aharoni, E.H. Fei, S. Shtrikman, D. Traves, Bul. Res. Conc. Israel, 6, 1957

[19]. L. Parreti, G. Turilli, J. Appl. Phys., 61, 1987, pp. 5098-5101

[20]. P.M.Sollis, P.R.Bissell, Journal of Physics D-Applied Physics 24 (1991) 1891

[21]. R.W. Chantrell, P.R. Bissell, P. Sollis, A. Hoare, T. Orth, JMMM 177 (1998), pp. 894-895

[22]. H.V. Jones, A.W.G. Duller, R.W. Chantrell, P.R. Bissell, A. Hoare, Jour. of Phys. D-Appl. Phys., 31, pp. 3028-3035, 1998

[23]. S.R. Hoon, G.R. Lawson, F. Thompson, B. Dean, R.W, Chantrell, JMMM, 1991

[24]. U. Netzelmann, J. Appl. Phys. vol.68 (4), 1990

[25]. S.V. Vonsovskii, Ferromagnetic Resonance, Pergamon, 1966

[26]. F.P. Valstyn, J.P. Hanton, A.H. Morrish, Phys. Rev., 128 (5), 1962

[27]. G. Asti, S. Rinaldi, J. Appl. Phys. vol.45 (8), pp. 3600-3610, 1974

[28]. G. Bottoni, D. Candolfo, A. Cecchetti, J. Appl. Phys. vol.81 (8), 3794 -3796, 1997

[29]. M. Vopsaroiu, P.R. Bissell, R. Cookson, Physica Status Solidi, 189, 2/3, 2002

[30]. L.A. Beardsley, V.S. Speriosu, IEEE Trans. on Magn., vol. 26 (5), 1990

[31]. A. Stancu, L. Stoleriu, M. Cerchez, J. Appl. Phys., 89 (11), 2001

[32]. G.W.D. Spratt, P.R. Bissell, R.W. Chantrell, E.P. Wohlfarth, JMMM, 75, pp. 309-318, 1988

[33]. O. Henkell, Phys. Status Solidi, 7, 919, 1964

[34]. P.E. Kelly, K.O'Grady, P.I. Mayo, R.W. Chantrell, IEEE Trans. Magn., 25, pp.3880, 1989

[35]. M.L. Williams, R.L. Comstock, AIP Conf. Proc., 5, pp. 738-742, 1971

[36].]. H.L.Lee, J. Appl. Phys., 63, pp. 2369, 1988

[37]. J.K.Howard, J. Appl. Phys., 63, pp. 3263, 1988

[38]. N. Inaba, Y. Uesaka, M. Futamoto, IEEE Trans. on Magn., vol. 35 (5), pp. 2670-2672, 1999

Chapter 4

[1]. P.M.Sollis, P.R.Bissell, Journal of Physics D-Applied Physics 24 (1991) 1991

[2]. P.R. Bissell, M. Vopsaroiu, R.D. Cookson, M.P. Sharrock, JMMM, 242-245, 2002, 331-334

[3]. M. Vopsaroiu, P.R. Bissell, R. Cookson, Physica Status Solidi, 189, 2/3, 2002

[4]. R.D. Cookson, P.R. Bissell, G.E. Kay, D.A. Parker, in press JMMM, 2002

[5]. S.R. McConochie, F. Schmidlin, P.R. Bissell, J.A. Gotaas, D.A. Parker, JMMM, 155 (1996), pp. 89-91

[6]. S.R. McConochie, P.R. Bissell, D.A. Parker, J.A. Gotaas, IEEE Trans. on Magn., 33 (5) 1997

Chapter 5

[1]. Y. Yu, J.W. Harrell, JMMM, 155, pp. 126, 1996

[2]. M. Shtrickman, D. Treves, J. Appl. Phys. 31, 58S, 1960

[3]. M. el-Hilo, P.E. Kelly, K. O'Grady, J. Popplewell, IEEE Trans. Magn., 26, pp. 210, 1990

[4]. S.R. Hoon, D.M. Paige, IEEE Trans. Magn., vol. 23, No. 1, pp. 183-185, 1987

[5]. H.G. Zolla, F. Spaepen, IEEE Trans. Magn., vol. 31, No. 6, pp. 3814-3816, 1995

[6]. J. Skilling, R.K. Bryan, Mon. Not. R. Astron. Soc., vol. 211, pp. 111-124, 1984

[7]. J.A. Potton, G.J. Daniell, D. Melville, J. Phys.: D, Appl. Phys. 17, pp. 1567-1581, 1984

[8]. J.W. Harrell, Y. YU, Y. YE, J.P. Parakka, D.E. Nikles, H.G. Zolla, J. Appl. Phys. vol.81 (8), pp. 3800-3802, 1997

[9]. W.T. Vetterling, F. Habbal, M. A. Wober, IEEE Trans. Magn., vol. 23, No. 5, pp. 2815-2817, 1987

[10]. C.E. Johnson, J. Appl. Phys. (D) vol.29, pp. 2266-2273, 1996

[11]. M.P. Morales, S.A. Walton, L.S. Prichard, C.J. Serna, D.P.E. Dickson and K. O'Grady, JMMM 190, 3, PP. 357-370, (1998)

[12]. N.N. Greenwood, T.C. Gibb, Mössbauer Spectroscopy, Chapman and Hall, London, 1971

[13]. H. Takano, T.T. Lam, J.G. Zhu, J.H. Judy, IEEE Trans. on Magn., vol. 29, 6, 1993.

[14]. F. Schmidllin, P.R. Bissell and J.A. Gotaas, J. Appl. Phys. vol.79 (8), 1996

[15]. M. Vopsaroiu, P.R. Bissell, R. Cookson, Physica Status Solidi, 189, 3, 2002

[16]. P.. Glijer, E. Abarra, H. Kisker, M.W. Muller, IEEE Trans. Magn., 32, pp. 3557-3562, 1996

[17]. M. Alex, J. Scott, T. Arnoldussen, IEEE Trans. Magn., 33, pp. 2956-2962, 1997

[18]. E.T. Yen, H.J. Richter, G.L. Chen, G.C. Rauch, IEEE Trans. Magn., 33, pp. 2701-2703, 1997

[19]. E.T. Yen, T. Thomson, G.L. Chen, H.J. Richter, R.Y. Ranjan, G.C. Rauch, IEEE Trans. Magn., 36, No. 5, pp. 2330-2332, 2000

[20]. T.J. Silva, H.N. Bertram, IEEE Trans. Magn., 26, pp. 3129-3139, 1990

[21]. H.N. Bertram, Cambridge Univ. Press, 1994, pp.306-308

[22]. T. Bolhuis, L. Abelmann, J.C.Lodder, E.O. Samwel, JMMM, 193, pp. 332-336, 1999.

[23]. Chemical Applications of Mössbauer spectroscopy, by V.I.Goldanskii and R.H.Herber, Academic Press (1968) 211-214

Appendixes

[1]. M. Vopsaroiu, P.R. Bissell, R. Cookson, Physica Status Solidi, 189, 3, 2002

[2]. V. Kuncser, M. Vopsaroiu, B.Sahoo, P.R.Bissell, W.Keune, in press - Hyperfine interactions, July 2002

[3]. K.E. Johnson, P.R. Ivett, D.R. Timmons, M. Mirzamaani, S.E. Lambert, T. Yogi, J. Appl. Phys., 67 (9), pp. 4686-4688, 1990

[4]. J. Daval, D. Randet, IEEE Trans. Magn. MAG-6, 768, 1970

[5]. T. Coughlin, J. Presseeky, S. Lee, N. Heiman, R.D. Fisher, K. Merchant, J. Appl. Phys., 67 (9), pp. 4689-4691, 1990

[6]. D.J. Sellmyer, D. Wang, J.A. Christner, J. Appl. Phys., 67 (9), pp. 4710-4712, 1990

[7]. H.Suzuki, P.R. Bissell, R.W. Chantrell, N. Kodama, JMMM, 146, pp.. 267-272, 1995

[8]. H.Suzuki, N. Kodama, P.R. Bissell, R.W. Chantrell, IEEE, 31, No. 6, pp.2800-2802, 1995

[9]. H.Suzuki, P.R. Bissell, R.W. Chantrell, N. Kodama, JMMM, 155, pp.196-198, 1996

[10]. Y. Tanaka, H. Ito, T. Sonoda, R. Nishikawa, IEEE Trans. Magn.,23 (1987) 2046

[11]. E.Teng, N. Ballard, IEEE Trans. Magn., 22 (1986) 579

[12]. H.M. Bertram, Theory of Magnetic Recording, Cam. Univ. Press, 1994

[13]. J.C. Mallinson, The Foundations of Magnetic Recording, San Diego, 1993

[14]. H. J. Richter, J. Phys. D: Appl. Phys., 32, pp.147-168, 1999

[15]. O. Karlqvist, Trans. R. Soc. Technol., 85, pp.1-27, 1954

[16]. J. Hong, J. Kane, J. Hashimoto, M. Yamagishi, K. Noma, H. Kanai, in press. IEEE Trans. Magn.

[17]. H. Kanai, K. Noma, J. Hong, Fujitsu Sci. Tech. J. 37, pp. 174-182, 2001

Publications

phys. stat. sol. (a) 189, No. 3, 759–762 (2002)

Anisotropy Field Measurements Using an Extended Rotational Remanence Technique

M. VOPSAROIU[1]), R. COOKSON, and P. R. BISSELL

Centre for Materials Science, Department of Physics, Astronomy and Mathematics, University of Central Lancashire, Preston PR1 2HE, UK

(Received May 1, 2001; accepted September 30, 2001)

Subject classification: 75.30.Gw; 75.50.Ss; 75.90.+w; S1.1

An extended method for anisotropy field measurements has been developed using a vector vibrating sample magnetometer (VSM). The technique, which relates the switching of particles nearly perpendicular to an applied field to the sample anisotropy, is suitable for magnetic media that contain orientated particles. Results measured as a function of angle are extrapolated to 90° for an improved measure of anisotropy field. *In plane* properties have been investigated for a series of four advanced double coated metal particle (MP) tapes. The results show that the *in plane* anisotropy field is related to the magnetic coating thickness, as a result of changes in magnetostatic interactions between the particles with thickness.

Introduction The anisotropy field and its distribution is a very important parameter for determining potential applications of magnetic recording media. In commercial applications, recording media properties are generally characterized by standard hysteresis parameters such as the coercivity. However, this is related not only to the magnetic particle properties but also to way the particles are incorporated into the matrix, such as the orientation of the particle easy axes. The advantage of anisotropy field distribution measurement is that, although the particle interactions still influence the results, other properties of the matrix are excluded so that results relate more to the potential of a "particle type" to the application rather than to the specific coating under investigation. This is because a single domain particle makes a contribution to the anisotropy field related to its switching field when its easy axis is aligned with the applied field but it is still under the influence of interactions with other constituent components of its magnetic environment. On the other hand, the particle contribution to coercivity is related to its switching field with the particle easy axis in its present orientation to the applied field. Many techniques have been developed to measure the anisotropy field and anisotropy field distribution using remanent torque magnetometry [1, 2] or vibrating sample magnetometer (VSM) measurements [3, 4]. Rotational hysteresis has also been extensively used for effective anisotropy field measurements [5, 6]. Many of the techniques determine the anisotropy field using experiments which involve switching processes. Anisotropy field can be also measured using non-switching techniques, such as transverse susceptibility. Sollis and Bissell [7] have been used transverse susceptibility for anisotropy field measurements and magnetic thickness calculation on CrO_2 systems. In this paper, we describe a method for determination of the anisotropy field distribution and the effective mean anisotropy field of the particles using a biaxial VSM. The technique is an extension of the remanent magnetometry method described

[1]) Corresponding author; Fax: +00-44-(0)1772-892996; Tel.: +00-44-(0)1772-893579; e-mail: mvopsaroiu@uclan.ac.uk; v.marian@lycos.com

 0031-8965/02/18902-0759 $ 17.50+.50/0

previously [3, 4], but higher precision results are reported using our extended experiment and involving an extrapolation for greater accuracy.

Experimental Method and Discussions An investigation of four samples is described in this paper. These were experimental double-coated advanced metal particle (MP) tapes as those used for digital data storage on systems such as the LTO format and have been selected because they exhibit different texture and magnetic thickness. They had a double coating consisting of a non-magnetic under-layer and a thin magnetic top-coat, which range from an $M_r t$ (saturation remanence × thickness) of 3 to 6 (T nm). The magnetic top layer contains Co–Fe metallic particles approximately 100 nm in length and with an aspect ratio ~5:1. Biaxial VMS experiments were carried out at room temperature on 1 cm diameter samples made of stacks of 16 single layers glued together to maintain their tape orientation. This produced a sample corresponding to 12.5 cm^2 and reduced the signal to noise ratio at satisfactory levels without compromising the sheet demagnetization factor of the sample. The disk samples were mounted in the VSM with the sample plane and the rotational axis coincident. Our technique is similar to remanent torque magnetometry, except that direct measurement of the magnetization change was used rather than in torque measurements. We determined the effective anisotropy field by identifying the field value required to produce switching if applied at an angle close to 90° from the *in plane* symmetry direction of the sample easy axis distribution (EAD). This mean direction was determined by measuring saturation remanence as a function of angle. The direction corresponding to maximum value was taken as the center of the EAD on the assumption that the distribution was symmetric about this direction. Starting from this point, the sample was rotated through 90° and a saturating field was applied and removed. In this remanent state, the sample was rotated through a small angle α. A small field was applied and removed and the change in remanence perpendicular to the applied field direction was recorded. Using gradually increasing fields, the change in remanence was due to the reversal of particle moments lying between 90° and (90° + α) to the center of the EAD. For small α, this corresponds to particle moments reversing at their anisotropy field. The differential of the remanence curve, or approximately the variation in the transverse remanent moment between two successive field applications and removals H_i and H_{i+1}, is the anisotropy field distribution of the particles.

This indicates how many particles with their easy axes between 90° and (90° + α), have an anisotropy field value between H_i and H_{i+1}. In Fig. 1 we present the *in plane* anisotropy field distributions measured for a 5° rotation

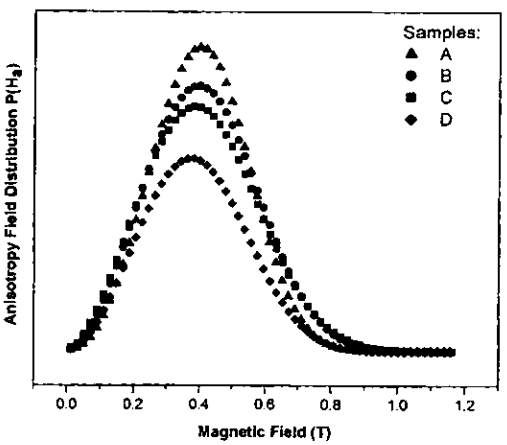

Fig. 1. Anisotropy field distribution measured for a 5° rotational angle

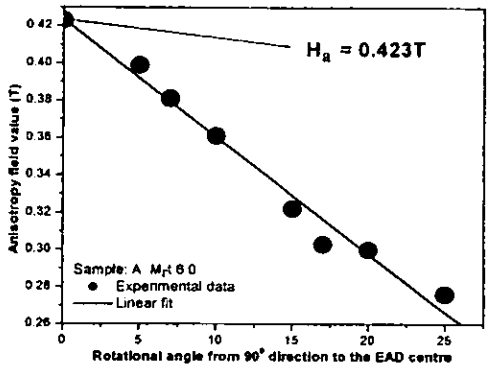

Fig. 2. Variation of the anisotropy field with measurement angle α. The straight-line extrapolation back to $\alpha = 0$ is a least-squares fit for the data points

angle and the mean anisotropy field is taken as the field value corresponding to the curve peak. Strictly speaking, this is only an approximate measure and will only be a true measure of anisotropy field if $\alpha \to 0$. Measurements for very smaller angles are difficult as the signal becomes too small to measure and the error increases. Most reported measurements using this technique therefore work with an angle of about 5°. We have extended the measurements by repeating them for up to seven different rotational angles from 5° to 25°. By plotting the peak field value against the rotational angle, it is found that these values lie approximately on a straight line which can be extrapolated back to $\alpha = 0$ (see Fig. 2).

The intersection point of the extrapolated line with the field axis gives a more accurate value of the anisotropy field. The experimental results are summarized in Table 1.

The experimental results show a correlation between the anisotropy field and magnetic coating thickness. The dependence (Fig. 3) suggests that as the magnetic thickness increases, the anisotropy field also increases.

This result could be understood in terms of interactions between the particles. In an ideal medium consisting of magnetically isolated particles, the measured anisotropy field value represents the anisotropy field of the individual particles. However, in a real system, the magnetic anisotropy field is reduced by inter-particular magnetostatic interactions, since this anisotropy field is mainly caused by the shape anisotropy due to magnetostatic energy [8]. Therefore, the measured anisotropy field values represent a mean effective anisotropy field, which includes the interaction effects. Recently, theoretical investigations on the magnetostatic interactions in particulate media have revealed a clear dependence of the magnetostatic interactions on the magnetic coating thickness [9]. It has been shown that a network of 2D particles has an enhanced magnetostatic

Table 1

Sample characteristics and experimental data resulting from standard and bi-axial VSM measurements. Magnetic thicknesses have been evaluated from demagnetizing field measurements using the transverse susceptibility technique [7]

samples	$M_r t$ (T nm)	magnetic thickness t (μm)	coercivity field H_c (T)	anisotropy field H_a (T)
A	6.0	0.26	0.191	0.423
B	4.5	0.19	0.192	0.418
C	4.0	0.17	0.192	0.411
D	3.0	0.12	0.194	0.400

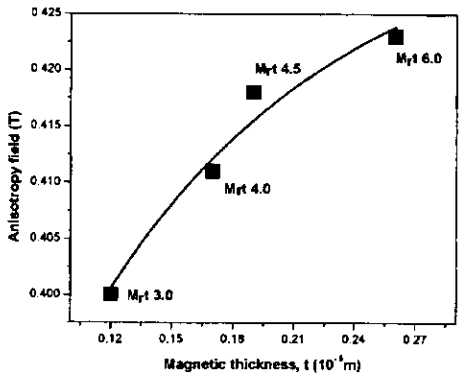

Fig. 3. Influence of the magnetic thickness on the effective anisotropy fields

interaction distribution over that of a 3D system of particles. As a consequence, the interaction effects are more pronounced for thinner medium. Since the anisotropy field of metal particles is reduced by the inter-particular magnetostatic interactions, as explained earlier, for a thinner medium, the anisotropy field is smaller. This theoretical result [9] is in agreement with our experimental data (see Fig. 3), where the anisotropy field increased as the magnetic thickness increased.

Conclusions An extended technique for anisotropy field measurements has been developed, which leads to a more precise anisotropy determination. Four experimental advanced double-coated metal particle tapes have been analyzed using our described method. The results point to an influence of the magnetic thickness on the anisotropy field, demonstrated by the anisotropy field variation with respect to the thickness. The experimental data are in agreement with recent theoretical studies of the interactions effects in particulate media [9].

Acknowledgements The authors would like to thank the National Storage Industries Consortium "Advanced Tape Program" and the Engineering and Physical Sciences Research Council for financial support for this work.

References

[1] P. J. FLANDERS and S. SHTRIKMAN, J. Appl. Phys. **33**, 216 (1962).
[2] S. R. HOON and D. M. PAIGE, IEEE Trans. Magn. **23**, 183 (1987).
[3] M. P. SHARROCK, IEEE Trans. Magn. **26**, 225 (1990).
[4] D. E. SPELIOTIS, IEEE Trans. Magn. **26**, 1891 (1990).
[5] G. BOTTONI, J. Magn. Magn. Mater. **140–144**, 2207(1995).
[6] T. L. TEMPLETON and A. S. ARROT, J. Appl. Phys. **81**, 3797(1997).
[7] P. M. SOLLIS and P. R. BISSELL, J. Phys. D **24**, 1891 (1991).
[8] M. IGAKI, H. NAGAMORI, T. SHIMATSU, and M. TAKAHASHI, J. Magn. Magn. Mater. **183**, 209 (1998).
[9] A. STANCU, L. STOLERIU, and M. CERCHEZ, J. Appl. Phys. **89**, 7260 (2001).

INSTITUTE OF PHYSICS PUBLISHING JOURNAL OF PHYSICS D: APPLIED PHYSICS
J. Phys. D: Appl. Phys. 35 (2002) 1296–1300 PII: S0022-3727(02)34369-9

Interaction effects on the anisotropy field in sputtered Co–Cr–Ta thin films and metal particle tapes

M Vopsaroiu[1] and P R Bissell[1,2]

[1] Centre for Materials Science, University of Central Lancashire, Preston PR1 2HE, UK

E-mail: pbissell@uclan.ac.uk

Received 28 February 2002
Published 31 May 2002
Online at stacks.iop.org/JPhysD/35/1296

Abstract

A comparative experimental study, regarding the effect of the interactions on the anisotropy field, is discussed in this paper. Two different sets of magnetic samples have been analysed using rotational hysteresis and standard remanence measurements. The results show variations of the anisotropy fields with respect to the magnetic thickness. This effect is related to the inter-particles interactions, which are also discussed in detail in the paper.

1. Introduction

Inter-particle interactions play an important role in magnetic materials including magnetic recording media. In thin films, exchange coupling can be dominant and is a major source of noise in magnetic recording sputtered hard disks. Modern disk materials have been developed with the structure controlled to reduce the exchange coupling between grains. In particulate media, the exchange between particles is rather week so that the magnetostatic interactions dominate. Central to interactions is the magnetic anisotropy of the medium.

In this paper, we have made an experimental comparative study between two different systems in order to analyse the interactions and their effects on the magnetic anisotropy fields. The samples consisted of a series of four metal particle (MP) tapes, which were typically representative of advanced archival information storage tape and four sputtered Co–Cr–Ta thin films. The latter were specially prepared to enhance their exchange coupling with a strong in-plane anisotropy and would not be suitable for information storage disk application. However, for our experimental study, since they exhibited very different properties from the particulate media, they provided a good comparison.

The systems have been experimentally analysed using rotational hysteresis (RH) to investigate the anisotropy and standard vibrating sample magnetometer (VSM) measurements of hysteresis loop and remanence properties. Isothermal remanent magnetization (IRM) and DC-demagnetization (DCD) were used to identify the type of interactions by using ΔM plots. The two series of samples showed opposite magnetic interactions, demagnetizing for the particulate media and opposing demagnetization for the thin films, the results pointing to an intimate relationship between magnetic anisotropy and interactions as will be shown in this paper.

[2] Author to whom correspondence should be addressed.

2. Experimental samples and their properties

2.1. Double coated (Fe–Co) MP tapes

Recently developed particulate tapes have been analysed in this paper. These were industrially produced experimental samples of double-coated advanced MP tapes with properties of those used for linear archival data storage such as the LTO and DLT formats. They were chosen because of their similar magnetic properties but different thickness and orientation distribution [1]. The tapes consisted of a thin magnetic coating on top of a non-magnetic underlayer. The magnetic layer thickness varied across the set of four samples from $t = 0.12$ to $0.26\,\mu$m. The non-magnetic underlayer most probably contained an α-Fe_2O_3 iron oxide [2], while the magnetic top layer contains Co–Fe metallic particles approximately 100 nm in length and with an aspect ratio ~5 : 1. It is expected that shape anisotropy will be significant in these particles, although doping with a small amount of Co will also increase their intrinsic coercivity. They have also been passivated (for protection against corrosion) by an induced oxidation of the surface and subsequently uniformly distributed in a non-magnetic polymer matrix using normal manufacturing techniques and alignment in a magnetic field prior to drying. It

is assumed that the same process has been used to produce all four samples and that the only significant difference was the thickness of the magnetic coating. Standard VSM experiments were made on 1 cm^2 samples and data are given in table 1.

2.2. *Sputtered Co–Cr–Ta thin films*

Uniaxial crystal anisotropy of the films is the major source of the magnetic anisotropy in cobalt based alloy thin films and strongly influences their magnetic properties. It has been reported [3–6] that the crystallographic orientation of cobalt based alloy thin films such as Co–Cr–Ta, depends strongly on the orientation of the underlayer as this affects the crystal orientation of the thin film during growth. In addition, other factors such as inter-grain interactions influence the magnetic properties of the films. Co based alloy films produced by magnetron sputtering are very convenient for generating high-density recording media. Usually, thin film media are sputtered on a rigid disk substrate during a static process.

An alternative method is transfer deposition, where the substrate is slowly moved passed the sputtering target on a continuously production line. In the case of sputtering perpendicular to the film plane on a static substrate, it would be expected that the magnetic properties would be isotropic in the film plane. Contrary, in the case of transfer deposition, the incidence angle will vary throughout the film thickness and this may generate an anisotropy in the film. Because the deposition angle changes throughout the film thickness, this process leads to a bowed columnar structure in the transfer direction [7]. Due to the induced anisotropy, our samples were selected as a series of four Co–Cr–Ta thin films on a Cr underlyer and produced by this technique. They have been extensively analysed and reported previously [8, 9] and their main properties and the codification are given in table 2.

The magnetic thickness has been varied from 40 to 100 nm in steps of 20 nm, while the Cr underlayer thickness was kept constant at 50 nm. The films were deposited on silicon wafers using a circuit processing apparatus in-line DC magnetron transfer sputtering system [10, 11]. In order to reduce texture effects of the substrate, naturally oxidized wafers were used and coated with 50 nm Cr underlayer before depositing the magnetic layer in the same system. The Co–Cr–Ta deposition rates varied from 1 to 2.5 $nm\,s^{-1}$ for film thickness of 40 and 100 nm, respectively. During deposition, each disk has been subjected to the same range of deposition angles and this produced a different depth profiles for films of different thickness. The substrate temperature was fixed at 250°C. Samples (1 cm^2) were cut from the wafers and have been used for standard VSM experiments and 1 cm disk samples were used for RH.

Table 1. Magnetic parameters for MP tapes obtained from VSM measurements.

MP tapes samples	Magnetic thickness (μm)	Coercivity $\mu_0 H_c$ (mT)	Orientation ration (OR)	Squareness Sq (M_r/M_s)
A	0.26	191	2.1	0.82
B	0.19	194	2.2	0.83
C	0.17	192	2.1	0.81
D	0.12	194	2.2	0.82

Table 2. Magnetic parameters for Co–Cr–Ta thin film samples obtained from VSM measurements.

Co–Cr–Ta samples	Co–Cr–Ta thickness (nm)	Coercivity $\mu_0 H_c$ (mT)	Orientation ratio (OR)	Squareness Sq (M_r/M_s)
E	40	117	1.05	0.84
F	60	106	1.06	0.78
G	80	98	1.11	0.78
H	100	96	1.10	0.71

3. Experimental techniques

The anisotropy field of the samples has been experimentally determined using RH. Despite this very time consuming technique, RH remains one of the most popular methods for anisotropy field measurements. Unlike other techniques, RH is applicable to any kind of magnetic material and does not depend on the orientation of the particles within the sample or the crystallographic structure of the sample. The anisotropy field value is identified as the field value where the RH loss (W_{RH}) curve reaches zero value. This technique was experimentally and theoretically introduced by Luborsky [12] and Jacobs [13]. Since then it has been intensively used. Bottoni [14, 15] and Templeton *et al* [16] have used RH to measure the magnetic anisotropy of metal particles for magnetic recording, and Igaki *et al* [17] has studied acicular particles for recording media also using RH. Anisotropy fields of Fe doped CrO_2 particles have been analysed by Keller and Schmidbauer [18] using RH, and the magnetocrystalline anisotropy constants of inter-metallic compounds were determined by Wyslocki *et al* [19] by rotational hysteresis energy studies.

Rotational hysteresis energy (W_R) is defined as the total work necessary to rotate the moment of a sample through 360° in the presence of a magnetic field. This is determined by measuring the torque τ exerted on a sample by a rotating magnetic field H. Mathematically it can be expressed as

$$\tau(\theta) = \bar{M} \times \bar{H} = MH\sin\theta = M_\perp H \qquad (1)$$

and

$$W_R = \int_0^{2\pi} \tau(\theta)\,d\theta = \int_0^{2\pi} MH\sin(\theta)\,d\theta \qquad (2)$$

Since the torque is proportional to the perpendicular magnetization of the sample, instead of measuring the torque, it is possible to determine rotational hysteresis energy by using a vector VSM. Bi-axial VMS experiments were carried out at room temperature on 1 cm diameter disk samples. During the experiment, a disk sample is rotated through 360° about its axis and with the field direction always in plane. Using steps of 10°, the in-plane magnetization transverse to the magnetic field ($M_\perp$) was recorded as a function of the rotation angle. A numerical value of the rotational hysteresis energy was obtained by integrating the 'torque' curve, which in our case was

$$W_R = \int_0^{2\pi} \tau(\theta)\,d\theta = \int_0^{2\pi} MH\sin(\theta)\,d\theta \qquad (3)$$

Valuable information could also be obtained only from RH loss, W_{RH}, rather than rotational hysteresis energy, W_R. The RH loss is determined by the algebraic sum of the rotational

hysteresis energies measured for a full 360° clockwise rotation followed by a full anticlockwise rotation.

$$W_{RH} = W_R^{clw} + W_R^{aclw} = \int_0^{2\pi} \tau(\theta)\,d\theta + \int_{2\pi}^{0} \tau(\theta)\,d\theta$$
$$= \oint \tau(\theta)\,d\theta \qquad (4)$$

The loss arises from the delay in the magnetization M suffers in following the rotating applied field. If the applied field is very small, moments do not switch and there is no irreversible variation of the magnetization and so no RH loss occurs. When the applied field is very large (bigger than the anisotropy field, H_a) the magnetization follows the field and is always (almost) parallel to it. This time there is no difference in the irreversible changes during the two rotations and so there is no RH loss. At intermediate fields, the magnetization tries to follow the rotation of H and suffers irreversible variations, which are different in the two rotation directions and lead to an energy loss.

The RH loss is no longer zero and in this range the W_{RH} initially increases with the field. These transitional phases can be seen in figure 1 where the transverse signal was recorded for a full 360° rotation in clockwise and anticlockwise directions for a range of different applied field values.

A better indication is given in figure 2, where W_{RH} has been plotted as a function of the inverse applied magnetic field $1/H$. From this graph, the anisotropy field is easily obtained by extrapolating the initial linear slope to $W_{RH} = 0$ where the intercept gives the values of $1/H_a$.

In addition to RH, standard remanence curves have been measured for all samples in order to generate the well-known ΔM plots [20]. These are accepted as a useful indication of the sign of the interactions in a magnetic material and of their variation with the applied field [21] and sample properties. The IRM and DCD curves were measured using well-established techniques [22].

4. Results and discussions

Using RH, the anisotropy fields for the two series of samples have been determined. In figures 3 and 4, we present the RH loss plotted against the reverse applied field for the two sets of samples.

Using the linear extrapolation described in section 3, the anisotropy fields have been determined. In table 3, the anisotropy results for the two sets of samples are summarized.

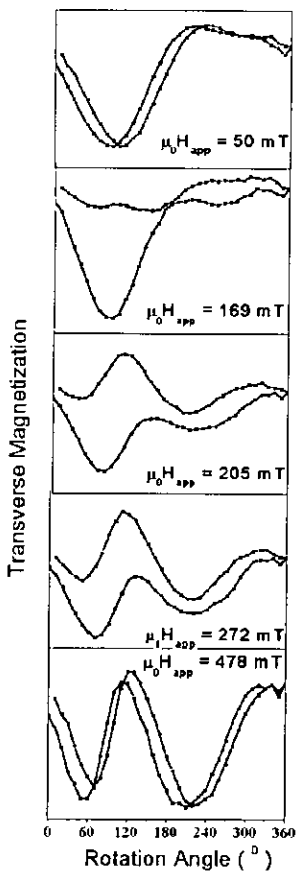

Figure 1. RH experimental data, for increasing values of the rotating field.

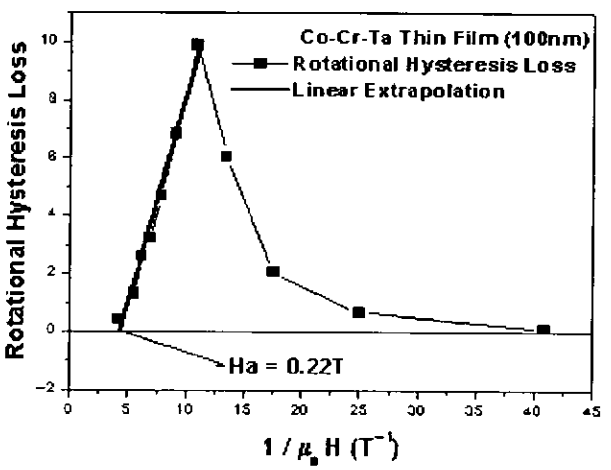

Figure 2. RH loss versus the inverse applied field. Linear extrapolation gives the anisotropy field at the intercept.

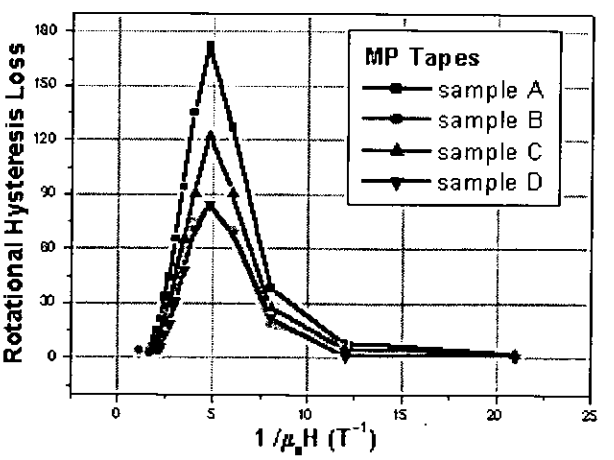

Figure 3. RH loss represented as function of the inverse field for the tape samples.

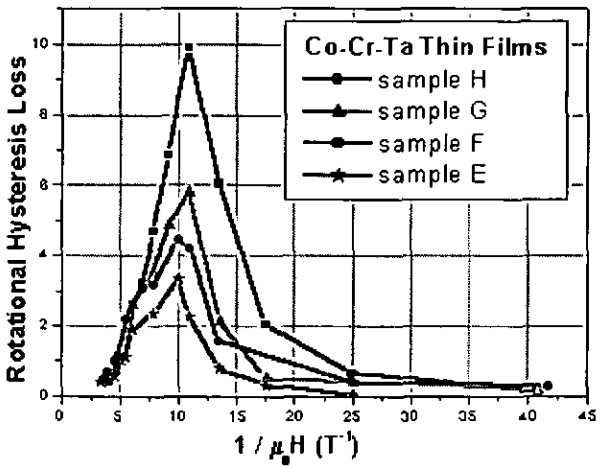

Figure 4. RH loss represented as function of the inverse field for the thin films samples.

Table 3. Experimental anisotropy fields for the MP tapes and Co–Cr–Ta thin films.

	Fe–Co MP tapes				Co–Cr–Ta thin films			
Samples	A	B	C	D	E	F	G	H
Anisotropy field $\mu_0 H_a$(mT)	420	413	409	395	360	330	290	220

However, these results represent only an effective anisotropy field since the particles are not isolated and they interact with each other via exchange and/or magnetostatic interactions. Such interactions are material dependent. In the two sets of samples the exhibited interactions are different (demagnetizing for $A \rightarrow D$ and opposing demagnetization for $E \rightarrow H$). In addition, they vary within each set resulting from the different magnetic coating thickness. Normally, one would expect the measured anisotropy field for samples belonging to the same set to be the same, since they were prepared under the same conditions and also contain identically components. However, it can be seen that the H_a values are not the same and a variation of the anisotropy field with respect to the magnetic thickness was found within both sets of samples as shown in figures 5 and 6.

For the MP tapes, it's been revealed that a thinner magnetic layer is associated with a smaller anisotropy field. The opposite is the case for the Co–Cr–Ta thin film samples where a thinner magnetic film is associated with a stronger anisotropy field. This result is explained in terms of interactions. Generally, in the particulate media, and also the case for the MP tapes, the magnetostatic or dipole–dipole coupling is the dominant interaction. It has been demonstrated theoretically that, as the magnetic thickness decreases, the constant of proportionality of the magnetostatic interactions to the applied field increases [23]. The dipole–dipole interactions will have a negative contribution to the effective field on a particle, and hence on the anisotropy field. This would account for the decrease in the anisotropy field with respect to the magnetic thickness. Furthermore, the change of the interactions with thickness has been confirmed experimentally by experimental remanence curves shown in figure 7. These are ΔM plots, which for an ideal medium with no interactions will present a flat line.

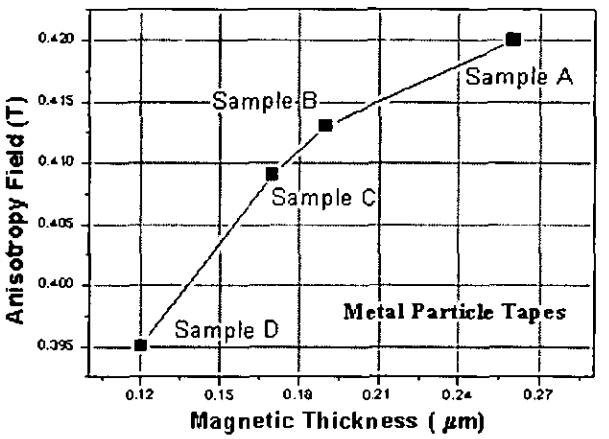

Figure 5. Anisotropy field variation with the magnetic thickness for the tape samples.

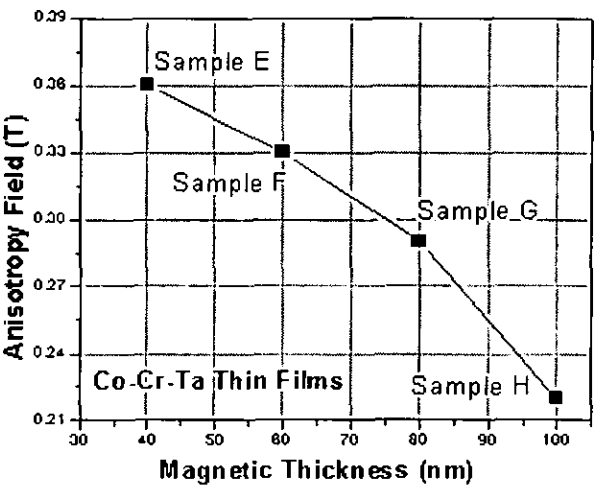

Figure 6. Anisotropy field variation with the magnetic thickness for the thin film samples.

In the case where the interactions within the medium are demagnetizing (negative), the curve is below the line and above the line for interactions, which oppose demagnetization (positive). As can be seen from figure 7, the experimental remanence studies indicate negative interactions that are becoming stronger as the magnetic coating is reduced in thickness.

The measured anisotropy fields corresponding to the thin film samples have also a variation with the magnetic thickness but, unlike the particulate tapes, they show the opposite behaviour, i.e. the thinner the magnetic layer, the higher the anisotropy field. We suggest that this is a direct effect of the positive exchange interactions that are dominant in these thin film media. Although the exchange coupling between neighbouring grains is a positive short-range interaction, it is not obvious why the strength of the exchange coupling should be thickness dependent. The explanation for that comes from the preparation procedure. The thin films are prepared using transfer deposition and this will facilitate the formation of a bowed columnar structure that would generate strong exchange anisotropy effects. Since the preparation time and the transit of the substrate in front of the target is fixed, as the magnetic

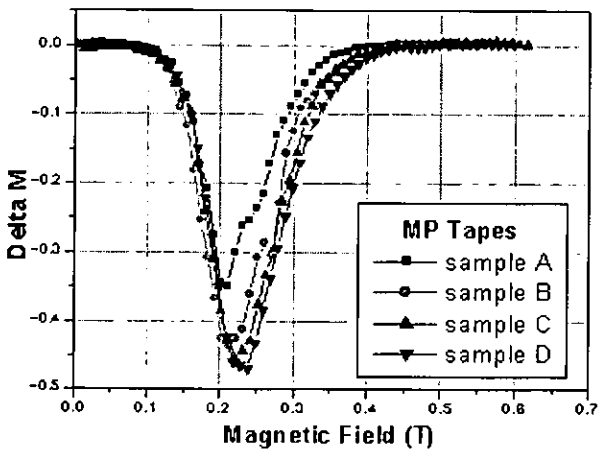

Figure 7. ΔM plots for the tape samples.

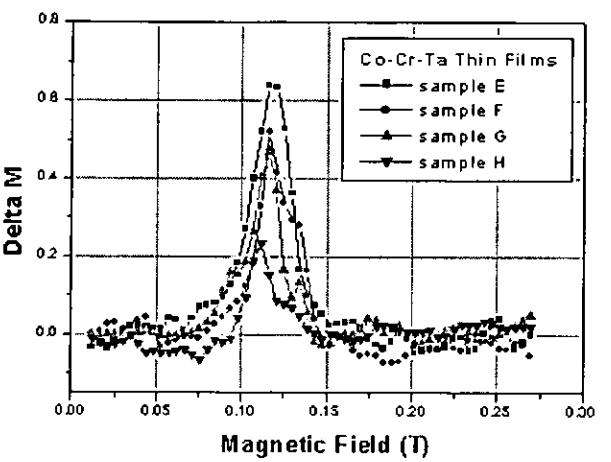

Figure 8. ΔM plots for the thin film samples.

layer gets thicker, the columnar structure becomes less bowed and reduces the in-plane anisotropy. This reduces the strength of the positive exchange coupling.

The change in the strength of the coupling is also confirmed by the remanece curves shown in figure 8, where the strongest positive interactions are for the thinnest Co–Cr–Ta thin film.

Another reason for the enhanced exchange anisotropy in thinner films could be the effect of the Cr underlayer on the crystallographic properties of the Co–Cr–Ta thin film [24]. It has been proved that Cr microstructure influences the grains morphology and the crystallographic texture of the sputtered magnetic film [25]. Consequently, a thicker magnetic layer will reduce the effect of Cr underlayer on the in-plane anisotropy properties of the sputtered films.

5. Conclusions

Two different sets of magnetic samples have been compared in order to analyse the effect of the inter-particle interactions on the general magnetic properties and magnetic anisotropy. RH and standard remanence measurements have been used as main experimental tools. Both sets of samples showed a variation of the anisotropy fields with the magnetic thickness. We have demonstrated that the inter-particle interactions are related to the anisotropy variation and are probably closely linked to the behaviour. The observed trends in the results are strongly supported by the experimental measurements of the interactions through remanence techniques and theoretical studies. For the samples investigated, the thinner Co–Cr–Ta films grown on Cr underlayer exhibit more in-plane magnetic anisotropy than the thick films. On contrary, the thinner magnetic coatings on MP tapes showed a smaller anisotropy fields than the thick MP coatings and they are related to the negative magnetostatic interaction.

Acknowledgments

The authors would like to thank the National Storage Industry Consortium's 'Advanced Tape Program' for financial support. We also acknowledge the assistance of Hiroyuki Suzuki from Hitachi who provided the thin film samples.

References

[1] Vopsaroiu M, Bissell P R and Cookson R 2002 *Phys. Status Solidi* **189** 2/3
[2] Kuncser V, Vopsaroiu M, Sahoo B, Bissell P R and Keune W 2002 presented at *ICAME 2001, Oxford, Hyperfine Interactions* at press
[3] Johnson K E, Ivett P R, Timmons D R, Mirzamaani M, Lambert S E and Yogi T 1990 *J. Appl. Phys.* **67** 4686–8
[4] Daval J and Randet D 1970 *IEEE Trans. Magn.* **6** 768
[5] Coughlin T, Presseeky J, Lee S, Heiman N, Fisher R D and Merchant K 1990 *J. Appl. Phys.* **67** 4689–91
[6] Sellmyer D J, Wang D and Christner J A 1990 *J. Appl. Phys.* **67** 4710–12
[7] Suzuki H, Bissell P R, Chantrell R W and Kodama N 1995 *JMMM* **146** 267–72
[8] Suzuki H, Kodama N, Bissell P R and Chantrell R W 1995 *IEEE* **31** 2800–2
[9] Suzuki H, Bissell P R, Chantrell R W and Kodama N 1996 *JMMM* **155** 196–8
[10] Tanaka Y, Ito H, Sonoda T and Nishikawa R 1987 *IEEE Trans. Magn.* **23** 2046
[11] Teng E and Ballard N 1986 *IEEE Trans. Magn.* **22** 579
[12] Luborsky F E, Mendelsohn L I and Paine T O 1957 *J. Appl. Phys.* **28** 334
[13] Jacobs I S and Luborsky F E 1957 *J. Appl. Phys.* **28** 467
[14] Bottoni G 1995 *JMMM* **140–144** 2207–8G
[15] Bottoni 1996 *JMMM* **155** 16–18
[16] Templeton T L and Arrot A S 1997 *J. Appl. Phys.* **81** 3797–9
[17] Igaki M, Nagamori H, Shimatsu T and Takahashi M 1998 *JMMM* **183** 209–19
[18] Keller R and Schmidbauer E 1998 *JMMM* **187** 160–8
[19] Wyslocki J J, Suski W, Pawlik P, Wochowski K, Kotur B and Bodak O I 1996 *JMMM* **162** 239–46
[20] Kelly P E, O'Grady K, Mayo P I and Chantrell R W 1989 *IEEE Trans. Magn.* **25** 3880
[21] Williams M L and Comstock R L 1971 *AIP Conf. Proc.* vol 5, pp 738–42
[22] Spratt G W D, Bissell P R, Chantrell R W and Wohlfarth E P 1988 *JMMM* **75** 309–18
[23] Stancu A, Stoleriu L and Cerchez M 2001 *J. Appl. Phys.* **89** 11
[24] Lee H L 1988 *J Appl. Phys.* **63** 2369
[25] Howard J K 1988 *J. Appl. Phys.* **63** 3263

ELSEVIER

Journal of Magnetism and Magnetic Materials 242–245 (2002) 331–334

Journal of magnetism and magnetic materials

www.elsevier.com/locate/jmmm

A magnetic evaluation of recording tape thickness

P.R. Bissell[a,*], M. Vopsaroiu[a], R.D. Cookson[a], M.P. Sharrock[b]

[a] *Centre for Materials Science, University of Central Lancashire, Preston PR1 2HE, UK*
[b] *Imation Corporation, Oakdale, MN 55128-3414, USA*

Abstract

Three techniques are compared that allow the magnetic thickness of recording media to be determined. The techniques rely on a measurement of the out-of-plane demagnetizing field and allow a standard vibrating sample measurement of a hysteresis loop to be calibrated in terms of magnetization. All three techniques give comparable results.

Keywords: Magnetic recording media; Anisotropy fields; Magnetization—demagnetization; Susceptibility—transverse

With the development of double-coated metal particle (MP) tapes where only the top layer is magnetic, measurement of magnetic coating thickness using mechanical techniques has become impossible and other techniques such as electron microscopy require specially prepared samples and introduce uncertainty through mechanical damage during preparation. An alternative non-destructive magnetic technique involving the measurement of the demagnetizing field in transverse AC susceptibility measurements has been previously described [1]. This involved measurement of the sheet-demagnetizing field of a tape sample by observing the transverse AC susceptibility anisotropy peak with an applied DC field in plane and out of plane. The position of the peak is very closely associated with particles with an orientation in the AC field direction so that the shift of the peak between the two measurements can be taken to be the difference in the demagnetizing fields experienced by these particles for the two DC field applications. This allows corresponding VSM hysteresis loop measurements to be calibrated in terms of magnetization intensity. When combined with the usual calibration for total moment against a reference sample and the known area of tape, then the thickness can be determined.

The principle of the technique can be extended to other magnetic properties of tapes that have properties and features specifically related to the applied magnetic field, which can be applied parallel and perpendicular to the plane of the tape. Based on this, we have added two further methods:

(1) Remanent rotational magnetometry measurement which involved the switching of particles nearly perpendicular to an applied field direction—as an extension of Flanders and Shtrikman [2];
(2) Comparison of the closure point of the transverse and perpendicular hysteresis loops.

Results from these two additional methods are described in this paper and compared with transverse susceptibility measurements. All three methods gave comparable values for magnetic layer thickness

Bi-axial VMS experiments were carried out on 1 cm diameter disk samples made of stacks of 16 single layers glued together to maintain their tape orientation. This produced a sample corresponding to 12.5 cm^2 and increased the signal-to-noise ratio to satisfactory levels without compromising the sheet-demagnetization factor of the sample (this technique involves measurement of changes in the magnetization perpendicular to the applied field direction so signals are therefore small). The samples were mounted in the VSM with the sample plane and the rotational axis coincident. Our technique is similar to remanent torque magnetometry, except that direct measurement of the magnetization change was used rather than torque measurement. The in-plane mean magnetic orientation of the sample was

*Corresponding author. Tel.: +44-1772-893563; fax: +44-1772-892996.
E-mail address: pbissell@uclan.ac.uk (P.R. Bissell).

0304-8853/02/$ - see front matter
PII: S0304-8853(01)01219-7

determined by measuring remanent magnetization as a function of angle and the maximum value was taken as the centre of the mean easy axis direction (EAD). Starting from this direction, the sample was rotated through 90° and a saturating field was applied and removed. In this remanent state, the sample was rotated through a small angle, α. A small field was applied and removed and the change in remanence perpendicular to the applied field direction was recorded, when the change in remanence was due to the reversal of particle moments lying between 90° and $(90+\alpha)°$ to the centre of the mean EAD. This process was repeated for increasing field values. For values of α approaching zero, this corresponds to particle moments reversing at their anisotropy field. The differential of the remanence curve, or approximately a plot of the variation in the transverse remanent moment between two successive field applications and removals H_i and H_{i+1}, is the anisotropy field distribution of the particles. This indicates how many particles with their easy axes between 90° and $(90+\alpha)°$, have an anisotropy field value between H_i and H_{i+1}. In Fig. 1 we present the in-plane anisotropy field distributions measured for a 5° rotation angle. The mean anisotropy field is taken as the applied field value corresponding to the peak of the curve. Strictly speaking, this is an approximate measure and it will only be a true measure of mean anisotropy field as $\alpha \to 0$. Measurements for very small angles are difficult as the signal becomes too small to measure and the experimental error increases. Most reported measurements using this technique therefore work with an angle of about 5°. We have extended the measurements by repeating for up to 7 different rotational angles from 5° to 25°. By plotting the peak field value against the rotational angle, it is found that these values lie approximately on a straight line which can be extrapolated back to $\alpha = 0$ (see Fig. 2).

The intersection point of the extrapolated line with the field axis gives a more accurate value of the anisotropy field, H_a. This technique was repeated with the applied field out of the sample plane and the anisotropy field, H_{a1}, was measured. It was found that H_{a1} was shifted to a higher value (see Fig. 2). Since the particle moments involved in the signal change are perpendicular to the applied field, the geometry of the measurement is the same as for the transverse AC susceptibility measurements and the shift in the anisotropy field peak is the result of the sample-demagnetizing field.

The second method was performed on a standard VSM and involved measurement of the in-plane and out-of-plane hysteresis loops of a sample. The closure points of the loops were determined and compared for in plane and out-of-plane loops. The difference was again related to the demagnetizing field. A hysteresis loop will close at a field when all the particles have switched. For Stoner Wohlfarth particles, this will correspond to the reversal of the particles with the largest anisotropy field and with their easy axes aligned with the applied field direction. Unlike the anisotropy field determination techniques, the closure points measured in plane and out of plane will likely be determined by different particles. The technique therefore also makes the assumption that the distributive properties of the particles are the same in plane and out of plane. Assuming a well-dispersed magnetic ink during coating and no preferential alignment of particles during manufacture, this seems to be a reasonable assumption. Furthermore, checks on the closure points of in-plane aligned and transverse loops indicate that these are at the same field, within experimental error. Fig. 3 shows an in-plane transverse and out-of-plane hysteresis loop. The difference in the

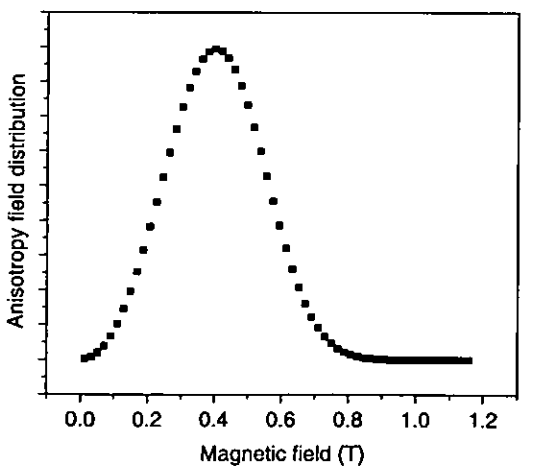

Fig. 1. Anisotropy field distribution determined by the rotational remanence method for sample A.

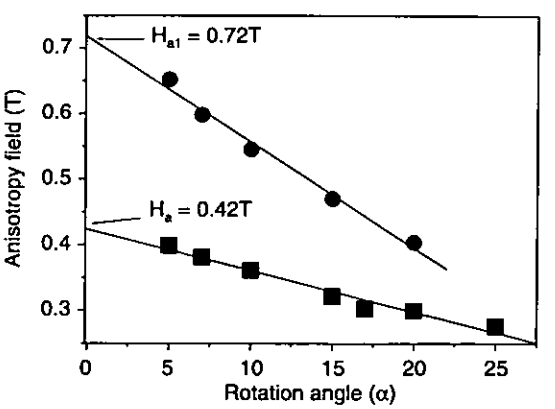

Fig. 2. Extrapolation of the mean remanence values in plane and out of plane for sample A.

field values for the closure points is taken as the difference in the demagnetizing fields of the sample.

Transverse susceptibility measurements were also made on all the samples using a method described fully in Ref. [1]. For the sake of brevity, experimental details are not given here, but measurement data for the four samples are included in Table 1.

The result of an investigation of four samples is given here. These were for experimental double-coated advanced MP tapes intended for digital data storage such as the LTO format. They were selected because they had different texture and magnetic thickness. The double coating consisted of a non-magnetic under-layer and a thin magnetic topcoat, which ranged from Mrt (saturation remanence × thickness) 3 to 6 memu cm^{-2} (0.03 to 0.06 A in SI units). In Table 1, a comparison of the results for all samples analysed for the demagnetizing field using the three methods is given. The results from these different techniques are in good agreement and the thickness values against the Mrt values of the samples are shown in Fig. 4. If the only variable in the production of these tapes were the thickness, then we would expect a straight-line relationship between Mrt and magnetic layer thickness.

Although results compare well, it should be noted that it is difficult to determine the closure point for hysteresis loops and it is prone to a certain amount of subjectivity. In addition, all the measurement techniques rely on the assumption that the demagnetizing factor for the sample is that of an infinite sheet. Two aspects of this require some comment:

The effect of stacking layers in order to increase the signal-to-noise ratio. Because the magnetic layer thickness is much less than the spacing between layers (magnetic layer to substrate thickness <0.03), a simple application of Gauss' law indicates that the demagnetizing field within a magnetic layer is unaffected by magnetic layers other than itself. Thus, stacking of infinite layers has no effect on the sheet-demagnetizing factor, but for finite sheets, there is an effect resulting from the free edges of the sample. This is small because of the dilution effect of the wide spacing of individual magnetic layers.

The effect of the particulate nature of the magnetic layers where thickness has been reduced to the order of a particle length. This has been the subject of a modelling study [3], which shows that for current media, the particulate nature does alter the demagnetizing factor by

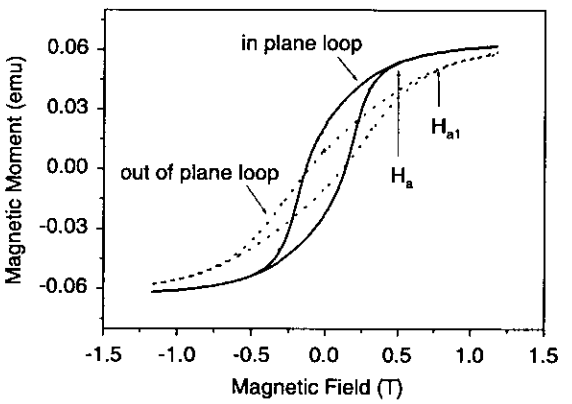

Fig. 3. Hysteresis loops for in-plane transverse and out of plane showing the effect of the demagnetizing field on the closure point.

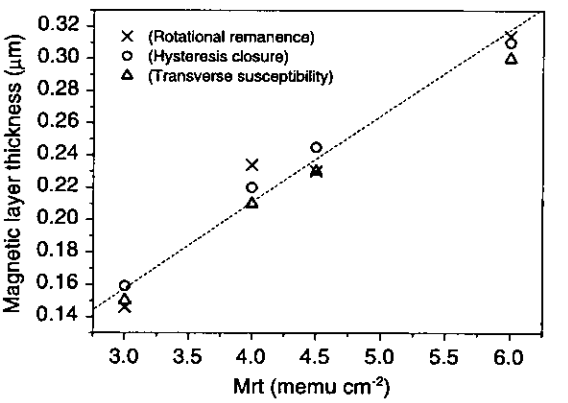

Fig. 4. Calculated magnetic layer thickness as a function of Mrt value for the four samples.

Table 1
Comparison of the demagnetizing fields calculated using the three described methods together with magnetic thickness determined by the transverse susceptibility method

Samples code	(Remanence × thickness) Mrt (memu cm^{-2})	Rotational remanent H_D (T)	Closure point detection H_D (T)	Transverse susceptibility H_D (T)	Transverse susceptibility film thickness (μm)
A	6.0	0.297	0.294	0.284	0.30
B	4.5	0.267	0.285	0.267	0.23
C	4.0	0.289	0.272	0.261	0.21
D	3.0	0.292	0.320	0.301	0.15

about 7%. Moreover, this will increase as the magnetic layer thickness is decreased unless there is an equivalent reduction in particle dimensions.

From this comparative study, we can conclude that the three methods to determine the demagnetizing field of the sample all give satisfactory results. On the assumption that the demagnetizing factor is that of an infinite sheet, which seems to be valid, this gives a non-destructive measure of the magnetic layer thickness. Although the measure of the closure points on the hysteresis loops measured in and out of plane has added experimental errors associated with determination of the closure points and the added assumption about the particle distribution, it is available within any laboratory that has standard vibrating sample magnetometer facilities. This technique therefore provides a useful method for determination of magnetic layer thickness in magnetic tape media.

Acknowledgements

The authors would like to thank the National Storage Industries Consortium "Advanced Tape Program" and the Engineering and Physical Sciences Research Council for financial support for this work.

References

[1] P.M. Sollis, P.R. Bissell, J. Phys. D 24 (1991) 1891.
[2] P.J. Flanders, S. Shtrikman, J. Appl. Phys. 33 (1962) 216.
[3] R.D. Cookson, P.R. Bissell, G.E. Kay, D.A. Parker, J. Magn. Magn. Mater. 242–245 (2002), this issue.

phys. stat. sol. (a) **189**, No. 3, 799–803 (2002)

Magnetic Coating Thickness Influence on the Texture in Metal Particle Systems

M. VOPSAROIU[1]), P. R. BISSELL, and R. COOKSON

Centre for Materials Science, University of Central Lancashire, Preston PR1 2HE, UK

(Received May 1, 2001; accepted September 30, 2001)

Subject classification: 75.30.Gw; 75.50.Ss; 75.90.+w; S1.1

The magnetic characterization of four experimental advanced double-coated MP tapes with different magnetic coating thickness has been completed. Although standard vibrating sample magnetometer (VSM) measurements show very similar characteristics such as coercivity, squareness and orientation ratio (OR), alternative measurements show distinct differences in addition to their magnetic thickness. The *in-plane* distribution of easy axes (EAD) measured using a bi-axial VSM, show that the distribution width increased as the magnetic coating thickness decreased. A theoretical relation between OR and EAD was used to determine the *out-of-plane* distribution width. This was found to be narrower than the *in-plane* equivalent, as expected. The *out-of-plane* distribution width decreased as the magnetic thickness decreases, contrary to the *in-plane* variation.

Introduction Magnetic recording media are often textured during manufacture by increasing the alignment of particle easy axes. The degree of texturing can be described by the Easy Axis Distribution (EAD) which can be different *in-plane* and *out-of-plane*. The effect of texturing increases the squareness of the hysteresis loop and reduces the switching field distribution (SFD), which is beneficial to recording performance. For simplicity of characterization, texture is often represented by the orientation ratio (OR). This is defined as the ratio of the remanent magnetization along the recording direction to that transverse to it. For randomly orientated particles OR = 1, while an OR > 1 indicates a partial alignment of the particles [1]. OR is a crude measure, which is insensitive to the distribution width for OR in the range 1 to ≈2 and a full measurement of the distribution of easy axes gives more detail. Several techniques have been developed to measure the *in-plane* EAD using either torque magnetometry [2, 3] or using vibrating sample magnetometer measurements [4, 6]. Most techniques are derivatives of the method introduced by Flanders and Shtrikman [5]. This is the case for our measurements, which were performed using a bi-axial VSM technique that was implemented by Schmidlin et al. [6].

Experimental Method Vector VMS experiments were carried out at room temperature on 1 cm diameter samples of advanced MP tape consisting of a stack of 16 disks glued together to maintain their magnetic orientation. This produced a sample corresponding to 12.5 cm^2 which reduced the signal to noise ratio to satisfactory levels without compromising the sheet demagnetization factor of the sample. The disk samples were mounted in the VSM with the sample plane and the rotational axis coincident. The mean easy axis direction of the sample was determined by measuring saturation remanence as a function of angle. The direction corresponding to maximum value was

[1]) Corresponding author; Fax: +00-44-1772-892996; Tel.: +00-44-1772-893579; e-mail: mvopsaroiu@uclan.ac.uk; v.marian@lycos.com

 0031-8965/02/18902-0799 $ 17.50+.50/0

taken as the center of the EAD on the assumption that the distribution was symmetric about this direction ($\alpha = 0$). All further measurements were made relative to this direction. The sample was saturated with a large magnetic field at ($\alpha = 0$), so that all the particle moments were switched into the field direction and, when the field was removed it was left in its remanent state with all particle moments switched to their easy axis directions closest to the field direction. The sample was then rotated through an angle $\Delta\alpha$ and a new remanence state produced by again saturating. The change in the vector remanence was due to the switching of moments for particles with easy axes between 90° and (90° + $\Delta\alpha$) to $\alpha = 0$. By repeating the measurement process for incremental increases in α between 0° and 180° the EAD can be obtained in that plane of measurement. *Out-of-plane* measurements of the EAD are almost impossible to measure with any reasonable accuracy because of demanding demagnetizing field corrections. We therefore used the relation between OR and EAD to determine the *out-of-plane* EAD.

Results and Discussions An investigation of four samples is described in this paper. These were experimental double-coated advanced metal particle (MP) tapes as those used for digital data storage on systems such as the LTO format. They had a double coating with a non-magnetic under-layer and a thin magnetic top coat containing Co–Fe metallic particles approximately 100 nm in length and with an aspect ratio ~5:1. Standard characterization of the hysteresis loops showed no major differences between the loops apart from the Mrt values (saturation remanence times thickness), which corresponded to different magnetic coating thicknesses (see Table 1). However, the *in-plane* EAD data showed that the samples had different texture varying with the magnetic coating thickness, as shown in Fig. 1.

The experimental distributions have been fitted by a Lorentzian function in order to obtain a numerical measure of the distribution width (also shown in Table 1),

$$f(\alpha) = \frac{ab}{\alpha^2 + b^2}, \tag{1}$$

where b is the distribution width parameter and a is a normalization parameter obtained from the condition

$$\int_{-90}^{90} f(\alpha)\, \mathrm{d}\alpha = 1, \tag{2}$$

Table 1
Sample characteristics including the experimental and derived results for both *in-plane* and *out-of-plane* orientation ratio and easy axis distribution parameters.

sample	Mrt	H_c	S_q	in-plane		out-of-plane	
	(nm T)	(T)		OR	b	OR	b
A	6.0	0.191	0.82	2.1	21°	2.5	18.4°
B	4.5	0.192	0.83	2.2	24.2°	2.8	15.7°
C	4.0	0.192	0.81	2.1	27.6°	2.9	15.5°
D	3.0	0.194	0.82	2.2	32.6°	3.1	15.0°

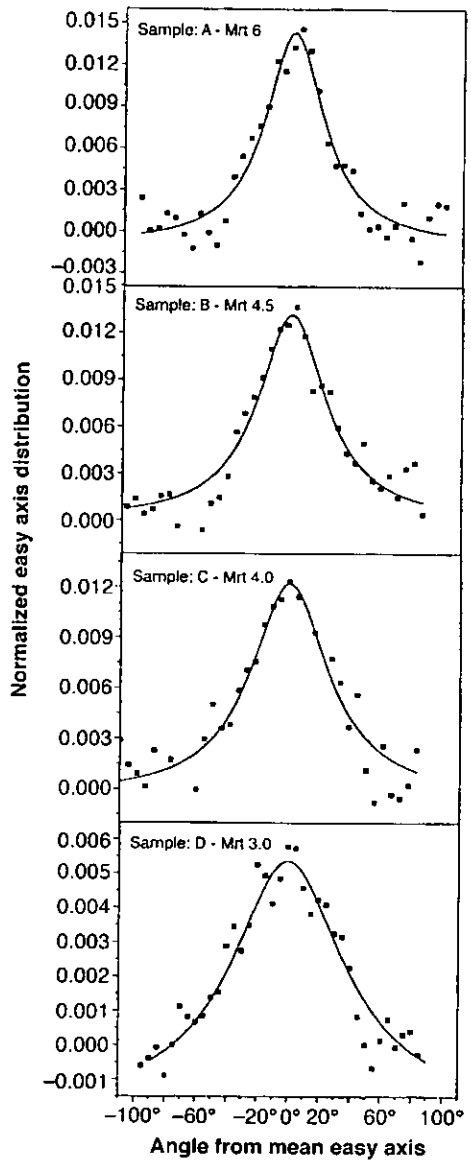

Fig. 1. *In-plane* experimental easy axis distributions for all four samples

$f(\alpha)$ represents the magnitude of the EAD and α is the *in-plane* rotation angle with respect to the sample mean easy axis direction. The estimated error in the EAD width is ±2°, which is comparative with the half rotational step angle. At the extremes of the EADs, the measured signal became increasingly noisy. This was a consequence of the measurement technique, which involves measuring changes in magnetization at right angles to the applied field direction.

The EAD can be linked to the orientation ratio. If a saturating field H_{app} is applied to a sample with an EAD $f(\alpha)$ at an angle β to $\alpha = 0$, then the resulting remanent magnetization in the field direction x is (M_x) and can be written as [7]

$$M_x(\beta) = I_s \int_{\beta-\frac{\pi}{2}}^{\frac{\pi}{2}} f(\alpha)\cos(\alpha-\beta)\,d\alpha + I_s \int_{\frac{\pi}{2}}^{\beta+\frac{\pi}{2}} f(\alpha-\pi)\cos(\alpha-\beta)\,d\alpha \tag{3}$$

where I_s is the total remanence magnetization. The OR can be calculated using the relation OR = $M_x(0)/M_x(90°)$. Figure 2 shows a plot of OR derived for a number of different distribution parameters, which may be used to estimate the corresponding b parameters for measured OR values.

It can be seen from Fig. 2 that for distribution widths greater than $b \cong 20°$, OR is insensitive to increasing b, i.e. for wide distributions, as in the case of the *in-plane* measurements, OR is not an effective measure of the EAD. However, as OR increases it can be used to calculate the distribution width more precisely and is more effective for *out-of-plane* distribution measurements. The *out-of-plane* OR was determined experimentally using the *in-plane* transverse and the *out-of-plane* hysteresis loops, the latter being corrected for demagnetizing effects. The *in-plane* EAD parameters showed that distribution width increased as the magnetic coating thickness is decreased (indicated by the Mrt value) and shown in Fig. 3.

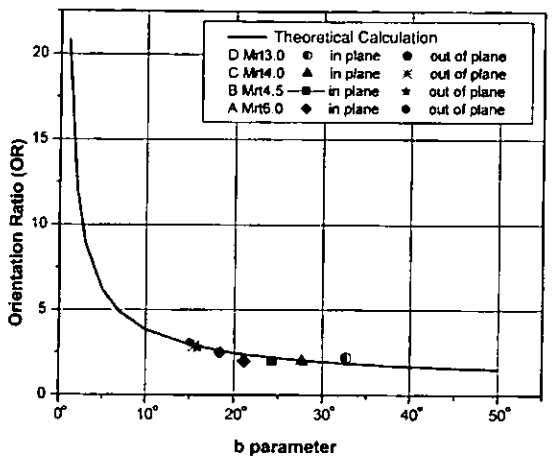

Fig. 2. Measured *in-plane* distribution parameter (b) and OR for all four samples shown on the theoretically derived relation. *Out-of-plane* measured OR values are also plotted on the theoretical curve to show the derived values of b

This indicates that, as the magnetic layer becomes thinner, the *in-plane* particle orientation is reduced resulting in a broader distribution. This could be related to the manufacturing process when a thinner coating will dry more rapidly and so reduce the effectiveness of the orienting magnets or be associated with changed rheology of the wet coat. The *out-of-plane* distribution parameters also show a variation with the magnetic thickness (Fig. 3) but, unlike the *in-plane* distribution parameter, the trend is in the opposite sense. This may be due to the geometrical influence of the magnetic thickness to the tape texture, where finished magnetic coat thickness is approximately equal to the particle length, as well as the mechanical shearing effects of the knife coater or doctor blade. The observed trend *out-of-plane* is much smaller than *in-plane*. In addition, all the *out-of-plane* distribution widths are much smaller than those measured in plane. Again this is probably related to the mechanical properties of the coating process.

Conclusions An experimental technique, for *in-plane* easy axis distribution measurement using a vector VSM, has been described and applied to *in-plane* measurements on a series of tapes with similar magnetic properties but different coating thickness. The relation between OR and distribution width has been established and is a good measure of the texture for narrow distributions, as in the case of *out-of-plane* measurements

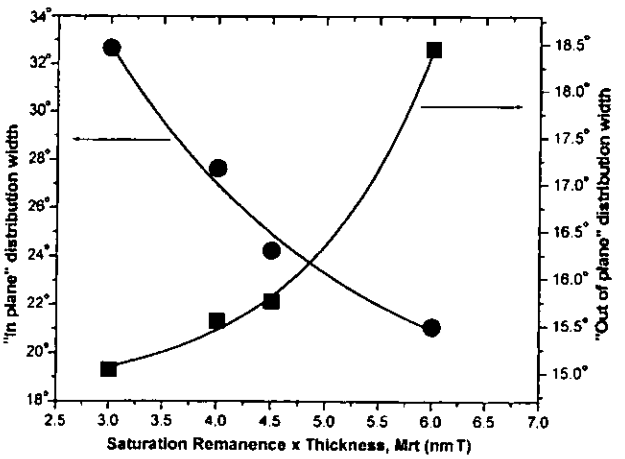

Fig. 3. Variation of the *in-plane* and *out-of-plane* easy axis distribution with the magnetic thickness

to which it has been applied. Results showed that the magnetic coating thickness was strongly related to tape texture both in plane and out of plane. In plane, the distribution width became narrower as the magnetic coating thickness was reduced. Out of plane, the distribution width, which was always narrower than that in plane, showed a contrary relationship to thickness.

Acknowledgements The authors would like to thank the National Storage Industries Consortium's Advanced Tape Program and the Engineering and Physical Sciences Research Council for financial support for this work.

References

[1] H. TAKANO, T. T. LAM, J. G. ZHU, and J. H. JUDY, IEEE Trans. Magn. **29**, 3709 (1993).
[2] S. R. HOON and D. M. PAIGE, IEEE Trans. Magn. **23**, 183 (1987).
[3] D. M. PAIGE and B. K. TANNER, Phys. E **15**, 128 (1982).
[4] T. L. TEMPLETON, A. ARROT, and Y. YOSHIDA, IEEE Trans. Magn. **30**, 4263 (1994).
[5] P. J. FLANDERS and S. SHTRIKMAN, J. Appl. Phys. **33**, 216 (1962).
[6] F. SCHMIDLLIN, P. R. BISSELL, and J. A. GOTAAS, J. Appl. Phys. **79**, 4746 (1996).
[7] J. W. HARRELL, Y. YU, Y. YE, J. P. PARAKKA, D. E. NIKLES, and H. G. ZOLLA, J. Appl. Phys. **81**, 3800 (1997).

ELSEVIER

Nuclear Instruments and Methods in Physics Research B 196 (2002) 135–147

NIM B
Beam Interactions with Materials & Atoms

www.elsevier.com/locate/nimb

The "in-plane" angular spin distribution in layered systems as obtained by ^{57}Fe Mössbauer spectroscopy

V. Kuncser [a,b], W. Keune [a,*], M. Vopsaroiu [c], P.R. Bissell [c]

[a] *Laboratorium für Angewandte Physik, Gerhard-Mercator-Universität Duisburg, Lotharstraße 1, D-47048 Duisburg, Germany*
[b] *National Institute for Materials Physics, MG7 76900 Bucharest-Magurele, Romania*
[c] *University of Central Lancashire, Magnetic Materials Research, Preston PR1 2HE, UK*

Received 12 February 2002; received in revised form 22 May 2002

Abstract

A practical approach for in-plane angular spin distributions in layered systems, as obtained by Mössbauer spectroscopy, is discussed. The line intensity ratio R_{23} of a Mössbauer pattern is expressed versus particular distribution parameters in unidirectional, step-shaped and ellipse-type models. The distribution parameters are deduced from experimental spectra taken by rotating the sample in its own plane. Three-dimensional spin distributions with small out-of-plane components can be analysed using the same method. The procedure is exemplified on four samples containing metallic nano-particles. The in-plane angular magnetic moment distributions derived with this method are compared with the results from bulk vector vibrating sample magnetometry in order to prove the accuracy of the described technique.

Keywords: Spin distribution; Mössbauer spectroscopy; Layered systems

1. Introduction

The most comprehensive theory about the evaluation of the spin texture by Mössbauer spectroscopy with both polarised and unpolarised source radiation was given by Pfannes and Fischer in 1977 [1]. The texture was described by atwo-variable density probability function, $D(\theta_m, \varphi_m)$, where θ_m and φ_m are the polar angles of the quantisation axis for the analysed nucleus in the laboratory fixed system. They showed that the maximum information obtainable from Mössbauer measurements for the magnetic dipolar radiation of ^{57}Fe is a set of nine expansion spherical harmonics coefficients of the texture distribution $D(\theta_m, \varphi_m)$. In the case of unpolarised dipole radiation, only five independent variables are required in order to construct a minimum texture function, $D^{min}(\theta_m, \varphi_m)$, which can properly approximate the real texture of the system. Subsequently, Greneche and Varret [2] have shown that by using a convenient rotation of the reference axes, a texture with a D_{2h} symmetry can be described by only three coefficients and three angular parameters, respectively. Further developments in the case of amorphous ribbons presenting spin-canting phenomena have been done by Pankhurst and Gibbs [3].

* Corresponding author. Tel.: +49-203-379-2387; fax: +49-203-379-3601.
E-mail address: keune@uni-duisburg.de (W. Keune).

0168-583X/02/$ - see front matter
PII: S0168-583X(02)01274-0

However, in spite of these important achievements, the practical determination of the angular spin distribution from the intensity ratio of the Mössbauer spectra is rather complicated. In many practical situations, there is an apriori knowledge of the texture symmetry which could simplify drastically the general procedures. Most often, metallic low dimensional systems such as thin films and multilayers present spins distributed predominantly in the sample plane. The peculiar magnetic properties of these systems depend strongly on the surface and/or interface spin distribution that could be intimately studied in connection with the microstructural behaviour by suitable Mössbauer techniques.

In this work we propose a simplified procedure for extracting the in-plane angular spin distribution from Mössbauer spectra acquired on two-dimensional magnetic systems in non-perpendicular geometry. Spin distributions with a small out-of-plane component and with mirror symmetry can be also treated within the assumption that the out-of-plane component can be derived independently in a perpendicular geometry. The procedure was experimentally verified on four samples of advanced double-coated metal particle tapes, and the results have been compared with easy axis distributions (EADs) obtained by using bulk vector vibrating sample magnetometry techniques.

2. Theory

Let us assume a spin distribution in the sample plane defined by the *Oxy* rectangular axes. The laboratory-fixed orthogonal system, *Oxyz*, has the *z*-axis normal to the sample plane (Fig. 1). The γ-beam is incident on the sample in the *Oxz*-plane under an angle ϕ relative to the *Ox*-axis. The orientation of the magnetic hyperfine field, B_{hf}, of an ^{57}Fe nucleus (anti-parallel to the Fe magnetic moment) is fully determined either by the angle φ made with the *Ox*-axis or by the angle ψ made with the direction of the γ-ray. Therefore, the angular density probability for the Fe hyperfine fields and hence for the magnetic moments depends on only one parameter and is described in the following by $P(\varphi)$ or alternatively, by $P(\psi)$. Furthermore, we

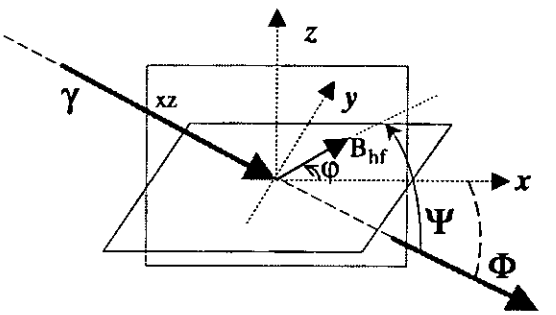

Fig. 1. Experimental arrangement of a Mössbauer experiment in non-perpendicular geometry. The laboratory fixed system, *Oxyz*, has the *Ox* and *Oz* axes co-planar with the γ-beam. Mössbauer spectra are taken by rotating the sample in the *Oxy*-plane.

relate the two densities via the relation $P(\varphi)d\varphi = P(\psi)d\psi$ where $d\psi$ is an infinitesimal increase of ψ corresponding to an infinitesimal increase, $d\varphi$, of angle φ. The physical meaning of the above equation is that the number of spins pointing to the angular interval $d\varphi$ equals the number of spins corresponding to $d\psi$. It is worth mentioning that the two densities of probability are not equal, $P(\varphi) \neq P(\psi)$, which can be simply observed from the normalisation conditions held for different ranges of φ and ψ, e.g. the overall integration should be done over 2π for angle φ and $2\pi - 2\phi$ for angle ψ, respectively (Fig. 1). Now let us consider ^{57}Fe nuclei with the in-plane magnetic hyperfine field forming the angle ψ relative to the γ-beam direction. The typical Mössbauer spectrum originating from such nuclei can be simply expressed as a superposition of six lines,

$$F(v; v_i, \psi) = \sum_{i=1}^{6} \xi_i \Gamma(v; v_i), \tag{1}$$

where $\Gamma(v; v_i)$ is a Lorentzian function centred at resonance velocity, v_i, whereas ξ_i represents the relative weight of line i related to the third inner line. For the magnetic dipolar radiation of ^{57}Fe (unpolarised source) and quasi-pure Zeeman splitting, ξ_i takes the values [4]:

$$\xi_1 = \xi_6 = 3; \quad \xi_2 = \xi_5 = \frac{4\sin^2\psi}{1+\cos^2\psi}; \quad \xi_3 = \xi_4 = 1. \tag{2}$$

Moreover, we take into account only the spin texture, and we will suppose that the magnitude of the hyperfine parameters remains constant for all the implied nuclei. Therefore, v_i as well as functions $\Gamma(v; v_i)$ are independent of ψ, and the overall spectrum due to spins with different in-plane orientations can be expressed as

$$F(v; v_i, \psi) = \int_{\psi} P(\psi)\,d\psi \sum_{i=1}^{6} \xi_i \Gamma(v; v_i) = \sum_{i=1}^{6} \langle \xi_i \rangle \Gamma(v; v_i), \quad (3)$$

where

$$\langle \xi_i \rangle = \int_{\psi} \xi_i P(\psi)\,d\psi.$$

The following mean coefficients $\langle \xi_i \rangle$ result from relation (2) and the normalisation of $P(\psi)$,

$$\langle \xi_1 \rangle = \langle \xi_6 \rangle = 3;$$
$$\langle \xi_2 \rangle = \langle \xi_5 \rangle = \int_{\psi} \frac{4\sin^2\psi}{1+\cos^2\psi} P(\psi)\,d\psi;$$
$$\langle \xi_3 \rangle = \langle \xi_4 \rangle = 1. \quad (4)$$

As a consequence, the overall magnetic Mössbauer spectrum due to in-plane spins with different orientations consists in the superposition of the six typical Lorentzian lines centred on v_i and with the intensity ratios respecting the sequence: $3{:}R_{23}{:}1{:}1{:}R_{23}{:}3$, where

$$R_{23} = 4\int_{\psi} \frac{\sin^2\psi}{1+\cos^2\psi} P(\psi)\,d\psi, \quad \text{with} \int_{\psi} P(\psi)\,d\psi = 1. \quad (5)$$

Practically, the spin distribution is related to a direction in the sample plane and, therefore, instead of ψ and $P(\psi)$, it is more convenient to work with the angular parameter φ and the corresponding density $P(\varphi)$ respectively, where φ is the angle between the x-axis and the magnetic hyperfine field vector, B_{hf} (see Fig. 1). Relations (5) can be easily transformed to the new variable starting from the equality $P(\varphi)d\varphi = P(\psi)d\psi$ and from the relation connecting angles ψ and φ: $\cos\psi = \cos\phi\cos\varphi$, which can be directly derived by analytical geometry (see Fig. 1). The new relation becomes

$$R_{23} = 4\int_0^{2\pi} \frac{1-\cos^2\phi\cos^2\varphi}{1+\cos^2\phi\cos^2\varphi} P(\varphi)\,d\varphi, \quad \text{with} \int_0^{2\pi} P(\varphi)\,d\varphi = 1. \quad (6)$$

Eq. (6) is a quite simple one, allowing us to derive useful information about the in-plane angular spin distribution via usual γ-ray Mössbauer spectroscopy in transmission geometry. Eq. (6) can be applied as well in the case of Mössbauer backscattering geometry (employing reemitted γ-rays, X-rays or conversion electrons and their registration by conventional (non-nuclear resonant) radiation detectors) under usual laboratory conditions (except in the extreme low temperature (mK) regime). Under usual conditions the excited ^{57}Fe nuclear Zeeman levels are equally thermally populated within the lifetime of the nuclear excited state, leading to an isotropic distribution of the emitted (scattered) radiation. Therefore, the additional consideration of the angle between B_{hf} and the direction of the reemitted radiation is not required, and Eq. (6) is also suitable for the case of Mössbauer backscattering under normal laboratory conditions.

Applying Eq. (6), the following procedure is suggested: (i) a theoretical density of probability depending on some unknown parameters is initially proposed according to the specific symmetry of the experiment, (ii) theoretical dependencies of the R_{23} ratio versus the unknown parameters are deduced from either the analytical or the numerical form of expression (6), (iii) experimental ratios R_{23}^{exp} are obtained from a number of Mössbauer spectra taken at different orientations (rotating the sample in the xy-plane or changing the incidence angle), (iv) the unknown parameters are obtained by solving an equation system of type (6) with the number of equations at least equal to the number of the unknown parameters. As we will see in the following, a maximum of two parameters are enough to describe realistic probability densities for the in-plane oriented spins in most practical situations. As expected, for a perpendicular geometry with the γ-beam normal to the sample plane ($\phi = 90°$), R_{23} is independent of $P(\varphi)$ and becomes

$$R'' = 4\int_0^{2\pi} P(\varphi)\,\mathrm{d}\varphi = 4. \tag{7}$$

R'' gives no information about the in-plane spin distribution. Contrary, for a three-dimensional distribution, such measurements give us valuable information about the out-of-plane component.

3. Particular cases

3.1. Unidirectional distribution

This is the simplest model assuming all Fe spins in the xy-plane and pointing to only one direction, e.g. described by φ_0. In this case we deal with a Dirac type probability distribution, $P(\varphi) = \delta(\varphi - \varphi_0)$ and relation (6) may be expressed as

$$R_{23} = 4\int_0^{2\pi} \frac{1-\cos^2\phi\cos^2\varphi}{1+\cos^2\phi\cos^2\varphi}\delta(\varphi-\varphi_0)\,\mathrm{d}\varphi = 4\frac{1-\cos^2\phi\cos^2\varphi_0}{1+\cos^2\phi\cos^2\varphi_0} = f(\varphi_0). \tag{8}$$

The spin orientation described by φ_0 may be deduced by only one experimental spectrum taken at an incidence angle ϕ. Theoretical dependencies of the R_{23} ratio versus φ_0 for different angles, ϕ, are shown in Fig. 2. The parameter φ_0 is determined from Fig. 2 for different experimental R_{23} ratios.

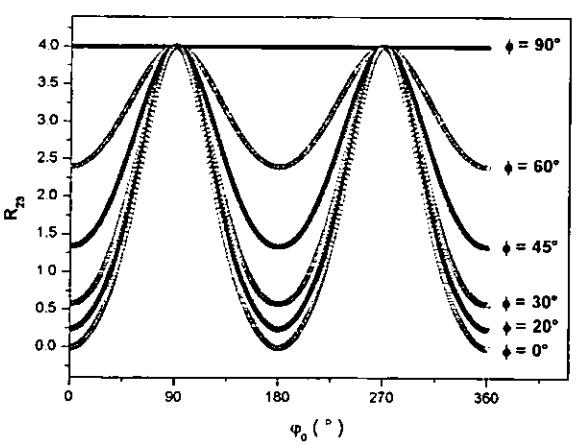

Fig. 2. Theoretical dependencies of the R_{23} ratio versus the in-plane spin orientation, φ_0, in the unidirectional model. Different incident angles ϕ of the γ-beam are considered.

As observed, φ_0 can be obtained with higher accuracy for angles ϕ approaching zero angle of incidence. However, because the resonant counting rate decreases drastically in this geometry, practically we have to make a compromise between an acceptable counting rate and the measurement accuracy. Angles ϕ between 20° and 30° seem to be most suitable for such experiments. It is worth mentioning that this is a very simplified model giving only qualitative information about a mean orientation of the spins in the sample plane.

3.2. Step-shaped distribution

This describes the situation where the in-plane spins (hyperfine fields) are pointing with the same probability only into the angular aperture $\Delta\varphi = 2\varphi'$, centred at φ_0. The density of probability is expressed as $P(\varphi) = P_0$ for $\varphi_0 - \varphi' < \varphi < \varphi_0 + \varphi'$ and $P(\varphi) = 0$ in the rest of the 2π interval. Relation (6) becomes

$$R_{23} = 4P_0\int_{\varphi_0-\varphi'}^{\varphi_0+\varphi'} \frac{1-\cos^2\phi\cos^2\varphi}{1+\cos^2\phi\cos^2\varphi}\,\mathrm{d}\varphi = f(\varphi_0,\varphi'), \tag{9}$$

where $P_0 = 1/\Delta\varphi$ results after normalisation. The function $f(\varphi_0,\varphi')$ admits an analytical form (see Appendix A), but careful attention has to be paid to critical angles. Due to these aspects, the direct numerical integration of relation (9) could be more useful.

In principle the two parameters of the angular spin distribution may be obtained from only two Mössbauer measurements at different angles. Fig. 3 presents the theoretical R_{23} ratios versus φ_0 at an angle of incidence $\phi = 30°$ and for different apertures, namely $2\varphi' = 10°$, 30° and 60°, respectively. The general trend of these curves has a minimum value at $\varphi_0 = 0°$ ($P(\varphi)$ centred on the Ox-axis) and a maximum value at $\varphi_0 = 90°$ ($P(\varphi)$ centred on the Oy-axis). Dependencies of theoretical R_{23} ratios versus φ' at an incidence angle of 30° and corresponding to $\varphi_0 = 0$ and 90° are shown in Fig. 4. It is worth mentioning that R_{23} shows a periodicity of π radians, and, therefore, we can determine only a φ_0 value between 0 and π (see Figs. 2 and 3). Practically, the minimum and the maximum value

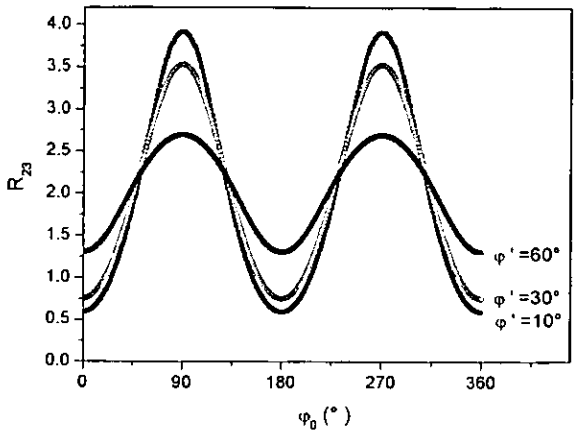

Fig. 3. Theoretical R_{23} ratio versus φ_0 for different angular distribution semi-apertures, φ', in the step-shaped distribution model. An angle of 30° between the γ-beam direction and the sample surface was considered.

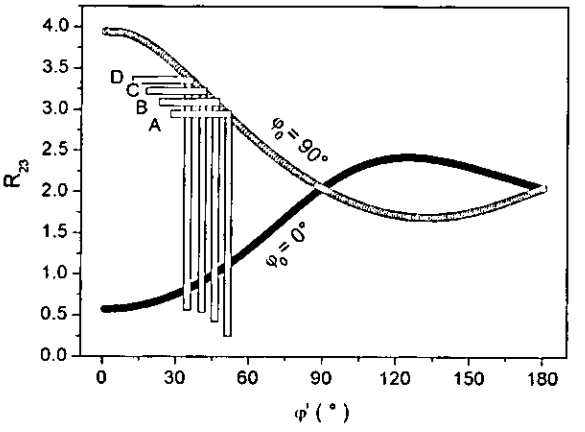

Fig. 4. Theoretical intensity ratios R_{23}^{Ox} ($\varphi_0 = 0°$) and R_{23}^{Oy} ($\varphi_0 = 90°$) versus the distribution semi-aperture, φ', in the step-shaped model. The parameter φ' is determined from this theoretical curve and the experimental R_{23} value. The experimental values A, B, C and D are discussed in Section 4. As in Fig. 3, the incident angle is $\phi = 30°$.

of the experimental R_{23} ratio should be obtained by rotating the sample in the xy-plane. The aperture $2\varphi'$ can be further derived from the two Mössbauer results corresponding to the distribution centred along the Ox ($\varphi_0 = 0°$) axis, i.e. R_{23}^{Ox}, and the Oy ($\varphi_0 = 90°$) axis, i.e. R_{23}^{Oy}. In this model, a more precise value for φ' can be found by the experimental difference $\Delta R_{23} = R_{23}^{Oy} - R_{23}^{Ox}$.

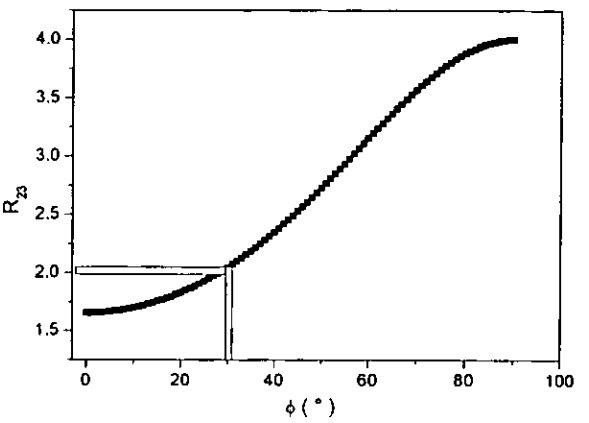

Fig. 5. R_{23} ratio versus the incident angle ϕ of the γ-beam for spins randomly distributed in the xy-plane (sample plane). A value close to 2 is obtained for an usual working angle of 30°.

3.3. In-plane randomly distributed spins

Such an analysis can be directly done by the extension of the step-shaped distribution over the complete 2π interval, namely $P(\varphi) = 1/2\pi$ for $0 < \varphi < 2\pi$. As can be seen in Appendix A, R_{23} takes a very simple form and, as expected, is dependent only on the incidence angle ϕ,

$$R_{23} = 4\left(\frac{2}{\sqrt{1+\cos^2\phi}} - 1\right). \tag{10}$$

The dependence of the R_{23} ratio versus the incident angle ϕ is presented in Fig. 5.

It is worth noticing that the situation with in-plane randomly distributed spins can be distinguished from other distributions leading potentially to the same value for the experimental R_{23} ratio by the constant behaviour of the experimental ratio with respect to any in-plane rotation of the sample.

3.4. Ellipse-type distribution

This is a more realistic model for a proper description of the planar spin distribution of a magnetic system with uniaxial anisotropy or with anisotropy induced by the presence of a magnetic field with an in-plane component. We propose the planar probability density as related to the radius vector connecting a focus with different points on

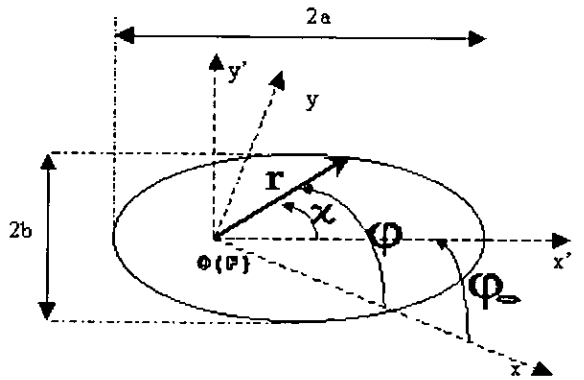

Fig. 6. Geometrical parameters related to an ellipse-type spin distribution in the film plane. By rotating the sample in its own plane we rotate the main symmetry axis of the ellipse (Ox') relative to the laboratory fixed axis Ox. This rotation is counted by the angle φ_0.

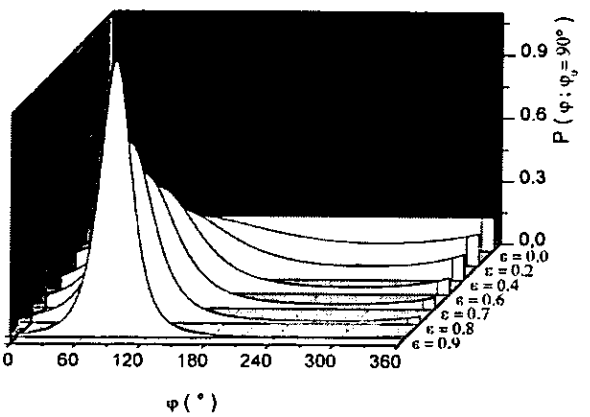

Fig. 7. Shape of the distribution probability versus eccentricity in the ellipse model for $\varphi_0 = 90°$. For eccentricities higher than 0.7, Lorentzian-like distributions can be considered.

the ellipse (see Fig. 6), namely by the relation: $P(\varphi) = r^2/2$. In the polar co-ordinates (r, φ), the density can be finally expressed as (Appendix B)

$$P(\varphi) = \frac{1}{2\pi} \frac{(1-\varepsilon^2)^{3/2}}{[1-\varepsilon\cos(\varphi-\varphi_0)]^2}, \tag{11}$$

where φ is the polar angle upon which we count the spin density in the Oxy co-ordinate system, φ_0 is the angle between the main symmetry axis of the ellipse (the Ox'- and Ox-axis), and ε is the ellipse eccentricity. Distribution (11) transforms into a random-type for $\varepsilon \to 0$, a Dirac-type for $\varepsilon \to 1$, and takes a quasi-Lorentzian-type shape for $\varepsilon > 0.7$ (see Fig. 7 and Appendix B). An analogous aperture $\Delta\varphi = 2b$ can be related to the width of the Lorentzian distribution at the half maximum. The following expression is obtained for the R_{23} intensity ratio:

$$R_{23} = 4\int_0^{2\pi} \frac{1-\cos^2\phi\cos^2\varphi}{1+\cos^2\phi\cos^2\varphi} \times \frac{1}{2\pi} \frac{(1-\varepsilon^2)^{3/2}}{[1-\varepsilon\cos(\varphi-\varphi_0)]^2}\,\mathrm{d}\varphi = f(\varphi_0,\varepsilon). \tag{12}$$

We can estimate the function $f(\varphi_0, \varepsilon)$ in this model only by a numerical integration. In principle, the two independent parameters of the probability distribution may be found again by taking only

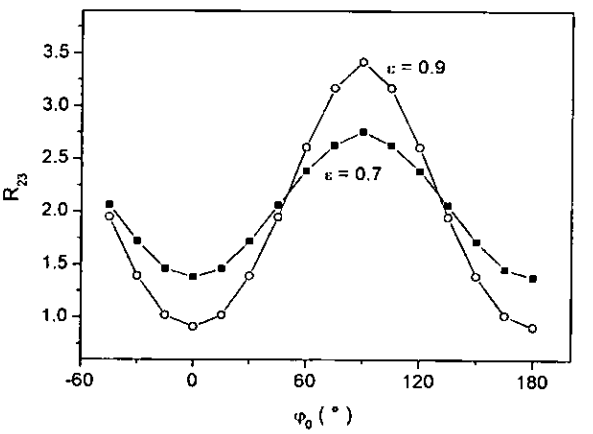

Fig. 8. Theoretical R_{23} intensity ratio versus φ_0 for different eccentricity, ε, in the ellipse type model.

two Mössbauer spectra. Fig. 8 presents the evolution of the R_{23} intensity ratio versus φ_0 for two different eccentricities. It shows the same π-periodicity specific to any in-plane distribution with mirror symmetry. The two extreme values are strongly dependent on the ellipse eccentricity. The dependence of R_{23} upon ε at $\varphi_0 = 90°$ is shown in Fig. 9(a). Unique values of R_{23} correspond to different ε values ($0 < \varepsilon < 1$). Practically, Mössbauer spectra should be taken by rotating the sample in the xy-plane. The maximum probability is along the Oy (Ox) direction where the intensity ratio takes the maximum (minimum) value. The ellipse

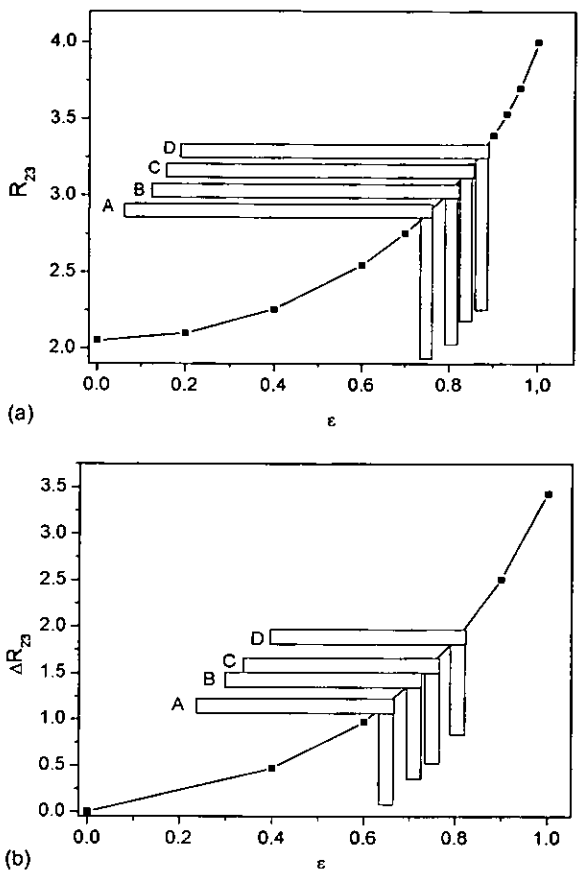

Fig. 9. (a) Theoretical intensity R_{23}^{Oy} ($\varphi_0 = 90°$) versus eccentricity, ε, at $\phi = 30°$. The parameter ε is determined from this theoretical curve and the experimental R_{23} value. The experimental values A, B, C and D are discussed in Section 4. (b) Theoretical difference $\Delta R_{23} = R_{23}^{Oy} - R_{23}^{Ox}$ versus eccentricity at $\phi = 30°$. By working with the experimental ΔR_{23} value, more reliable parameters ε can be derived.

eccentricity can be unambiguously deduced from the maximum (minimum) value, e.g. at the ordinate of the experimental R_{23} value in Fig. 9(a). By using more experimental data taken for different in-plane rotation angles the accuracy of the derived results can be substantially increased. In fact, the contribution of the $(f_{\text{theor}} - f_{\text{exp}})^2$ quantities for angles φ_0 around $(2k+1)\pi/4$, close to the inflection points of function f, is not significant and, therefore, only the minimum and maximum values of the function f may be used. The theoretical difference $\Delta R_{23} = R_{23}^{Oy} - R_{23}^{Ox}$ can be calculated versus ε, and then the distribution eccentricity is derived from the ordinate of the experimental ΔR_{23} difference between the maximum and the minimum intensity ratio (Fig. 9(b)).

3.5. Three-dimensional spin distribution with small out-of-plane component

The usual case of three-dimensional angular distributions with small out-of-plane components present double mirror symmetry and may be described by symmetric quadratic surfaces, e.g. by ellipsoidal distributions with the main axis oriented in the sample plane along φ_0. These can be further decomposed in two-dimensional uncorrelated in-plane and out-of-plane components, which separately can be analysed by the above-mentioned models.

The out-of-plane component is deduced from the experimental R_{23} ratio (equal to R'') obtained in perpendicular geometry ($\phi = 90°$). The case corresponds to a planar distribution (normal to the sample plane) centred at $\varphi_0 = 90°$ and analysed with the incident radiation in the distribution plane. Therefore models 3.2/3.4 within the conditions $\varphi_0 = 90°$ and $\phi = 0°$ can be applied in order to find the out-of-plane distribution aperture $\Delta\varphi$.

Models 3.2/3.4 in a non-perpendicular geometry should provide the in-plane component of the distribution. In fact, even in the limit $\Delta\varphi \to 0$ and $\varphi_0 \to 90°$ for the in-plane component of the distribution, the experimental intensity ratio R_{23} does not reach the maximum value of 4, due to the out-of-plane component. In conditions of a small out-of-plane component, the general trend of the experimental intensity ratio versus the parameters of the in-plane distribution is expected to follow the previously deduced trends for completely in-plane spins. The out-of-plane component will modify especially the limits of these variations, in the sense that for an in-plane spin component centred at $\varphi_0 = 90°$ the experimental intensity ratio R_{23} will be lower than in the case of no out-of-plane component, whereas for an in-plane component centred at $\varphi_0 = 0°$, the intensity ratio will be higher. Moreover it is expected that these deviations from the formal values of an ideal in-plane component will depend on the angle ϕ. If we are able to approximate the out-of-plane influence

on the intensity ratio, the experimental values can be properly modified in order to get the intensity ratio corresponding to only the in-plane spin component of the distribution. For this modified value, R^*_{23}, we may use directly relations (8)–(12), and hence the results derived for an ideal in-plane distribution. The modified intensity ratio related to only the in-plane component of the distribution may be approximated by the following relationship (Appendix C):

$$R^*_{23} = R^{\exp}_{23} + (4 - R^n)(\sin\phi - \cos\phi\cos\varphi_0) \qquad (13)$$

with $R^{\exp}_{23}$ the experimental intensity ratio obtained in non-perpendicular geometry and R^n the intensity ratio in perpendicular geometry. It is worth noticing that for high out-of-plane components of the spin distribution or for high incident angles, the intensity ratio in non-perpendicular geometry becomes almost insensitive to the in-plane rotation of the sample and, consequently, the parameters of the in-plane spin distribution cannot be properly obtained.

4. Experimental results

The above-presented procedures will be used in order to find the magnetic EAD in four samples of advanced double-coated metal particle tapes. The analysed double-coated metal particle tapes present a magnetic layer and a non-magnetic under-layer. The magnetic layer contains ellipsoidal particles of metallic iron (doped with a very small amount of Co) embedded in a polymer matrix, whereas the non-magnetic under-layer is based on antiferromagnetic α-Fe_2O_3 particles. The metallic ellipsoids have an aspect ratio of 1:5 and a length of approximately 100 nm. The embedding process has been done in the presence of a small longitudinal applied field, in order to orient the ellipsoids with their easy axis along the tape direction. The metallic nano-particles are magnetic monodomains, and due to the shape anisotropy, both the internal moments as well as the overall particle magnetic moments prefer an orientation along the main ellipsoidal axis. It is well known that the magnetic orientation of the metallic particles has a major effect on the recording performances and therefore should be carefully analysed by suitable techniques. The characterisation of the iron species and the out-of-plane component of the particle EAD were analysed in our previous work [6], using both Mössbauer spectroscopy and magnetometry. In this paper we focus on the in-plane component of the EAD deduced by Mössbauer spectroscopy. The in-plane EAD for the four analysed samples (labeled A, B, C, D) with different effective thicknesses as described in [6], was previously reported and derived by Vopsaroiu and Bissell [7] via magnetic measurements based on the bi-axial VSM technique. The analysed samples as well as some specific magnetic parameters are given in Table 1. Mrt represents the remanent magnetisation per unit volume multiplied by the effective magnetic coating thickness, whereas $2b$ is the angular width at half maximum of a Lorentzian function that gives the best fit of the experimental in-plane EAD [7].

Room temperature Mössbauer spectra have been acquired in transmission geometry using a spectrometer with constant acceleration and a ^{57}Co source in a Rh matrix. All samples were

Table 1
Magnetic and Mössbauer parameters of the four analysed samples

Sample	Mrt (memu/cm^2)	$2b$ (°)	R^n	R^{*Oy}_{23}	$2\varphi'$ (°)	ε (Fig. 9(a))	$2b_1$ (°)	R^{*Ox}_{23}	ΔR^*	ε (Fig. 9(b))	$2b_2$ (°)
A	3.0	65(3)	3.65(5)	2.90(5)	103(3)	0.74(2)	56(3)	1.70(5)	1.2(1)	0.65(2)	67(3)
B	4.0	55(3)	3.70(5)	3.10(5)	90(3)	0.81(2)	47(3)	1.65(5)	1.5(1)	0.72(2)	57(3)
C	4.5	48(3)	3.55(5)	3.20(5)	80(3)	0.84(2)	43(3)	1.60(5)	1.6(1)	0.76(2)	51(3)
D	6.0	42(3)	3.65(5)	3.35(5)	70(3)	0.87(2)	40(3)	1.45(5)	1.9(1)	0.81(2)	45(3)

Data corresponding to angular spin-distribution parameters obtained by different methods are also presented. The parameters $2b$ were obtained by magnetometry. The parameter $2b_1$ was obtained from Fig. 9(a) by using one intensity ratio (R^{*Oy}_{23}) in Mössbauer spectroscopy (MS1), and $2b_2$ was determined via ΔR^* (see Fig. 9(b)) by using two experimental intensity ratios (MS2).

previously studied with the γ radiation perpendicular to the sample plane in order to deduce the average out-of-plane spin component [6]. The corresponding R'' intensity ratios are given also in Table 1. It can be observed that only a small out-of-plane component of the particle magnetic moments ($3.5 < R'' < 3.7$) is present, and, therefore, models 3.2 or 3.4 may be successfully applied.

New measurements in non-perpendicular geometry at $\phi = 30°$ have been performed. We naturally assumed that the maximum moment density should be along the direction of the applied field during the coating procedure (which was previously marked on the samples). Some typical Mössbauer spectra taken for sample D at different angles φ_0 between the applied field direction (along the tape direction) and the Ox axis are shown in Fig. 10. The more intense Mössbauer sub-spectrum (outer sextet) with a hyperfine field of 49.5 T originates from the α-Fe_2O_3 nanoparticles in the under-layer [6]; it has been least-squares fitted via a distribution of hyperfine fields,

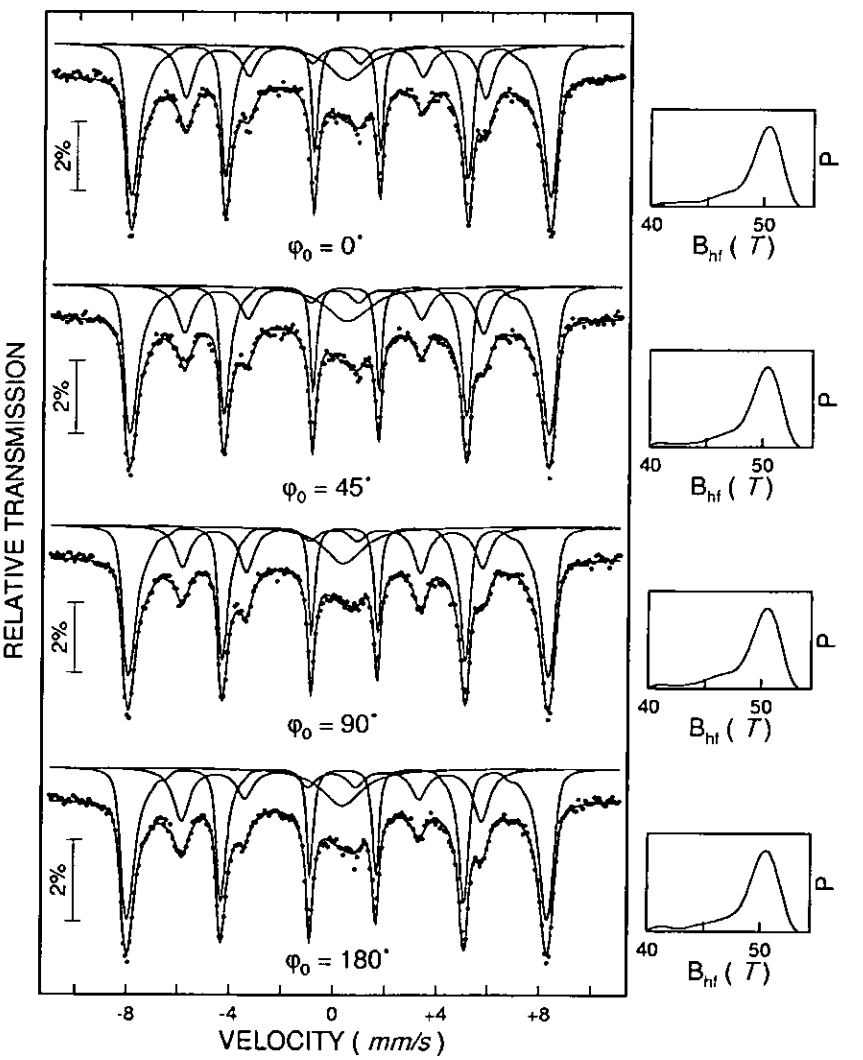

Fig. 10. Typical Mössbauer spectra of sample D taken at an incident angle $\phi = 30°$ and different angles φ_0. The inner sextet originates from the magnetic single-domain metallic particles. Right-hand side: hyperfine field distributions, $P(B_{hf})$, of the α-Fe_2O_3 underlayer.

$P(B_{hf})$. The Mössbauer pattern corresponding to the α-Fe(Co) metallic particles is the less intense inner sextet with a hyperfine field of about 36 T [6] and it has been fitted with only one usual Lorentzian sextet. It may be observed that the relative intensity of the second (fifth) line of the α-Fe(Co) sextet depends sensitively on the angle φ_0. The experimental R_{23} ratio shows a minimum at $\varphi_0 = 0°$ (180°) and a maximum at 90° (Fig. 11), in agreement with the assumption of a maximum EAD along the applied field direction. Once knowing the direction of the maximum spin density, the aperture of the distribution may be found by one measurement per sample (e.g. at $\varphi_0 = 90°$). The obtained R_{23}^* intensity ratios and the $2b_1$ parameters derived via ε within the 3.4 model (see Fig. 9(a)) and $2\varphi'$ aperture obtained within the 3.2 model (Fig. 4), respectively, are presented in Table 1. Results concerning the evaluation of the distribution parameters via the difference $\Delta R_{23}^* = R_{23}^{*Oy} - R_{23}^{*Ox}$ (Fig. 9(b)) estimated from two Mössbauer spectra taken at $\varphi_0 = 90°$ and 0°, respectively, are given in the same table.

Fig. 12 displays the evolution of the in-plane Lorentzian-like distribution parameters obtained from different methods versus the Mrt product of the analysed samples. The apertures in the step-shaped model are compared. For narrow distributions, an acceptable agreement is observed between magnetic (full squares) and Mössbauer (open circles) data obtained by only one experimental spectrum. The agreement between the magnetic and the Mössbauer results (open triangles) improves substantially by taking into account two different Mössbauer spectra. The apertures $2\varphi'$ in the step-shaped model (asterisks) follow the same trend as the $2b$ parameters, but are about 65% higher. They seem to be related to Lorentzian widths at around 1/3 of the maximum probability.

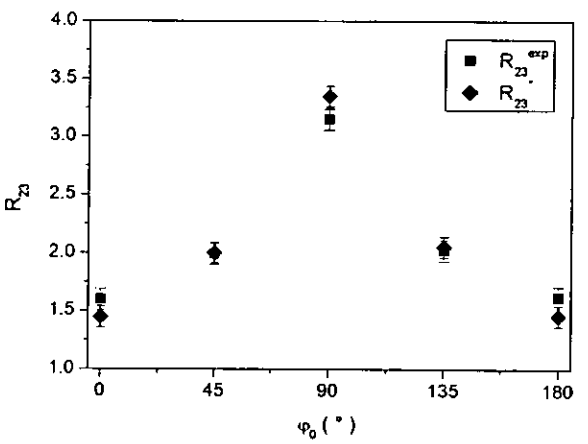

Fig. 11. Experimental intensity ratios R_{23}^{exp} for sample D (full squares) obtained by least-squares fitting the Mössbauer spectra taken at $\phi = 30°$ and different angles φ_0. The modified experimental intensity ratio R_{23}^* related to only the in-plane component (according to Eq. (13)) is also presented (full diamonds).

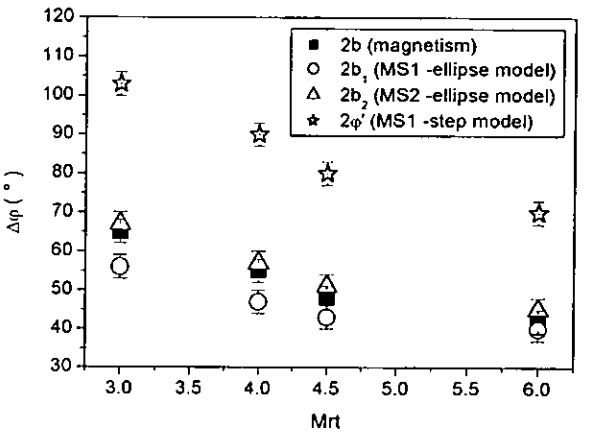

Fig. 12. Full widths at half maximum for a Lorentzian-like EAD of metallic particles versus the Mrt values of the analysed samples. Results from magnetic (full squares) and Mössbauer methods (open circles and open triangles) are considered. Apertures $2\varphi'$ in the step-shaped model (asterisks) are also plotted.

It is worth noticing that the advantage of the biaxial VSM technique consists in a better reliability of the derived distributions, while the Mössbauer techniques give the possibility to deduce the in-plane EAD over a large regime of temperatures.

5. Conclusions

Simple procedures for deducing in-plane angular spin distributions by Mössbauer spectroscopy are described. A convenient type of distribution is initially proposed. Theoretical R_{23} intensity ratios in Mössbauer patterns are expressed in terms of the distribution parameters. Experimental R_{23} ratios fix subsequently the proper values of the parameters in the analysed distributions. The procedure was applied in order to derive the an-

gular magnetic moment distributions of metallic nano-particles in advanced double-coated tapes for magnetic recording. The results obtained by Mössbauer spectroscopy are in agreement with results obtained from the bi-axial VSM technique.

The angular spin distribution correlated with the Fe phase composition at interfaces or in very thin films may be obtained with such a procedure by using backscattering Mössbauer techniques.

Acknowledgements

Financial support by the Alexander-von-Humboldt Stiftung is highly acknowledged by one of the authors (V. Kuncser). The authors wish to thank U. von Hörsten for valuable technical assistance. Work partially supported by the Deutsche Forschungsgemeinschaft (SFB 491).

Appendix A

With the notation $c = \cos\phi$, relation (9) becomes

$$R_{23} = 4\frac{1}{2\varphi'}\int_{\varphi_0-\varphi'}^{\varphi_0+\varphi'}\frac{1-c^2\cos^2\varphi}{1+c^2\cos^2\varphi}\,d\varphi = 4\frac{1}{2\varphi'}\left[(1-c^2)\int_{\varphi_0-\varphi'}^{\varphi_0+\varphi'}\frac{d\varphi}{1+c^2\cos^2\varphi} + c^2\int_{\varphi_0-\varphi'}^{\varphi_0+\varphi'}\frac{\sin^2\varphi}{1+c^2\cos^2\varphi}\right]$$

and further ([5], pp. 958 and 962),

$$R_{23} = 4\frac{1}{2\varphi'}\left[\left(\frac{1-c^2}{\sqrt{1+c^2}}\arctan\frac{\tan\varphi}{\sqrt{1+c^2}}\right)_{\varphi_0-\varphi'}^{\varphi_0+\varphi'} + c^2\left(\frac{\sqrt{1+c^2}}{c^2}\arctan\frac{\tan\varphi}{\sqrt{1+c^2}} - \frac{\varphi}{c^2}\right)_{\varphi_0-\varphi'}^{\varphi_0+\varphi'}\right] = 4\frac{1}{2\varphi'}\left(\frac{2}{\sqrt{1+c^2}}\arctan\frac{\tan\varphi}{\sqrt{1+c^2}}\Bigg|_{\varphi_0-\varphi'}^{\varphi_0+\varphi'} - 2\varphi'\right).$$

Finally,

$$R_{23} = 4\frac{1}{2\varphi'}\left[\frac{2}{\sqrt{1+c^2}}\left(\arctan\frac{\tan(\varphi_0+\varphi')}{\sqrt{1+c^2}} - \arctan\frac{\tan(\varphi_0-\varphi')}{\sqrt{1+c^2}} + k\pi\right) - 2\varphi'\right]. \tag{A.1}$$

For $\varphi' \to 0$ (limit toward a δ-type distribution), we have

$$\lim_{\varphi'\to 0}\frac{\arctan\frac{\tan(\varphi_0+\varphi')}{\sqrt{1+c^2}} - \arctan\frac{\tan(\varphi_0-\varphi')}{\sqrt{1+c^2}}}{2\varphi'} = \frac{1}{1+\frac{(\tan\varphi_0)^2}{1+c^2}}\frac{1}{\sqrt{1+c^2}}\frac{1}{\cos^2\varphi_0},$$

and consequently, relation (A.1) becomes

$$R_{23} = 4\frac{2\varphi'}{2\varphi'}\left(\frac{2}{\sqrt{1+c^2}}\times\frac{\sqrt{1+c^2}}{\cos^2\varphi_0+c^2\cos^2\varphi_0+\sin^2\varphi_0} - 1\right) = 4\frac{1-c^2\cos^2\varphi_0}{1+c^2\cos^2\varphi_0},$$

namely, the specific intensity ratio of an unidirectional distribution.

The intensity ratio for in-plane randomly distributed spins can be easily deduced from relation (A.1) by the conditions $\varphi' = \pi$ and $0 < R_{23} < 4$. Based on the π periodicity of the *tan* function, it results directly,

$$R_{23} = 4\frac{1}{2\pi}\left[\frac{4\pi}{\sqrt{1+c^2}} - 2\pi\right]. \tag{A.2}$$

Appendix B

We define the angular density of probability in the ellipsoidal model as related to the vector radius of an ellipse. In the $Ox'y'$ coordinate system, we propose, for spins pointing toward a direction χ versus Ox', a spin density respecting the relation $P(\chi) = r^2/2$. With this definition, the normalisation condition is written as

$$\int_0^{2\pi}P(\chi)\,d\chi = \int_0^{2\pi}\frac{1}{2}r\cdot r\,d\chi = \int_{A_{\text{ellipse}}}dA = A_{\text{ellipse}} = \pi ab = ct. \tag{B.1}$$

The normalisation may be simply fulfilled for ellipses of unit area, namely for $\pi ab = 1$ (a and b are the two semi-axes of the ellipse, see Fig. 6.)

In polar co-ordinates r and χ (system $Ox'y'$), r can be expressed as [4]

$$r = \frac{2p}{1 - \varepsilon\cos\chi}, \tag{B.2}$$

where the two ellipse parameters p and ε are related to the two semi-axes by the relations

$$\varepsilon = \sqrt{1 - b^2/a^2} \quad \text{and} \quad p = b^2/a. \tag{B.3}$$

Within relation $\pi ab = 1$, the following connection between p and ε can be found from (B.3):

$$4p^2 = \frac{(1-\varepsilon^2)^{3/2}}{\pi}. \tag{B.4}$$

Moreover, the spin densities in the two systems $Ox'y'$ and Oxy, respectively, obey the relation

$$P(\chi)|_{Ox'y'} = P(\varphi - \varphi_0)|_{Oxy}. \tag{B.5}$$

By taking into account (B.2), (B.4) and (B.5), the spin density in the Oxy system is expressed only as a function of the ellipse eccentricity, ε, and the direction of maximum probability, φ_0,

$$P(\varphi;\varphi_0,\varepsilon) = \frac{r^2}{2} = \frac{1}{2}\frac{4p^2}{[1-\varepsilon\cos(\varphi-\varphi_0)]^2} = \frac{1}{2\pi}\frac{(1-\varepsilon^2)^{3/2}}{[1-\varepsilon\cos(\varphi-\varphi_0)]^2}. \tag{B.6}$$

Two limiting cases should be analysed:

(a) $\varepsilon \to 0$ (ellipse $\to$ circle):

$$P(\varphi) = \frac{1}{2\pi} = ct,$$

which is the typical expression we used for randomly distributed spins.

(b) $\varepsilon \to 1$ (ellipse $\to$ unidirectional distribution):

$$P(\varphi) = \begin{cases} 0 & \text{for} \quad \varphi \neq \varphi_0 \\ \infty & \text{for} \quad \varphi = \varphi_0 \end{cases}$$

$$\text{and} \int_0^{2\pi} P(\varphi)\,\mathrm{d}\varphi = 1,$$

namely conditions that define a $\delta(\varphi - \varphi_0)$ function.

Appendix C

The following indirect way for estimating the influence of the out-of-plane spin component on the experimental intensity ratio is proposed: (i) we look for a relationship between the experimental intensity ratio, R_{23}^{exp}, and a formal intensity ratio, R_{23}^{*}, corresponding to an in-plane distribution that should be verified in some known limiting cases, (ii) the intensity ratio in Figs. 2 and 3 are compatible with a harmonic type dependence on φ_0, and hence we assume the same dependence for the deviation $R_{23}^{exp} - R_{23}^{*}$, (iii) an out-of-plane angular spin aperture described by $4 - R^n$ corresponds to the intensity ratio in perpendicular geometry R^n, (iv) the maximum deviation due to the out-of-plane component should be $4 - R^n$, (v) the deviation depends on the incident angle and takes values between zero and the maximum deviation, and, therefore, a harmonic dependence upon angle ϕ may be supposed, too.

The limiting cases are

- For $\varphi_0 = 90°$ and $\phi = 0°$, $R_{23}^{exp} = R_{23}^{*}$.
- For $\varphi_0 = 90°$ and $\phi = 90°$, $R_{23}^{exp} = R^n$.
- For $\varphi_0 = 0°$ and $\phi = 0°$, $R_{23}^{exp} = R_{23}^{*} + (4 - R^n)$.
- For $\varphi_0 = 0°$ and $\phi = 90°$, $R_{23}^{exp} = R^n$.

The experimental intensity ratio respecting all the above mentioned conditions can be described by the following relationship:

$$R_{23}^{exp} = R_{23}^{*} - (4 - R^n)\sin\phi + (4 - R^n)\cos\phi\cos\varphi_0. \tag{C.1}$$

It may be observed that for $\varphi_0 = 90°$ the last term is zero and R_{23}^{exp} becomes

$$R_{23}^{exp} = R_{23}^{*} - (4 - \mathrm{R}^n)\sin\phi. \tag{C.2}$$

In this case the effect of the out-of-plane component is to decrease the maximum intensity ratio that would correspond to a complete in-plane spin distribution (see Fig. 3).

Further, (C.2) gives

- For $\phi = 0°$, $R_{23}^{exp} = R_{23}^{*}$.
- For $\phi = 90°$, the formal intensity ratio corresponding to an in-plane distribution, R_{23}^{*}, becomes 4 and therefore $R_{23}^{exp} = R^n$.

For $\varphi_0 = 0°$, relation (C.1) reduces to

$$R_{23}^{exp} = R_{23}^{*} - (4 - R^n)\sin\phi + (4 - R^n)\cos\phi. \quad (C.3)$$

For small incidence angles, the effect of the out-of-plane component is to increase the minimum intensity ratio that would correspond to a complete in-plane spin distribution (see Fig. 3).

Further, (C.3) gives

- For $\phi = 0°$, $R_{23}^{exp} = R_{23}^{*} + (4 - R^n)$.
- For $\phi = 90°$, the last term is zero and $R_{23}^{exp} = R^n$.

The formal intensity ratio corresponding to only the in-plane component of the distribution can be easy subtracted from relation (C.1):

$$R_{23}^{*} = R_{23}^{exp} + (4 - R^n)(\sin\phi - \cos\phi\cos\varphi_0). \quad (C.4)$$

References

[1] H.D. Pfannes, H. Fischer, Appl. Phys. 13 (1977) 317.

[2] J.M. Greneche, F. Varret, J. Phys. C: Solid State Phys. 15 (1982) 5333.

[3] Q.A. Pankhurst, M.R.J. Gibbs, J. Phys. C: Condens. Matter 5 (1993) 3275, and references therein.

[4] U. Gonser, Mossbauer spectroscopy, in: U. Gonser (Ed.), Topics in Applied Physics, Vol. 5, Springer, Berlin, 1975, p. 1.

[5] G.A. Korn, T.M. Korn, Mathematical Handbook For Scientists and Engineers, Mc Graw-Hill, New York, 1968.

[6] V. Kuncser, M. Vopsaroiu, B. Sahoo, P.R. Bissell, W. Keune, Proceedings of the International Conference on Applications of the Mössbauer Effect (ICAME 2001), Oxford, UK, September 2001, Hyperfine Int., in press.

[7] M. Vopsaroiu, P.R. Bissell, R. Kookson, Phys. Stat. Sol. (b), in press.